WL-TR-96-1108

WIDEBAND ELECTROMAGNETIC SCATTERING/ANALYSIS PROGRAM

A CAUSTIC CORRECTED UNIFORM GEOMETRICAL THEORY OF DIFFRACTION FOR EVALUATING HIGH FREQUENCY ELECTROMAGNETIC FIELDS NEAR THE CUSP OF THE CAUSTIC CAUSED BY THE CURVATURE OF AN EDGE

J. H. Meloling and R. J. Marhefka
THE OHIO STATE UNIVERSITY
ELECTROSCIENCE LABORATORY
1320 KINNEAR ROAD
COLUMBUS OH 43212

OCTOBER 1994

INTERIM REPORT FOR PERIOD JANUARY 1994 TO MAY 1994

Approved for public release; distribution unlimited

AVIONICS DIRECTORATE
WRIGHT LABORATORY
AIR FORCE MATERIEL COMMAND
WRIGHT-PATTERSON AIR FORCE BASE, OH 45433-7623

NOTICE

WHEN GOVERNMENT DRAWINGS, SPECIFICATIONS, OR OTHER DATA ARE USED FOR ANY PURPOSE OTHER THAN IN CONNECTION WITH A DEFINITE GOVERNMENT-RELATED PROCUREMENT, THE UNITED STATES GOVERNMENT INCURS NO RESPONSIBILITY OR ANY OBLIGATION WHATSOEVER. THE FACT THAT THE GOVERNMENT MAY HAVE FORMULATED OR IN ANY WAY SUPPLIED THE SAID DRAWINGS, SPECIFICATIONS, OR OTHER DATA, IS NOT TO BE REGARDED BY IMPLICATION, OR OTHERWISE IN any MANNER CONSTRUED, AS LICENSING THE HOLDER, OR ANY OTHER PERSON OR CORPORATION; OR AS CONVEYING ANY RIGHTS OR PERMISSION TO MANUFACTURE, USE, OR SELL ANY PATENTED INVENTION THAT MAY IN ANY WAY BE RELATED THERETO.

THIS REPORT IS RELEASABLE TO THE NATIONAL TECHNICAL INFORMATION SERVICE (NTIS). AT NTIS, IT WILL BE AVAILABLE TO THE GENERAL PUBLIC, INCLUDING FOREIGN NATIONS.

THIS TECHNICAL REPORT HAS BEEN REVIEWED AND IS APPROVED FOR PUBLICATION.

RICHARD J. KOESEL
Project Engineer
Radar Branch
Avionics Directorate

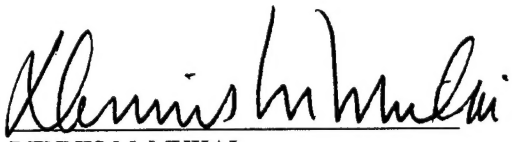

DENNIS M. MUKAI
Chief, Radar Branch
RF Technology Division
Avionics Directorate

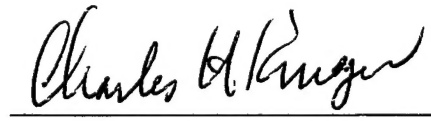

CHARLES H. KRUEGER, Chief
RF Technology Division
Avionics Directorate

IF YOUR ADDRESS HAS CHANGED, IF YOU WISH TO BE REMOVED FROM OUR MAILING LIST, OR IF THE ADDRESSEE IS NO LONGER EMPLOYED BY YOUR ORGANIZATION PLEASE NOTIFY WL/AAMR, 2241 AVIONICS CIRCLE, WRIGHT-PATTERSON AFB OH 45433-78333 TO HELP MAINTAIN A CURRENT MAILING LIST.

Copies of this report should not be returned unless return is required by security considerations, contractual obligations, or notice on a specific document.

REPORT DOCUMENTATION PAGE

Form Approved
OMB No. 0704-0188

1. AGENCY USE ONLY (Leave blank)	2. REPORT DATE	3. REPORT TYPE AND DATES COVERED
	October 1994	Interim 1/1/94 – 5/31/94

4. TITLE AND SUBTITLE

WIDEBAND ELECTROMAGNETIC SCATTERING/ANALYSIS PROGRAM
A Caustic Corrected Uniform Geometrical Theory of Diffraction for Evaluating High Frequency Electromagnetic Fields near the Cusp of the Caustic Caused by the Curvature of an Edge

5. FUNDING NUMBERS

C: F33615-91-C-1729
PE: 62204F
PR: 7622
TA 07
WU 71

6. AUTHOR(S)

J.H. Meloling and R.J. Marhefka

7. PERFORMING ORGANIZATION NAME(S) AND ADDRESS(ES)

The Ohio State University
ElectroScience Laboratory
1320 Kinnear Road
Columbus, OH 43212

8. PERFORMING ORGANIZATION REPORT NUMBER

724733-5

9. SPONSORING / MONITORING AGENCY NAME(S) AND ADDRESS(ES)

Avionics Directorate
Wright Laboratory
Air Force Materiel Command
Wright Patterson AFB OH 45433-7623
POC: R. Koesel, WL/AAMR, (513) 255-6427

10. SPONSORING / MONITORING AGENCY REPORT NUMBER

WL-TR-96-1108

11. SUPPLEMENTARY NOTES

12a. DISTRIBUTION / AVAILABILITY STATEMENT

Approved for public release

12b. DISTRIBUTION CODE

13. ABSTRACT *(Maximum 200 words)*

An improvement to the Uniform Geometrical Theory of Diffraction (UTD) is developed for determining the high frequency electromagnetic fields near the caustic caused by the curvature of an edge. Although the classic UTD correctly compensates for the discontinuities of the Geometrical Optics fields, it does not correct for caustics created by a curved edge. In particular, for a flat plate with a curved edge that is symmetric about a line, a caustic will occur for a source or observer, when two or more diffraction points merge.

This work is devoted to the development of a caustic corrected UTD solution. This means that uniform asymptotic techniques are used to obtain a solution that reduces to the classical UTD result away from, is bounded near, and reduces to the known result at the caustic.

Results are calculated for several geometries and compared with the Method of Moments. The results are shown to be in excellent agreement in the caustic regions and smoothly reduce to the UTD away from the caustic regions. Finally, the resulting solution is a very fast and efficient way of computing the high frequency field diffracted by a curved edge due to its ray optical nature.

14. SUBJECT TERMS

GTD (GEOMETRICAL THEORY OF DIFFRACTION)
UTD (UNIFORM THEORY OF DIFFRACTION)
ASYMPTOTIC
DIFFRACTION
MODELLING

15. NUMBER OF PAGES
273

16. PRICE CODE

17. SECURITY CLASSIFICATION OF REPORT	18. SECURITY CLASSIFICATION OF THIS PAGE	19. SECURITY CLASSIFICATION OF ABSTRACT	20. LIMITATION OF ABSTRACT
Unclassified	Unclassified	Unclassified	UL

Contents

Figures

SECTION 1

Introduction

An improvement to the Uniform Geometrical Theory of Diffraction (UTD) is developed for determining the high frequency electromagnetic fields near the caustic caused by the curvature of an edge. This improved solution will be referred to as a caustic corrected UTD (CC-UTD). Although the UTD of Kouyoumjian and Pathak [1] correctly compensates for the discontinuities of the Geometrical Optics (GO) fields, it does not correct for caustics created by a curved edge. In particular, a flat plate with a curved edge that is symmetric about a line will create caustics in the diffracted fields. A caustic will occur when the source or observation point is in the near-zone. In this case, there are two smooth caustics caused by the diffracted rays that form a cusp in the plane of symmetry. In terms of the UTD, the two caustics are created when two diffraction points merge (coalesce). The cusp of these caustics is formed when three diffraction points coalesce. There are two different regions in the plane of symmetry. The caustic lit region is the region where there are three distinct diffraction points that merge at the cusp. There is just one diffraction point on the other side of the cusp. This is called the caustic shadow region.

In the past, much effort as been spent on analyzing the far-zone diffraction from objects with curved edges and curved apertures in plane screens. Many of these solutions have been obtained using electric and magnetic current elements that flow along the curved edge. These currents are called equivalent currents because they represent the distributed effects of the surface current on the faces of the wedge. Many far-zone solutions have been obtained using this type of solution.

Millar [2, 3] used equivalent currents to determine the far-zone transmission of a plane wave through apertures in plane screens. Equivalent currents are derived and applied to the transmission through a circular aperture in [2]. Later, in [3], the transmission through more general curved apertures is discussed and the special case of an elliptic aperture is analyzed.

A similar equivalent current solution was used by Ryan and Peters [4, 5] to obtain edge diffracted fields in the axial caustic regions of circular disks and cones. The equivalent currents used by Ryan and Peters are not only valid for half-plane diffraction but also wedge diffraction. These equivalent currents were also generalized to try and account for obliquely diffracted waves. Many other solutions have been obtained using the equivalent currents of Ryan and Peters.

The scattering by a finite cone has been studied extensively using equivalent currents. Burnside and Peters [6, 7] analyzed the scattering by a cone using equivalent currents to determine the fields in the axial caustic regions and to include higher-order diffraction mechanisms. Also, creeping wave excited diffractions on a cone is analyzed by Choi, Wang, Peters and Levy [8]. All of these solutions are valid for the far-zone scattering of a plane wave by a finite length cone.

Several heuristic modifications to the Ryan and Peters equivalent currents have been proposed. First, Knott and Senior [9], proposed the substitution $\sin^2\beta = \sin\beta\sin\beta'$ to enforce reciprocity. Next, it was discovered that these equivalent currents tend to account for the surface more than one time. Sikta and Peters [10] used a modified edge vector to heuristically correct for this problem. This modified edge vector is commonly called a stripping vector. Finally, the Ryan and Peters equivalent currents are only valid for far-zone diffraction problems. To use this concept to analyze near-zone problems, the GTD diffraction coefficients are replaced with the UTD diffraction coefficients. This modification was first made by Greer and Burnside [11] and later by Albertsen, Balling and Jensen [12].

Greer and Burnside [11] used the equivalent current concept in the near-zone to predict the high frequency fields in the caustic regions. This solution consists of the formulation of a diffraction integral using equivalent currents and numerically

integrating them to obtain the diffracted field contribution to the total field. Although their solution accurately predicts the field in and away from the caustic regions, the physical insight that is gained from a ray optical solution is not obtained. Also, this solution can take a considerable amount of computer time because the diffraction integral is integrated numerically.

Later; Albertsen, Balling and Jensen [12] developed an equivalent current solution and obtained approximate ray optical expressions. Their solution begins with the development of a diffraction integral using near-zone equivalent currents similar to Greer and Burnside. Next, they develop approximate ray optical expressions by making some stationary phase approximations. However, they do not use uniform asymptotic techniques so they do not obtain a complete or uniform solution. This means that their solution is bounded in the caustic regions, but it does not reduce to the classical UTD solution away from the caustic. Therefore, this solution is only applicable in the immediate vicinity of the caustics. The classical UTD solution must be used away from the caustics. This makes for a cumbersome solution. They are also unclear about where and how the two solutions should be blended.

Although the equivalent current solutions of Greer and Burnside or Albertsen, Balling and Jensen do a good job of correcting for the diffracted field caustics, they do not account for the regions where the reflection point is near the edge when diffraction points are coalescing. This is not a problem in the far-zone because the reflected field exists only along the specular direction. This phenomena is not accounted for because the equivalent currents are derived for a straight edge and then applied to a curved edge. We should not expect these equivalent currents alone to correct for this phenomena since a straight edge has only one diffraction point and a curved edge has more than one diffraction point in the near-zone.

In order to correct for the coalescence of reflection and diffraction points, a formulation must be used that does not use the classical GO fields. In this way, all the reflection and diffraction points can be accounted for by the uniform asymptotic expansion. The Physical Optics (PO) integral is typically used for this part of

the formulation. Once the evaluation of the PO integral has been performed either numerically or asymptotically, the contribution from the edge must be corrected.

One method of correcting for the incorrect edge contribution is to use the Physical Theory of Diffraction (PTD). The PTD consists of the PO contribution plus a fringe equivalent current contribution that flows along the edge of the wedge. This fringe current is obtained by asymptotically integrating the difference between the exact diffracted surface currents and the PO diffracted surface currents up to the edge of the wedge. A fringe equivalent current has been formulated by Michaeli [13] and Butorin, Martynov and Ufimtsev [14] which is valid for far-zone incidence and observation locations. These two solutions are commonly known to be identical.

More recently, the Incremental Theory of Diffraction (ITD) is formulated by Tiberio, Maci and Toccafondi [15, 16, 17]. The ITD consists of three integral contributions. The first of these integrals is the PO surface integral. The remaining two integrals are line integrals along the edge of the wedge. These line integrals are used to correct for the incorrect edge information of the PO integral. The exact diffracted field and the PO diffracted field are localized using a Fourier transform pair. In doing so, they obtain incremental diffracted field expressions that are valid in the near-zone.

Both the PTD and the ITD methods allow for a more complete formulation of radiation and scattering problems than the classical equivalent current formulations. However, to obtain a ray optical solution to a problem, the PO integral must be asymptotically evaluated. If this can not be accomplished, some approximations must be made in order to obtain a useful engineering solution. One of the most common of these approximations is to assume that the PO surface integral minus its edge contribution is the GO field. For near-zone problems, only the ITD can be used in this manner since the PTD fringe equivalent currents are derived for only far-zone cases. This will result in a solution that is similar to that of Greer and Burnside or Albertsen, Balling and Jensen. However, the heuristic modification made to the far-zone equivalent currents are not the same as the results of the more rigorous ITD formulation.

The ultimate goal of this report is to develop a useful and efficient solution that can be used to solve more complicated electromagnetic radiation and scattering problems dealing with the diffraction by curved edges. Curved edges cause caustics in the classical UTD ray optical solutions. The work presented in this report is devoted to the development of a caustic corrected UTD solution. This means that uniform asymptotic techniques are used to obtain a solution in the form of the classical UTD except that the information about the caustics is included. One of the requirements for a solution to be uniform is that it must reduce to the classical UTD result away from the caustics. The solution must also be bounded near the caustic and reduce to the known result at the caustic. This is accomplished here. Finally, the resulting solution is a very fast and efficient way of computing the high frequency field diffracted by a curved edge due to its ray optical nature.

This solution begins in a way that is very similar to that of Greer and Burnside or Albertsen, Balling and Jensen. A diffraction integral is formulated using the Incremental Theory of Diffraction (ITD) recently developed by Tiberio and Maci [15, 16, 17]. These integrals turn out to be very similar to those obtained using near-zone equivalent currents. Next, these integrals are asymptotically reduced on the lit and shadow sides of the caustic. A uniform asymptotic expansion similar to the one developed by Chester, Friedman and Ursell [18] is used to obtain a caustic corrected UTD solution on the lit side of the caustic. A uniform asymptotic expansion using classical stationary phase techniques is used to obtain a caustic corrected UTD solution on the shadow side of the caustic.

The caustic corrected UTD solution obtained in this report is consistent with the classical UTD. The CC-UTD solution smoothly reduces to the classical UTD solution of Kouyoumjian and Pathak on both sides of the caustic. Caustic correction transition functions are multiplied by the classical UTD solution which allow the coalescing diffraction points to properly combine and produce the correct field near the caustic. Only one diffraction point remains on the shadow side of the caustic; however, the ray field expression includes several different parts to obtain a uniform result. The first part of this diffracted field expression consists of the classical UTD

field expression multiplied by a caustic correction transition function. The remaining parts of this diffracted field expression are curvature dependent expressions that are not obtainable using classical UTD techniques. These expressions are cast in the form of the UTD diffracted field expression multiplied by caustic correction transition functions and new curvature dependent diffraction coefficients.

Chapter 2 of this report is a brief review of the classical UTD. The diffracted field caustics and the problems they cause are also discussed. Next, Chapter 3 is a derivation of many of the common incremental diffracted field and equivalent current expressions. These expressions are derived using a consistent procedure that allows for the derivation of incremental diffracted fields consistent with the Physical Theory of Diffraction and the Geometrical Theory of Diffraction. These different expressions are compared to determine which expression is the best one for the problem to be solved here. The formulation chosen is that of the ITD. In Chapter 4, the ITD is discussed and the diffracted field contribution is derived by determining the field diffracted by a wedge and the Fourier transform used to convert it to the incremental diffracted field expression. This result is then asymptotically reduced to obtain a closed form expression that is easy to use.

The field radiated by a source located on a flat plate with a curved edge is derived in Chapter 5. The ITD diffracted field integral equation is formulated and asymptotically reduced on the lit and shadow sides of the caustic. Two geometries are studied in Chapter 6 using this solution. First, the radiation by a monopole mounted on a flat plate with an edge defined by a parabolic equation is found. This geometry is useful in isolating just the phenomena of interest because it is semi-infinite in extent. It is also a simple geometry that gives valuable insight into the physical nature of the solution. The CC-UTD is compared with the classical UTD for this geometry. Next, the field radiated by a monopole mounted in the center of an elliptic disk is determined. This geometry is used to show the applicability of this solution. The CC-UTD solution is compared to the classical UTD solution and a Moment Method (MM) solution for this geometry.

Chapter 7 is devoted to the derivation of the more general scattering solution. The ITD diffracted field expression is derived and then asymptotically reduced on the lit and shadow sides of the caustic to obtain closed form ray optical expressions consistent with the classical UTD. In Chapter 8, the field scattered by a flat plate with an edge defined by a parabolic equation and the field scattered by an elliptic disk are determined. Again, the plate with the parabolic edge is used to illustrate the physical nature of the solution and the elliptic disk is used to illustrate the practical use of the resulting CC-UTD solution. The CC-UTD solution for the plate with the parabolic edge is compared to the classical UTD solution. The CC-UTD solution is compared with the classical UTD solution and a MM solution for the scattering by the elliptic disk. Finally, Chapter 9 is a summary of the work in this report along with some concluding remarks.

This report also includes several appendices. First, Appendix A is the closed form evaluation of three auxiliary integrals used in the determination of the incremental diffracted field expressions of Chapter 3. Appendix B is a derivation of the uniform asymptotic expansions used to determine the diffracted fields on the lit and shadow sides of the caustic. This appendix also proves that the two different expansions are indeed uniform. Next, Appendix C contains useful formulas for the calculation of the Parabolic Cylinder functions used in the caustic correction transition functions. Finally, Appendix D is a derivation of the phase function, diffraction parameter and half-plane diffraction coefficient derivatives used in the uniform asymptotic expansions.

All of the fields in this work are time harmonic with an assumed time dependance of $e^{j\omega t}$. This time dependance will be suppressed throughout this report. It will also be assumed that the free space wavenumber, k, has a small negative imaginary part. This will ensure that the radiation condition is satisfied at infinity. In addition, the plates are assumed to perfectly conducting.

SECTION 2

The Classical Uniform Geometrical Theory of Diffraction

Many geometries considered in high frequency problems can be evaluated using classical diffraction techniques. An important class of these techniques uses the Geometrical Optics (GO) fields along with diffracted fields to correct them. One of the most commonly used diffraction theories is the Geometrical Theory of Diffraction (GTD) and its uniform version the Uniform Geometrical Theory of Diffraction (UTD). This chapter is a brief overview of the UTD.

The GTD was developed in great detail by Keller [19] and is a ray optical technique that separates the total field into the sum of various types of fields each propagating according to its own specific set of rules. For a perfectly conducting wedge, the three types of fields used to determine the total field are the incident field, the reflected field, and the edge diffracted field. The incident and reflected fields are the same as those typically found using GO techniques. The diffracted field derived by Keller [19] is valid in the far-zone but does not correctly compensate for the discontinuities of the GO fields in the near-zone. Along the incident and reflection shadow boundaries, the GTD diffracted field is singular.

The UTD derived by Kouyoumjian and Pathak [1] corrects for the singularities of the diffracted field along the incident and reflection shadow boundaries which the GTD does not. Their solution is in the form of the general diffracted ray of the GTD except uniform diffraction coefficients are used. The general solution to a problem

has the form

$$\vec{E}^t(P) = \vec{E}^i(P) + \vec{E}^r(P) + \vec{E}^d(P) \tag{1}$$

where $\vec{E}^i(P)$ is the incident field at the observation point P and $\vec{E}^r(P)$ is the reflected field at P. These are the GO fields. There are also diffracted fields of the form

$$\vec{E}^d(P) = \vec{E}^i(Q_e) \cdot \overline{\overline{D}}(Q_e) \sqrt{\frac{\rho^d(Q_e)}{s\left[\rho^d(Q_e)+s\right]}}\, e^{-jks} \tag{2}$$

where $\overline{\overline{D}}(Q_e)$ is a dyadic diffraction coefficient given by

$$\overline{\overline{D}}(Q_e) = -\hat{\beta}'\hat{\beta} D_s(Q_e) - \hat{\psi}'\hat{\psi} D_h(Q_e) \tag{3}$$

and $\vec{E}^i(Q_e)$ is the incident field at the point of diffraction Q_e. The geometry for these diffracted rays is shown in Figure 1. This solution is also in the standard ray fixed coordinate system where the polarization vectors

$$\hat{\psi} = \frac{\hat{s} \times \hat{e}}{|\hat{s} \times \hat{e}|} = \frac{\hat{s} \times \hat{e}}{\sin\beta} \tag{4a}$$

$$\hat{\psi}' = \frac{\hat{e} \times \hat{s}'}{|\hat{e} \times \hat{s}'|} = \frac{\hat{e} \times \hat{s}'}{\sin\beta'} \tag{4b}$$

$$\hat{\beta} = \hat{s} \times \hat{\psi} \tag{4c}$$

$$\hat{\beta}' = \hat{s}' \times \hat{\psi}' \tag{4d}$$

form a spherical coordinate system about the diffraction point Q_e. The rays diffracted by the edge will propagate along lines which minimize the distance from the source to the edge and to the observation point according to the generalized Fermat's principle. The diffraction point can be shown to be located where $\beta = \beta'$. It is also clear that this distance is minimum for any point on the cone with a half angle of β. This is known as the diffraction cone or the Keller cone and it is shown in Figure 2.

The UTD diffraction coefficients $D_s(Q_e)$ and $D_h(Q_e)$ corresponding to the soft and hard polarizations are,

$$D_{s,h}(Q_e) = \frac{-e^{-j\pi/4}}{2n\sqrt{2\pi k}\sin\beta} \left[\left\{ \cot\left(\frac{\pi+\Psi^-}{2n}\right) F\left[kL^i a^+(\Psi^-)\right] + \cot\left(\frac{\pi-\Psi^-}{2n}\right) F\left[kL^i a^-(\Psi^-)\right] \right\} \right.$$

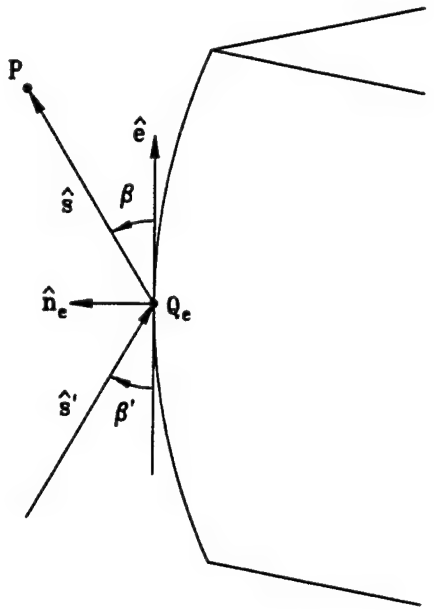

(a)

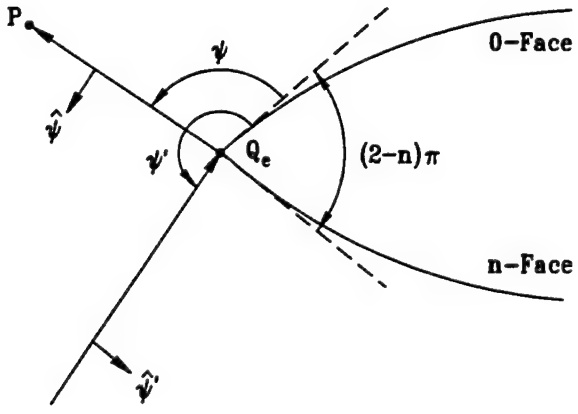

(b)

Figure 1: Canonical geometry for the diffraction by a wedge: (a) oblique incidence and (b) top view.

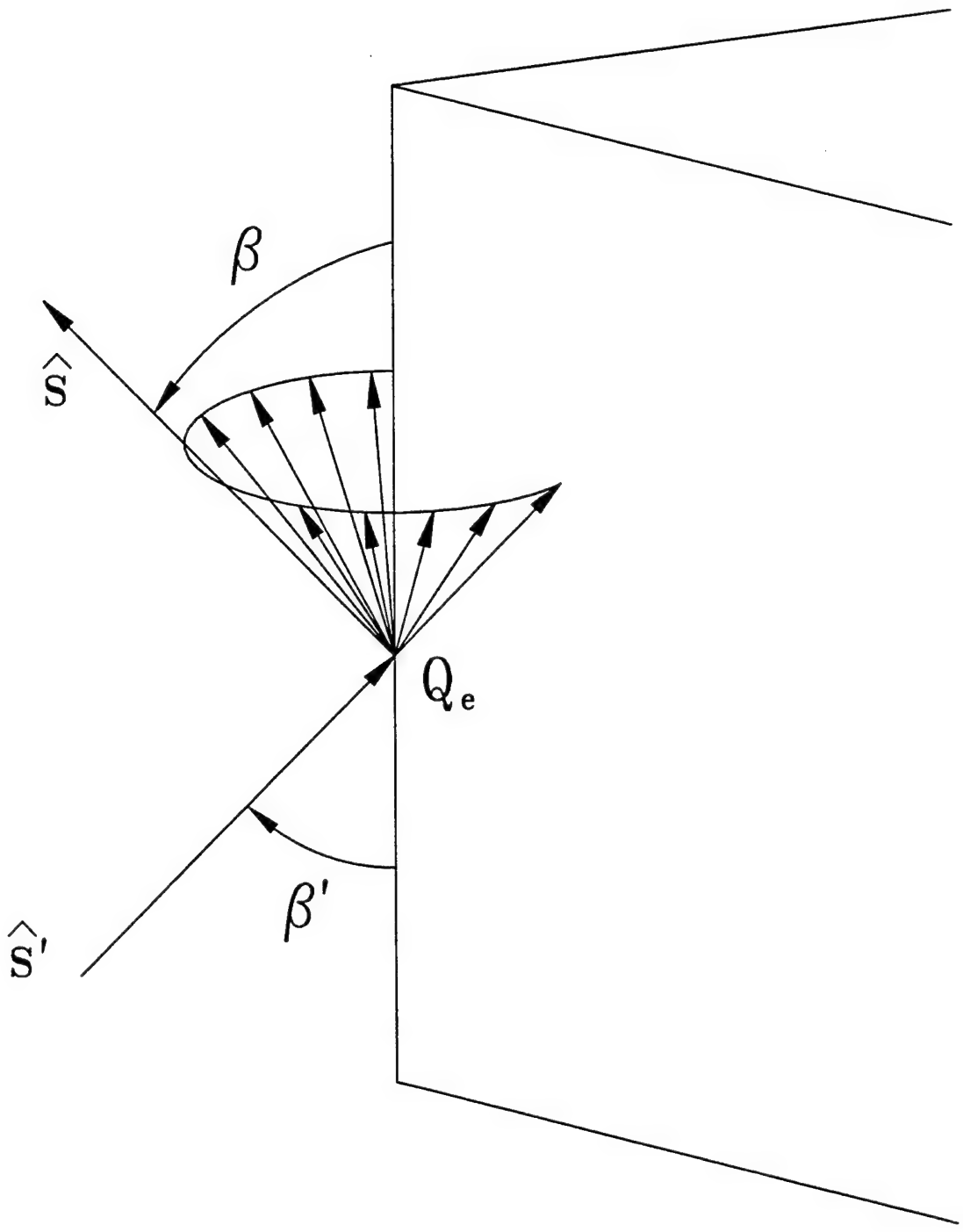

Figure 2: Diffraction cone for an obliquely incident wave.

$$\mp\left\{\cot\left(\frac{\pi+\Psi^+}{2n}\right)F\left[kL^{ro}a^+(\Psi^+)\right]\right.$$
$$\left.+\cot\left(\frac{\pi-\Psi^+}{2n}\right)F\left[kL^{rn}a^-(\Psi^+)\right]\right\}\Bigg] \tag{5}$$

where $\Psi^{\mp}=\psi\mp\psi'$. The Fresnel transition function in (5) is

$$F[x]=2j\sqrt{x}e^{jx}\int_{\sqrt{x}}^{\infty}e^{-j\tau^2}d\tau \tag{6}$$

where

$$a^{\pm}(\gamma)=2\cos^2\left(\frac{2\pi nN^{\pm}-\gamma}{2}\right) \tag{7}$$

and $N^{\pm}$ is the nearest integer satisfying

$$2\pi nN^{\pm}-\gamma=\pm\pi. \tag{8}$$

This transition function is used to bound the diffracted field and correctly compensate for the discontinuities of the GO fields. The distance parameters L^i, L^{ro} and L^{rn} have been obtained for a general curved wedge by Kouyoumjian and Pathak [1]. For the cases of interest in this work, the wedge is formed by two flat faces. In this case, the distance parameters are

$$L^i=L^{ro}=L^{rn}=\frac{s\left(\rho_e^i+s\right)\rho_1^i\rho_2^i}{\rho_e^i\left(\rho_1^i+s\right)\left(\rho_2^i+s\right)}\sin^2\beta \tag{9}$$

where ρ_e^i is the radius of curvature of the incident wave in the edge fixed plane and ρ_1^i and ρ_2^i are the two principle radii of curvature of the incident wave at the point of diffraction. A special case of interest here is for a plane wave incident on the wedge. For this case, the distance parameters become $L^i=L^{ro}=L^{rn}=s\sin^2\beta$.

For the general case of a curved edge, the incident field is diffracted astigmatically. This means the diffracted field wavefront has two different principle radii of curvature. This is accounted for by an amplitude spreading factor in the diffracted field expression. This amplitude spreading factor is defined as the square root term in (2). The astigmatic tube of rays diffracted by a curved edge is shown graphically in Figure 3. Since the diffracted field exists along the diffraction cones, the edge is the first caustic of the diffracted field. The second caustic of the diffracted field is ρ^d

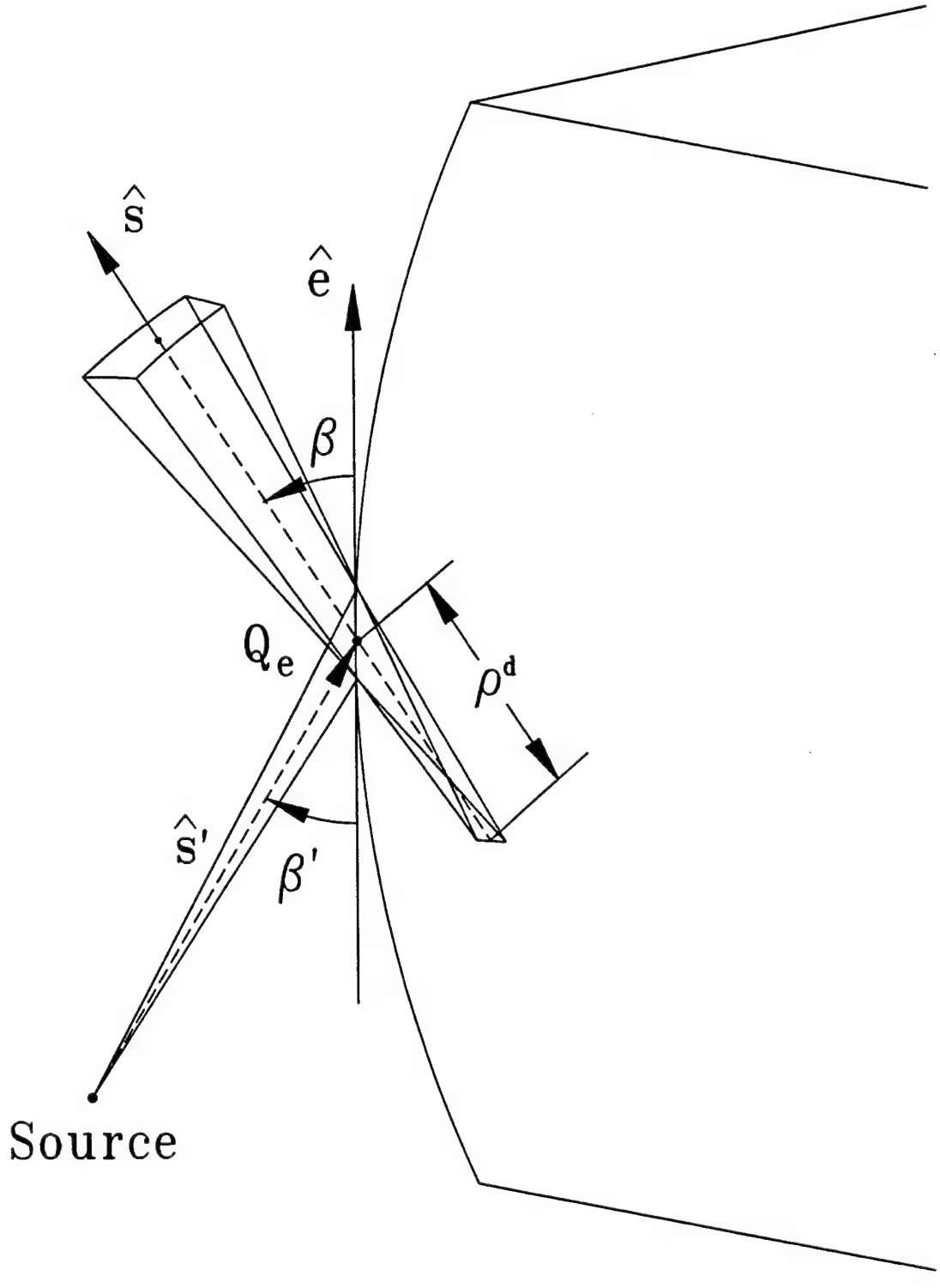

Figure 3: Astigmatic tube of rays diffracted by a wedge.

and is given by

$$\frac{1}{\rho^d} = \frac{1}{\rho_e} + \frac{(\hat{s} - \hat{s}') \cdot \hat{n}_e}{\rho_g \sin^2 \beta} \tag{10}$$

where ρ_e is the radius of curvature of the incident wave in the edge fixed plane, $\hat{n}_e$ is the unit vector normal to the edge and directed away from the center of curvature and ρ_g is the radius of curvature of the edge at the point of diffraction.

Although the UTD diffraction coefficients do correct the GO fields at the incident and reflection shadow boundaries, they do not correct for any problems that may be caused by the amplitude spreading factor. The observation point is in the near-zone for the case of interest here. This means that it is possible for the observation point to approach the second caustic of the diffracted field. When this occurs, the UTD diffracted field expression becomes infinite. It also turns out that this happens at the same time two or more diffraction points merge (coalesce).

In an attempt to correct for these caustic problems, various equivalent current and incremental diffracted field expressions have been derived. Equivalent currents are filament currents that are placed along the edge of the wedge. These equivalent currents are then substituted into the radiation integral and integrated along the edge to obtain the total diffracted field contribution. An incremental diffracted field is the field diffracted by an infinitesimal length of the edge of a wedge. This incremental diffracted field is then integrated along the edge to obtain the total diffracted field contribution. These techniques will be used in this work to find the field near the caustic of the diffracted field.

SECTION 3

Incremental Diffracted Fields

There are two main approaches used to determine the field diffracted by an infinitesimal length of the edge of a wedge. The first of these is based on the currents induced on the faces of the canonical wedge geometry. This approach is consistent with the Physical Theory of Diffraction (PTD). The second approach is based on the field diffracted by the canonical wedge geometry. This method is consistent with the Geometrical Theory of Diffraction (GTD).

Many people have worked on the development of the field diffracted by an infinitesimal length of the edge of a wedge from the current point of view. Mitzner [20] derived incremental length diffraction coefficients for arbitrary aspects of observation using the non-uniform current induced on the two faces of the wedge. Later, Michaeli [21, 22] derived equivalent currents for arbitrary aspects of observation using the total current induced on the two faces of the wedge. It was then shown by Knott [23] that the total current part of Mitzner's solution is identical to Michaeli's solution. Both of these formulations suffer from singularities along certain aspects of observation. Michaeli [13] rederived his equivalent currents using a different direction of integration of the current along the faces of the wedge to eliminate these infinities. He also used the non-uniform current and obtained a result with fewer singularities. This result was also obtained by Butorin and Ufimtsev [24] for the scalar case and by Butorin, Martynov and Ufimtsev [14] for the vector case. The equivalent current formulation of Ando, Murasaki and Kinoshita [25] follows the same procedure as Michaeli [13] except a different integration direction is chosen for the integration

of the surface current. Shore and Yaghjian [26] derived expressions of a similar form that are used to determine the scattering by cracks and struts of reflector antennas.

A different approach to the derivation of the field diffracted by an infinitesimal length of the edge of a wedge begins with the actual diffracted field. Ryan and Peters [4, 5] compared the asymptotic form of the diffracted field with the asymptotic form of the field radiated by a line source. These expressions were equated and solved for the equivalent currents. However, their result is only approximate away from normal incidence. Knott and Senior [9] enforced reciprocity to heuristically modify the Ryan and Peters solution to improve the method for oblique incidence. This formulation has been used primarily for far-zone problems. Later, the concept of stripping was used to improve the accuracy of these solutions. A separate field based formulation is that of Arnold [27]. He assumes a double spectral integral formula and compares its asymptotic result to that of the GTD. This is then used to solve for the unknown argument of the integral. The most recent field based derivation is that of Tiberio and Maci [15, 16, 17]. This method uses a Fourier transform pair to convert the field diffracted by the canonical wedge geometry into the field diffracted by an infinitesimal length of the edge.

These methods are all very different in formulation, but are all used to describe the same physical phenomena. Therefore, there should be some consistent method for formulating them all in the same basic manner. This chapter is devoted to the development of a unified formulation of the field diffracted by an infinitesimal length of the edge of a wedge. This is accomplished by deriving the PTD equivalent currents from the current on the faces of the wedge. This is then transformed to obtain the field based GTD equivalent currents. Finally, all of these solutions are compared.

1 Double Spectral Integral Formulation of the Field Diffracted by an Infinitesimal Length of the Edge of a Wedge

In the determination of an incremental diffracted field, it is typical to find the field diffracted by an incremental length of an infinite two dimensional wedge. This is

usually accomplished by integrating the exact surface currents of each face of the wedge up to the edge. This is the procedure that will be used here except the result will be put in a general form that will allow for an easy comparison between the various formulations. This section is a derivation of the double spectral integral form of the field diffracted by an infinitesimal length of the edge of a wedge.

The magnetic field scattered by an object is easily found [28, 29] as,

$$\vec{H}^s(\vec{R}) = \iint_S \nabla G_0(\vec{R},\vec{R}') \times \vec{J}_s(\vec{R}')\, ds' \tag{11}$$

where $G_0(\vec{R},\vec{R}')$ is the scalar free space Green's function and $\vec{J}_s(\vec{R}')$ is the induced surface current. For the specific case of the field scattered by the 0-face of a two dimensional, perfect electrically conducting wedge as shown in Figure 4,

$$\vec{H}^s_o(\vec{R}) = \int_{-\infty}^{\infty}\int_{0}^{\infty} \nabla G_0(\vec{R},\vec{R}') \times \vec{J}^o_s(\vec{R}')\, dx'dz' = \int_{-\infty}^{\infty} d\vec{H}^s_o(\vec{R}), \tag{12}$$

where the incremental magnetic field scattered by the 0-face of an infinitesimal length of the edge is

$$d\vec{H}^s_o(\vec{R}) = dz' \int_0^{\infty} \nabla G_0(\vec{R},\vec{R}') \times \vec{J}^o_s(\vec{R}')\, dx' \tag{13}$$

and $\vec{J}^o_s(\vec{R}')$ is the surface current on the 0-face of the wedge. The spectral domain form of the scalar free space Green's function is

$$G_0(\vec{R},\vec{R}') = \frac{e^{-jk|\vec{R}-\vec{R}'|}}{4\pi|\vec{R}-\vec{R}'|} = \frac{1}{8\pi^2 j}\iint_{-\infty}^{\infty} e^{-j[k_x(x-x')+k_z(z-z')+k_y|y|]}\,\frac{dk_x dk_z}{k_y}, \tag{14}$$

where

$$k_y = \begin{cases} \sqrt{k^2-k_x^2-k_z^2} & ;\text{ if } k^2 > k_x^2+k_z^2 \\ -j\sqrt{k_x^2+k_z^2-k^2} & ;\text{ if } k^2 < k_x^2+k_z^2 \end{cases} \tag{15}$$

is to be used here. The gradient of the scalar free space Green's function is define in cartesian coordinates as

$$\nabla G_0(\vec{R},\vec{R}') = \hat{x}\,\frac{\partial G_0(\vec{R},\vec{R}')}{\partial x} + \hat{y}\,\frac{\partial G_0(\vec{R},\vec{R}')}{\partial y} + \hat{z}\,\frac{\partial G_0(\vec{R},\vec{R}')}{\partial z} \tag{16}$$

where

$$\frac{\partial G_0(\vec{R},\vec{R}')}{\partial x} = \frac{-1}{8\pi^2}\iint_{-\infty}^{\infty} k_x e^{-j[k_x(x-x')+k_z(z-z')+k_y|y|]}\,\frac{dk_x dk_z}{k_y}, \tag{17}$$

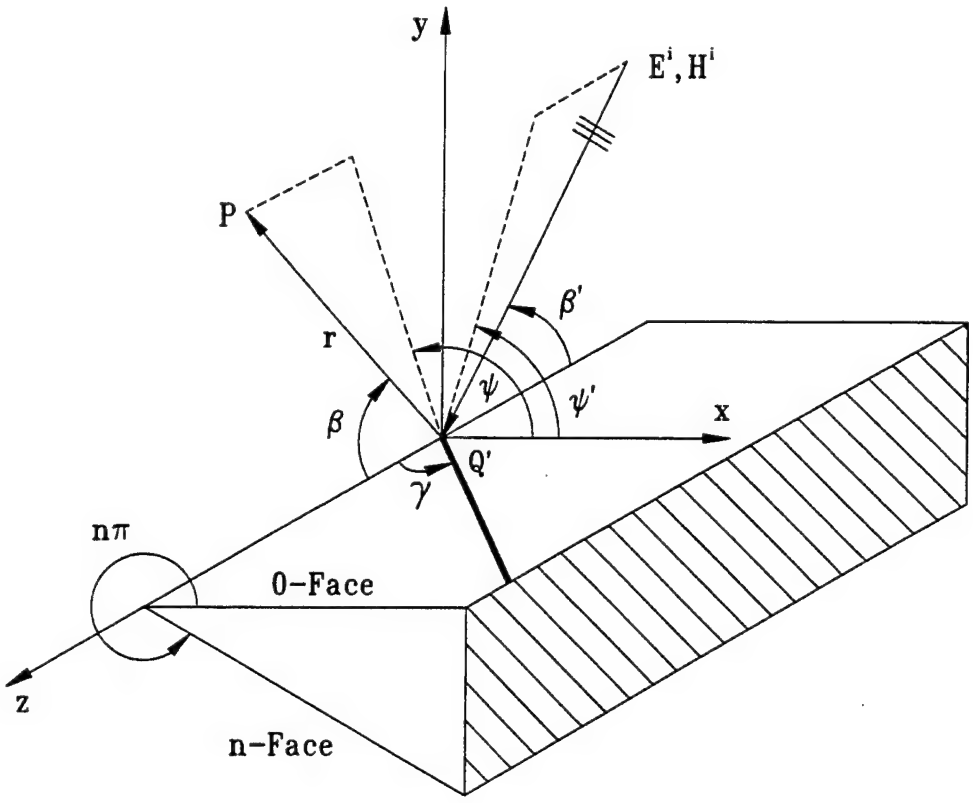

Figure 4: Canonical geometry for the scattering by a wedge.

$$\frac{\partial G_0(\vec{R},\vec{R}')}{\partial y} = \frac{-1}{8\pi^2}\iint_{-\infty}^{\infty} \varepsilon_y k_y e^{-j[k_x(x-x')+k_z(z-z')+k_y|y|]}\,\frac{dk_x dk_z}{k_y} \tag{18}$$

and

$$\frac{\partial G_0(\vec{R},\vec{R}')}{\partial z} = \frac{-1}{8\pi^2}\iint_{-\infty}^{\infty} k_z e^{-j[k_x(x-x')+k_z(z-z')+k_y|y|]}\,\frac{dk_x dk_z}{k_y} \tag{19}$$

with $\varepsilon_y = \text{sgn}\{y\} = \text{sgn}\{\sin\psi\}$. Since the 0-face of the wedge lies in the x-z plane,

$$\vec{J}_s^o(\vec{R}') = \hat{x}J_x^o(\vec{R}') + \hat{z}J_z^o(\vec{R}'). \tag{20}$$

Substituting (16) through (20) into (13) and interchanging the order of the spectral and spatial integrals,

$$d\vec{H}_o^s(\vec{R}) = dz'\frac{1}{8\pi^2 j}\iint_{-\infty}^{\infty} \vec{I}(k_x,k_z;z')\frac{dk_x dk_z}{k_y} \tag{21}$$

where

$$\vec{I}(k_x,k_z;z') = \int_0^{\infty} \vec{F}(k_x,k_z;R')\,e^{-jh(k_x,k_z;R')}\,dx', \tag{22}$$

$$h(k_x,k_z;R') = k_x(x-x') + k_z(z-z') + k_y|y| \tag{23}$$

and

$$\begin{aligned}\vec{F}(k_x,k_z;R') \;=\; \hat{x}\left[-j\varepsilon_y k_y J_z^o(\vec{R}')\right] \;&+\; \hat{y}\left[jk_x J_z^o(\vec{R}') - jk_z J_x^o(\vec{R}')\right] \\ &+\; \hat{z}\left[j\varepsilon_y k_y J_x^o(\vec{R}')\right].\end{aligned} \tag{24}$$

Next, the surface current on the 0-face of the wedge must be found. Since the 0-face of the wedge lies in the $y = 0$ plane,

$$\vec{J}_s^o(\vec{R}') = \hat{n}_o \times \vec{H}^t(\vec{R}')\Big|_{y=0} \tag{25}$$

where $\hat{n}_o = \hat{y}$ is the unit normal vector to the 0-face of the wedge and $\vec{H}^t(\vec{R}')$ is the total magnetic field. Therefore, we find that

$$J_x^o(\vec{R}') = H_z^t(\vec{R}')\Big|_{y=0} = H_z^t(\vec{R}')\Big|_{\substack{\psi=0\\ \rho=x'}} \tag{26}$$

and

$$J_z^o(\vec{R}') = -H_x^t(\vec{R}')\Big|_{y=0} = -H_\rho^t(\vec{R}')\Big|_{\substack{\psi=0\\ \rho=x'}} \tag{27}$$

are the x- and z-components of the 0-face surface current, respectively. The incident wave is assumed to be planar for the remainder of this chapter; however, the procedure used here can be applied to other incident wave types. The components of the surface current are determined from the expressions for the exact fields in the presence of a wedge. The z-components of the total electric field and the total magnetic field in the presence of the wedge are [30],

$$E_z^t(\vec{R}) = E_z^i(0)e^{-jkz'\cos\beta'}\left[u(k\rho\sin\beta', \Psi^-) - u(k\rho\sin\beta', \Psi^+)\right] \tag{28}$$

and

$$H_z^t(\vec{R}) = H_z^i(0)e^{-jkz'\cos\beta'}\left[u(k\rho\sin\beta', \Psi^-) + u(k\rho\sin\beta', \Psi^+)\right]; \tag{29}$$

respectively, where $\Psi^{\mp} = \psi \mp \psi'$ and the function $u(X, \Psi)$ is

$$u(X,\Psi) = \frac{1}{n} + \frac{2}{n}\sum_{m=1}^{\infty}(j)^{m/n}J_{m/n}(X)\cos\left(\frac{m}{n}\Psi\right) \tag{30}$$

$$= \frac{1}{2\pi jn}\int_{\Gamma}\frac{\sin(\frac{\xi}{n})e^{jX\cos\xi}}{\cos(\frac{\xi}{n}) - \cos(\frac{\Psi}{n})}d\xi. \tag{31}$$

The contour of integration in (31) is shown in Figure 5. Substituting (29) into (26) and using the fact that $H_z^i(0) = H_{\beta'}^i(0)\sin\beta'$, we can find the x-component of the surface current as

$$J_x^o(\vec{R}\,') = 2H_{\beta'}^i(0)e^{-jkz'\cos\beta'}\sin\beta' u(X, \psi'), \tag{32}$$

where $X = kx'\sin\beta'$. Also, due to the cylindrical uniformity of the wedge, the transverse components of the total magnetic field can be determined from the z-components using [31]

$$\vec{H}_t^t(\vec{R}) = \frac{k_z^i}{jk_t^2}\nabla_t H_z^t(\vec{R}) + \frac{\omega\epsilon}{jk_t^2}\hat{z}\times\nabla_t E_z^t(\vec{R}) \tag{33}$$

which allows us to determine the ρ-component of the total magnetic field as

$$H_\rho^t(\vec{R}) = -j\cot\beta'\,\frac{\partial H_z^t(\vec{R})}{\partial X} - \frac{\omega\epsilon}{jk_t^2\rho}\,\frac{\partial E_z^t(\vec{R})}{\partial\Psi}. \tag{34}$$

Using (29) and the fact that $H_z^i(0) = H_{\beta'}^i(0)\sin\beta'$, we find that

$$\left.\frac{\partial H_z^t(\vec{R})}{\partial X}\right|_{\substack{\psi=0\\ \rho=x'}} = 2H_{\beta'}^i(0)e^{-jkz'\cos\beta'}\sin\beta'\,\frac{\partial u(X,\psi')}{\partial X} \tag{35}$$

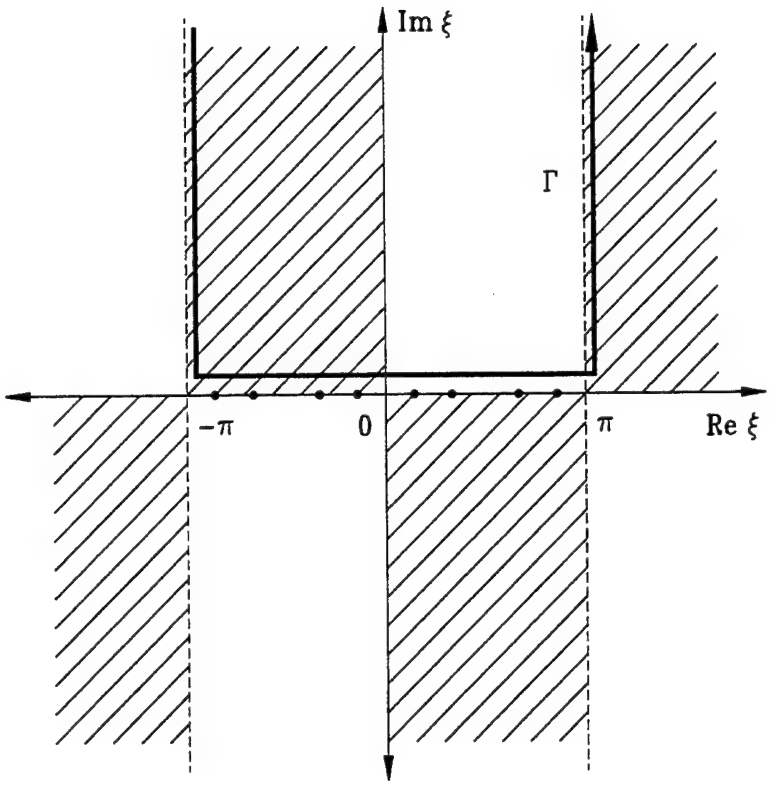

Figure 5: Contour of integration for the exact wedge solution.

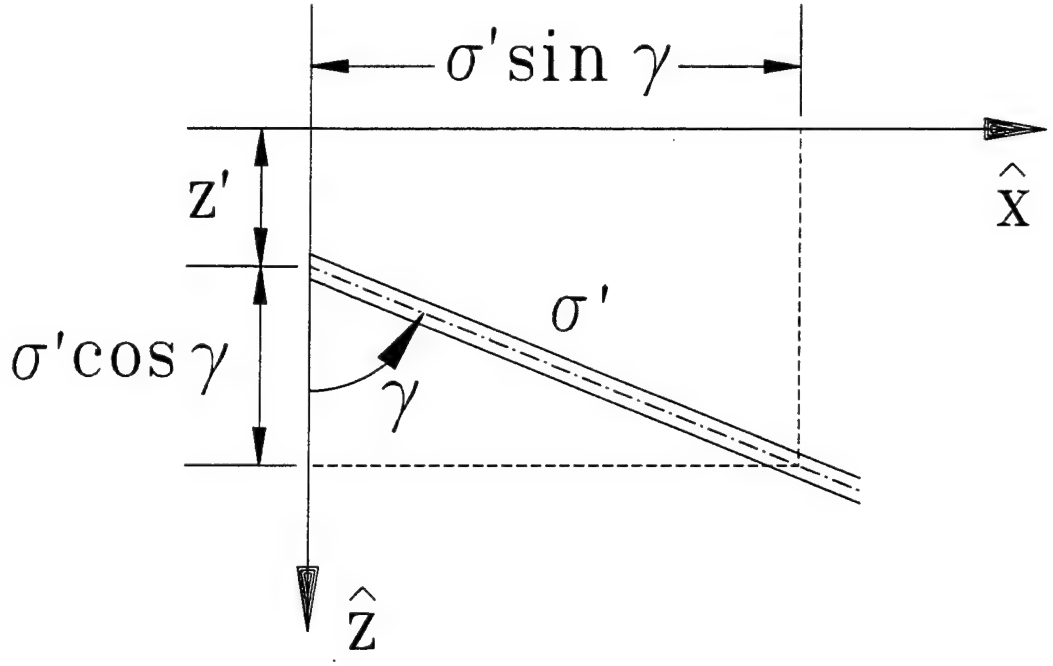

Figure 6: Change of integration direction along the face of a wedge.

and using (28) and $E_z^i(0) = H_{\psi'}^i(0) Z_c \sin\beta'$,

$$\left.\frac{\partial E_z^t(\vec{R})}{\partial \Psi}\right|_{\substack{\psi=0 \\ \rho=x'}} = -2H_{\psi'}^i(0) e^{-jkz'\cos\beta'} Z_c \sin\beta' \, \frac{\partial u(X,\psi')}{\partial \psi'}. \tag{36}$$

Therefore, substituting (35) and (36) into (34) the z-component of the 0-face surface current is given by

$$\begin{aligned} J_z^o(\vec{R}') &= 2jH_{\beta'}^i(0) e^{-jkz'\cos\beta'} \cos\beta' \, \frac{\partial u(X,\psi')}{\partial X} \\ &+ 2jH_{\psi'}^i(0) e^{-jkz'\cos\beta'} \, \frac{1}{X} \frac{\partial u(X,\psi')}{\partial \psi'} \end{aligned} \tag{37}$$

where again $X = kx' \sin\beta'$.

The integration along a strip of infinitesimal width in the x' direction will be changed to an integration along an arbitrarily directed strip as shown in Figure 6 in an attempt to make the final result as general as possible. The change of variables

$$x' \rightarrow \sigma' \sin\gamma \tag{38}$$

$$z' \rightarrow z' + \sigma' \cos\gamma \tag{39}$$

$$dx' \rightarrow \frac{dX}{k \sin\beta'} \tag{40}$$

is used to reorient the integration along the face of the wedge to be in an arbitrary direction. Therefore, substituting (39) into (32) we obtain the x-component of the surface current

$$\begin{aligned} J_x^o(\vec{R}') &= 2H^i_{\beta'}(0)e^{-jkz'\cos\beta'}e^{-jX\cot\gamma\cot\beta'}\sin\beta' u(X,\psi') \\ &= 2\left[\widehat{\beta}'\cdot\vec{H}^i(z')\right]e^{-jX\cot\gamma\cot\beta'}\sin\beta' u(X,\psi') \end{aligned} \tag{41}$$

and substituting (39) into (37) we obtain the z-component of the surface current

$$\begin{aligned} J_z^o(\vec{R}') &= 2jH^i_{\beta'}(0)e^{-jkz'\cos\beta'}e^{-jX\cot\gamma\cot\beta'}\cos\beta'\,\frac{\partial u(X,\psi')}{\partial X} \\ &+ 2jH^i_{\psi'}(0)e^{-jkz'\cos\beta'}e^{-jX\cot\gamma\cot\beta'}\,\frac{1}{X}\frac{\partial u(X,\psi')}{\partial\psi'} \\ &= 2j\left[\widehat{\beta}'\cdot\vec{H}^i(z')\right]e^{-jX\cot\gamma\cot\beta'}\cos\beta'\,\frac{\partial u(X,\psi')}{\partial X} \\ &+ 2j\left[\widehat{\psi}'\cdot\vec{H}^i(z')\right]e^{-jX\cot\gamma\cot\beta'}\,\frac{1}{X}\frac{\partial u(X,\psi')}{\partial\psi'}. \end{aligned} \tag{42}$$

This change of variables also results in the change $X = k\sigma'\sin\gamma\sin\beta'$. Using this result and the change of variables of (38) and (39), (23) becomes

$$h(k_x,k_z;R') = q(k_x,k_z;z') - X\left(\frac{k_x\sin\gamma + k_z\cos\gamma}{k\sin\gamma\sin\beta'}\right) \tag{43}$$

where

$$q(k_x,k_z;z') = k_x x + k_z(z-z') + k_y|y|. \tag{44}$$

Next, substituting (41) through (43) into (22) we get

$$\begin{aligned} \vec{I}(k_x,k_z;z') &= \Bigg\{\widehat{x}\left(2\left[\widehat{\beta}'\cdot\vec{H}^i(z')\right]\varepsilon_y\frac{k_y}{k}\cot\beta'\,U_2\right. \\ &\qquad \left. + 2\left[\widehat{\psi}'\cdot\vec{H}^i(z')\right]\varepsilon_y\frac{k_y}{k}\frac{1}{\sin\beta'}U_3\right) \\ &+\widehat{y}\left(-2\left[\widehat{\beta}'\cdot\vec{H}^i(z')\right]\frac{k_x}{k}\cot\beta'\,U_2 - 2\left[\widehat{\psi}'\cdot\vec{H}^i(z')\right]\frac{k_x}{k}\frac{1}{\sin\beta'}U_3\right. \\ &\qquad \left. - 2j\left[\widehat{\beta}'\cdot\vec{H}^i(z')\right]\frac{k_z}{k}U_1\right) \\ &+\widehat{z}\left(2j\left[\widehat{\beta}'\cdot\vec{H}^i(z')\right]\varepsilon_y\frac{k_y}{k}U_1\right)\Bigg\}e^{-jq(k_x,k_z;z')} \end{aligned} \tag{45}$$

where the auxiliary integrals are defined as

$$U_1 = \int_0^\infty u(X,\psi')e^{jX\zeta}dX, \tag{46}$$

$$U_2 = \int_0^\infty \frac{\partial u(X,\psi')}{\partial X} e^{jX\zeta} dX \tag{47}$$

and

$$U_3 = \int_0^\infty \frac{1}{X} \frac{\partial u(X,\psi')}{\partial \psi'} e^{jX\zeta} dX \tag{48}$$

with

$$\zeta = \frac{k_x \sin\gamma + (k_z - k\cos\beta')\cos\gamma}{k \sin\gamma \sin\beta'}. \tag{49}$$

It is found in Appendix A that the closed form endpoint contributions (i.e., the contribution from the edge) of the auxiliary integrals (46) through (48) are

$$U_1 = \frac{1}{j\sin\alpha} G_h^o(\alpha), \tag{50}$$

$$U_2 = -\cot\alpha\, G_h^o(\alpha) - \frac{1}{n} \tag{51}$$

and

$$U_3 = G_s^o(\alpha), \tag{52}$$

respectively. The functions $G_{s,h}^o(\alpha)$ are the spectral diffraction coefficients of the 0-face of the wedge

$$G_{s,h}^o(\alpha) = \frac{-1}{2n}\left[\cot\left(\frac{\pi-(\alpha-\psi')}{2n}\right) \mp \cot\left(\frac{\pi-(\alpha+\psi')}{2n}\right)\right] \tag{53}$$

for the soft and hard polarizations and $\alpha = \cos^{-1}\zeta$ where ζ is given in (49). The proper definition of the inverse cosine function is given in (594) and (595) of Appendix A. Lastly, the cartesian-to-spherical coordinate transformation

$$\hat{x} = \hat{r}\sin\beta\cos\psi + \hat{\beta}\cos\beta\cos\psi - \hat{\psi}\sin\psi \tag{54}$$

$$\hat{y} = \hat{r}\sin\beta\sin\psi + \hat{\beta}\cos\beta\sin\psi + \hat{\psi}\cos\psi \tag{55}$$

$$\hat{z} = \hat{r}\cos\beta - \hat{\beta}\sin\beta \tag{56}$$

is used in (45) to convert the answer into the standard spherical ray fixed coordinate system. The resulting solution can now be written in the standard dyadic form

$$d\vec{H}_o^d(\vec{R}) = \vec{H}^i(z') \cdot \overline{\overline{G}}^o(z')\, dz' \tag{57}$$

where

$$\overline{\overline{G}}^{o}(z') = \frac{1}{8\pi^2 j}\int\int_{-\infty}^{\infty} \overline{\overline{K}}(k_x, k_z; z')e^{-j[k_x x + k_z(z-z') + k_y|y|]}\,\frac{dk_x dk_z}{k_y}. \tag{58}$$

The amplitude function of this double spectral integral is a dyadic of the form

$$\begin{aligned}\overline{\overline{K}}(k_x, k_z; z') \;=\; & -\hat{\beta}'\hat{r}\,K_{\beta' r}(k_x, k_z; z') - \hat{\psi}'\hat{r}\,K_{\psi' r}(k_x, k_z; z') \\ & -\hat{\beta}'\hat{\beta}\,K_{\beta'\beta}(k_x, k_z; z') - \hat{\psi}'\hat{\beta}\,K_{\psi'\beta}(k_x, k_z; z') \\ & -\hat{\beta}'\hat{\psi}\,K_{\beta'\psi}(k_x, k_z; z') - \hat{\psi}'\hat{\psi}\,K_{\psi'\psi}(k_x, k_z; z')\end{aligned} \tag{59}$$

where the terms in the dyadic are:

$$\begin{aligned}K_{\beta' r}(k_x, k_z; z') \;=\; & \left\{2\,\varepsilon_y \frac{k_y}{k}\sin\beta\cos\psi\cot\beta'\cot\alpha - 2\,\frac{k_x}{k}\sin\beta\sin\psi\cot\beta'\cot\alpha\right. \\ & \left. + 2\,\frac{k_z}{k}\,\frac{\sin\beta\sin\psi}{\sin\alpha} - 2\,\varepsilon_y\frac{k_y}{k}\,\frac{\cos\beta}{\sin\alpha}\right\} G_h^o(\alpha) \\ & + \left\{2\,\varepsilon_y\frac{k_y}{k}\,\frac{\sin\beta\cos\psi\cot\beta'}{n} - 2\,\frac{k_x}{k}\,\frac{\sin\beta\sin\psi\cot\beta'}{n}\right\}\end{aligned} \tag{60a}$$

$$K_{\psi' r}(k_x, k_z; z') \;=\; \left\{2\,\frac{k_x}{k}\,\frac{\sin\beta\sin\psi}{\sin\beta'} - 2\,\varepsilon_y\frac{k_y}{k}\,\frac{\sin\beta\cos\psi}{\sin\beta'}\right\} G_s^o(\alpha) \tag{60b}$$

$$\begin{aligned}K_{\beta'\beta}(k_x, k_z; z') \;=\; & \left\{2\,\varepsilon_y \frac{k_y}{k}\cos\beta\cos\psi\cot\beta'\cot\alpha - 2\,\frac{k_x}{k}\cos\beta\sin\psi\cot\beta'\cot\alpha\right. \\ & \left. + 2\,\frac{k_z}{k}\,\frac{\cos\beta\sin\psi}{\sin\alpha} + 2\,\varepsilon_y\frac{k_y}{k}\,\frac{\sin\beta}{\sin\alpha}\right\} G_h^o(\alpha) \\ & + \left\{2\,\varepsilon_y\frac{k_y}{k}\,\frac{\cos\beta\cos\psi\cot\beta'}{n} - 2\,\frac{k_x}{k}\,\frac{\cos\beta\sin\psi\cot\beta'}{n}\right\}\end{aligned} \tag{60c}$$

$$K_{\psi'\beta}(k_x, k_z; z') \;=\; \left\{2\,\frac{k_x}{k}\,\frac{\cos\beta\sin\psi}{\sin\beta'} - 2\,\varepsilon_y\frac{k_y}{k}\,\frac{\cos\beta\cos\psi}{\sin\beta'}\right\} G_s^o(\alpha) \tag{60d}$$

$$\begin{aligned}K_{\beta'\psi}(k_x, k_z; z') \;=\; & \left\{-2\,\varepsilon_y \frac{k_y}{k}\sin\psi\cot\beta'\cot\alpha - 2\,\frac{k_x}{k}\cos\psi\cot\beta'\cot\alpha\right. \\ & \left. + 2\,\frac{k_z}{k}\,\frac{\cos\psi}{\sin\alpha}\right\} G_h^o(\alpha) \\ & + \left\{-2\,\varepsilon_y\frac{k_y}{k}\,\frac{\sin\psi\cot\beta'}{n} - 2\,\frac{k_x}{k}\,\frac{\cos\psi\cot\beta'}{n}\right\}\end{aligned} \tag{60e}$$

$$K_{\psi'\psi}(k_x, k_z; z') \;=\; \left\{2\,\frac{k_x}{k}\,\frac{\cos\psi}{\sin\beta'} + 2\,\varepsilon_y\frac{k_y}{k}\,\frac{\sin\psi}{\sin\beta'}\right\} G_s^o(\alpha) \tag{60f}$$

This is a convenient form of the solution because it allows for an easy comparison between the incremental diffracted field solutions consistent with the PTD and the

GTD. It is also convenient because if we compare (58) with (14), we see that they both have a very similar form. Therefore, (58) may be interpreted as a spherical wave propagating outward from a point z' on the z-axis. Each of these spherical waves are weighted differently for each co-polarized and cross-polarized diffracted field component. These weighting functions are related to the soft and hard diffraction coefficients as expected.

This result is similar to that of Arnold [27] except for a few key points. The result obtained by Arnold is only a scalar formulation. Also, Arnold's result is obtained using a different procedure which assumes that the integral along the edge is performed first and then the spectral integrals. For this case, he concludes that the amplitude function of this integral need only contain information along the Keller cone directions. This is true because once the integral along the edge is performed, the spectral integrals have dominant contributions near the Keller cone directions. According to the method of stationary phase, the spectral integrals can be approximated using only the values of the integrand near the Keller cone directions. Therefore, the information about the fields along the Keller cone directions can be continued to other directions with little change in the resulting solution.

Although this formulation is mathematically precise, it is practical for only a few specific problems. It is assumed that the integral along the edge can be done in closed form. This can be done only for simple geometries. In order to encompass a wider class of problems, it is desired to determine a closed form result for the spectral integrals and leave only the integral along the edge. This can not be accomplished using Arnold's procedure.

2 Incremental Diffracted Fields Consistent with the Physical Theory of Diffraction

The procedures used to determine PTD equivalent currents are used here to obtain the field diffracted by an infinitesimal length of the edge of a wedge. This is accomplished simply by asymptotically reducing (58) to obtain a closed form result. In this section,

an asymptotic expression for the incremental diffracted field from the total surface current is determined.

It should be noted that the PTD method uses the non-uniform current to correct the Physical Optics (PO) current near an edge. This non-uniform current is usually asymptotically integrated up to the edge of the wedge to obtain a fringe equivalent current. The PO current subtracted from the total current is the non-uniform current. The expressions derived in this section correspond to the total current component of the fringe equivalent current written in diffracted field form. Also, (57) will be evaluated assuming a far-zone observation point. In this way, simpler formulas are obtained which makes the comparison with the incremental diffracted field that is consistent with the GTD much easier.

The asymptotic expansion of (58) begins by determining the stationary phase point of the double spectral integral. It is a straightforward and simple exercise to show that the stationary phase point of (58) is located at $(k_{xs}, k_{zs}) = (k\sin\beta\cos\psi, k\cos\beta)$. It is also easy to show that $k^2 > k_{xs}^2 + k_{zs}^2$ and therefore (15) evaluated at the stationary phase point is

$$k_{ys} = \varepsilon_y k \sin\beta \sin\psi. \tag{61}$$

The asymptotic expansion of (58) using the double integral stationary phase method [32] is

$$\begin{aligned} \overline{\overline{G}}^o(z') &= \frac{1}{8\pi^2 j}\int\int_{-\infty}^{\infty} \overline{\overline{K}}(k_x, k_z; z') e^{-j[k_x x + k_z(z-z') + k_y|y|]} \frac{dk_x dk_z}{k_y} \\ &\sim \frac{\sigma}{4\pi k_{ys}\sqrt{|AB - H^2|}} \overline{\overline{K}}(k_{xs}, k_{zs}; z') e^{-jq(k_{xs}, k_{zs}; z')} \end{aligned} \tag{62}$$

where it is assumed that $\overline{\overline{K}}(k_x, k_z; z')$ is a smooth and slowly varying function of k_x and k_z near the stationary phase point. This is valid for far-zone observations. The phase σ, of the asymptotic expansion is defined as

$$\sigma = \begin{cases} +1 & ; \text{if } AB > H^2 \text{ and } A > 0 \\ -1 & ; \text{if } AB > H^2 \text{ and } A < 0 \\ -j & ; \text{if } AB < H^2 \end{cases} \tag{63}$$

where the functions A,B and H are

$$A = - \left. \frac{\partial^2 q(k_x, k_z; z')}{\partial k_x^2} \right|_{(k_x,k_z)=(k_{xs},k_{zs})} = \frac{r}{k \sin^2 \psi} > 0, \tag{64}$$

$$B = - \left. \frac{\partial^2 q(k_x, k_z; z')}{\partial k_z^2} \right|_{(k_x,k_z)=(k_{xs},k_{zs})} = \frac{r \left(\sin^2 \beta \sin^2 \psi + \cos^2 \beta \right)}{k \sin^2 \beta \sin^2 \psi} \tag{65}$$

and

$$H = - \left. \frac{\partial^2 q(k_x, k_z; z')}{\partial k_x \partial k_z} \right|_{(k_x,k_z)=(k_{xs},k_{zs})} = \frac{r \cos \beta \cos \psi}{k \sin \beta \sin^2 \psi}, \tag{66}$$

respectively. Also, r is the radial distance between any point on the edge and the observation point. Using (64) through (66) it is a simple task to show

$$\frac{1}{\sqrt{|AB - H^2|}} = \frac{k_{ys}}{r} \tag{67}$$

and that $AB > H^2$ and $A > 0$ which, from (63), leads to the fact that $\sigma = +1$. Lastly, evaluating (60)

$$\begin{aligned} \overline{\overline{K}}(k_{xs}, k_{zs}; z') \;=\; & -\widehat{\beta}'\widehat{\beta} \left\{ 2 \frac{\sin \psi}{\sin \alpha} G_h^o(\alpha) \right\} - \widehat{\psi}'\widehat{\psi} \left\{ 2 \frac{\sin \beta}{\sin \beta'} G_s^o(\alpha) \right\} \\ & -\widehat{\beta}'\widehat{\psi} \left\{ 2 \frac{\sin \beta \left(\cos \psi \cot \beta - \cos \alpha \cot \beta' \right)}{\sin \alpha} G_h^o(\alpha) \right. \\ & \left. - \; 2 \frac{\sin \beta \cot \beta'}{n} \right\} \end{aligned} \tag{68}$$

and (44)

$$q(k_{xs}, k_{zs}; z') = kr \tag{69}$$

at the stationary phase point, all the quantities in (62) are completely determined. Therefore, the far-zone asymptotic expansion of (57) is

$$d\vec{H}_o^d(\vec{R}) \sim \vec{H}^i(z') \cdot \overline{\overline{\mathcal{D}}}(z') \frac{e^{-jkr}}{4\pi r} \, dz' \tag{70}$$

where

$$\begin{aligned} \overline{\overline{\mathcal{D}}}(z') \;=\; & -\widehat{\beta}'\widehat{\beta} \left\{ 2 \frac{\sin \psi}{\sin \alpha} G_h^o(\alpha) \right\} - \widehat{\psi}'\widehat{\psi} \left\{ 2 \frac{\sin \beta}{\sin \beta'} G_s^o(\alpha) \right\} \\ & -\widehat{\beta}'\widehat{\psi} \left\{ 2 \frac{\sin \beta \left(\cos \psi \cot \beta - \cos \alpha \cot \beta' \right)}{\sin \alpha} G_h^o(\alpha) \right. \\ & \left. - \; 2 \frac{\sin \beta \cot \beta'}{n} \right\} \end{aligned} \tag{71}$$

and

$$\alpha = \cos^{-1}\left\{\frac{\sin\beta\cos\psi}{\sin\beta'} + \frac{(\cos\beta - \cos\beta')}{\sin\beta'}\cot\gamma\right\}. \tag{72}$$

Again, the proper definition of the inverse cosine function is defined in (594) and (595) of Appendix A. It is now a simple task to compare this solution with other existing equivalent current and incremental diffracted field solutions.

If the orientation of the integration strips along the face of the wedge is normal to the edge (i.e., $\gamma = \frac{\pi}{2}$) we get the solutions of Mitzner [20] and Michaeli [21, 22]. Recalling the fact that Mitzner used the non-uniform current in his solution, the field from the total current was shown by Knott [23] to be the same as that obtained by Michaeli. As discussed by Michaeli, this solution predicts singular fields for certain aspects of observation. To eliminate most of these singularities, the orientation of the integration strips is changed.

By reorienting the integration along the face of the wedge to be along the direction of the grazing diffracted ray (i.e., $\gamma = \beta'$) the solutions of Michaeli [13], Butorin and Ufimtsev [24] and Butorin, Martynov and Ufimtsev [14] are obtained. The paper by Butorin and Ufimtsev is a scalar version of the more general vector electromagnetic solution of Butorin, Martynov and Ufimtsev. It is also commonly understood that the solution of Butorin, Martynov and Ufimtsev is identical to that of Michaeli. In all three of these solutions, the non-uniform current is used. However, if the solutions in these papers were performed using the total surface current, we obtain the solution found in this section with $\gamma = \beta'$.

Another direction of integration of the strips along the face of the wedge is proposed by Ando, Murasaki and Kinoshita [25]. The direction they propose is the projection onto the half-plane of the difference between the directions of observation and the Keller cone. Although this choice of directions does produce an equivalent current with no singularities, it has no physical meaning since the current flows in the $\gamma = \beta'$ direction.

3 Incremental Diffracted Fields Consistent with the Geometrical Theory of Diffraction

The important difference in the formulation of the incremental diffracted fields that are consistent with the PTD and the GTD is the choice of the coordinate system for the spectra. The PTD incremental diffracted field, as derived in Section 2, was found using a cartesian spectral integration. On the other hand, the GTD incremental diffracted field can be obtained by converting the cartesian spectral integration to a spherical spectral integration. This section is devoted to the conversion of the double spectral integral in (58) from cartesian coordinates to spherical coordinates. This is then asymptotically reduced to obtain a closed form result.

To obtain the proper variable substitution, we recall from (49) and (594) that

$$\begin{aligned} \zeta = \cos\alpha &= \frac{k_x \sin\gamma + (k_z - k\cos\beta')\cos\gamma}{k\sin\gamma\sin\beta'} \\ &= \frac{k_x}{k\sin\beta'} + (k_z - k\cos\beta')\frac{\cot\gamma}{k\sin\beta'}. \end{aligned} \tag{73}$$

If this equation is used to define the coordinate transformation, we can choose

$$k_x = k\sin\beta'\cos\alpha \tag{74}$$

and

$$k_z = k\cos\beta' \tag{75}$$

for our substitutions. This is easily recognized as two of the three variable changes from cartesian coordinates to spherical coordinates. Using a standard spherical coordinate transformation, we find

$$k_y = k\sin\beta'\sin\alpha \tag{76}$$

as the remaining variable change. It is important to understand that integrating the spectra in cartesian coordinates is the same as integrating the projection of the spherical spectra on the k_x-k_z plane. Therefore, the infinitesimal area of the projection is [33]

$$\frac{dk_x dk_z}{k_y} = k\sin\beta'\,d\alpha\,d\beta'. \tag{77}$$

This completes the required variable substitutions. However, to avoid confusion, a dummy variable substitution of $\beta' \rightarrow \theta'$ will be used. Therefore, the change of variables becomes

$$k_x = k \sin\theta' \cos\alpha \tag{78a}$$

$$k_y = k \sin\theta' \sin\alpha \tag{78b}$$

$$k_z = k \cos\theta' \tag{78c}$$

$$\frac{dk_x dk_z}{k_y} = k \sin\theta' \, d\alpha \, d\theta'. \tag{78d}$$

Next, to obtain a convenient and standard result, the directions of integration of both spectral integrals are reversed

$$\overline{\overline{G^o}}(z') = \frac{1}{8\pi^2 j} \int_{\infty}^{-\infty}\int \overline{\overline{K}}(k_x, k_z; z') e^{-j[k_x x + k_z(z-z') + k_y|y|]} \frac{dk_x dk_z}{k_y}. \tag{79}$$

The contours of integration must now be properly mapped. The contour of integration in the θ' plane is simple to determine. The angle θ' is real between 0 and π from the spherical coordinate transformation. The remainder of the contour is mapped into the complex θ' plane from $-j\infty \rightarrow 0$ and $\pi \rightarrow \pi + j\infty$. This contour of integration is shown in Figure 7.

The contour of integration in the α plane requires more care. The result in (57) through (60) expresses the radiation from a narrow strip of current on the 0-face of the wedge in free space. Therefore, this result no longer has any explicit information about the 0-face. It is important to take this information into account when making the transformation.

To attain the correct transformation, the condition that the field scattered by each strip on the 0-face of the wedge must be invariant under reflection. Therefore, the range of ψ and ψ' must be restricted to be $0 < \psi, \psi' < \pi$ which makes $\varepsilon_y = +1$. Once the transformation is made under this condition, the angles ψ and ψ' can be analytically continued for all possible angles.

Recall that the integration of the spectra in cartesian coordinates is the same as the integration of the projection of the spherical spectra on the k_x-k_z plane. Also, the spherical spectral integration is only performed over the upper hemisphere because

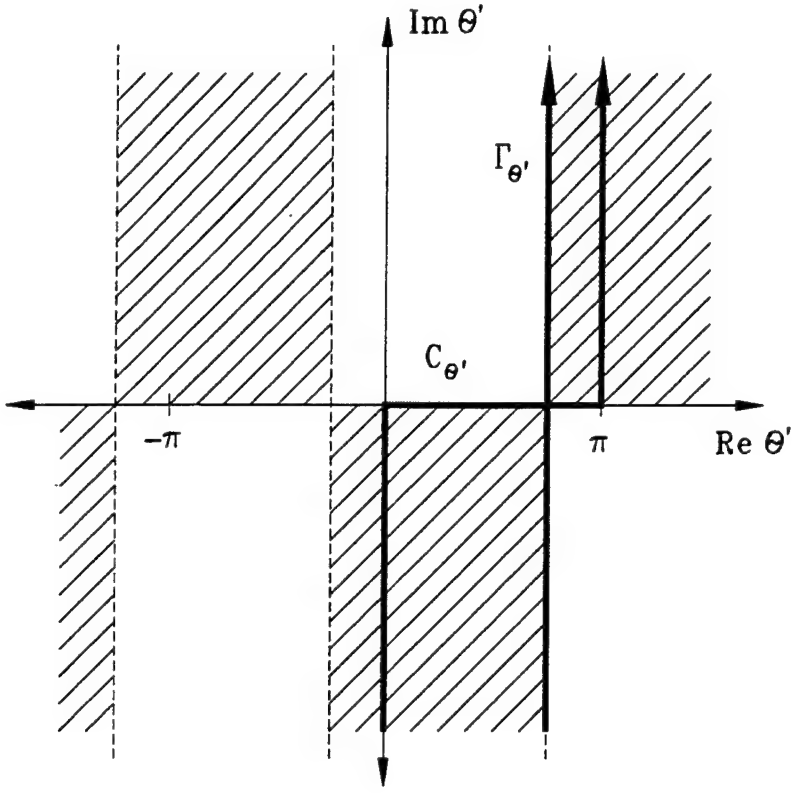

Figure 7: Contour of integration in the θ' plane.

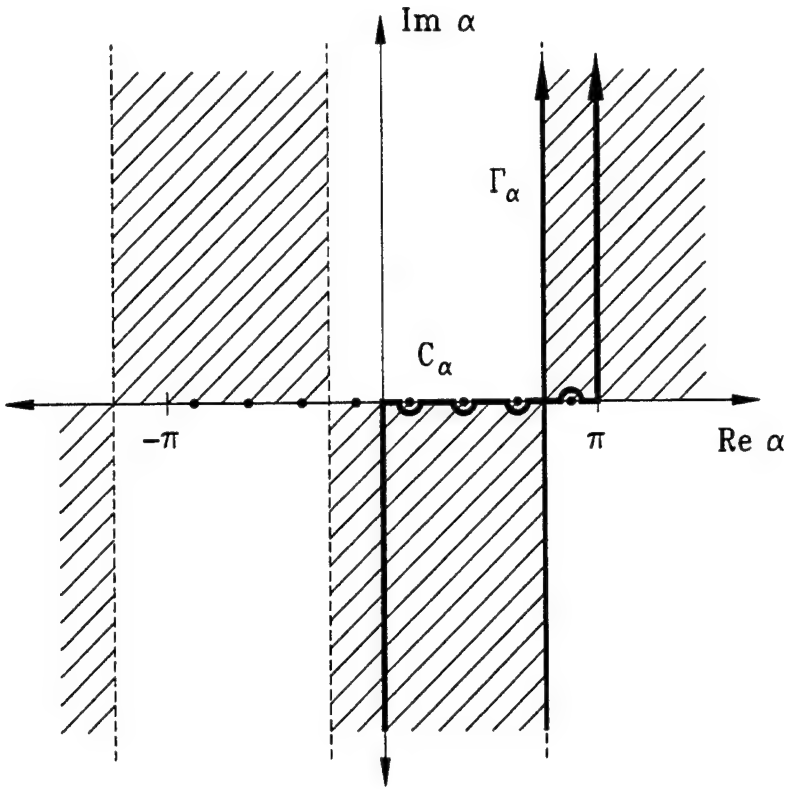

Figure 8: Contour of integration in the α plane.

$\varepsilon_y = +1$. Therefore, the angle α is real between 0 and π. Again, the remainder of the contour is mapped into the complex α plane from $-j\infty \rightarrow 0$ and $\pi \rightarrow \pi + j\infty$. It is also important to remember that this is an incremental diffracted field and so the contour of integration must be properly indented such that none of the Geometrical Optics (GO) poles are crossed by a deformation of the contour of integration to its steepest descent path. The contour of integration depends on the location of both the GO poles and the saddle point; however, an example of this contour of integration is shown in Figure 8.

Using the change of variables of (78) in (79), the resulting solution can be written in the standard dyadic form

$$\overline{\overline{G}}^{o}(z') = \frac{k}{8\pi^2 j} \int_{C_{\theta'}} \int_{C_\alpha} \overline{\overline{K}}_s(\theta', \alpha; z') e^{-jkrg(\theta', \alpha; z')} \sin\theta' \, d\alpha \, d\theta' \tag{80}$$

and

$$g(\theta', \alpha; z') = \cos\theta' \cos\beta + \cos(\alpha - \psi) \sin\theta' \sin\beta \tag{81}$$

where $0 < \psi, \psi' < \pi$ and the contours of integration $C_{\theta'}$ and C_α are shown in Figures 7 and 8, respectively. From (60), the amplitude function of this double spectral integral is a dyadic of the form

$$\begin{aligned}
\overline{\overline{K}}_s(\theta', \alpha; z') &= -\hat{\beta}'\hat{r}\, K_{\beta' r}(\theta', \alpha; z') - \hat{\psi}'\hat{r}\, K_{\psi' r}(\theta', \alpha; z') \\
&\quad -\hat{\beta}'\hat{\beta}\, K_{\beta'\beta}(\theta', \alpha; z') - \hat{\psi}'\hat{\beta}\, K_{\psi'\beta}(\theta', \alpha; z') \\
&\quad -\hat{\beta}'\hat{\psi}\, K_{\beta'\psi}(\theta', \alpha; z') - \hat{\psi}'\hat{\psi}\, K_{\psi'\psi}(\theta', \alpha; z')
\end{aligned} \tag{82}$$

where the terms in the dyadic are:

$$\begin{aligned}
K_{\beta' r}(\theta', \alpha; z') &= 2\{\sin\beta \cos\theta' \cos(\alpha - \psi) - \cos\beta \sin\theta'\} G_h^o(\alpha) \\
&\quad + \left\{ 2 \frac{\sin\beta \cos\theta'}{n} \sin(\alpha - \psi) \right\} && \text{(83a)} \\
K_{\psi' r}(\theta', \alpha; z') &= -2 \sin\beta \sin(\alpha - \psi)\, G_s^o(\alpha) && \text{(83b)} \\
K_{\beta'\beta}(\theta', \alpha; z') &= 2\{\cos\beta \cos\theta' \cos(\alpha - \psi) + \sin\beta \sin\theta'\} G_h^o(\alpha) \\
&\quad + \left\{ 2 \frac{\cos\beta \cos\theta'}{n} \sin(\alpha - \psi) \right\} && \text{(83c)} \\
K_{\psi'\beta}(\theta', \alpha; z') &= -2 \cos\beta \sin(\alpha - \psi)\, G_s^o(\alpha) && \text{(83d)} \\
K_{\beta'\psi}(\theta', \alpha; z') &= 2 \cos\theta' \sin(\alpha - \psi)\, G_h^o(\alpha) \\
&\quad + \left\{ -2 \frac{\cos\theta'}{n} \cos(\alpha - \psi) \right\} && \text{(83e)} \\
K_{\psi'\psi}(\theta', \alpha; z') &= 2 \cos(\alpha - \psi)\, G_s^o(\alpha) && \text{(83f)}
\end{aligned}$$

The angle ψ can not be analytically continued since the saddle point in the α plane is located at $\alpha_s = \psi$. The saddle point would move outside the range of integration if this result was analytically continued. Therefore, a second change of variables should be made to shift the saddle point location in the α plane to a constant.

To transform this integral to an integral with a typical diffraction integral contour, let us assume the medium is slightly lossy so that k possesses a small negative imaginary part. The contour of integration in the α plane can now be deformed from C_α to Γ_α as shown in Figure 8. Next, we use the change of variables

$$\alpha - \psi = \pi - \xi \tag{84}$$

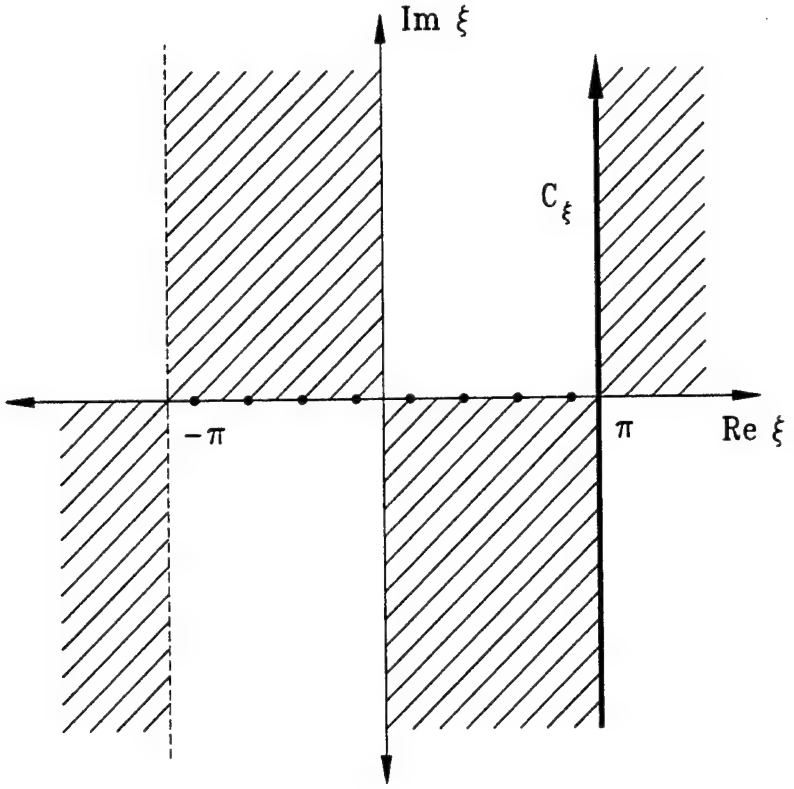

Figure 9: Contour of integration in the ξ plane.

and

$$d\alpha = -d\xi \tag{85}$$

which maps the contour of integration Γ_α to the negative of the contour C_ξ shown in Figure 9. Finally, changing the direction of integration in the ξ plane, the solution can now be written in the standard dyadic form

$$d\vec{H}_o^d(\vec{R}) = \vec{H}^i(z') \cdot \overline{\overline{G}}^o(z')\, dz' \tag{86}$$

where

$$\overline{\overline{G}}^o(z') = \frac{k}{8\pi^2 j} \int_{C_{\theta'}} \int_{C_\xi} \overline{\overline{K}}_s(\theta', \xi; z') e^{-jkrg(\theta', \xi; z')} \sin\theta'\, d\xi\, d\theta' \tag{87}$$

and

$$g(\theta', \xi; z') = \cos\theta' \cos\beta - \cos\xi \sin\theta' \sin\beta \tag{88}$$

with the contour of integration in the ξ plane being shown in Figure 9. The amplitude function of this double spectral integral is a dyadic of the form

$$\begin{aligned}\overline{\overline{K}}_s(\theta',\xi;z') &= -\widehat{\beta}'\widehat{\tau}\,K_{\beta'\tau}(\theta',\xi;z') - \widehat{\psi}'\widehat{\tau}\,K_{\psi'\tau}(\theta',\xi;z') \\ &\quad -\widehat{\beta}'\widehat{\beta}\,K_{\beta'\beta}(\theta',\xi;z') - \widehat{\psi}'\widehat{\beta}\,K_{\psi'\beta}(\theta',\xi;z') \\ &\quad -\widehat{\beta}'\widehat{\psi}\,K_{\beta'\psi}(\theta',\xi;z') - \widehat{\psi}'\widehat{\psi}\,K_{\psi'\psi}(\theta',\xi;z') \qquad (89)\end{aligned}$$

where the terms in the dyadic are:

$$\begin{aligned}K_{\beta'\tau}(\theta',\xi;z') &= -2\left\{\sin\beta\cos\theta'\cos\xi + \cos\beta\sin\theta'\right\}\tilde{G}_h^o(\xi) \\ &\quad + \left\{2\,\frac{\sin\beta\cos\theta'}{n}\,\sin\xi\right\} \qquad (90a)\\ K_{\psi'\tau}(\theta',\xi;z') &= -2\sin\beta\sin\xi\,\tilde{G}_s^o(\xi) \qquad (90b)\\ K_{\beta'\beta}(\theta',\xi;z') &= -2\left\{\cos\beta\cos\theta'\cos\xi - \sin\beta\sin\theta'\right\}\tilde{G}_h^o(\xi) \\ &\quad + \left\{2\,\frac{\cos\beta\cos\theta'}{n}\,\sin\xi\right\} \qquad (90c)\\ K_{\psi'\beta}(\theta',\xi;z') &= -2\cos\beta\sin\xi\,\tilde{G}_s^o(\xi) \qquad (90d)\\ K_{\beta'\psi}(\theta',\xi;z') &= 2\cos\theta'\sin\xi\,\tilde{G}_h^o(\xi) + 2\,\frac{\cos\theta'}{n}\,\cos\xi \qquad (90e)\\ K_{\psi'\psi}(\theta',\xi;z') &= -2\cos\xi\,\tilde{G}_s^o(\xi) \qquad (90f)\end{aligned}$$

and the new spectral diffraction coefficients are

$$\tilde{G}_{s,h}^o(\xi) = \frac{-1}{2n}\left[\cot\left(\frac{\xi-(\psi-\psi')}{2n}\right) \mp \cot\left(\frac{\xi-(\psi+\psi')}{2n}\right)\right] \qquad (91)$$

for the soft and hard polarizations. Since the saddle point in the ξ plane is located at $\xi_s = \pi$, the angles ψ and ψ' can now be analytically continued for angles greater than π. An important note at this point is that the new spectral diffraction coefficients in (91) for the 0-face of the wedge are identical to those found by Michaeli [34].

In order to compare this solution to the solution found in Section 2 it is convenient to convert the integral in (87) to a double stationary phase integral. To accomplish this, we again assume the medium is slightly lossy so that k possesses a small negative imaginary part so that the contour of integration in the θ' plane can be deformed from $C_{\theta'}$ to $\Gamma_{\theta'}$ as shown in Figure 7. Finally, changing the variables of integration

$$\theta' \;\rightarrow\; \beta + j\delta \qquad (92)$$

$$\xi \rightarrow \pi + j\nu \tag{93}$$

$$d\theta'\, d\xi \rightarrow -d\delta\, d\nu \tag{94}$$

in (87) results in the double stationary phase integral

$$\overline{\overline{G}}^{\circ}(z') = \frac{-k}{8\pi^2 j} \iint_{-\infty}^{\infty} \overline{\overline{K}}_s(\beta + j\delta, \pi + j\nu; z') e^{-jkrg(\beta+j\delta,\pi+j\nu;z')} \sin(\beta + j\delta)\, d\delta\, d\nu \tag{95}$$

where

$$-jkrg(\beta + j\delta, \pi + j\nu; z') = -krh(\delta, \nu; z') + jkrf(\delta, \nu; z'), \tag{96}$$

$$h(\delta, \nu; z') = \sin\beta \cos\beta \sinh\delta\,(1 - \cosh\nu) \tag{97}$$

and

$$f(\delta, \nu; z') = -\cos^2\beta \cosh\delta - \sin^2\beta \cosh\nu \cosh\delta. \tag{98}$$

It is a simple task to show that the stationary phase point is located at $(\delta_s, \nu_s) = (0, 0)$.

As was done in Section 2, the high frequency expression of (95) will be found assuming a far-zone observation point. Therefore, using the double integral stationary phase method [32]

$$\overline{\overline{G}}^{\circ}(z') \sim \frac{-\sigma \sin\beta}{4\pi r\sqrt{|AB - H^2|}} \overline{\overline{K}}_s(\beta, \pi; z') e^{-jkrg(\beta,\pi;z')} \tag{99}$$

where it is assumed that $\overline{\overline{K}}_s(\beta + j\delta, \pi + j\nu; z')$ is a smooth and slowly varying function of δ and ν near the stationary phase point. This is valid for far-zone observations. Also, σ is defined in (63) and the functions A,B and H are

$$A = \left.\frac{\partial^2 f(\delta, \nu; z')}{\partial\delta^2}\right|_{(\delta,\nu)=(0,0)} = f(0, 0; z') = -1 < 0, \tag{100}$$

$$B = \left.\frac{\partial^2 f(\delta, \nu; z')}{\partial\nu^2}\right|_{(\delta,\nu)=(0,0)} = -\sin^2\beta \tag{101}$$

and

$$H = \left.\frac{\partial^2 f(\delta, \nu; z')}{\partial\delta\,\partial\nu}\right|_{(\delta,\nu)=(0,0)} = 0, \tag{102}$$

respectively. Using (100) through (102) it is a simple task to show that

$$\frac{1}{\sqrt{|AB - H^2|}} = \frac{1}{\sin\beta} \tag{103}$$

and that $AB > H^2$ and $A < 0$ which, from (63), leads to the fact that $\sigma = -1$. Lastly, evaluating (90)

$$\overline{\overline{K}}_s(\beta, \pi; z') = -\hat{\beta}'\hat{\beta}\ \left\{2\,\tilde{G}_h^o(\pi)\right\} - \hat{\psi}'\hat{\psi}\ \left\{2\,\tilde{G}_s^o(\pi)\right\} - \hat{\beta}'\hat{\psi}\ \left\{-2\,\frac{\cos\beta}{n}\right\} \tag{104}$$

and (88)

$$g(\beta, \pi; z') = 1 \tag{105}$$

at the stationary phase point, all the quantities in (99) are completely determined. Therefore, the far-zone asymptotic expansion of (86) is

$$d\vec{H}_o^d(\vec{R}) \sim \vec{H}^i(z') \cdot \overline{\overline{\mathcal{D}}}(z')\ \frac{e^{-jkr}}{4\pi r}\ dz' \tag{106}$$

where

$$\overline{\overline{\mathcal{D}}}(z') = -\hat{\beta}'\hat{\beta}\ \left\{2\,\tilde{G}_h^o(\pi)\right\} - \hat{\psi}'\hat{\psi}\ \left\{2\,\tilde{G}_s^o(\pi)\right\} - \hat{\beta}'\hat{\psi}\ \left\{-2\,\frac{\cos\beta}{n}\right\}. \tag{107}$$

To allow for an easy comparison between this solution and the solution found in Section 2, we recognize that

$$\tilde{G}_{s,h}^o(\pi) \equiv G_{s,h}^o(\psi) \tag{108}$$

where $G_{s,h}^o(\alpha)$ are the diffraction coefficients defined in (53) that were used in Section 2. Therefore, (107) can be written as

$$\overline{\overline{\mathcal{D}}}(z') = -\hat{\beta}'\hat{\beta}\ \{2\,G_h^o(\psi)\} - \hat{\psi}'\hat{\psi}\ \{2\,G_s^o(\psi)\} - \hat{\beta}'\hat{\psi}\ \left\{-2\,\frac{\cos\beta}{n}\right\} \tag{109}$$

where this is now in a form that allows for an easy comparison with the results in Section 2.

This result is very similar to the GTD equivalent currents that are derived from a field point of view. The equivalent currents of Ryan and Peters [4, 5] were derived for the case where $\beta = \beta' = \frac{\pi}{2}$. These equivalent currents were then heuristically generalized for oblique incidence by Knott and Senior [9] by enforcing reciprocity. Rewriting this result in the form of an incremental diffracted field we obtain the same expression as that in (106). Also, since it can be shown that the double spectral integral representation of (86) is identical to the one obtained by Tiberio and Maci [15, 16, 17], the asymptotic expression in (106) is also. Therefore, the derivation of Tiberio and Maci is a rigorous derivation of the Ryan and Peters result with the heuristic modifications of Knott and Senior.

4 Comparison of Incremental Diffracted Field Solutions

Since the PTD and GTD incremental diffracted fields are all derived from the same point of view, we are now in a position to compare the results of each of the different formulations. This section is a comparison of the PTD and the GTD incremental diffracted fields. The advantages and disadvantages of each is also discussed.

The double spectral integral forms in cartesian and spherical coordinates produce the same results in this form. Therefore, if we follow the procedure proposed by Arnold [27] and the integral along the edge is performed first, both spectra will produce the same result. However, as discussed earlier, it is rare to work a problem in which the integral along the edge can be done in closed form. This means that Arnold's procedure is not very practical. The most practical incremental diffracted field solution is obtained by asymptotically reducing the spectral integrals.

The only difference between the various PTD solutions is the direction taken for the integral of the current along the faces of the wedge. The most physically meaningful direction for this integration is that of the grazing diffracted ray as pointed out by Michaeli [13] and Butorin, Martynov and Ufimtsev [14]. This produces a result that predicts fields off the Keller cone. It is yet to be shown what the significance of using this type of formulation has in the near-zone.

The GTD incremental diffracted field can be obtained from the PTD incremental diffracted field by restricting the observation point to lie on the Keller cone. It is then reasoned that according to the method of stationary phase the integral along the edge is dominated by the contribution near the Keller cone direction. Therefore, the information about the fields along the Keller cone directions can be continued to other directions with little change in the resulting solution. The main advantage of this type of formulation is that a near-zone incremental diffracted field can be obtained. For this reason, the incremental diffracted field formulation of Tiberio and Maci [15, 16, 17] will be used for the remainder of this work. A more detailed

derivation of the near-zone diffracted field contribution of the ITD is performed in the next chapter.

SECTION 4

The Diffracted Field Contribution of the Incremental Theory of Diffraction

The derivation of the diffracted field contribution of the Incremental Theory of Diffraction (ITD) consists of several steps. First, the exact expression for the field diffracted by the canonical wedge problem is determined. Next, a Fourier transform pair relation is derived. This is then used to find the field diffracted by an infinitesimal length of the edge of the wedge. Finally, this expression is asymptotically reduced to obtain a closed form expression that permits its easy application to more general geometries. This is the procedure developed by Tiberio and Maci [15, 16, 17]. This chapter is a more complete discussion of the ITD as opposed to Chapter 3 which is a derivation of the diffracted field contribution of the ITD. The diffracted field contribution formulated in this chapter is obtained using the procedure proposed by Tiberio and Maci [15, 16, 17] and not from the current as was done in Chapter 3. This chapter is devoted to the discussion of the ITD method and the development of the near-zone diffracted field contribution of the ITD.

1 The Incremental Theory of Diffraction

The ITD is a recently proposed method for determining electromagnetic fields. The ITD consists of three separate field terms as formulated by Tiberio and Maci [15, 16, 17]. This section is devoted to a discussion of the ITD.

The ITD consists of one surface integral contribution and two line integral contributions. The surface integral is the integral of the field radiated by an infinitesimal patch of the surface. This surface integral is taken to be the Physical Optics (PO) integral. To compensate for the incorrect edge contribution of the PO integral, the PO edge contribution is subtracted out and a more accurate diffracted field contribution is added. These are the two line integrals.

Tiberio and Maci propose the use of a Fourier transform pair to obtain the contributions from an infinitesimal length of the edge. This consists simply of Fourier transforming the solution for the infinite wedge case. This results in incremental contributions that can be written in terms of incremental diffracted fields corresponding to the PO diffraction and the exact diffraction by the wedge.

Although all three of these contributions are required for a complete ITD solution, very good results can be obtained by only including the diffracted field contribution and the classical Geometrical Optics (GO) fields. Since the PO integral without its edge contribution is essentially the GO fields, the PO and PO edge contributions can be determined approximately using the classical GO theory. Although these contributions are not identical, the difference is small for most cases. For this reason, the field calculations for the remainder of this work will consist of the GO fields being generated using classical GO techniques and the diffracted field being generated by the incremental diffracted field contribution of the ITD.

2 The Canonical Wedge Solution

The derivation of the diffracted field contribution of the ITD begins with the exact solution for the field diffracted by an infinite straight edge of a wedge with two flat faces. This geometry is shown in Figure 10. This section is a brief derivation of the exact diffracted field in vector form. This solution is written in a form that is convenient for the remainder of the ITD diffracted field solution.

An important and useful fact about the total field exterior to a cylindrically symmetric geometry with a plane wave incident is that the transverse field components can be completely determined from the axial field component. For the geometry of

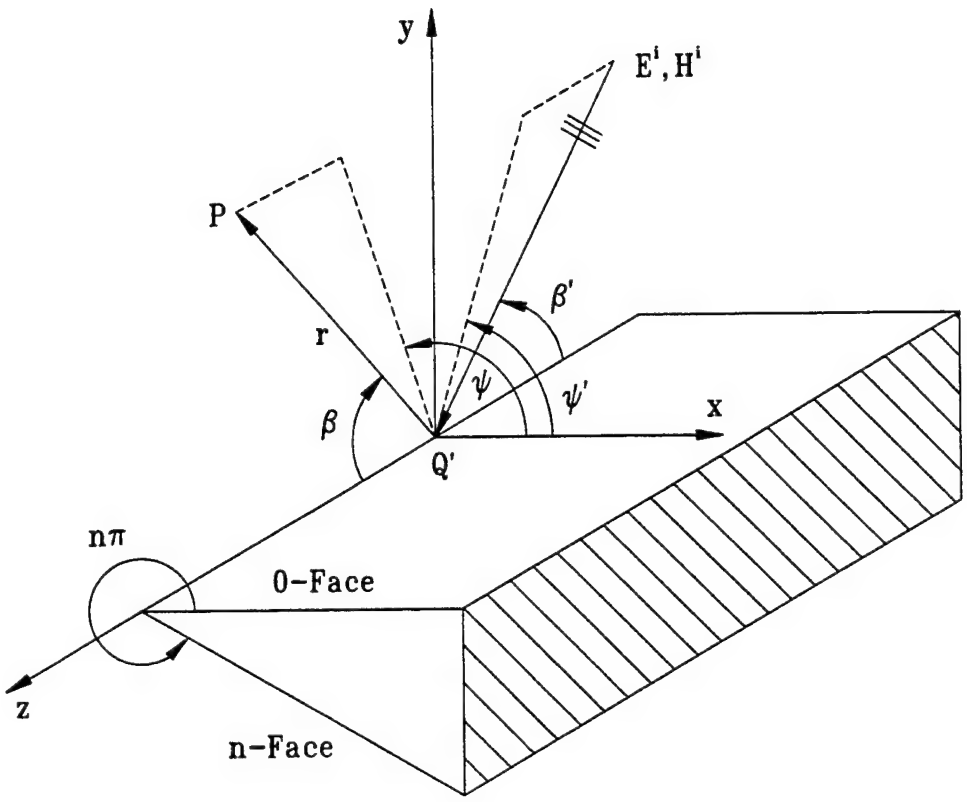

Figure 10: Geometry for the canonical wedge.

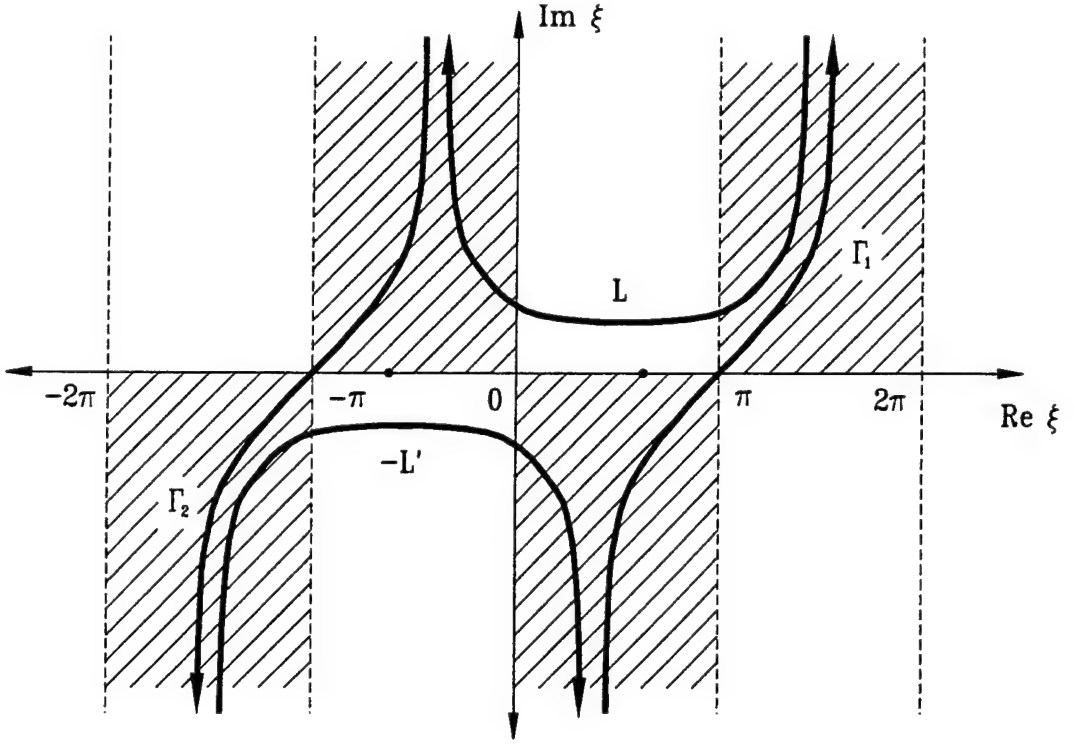

Figure 11: Contour of integration for the canonical wedge geometry.

interest here, this means that the total field in the transverse directions can be determined from the z-components of the electric and magnetic fields. The z-components of the electric and magnetic fields were derived by Pathak and Kouyoumjian [31] and are

$$E_z(P) = -E_z^i \frac{e^{-jk_z^i z'}}{2\pi j} \int_{L-L'} G_s(\xi) e^{jk_t \rho \cos\xi} \, d\xi \tag{110}$$

and

$$H_z(P) = -H_z^i \frac{e^{-jk_z^i z'}}{2\pi j} \int_{L-L'} G_h(\xi) e^{jk_t \rho \cos\xi} \, d\xi, \tag{111}$$

respectively; where $k_z^i = k\cos\beta'$ and $k_t = k\sin\beta'$. Also, the spectral diffraction coefficients are

$$G_{s,h}(\xi) = \frac{-1}{2n}\left\{\cot\left(\frac{\xi + \Psi^-}{2n}\right) \mp \cot\left(\frac{\xi + \Psi^+}{2n}\right)\right\} \tag{112}$$

where $\Psi^{\mp} = \psi \mp \psi'$. The contour of integration for the field expressions in (110) and (111) is shown in Figure 11. The total electric field exterior to the wedge can

now be written as

$$\vec{E}_\infty(P) = \vec{E}_t(P) + \hat{z}E_z(P) \tag{113}$$

where $\vec{E}_t(P)$ are the transverse field components of the total electric field. This is shown by Pathak and Kouyoumjian [31] to be related to the z-components of the electric and magnetic field

$$\vec{E}_t(P) = \frac{k_z^i}{jk_t^2}\nabla_t E_z(P) + \frac{j\omega\mu}{k_t^2}\hat{z}\times\nabla_t H_z(P) \tag{114}$$

where

$$\nabla_t = \hat{\rho}\frac{\partial}{\partial\rho} + \hat{\psi}\frac{1}{\rho}\frac{\partial}{\partial\psi}. \tag{115}$$

It is a simple task to show that the derivatives with respect to ρ of the z-components of the electric and magnetic fields are

$$\begin{aligned}\frac{\partial}{\partial\rho}E_z(P) &= -E_z^i\,\frac{e^{-jk_z^i z'}}{2\pi j}\int\limits_{L-L'} G_s(\xi)\left\{\frac{\partial}{\partial\rho}e^{jk_t\rho\cos\xi}\right\}d\xi \\ &= -E_z^i\,e^{-jk_z^i z'}\frac{k_t}{2\pi}\int\limits_{L-L'}\cos\xi\,G_s(\xi)\,e^{jk_t\rho\cos\xi}\,d\xi\end{aligned} \tag{116}$$

and

$$\begin{aligned}\frac{\partial}{\partial\rho}H_z(P) &= -H_z^i\,\frac{e^{-jk_z^i z'}}{2\pi j}\int\limits_{L-L'} G_h(\xi)\left\{\frac{\partial}{\partial\rho}e^{jk_t\rho\cos\xi}\right\}d\xi \\ &= -H_z^i\,e^{-jk_z^i z'}\frac{k_t}{2\pi}\int\limits_{L-L'}\cos\xi\,G_h(\xi)\,e^{jk_t\rho\cos\xi}\,d\xi,\end{aligned} \tag{117}$$

respectively. The derivatives with respect to ψ of the z-components of the electric and magnetic fields require more care. The differentiation process begins with

$$\frac{1}{\rho}\frac{\partial}{\partial\psi}E_z(P) = -E_z^i\,\frac{e^{-jk_z^i z'}}{2\pi j\rho}\int\limits_{L-L'}\left\{\frac{\partial}{\partial\psi}G_s(\xi)\right\}e^{jk_t\rho\cos\xi}\,d\xi. \tag{118}$$

Next, we recognize that

$$\frac{\partial}{\partial\psi}G_s(\xi) = \frac{\partial}{\partial\xi}G_s(\xi) \tag{119}$$

which makes (118)

$$\frac{1}{\rho}\frac{\partial}{\partial\psi}E_z(P) = -E_z^i\,\frac{e^{-jk_z^i z'}}{2\pi j\rho}\int\limits_{L-L'}\left\{\frac{\partial}{\partial\xi}G_s(\xi)\right\}e^{jk_t\rho\cos\xi}\,d\xi. \tag{120}$$

This integral is now in a form that can be easily evaluated using integration-by-parts. Using integration-by-parts

$$\int u \frac{dv}{dx} dx = uv - \int v \frac{du}{dx} dx \tag{121}$$

and noting that the values of the integral at its endpoints is zero, (120) becomes

$$\begin{aligned} \frac{1}{\rho}\frac{\partial}{\partial\psi}E_z(P) &= E_z^i \frac{e^{-jk_z^i z'}}{2\pi j\rho} \int\limits_{L-L'} G_s(\xi)\left\{\frac{\partial}{\partial\xi} e^{jk_t\rho\cos\xi}\right\} d\xi \\ &= -E_z^i\, e^{-jk_z^i z'}\frac{k_t}{2\pi}\int\limits_{L-L'} \sin\xi\, G_s(\xi)\, e^{jk_t\rho\cos\xi}\, d\xi \end{aligned} \tag{122}$$

which is the derivative of the z-component of the electric field with respect to ψ as desired. The derivative of the z-component of the magnetic field with respect to ψ is

$$\frac{1}{\rho}\frac{\partial}{\partial\psi}H_z(P) = -H_z^i e^{-jk_z^i z'}\frac{k_t}{2\pi}\int\limits_{L-L'} \sin\xi G_h(\xi) e^{jk_t\rho\cos\xi}\, d\xi \tag{123}$$

following a similar procedure. Noting that $E_z^i = E_{\beta'}^i \sin\beta'$, $H_z^i = -\frac{1}{Z_c} E_{\psi'}^i \sin\beta'$ and using the coordinate transformation

$$\hat{\rho} = \hat{r}\sin\beta + \hat{\beta}\cos\beta \tag{124}$$

$$\hat{z} = \hat{r}\cos\beta - \hat{\beta}\sin\beta\,, \tag{125}$$

the resulting solution will be in the standard ray fixed coordinate system. Substituting (114), (116), (117), (122), (123) into (113) and simplifying, we obtain an expression for the total electric field given by,

$$\vec{E}_\infty(P) = \vec{E}^i(Q')\cdot\frac{1}{2\pi j}\int\limits_{L-L'} \overline{\overline{F}}_\infty(\xi,\beta') e^{-jkrf(\xi,\beta')} d\xi \tag{126}$$

where

$$f(\xi,\beta') = \cos\beta\cos\beta' - \cos\xi\sin\beta\sin\beta'. \tag{127}$$

Also, the dyadic $\overline{\overline{F}}_\infty(\xi,\beta')$ is given by

$$\begin{aligned} \overline{\overline{F}}_\infty(\xi,\beta') &= -\hat{\beta}'\hat{r}\, F_{\beta' r}(\xi,\beta')\, G_s(\xi) - \hat{\psi}'\hat{r}\, F_{\psi' r}(\xi,\beta')\, G_h(\xi) \\ &\quad -\hat{\beta}'\hat{\beta}\, F_{\beta'\beta}(\xi,\beta')\, G_s(\xi) - \hat{\psi}'\hat{\beta}\, F_{\psi'\beta}(\xi,\beta')\, G_h(\xi) \\ &\quad -\hat{\beta}'\hat{\psi}\, F_{\beta'\psi}(\xi,\beta')\, G_s(\xi) - \hat{\psi}'\hat{\psi}\, F_{\psi'\psi}(\xi,\beta')\, G_h(\xi) \end{aligned} \tag{128}$$

and the terms in the dyadic are:

$$F_{\beta'_r}(\xi,\beta') = \sin\beta\cos\beta'\cos\xi + \cos\beta\sin\beta' \quad (129a)$$

$$F_{\psi'_r}(\xi,\beta') = -\sin\beta\sin\xi \quad (129b)$$

$$F_{\beta'\beta}(\xi,\beta') = \cos\beta\cos\beta'\cos\xi - \sin\beta\sin\beta' \quad (129c)$$

$$F_{\psi'\beta}(\xi,\beta') = -\cos\beta\sin\xi \quad (129d)$$

$$F_{\beta'\psi}(\xi,\beta') = \cos\beta'\sin\xi \quad (129e)$$

$$F_{\psi'\psi}(\xi,\beta') = \cos\xi \quad (129f)$$

To obtain only the diffracted field contribution of the total field, we begin by closing the contour of integration. This is accomplished by including the steepest descent paths through the points $\xi = \pm\pi$ as shown in Figure 11. Now, if we define the contours $C = L - L' + \Gamma_1 + \Gamma_2$ and $\Gamma_d = \Gamma_1 + \Gamma_2$, the total electric field is

$$\begin{aligned}\vec{E}_\infty(P) &= \vec{E}^i(Q')\cdot\frac{1}{2\pi j}\oint_C \overline{\overline{F}}_\infty(\xi,\beta')e^{-jkrf(\xi,\beta')}d\xi \\ &- \vec{E}^i(Q')\cdot\frac{1}{2\pi j}\int_{\Gamma_d} \overline{\overline{F}}_\infty(\xi,\beta')e^{-jkrf(\xi,\beta')}d\xi. \end{aligned} \quad (130)$$

It is shown by Pathak and Kouyoumjian [31] that the integral on the contour C produces the GO fields and the integral on the contour Γ_d produces the diffracted field. Finally, the field diffracted by a wedge with a plane wave incidence is

$$\vec{E}^d_\infty(P) = -\vec{E}^i(Q')\cdot\frac{1}{2\pi j}\int_{\Gamma_d} \overline{\overline{F}}_\infty(\xi,\beta')e^{-jkrf(\xi,\beta')}d\xi \quad (131)$$

where $f(\xi,\beta')$ and $\overline{\overline{F}}_\infty(\xi,\beta')$ are given by (127) and (128), respectively.

3 The Fourier Transform

The next step in the development of the ITD diffracted field expression is the derivation of a specialized Fourier transform pair. This is used to obtain an incremental quantity from the infinite wedge solution of Section 2. This section is devoted to the derivation of the Fourier transform pair used by Tiberio and Maci [15, 16, 17] to obtain this incremental quantity.

It is necessary at this point to make some assumptions about the desired form of the resulting solution. It is assumed here that the diffracted field can be written in the form,

$$\vec{E}^d_\infty(P) = \int_{-\infty}^{\infty} \vec{I}^d(z') e^{-jkz' \cos\beta'} dz' \tag{132}$$

where $\vec{I}^d(z')$ is an incremental quantity yet to be found. This quantity is determined by recalling the traditional Fourier transform pair:

$$A(x) = \int_{-\infty}^{\infty} B(\alpha) e^{-j\alpha x} d\alpha \tag{133a}$$

$$B(\alpha) = \frac{1}{2\pi} \int_{-\infty}^{\infty} A(x) e^{j\alpha x} dx \tag{133b}$$

Next, comparing (132) and (133a), we obtain the change of variables

$$\alpha = z' \tag{134a}$$

$$x = k \cos\beta' \tag{134b}$$

$$B(\alpha) = \vec{I}^d(z') \tag{134c}$$

$$A(x) = \vec{E}^d_\infty(P) \tag{134d}$$

that will allow us to use the Fourier transform pair in (133) to determine $\vec{I}^d(z')$. Thus, substituting (134) into (133b),

$$\vec{I}^d(z') = \frac{k}{2\pi} \int_{-\infty}^{\infty} \vec{E}^d_\infty(P) e^{jkz' \cos\beta'} d(\cos\beta') \tag{135}$$

is the unknown incremental quantity. The variable of integration is changed to β' to put this result in a more convenient form. The dummy variable θ' is used to avoid confusion. Finally, the desired Fourier transform pair is:

$$\vec{E}^d_\infty(P) = \int_{-\infty}^{\infty} \vec{I}^d(z') e^{-jkz' \cos\beta'} dz' \tag{136a}$$

$$\vec{I}^d(z') = \frac{k}{2\pi} \int_{C_{\theta'}} \vec{E}^d_\infty(P) \sin\theta' e^{jkz' \cos\theta'} d\theta' \tag{136b}$$

where the contour of integration in the θ' plane is shown in Figure 12.

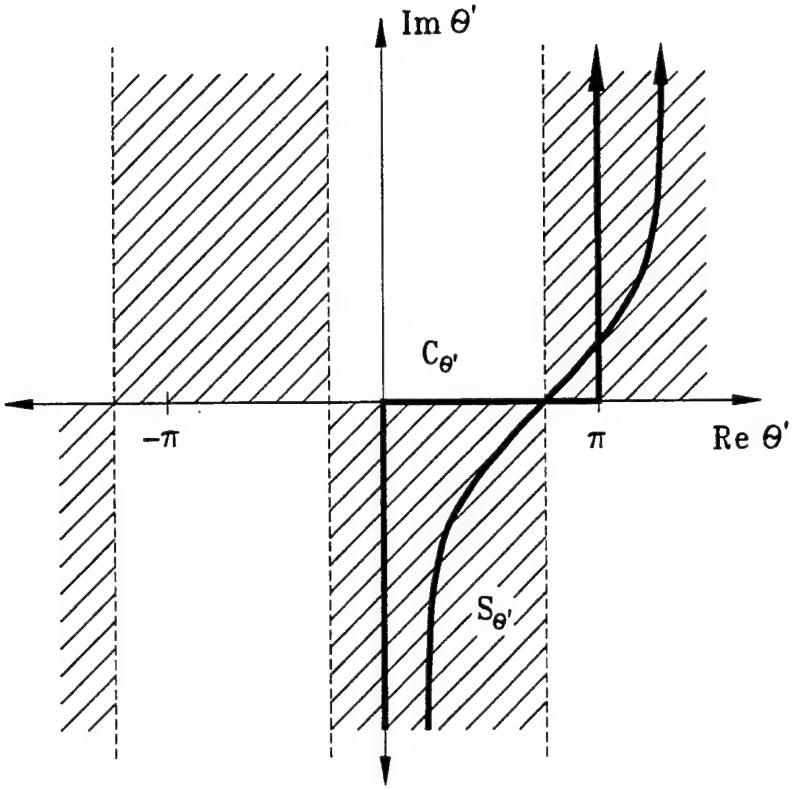

Figure 12: Contour of integration for the θ' plane integral.

4 Formulation of the Diffracted Field Contribution of the Incremental Theory of Diffraction

The next step of the ITD diffracted field formulation is simply to use the Fourier transform pair developed in Section 3 to convert the solution of the infinite wedge of Section 2 into the field diffracted by an infinitesimal length of the edge. This section develops the final ITD diffracted field expression and converts it into a convenient form for its use on more general problems.

Although (136) is a valid form for the ITD diffracted field, it is not the most convenient. The Fourier transform pair in (136) can be written in the more convenient form,

$$\vec{E}^d(P) = \int_{-\infty}^{\infty} d\vec{E}^d(z') \tag{137}$$

with

$$d\vec{E}^d(z') = dz' e^{-jkz'\cos\beta'} \frac{k}{2\pi} \int_{C_{\theta'}} \vec{E}^d_\infty(P) \sin\theta' e^{jkz'\cos\theta'} d\theta' \tag{138}$$

where $d\vec{E}^d(z')$ is the field diffracted by an infinitesimal length of the edge as desired. Since this expression is for an infinitesimal length of the edge, the edge can be changed to any general edge geometry. Thus, substituting (131) into (138) we obtain for any general shaped edge,

$$\vec{E}^d(P) = \int_{C_e} d\vec{E}^d(l) \tag{139}$$

where C_e is the contour along the actual edge,

$$d\vec{E}^d(l) = -\,dl\ \vec{E}^i(Q') \cdot \frac{k}{4\pi^2 j} \int_{C_{\theta'}} \int_{\Gamma_d} \overline{\overline{F}}_\infty(\xi,\theta') \sin\theta' e^{-jkrf(\xi,\theta')} d\xi d\theta' \tag{140}$$

and

$$f(\xi,\theta') = \cos\beta\cos\theta' - \cos\xi\sin\beta\sin\theta'. \tag{141}$$

Also, the dyadic $\overline{\overline{F}}_\infty(\xi,\theta')$ is given by

$$\begin{aligned} \overline{\overline{F}}_\infty(\xi,\theta') \;=\; & -\hat{\beta}'\hat{\tau}\, F_{\beta'\tau}(\xi,\theta')\, G_s(\xi) - \hat{\psi}'\hat{\tau}\, F_{\psi'\tau}(\xi,\theta')\, G_h(\xi) \\ & -\hat{\beta}'\hat{\beta}\, F_{\beta'\beta}(\xi,\theta')\, G_s(\xi) - \hat{\psi}'\hat{\beta}\, F_{\psi'\beta}(\xi,\theta')\, G_h(\xi) \\ & -\hat{\beta}'\hat{\psi}\, F_{\beta'\psi}(\xi,\theta')\, G_s(\xi) - \hat{\psi}'\hat{\psi}\, F_{\psi'\psi}(\xi,\theta')\, G_h(\xi) \end{aligned} \tag{142}$$

and the terms in the dyadic are:

$$F_{\beta'r}(\xi,\theta') = \sin\beta\cos\theta'\cos\xi + \cos\beta\sin\theta' \quad (143a)$$

$$F_{\psi'r}(\xi,\theta') = -\sin\beta\sin\xi \quad (143b)$$

$$F_{\beta'\beta}(\xi,\theta') = \cos\beta\cos\theta'\cos\xi - \sin\beta\sin\theta' \quad (143c)$$

$$F_{\psi'\beta}(\xi,\theta') = -\cos\beta\sin\xi \quad (143d)$$

$$F_{\beta'\psi}(\xi,\theta') = \cos\theta'\sin\xi \quad (143e)$$

$$F_{\psi'\psi}(\xi,\theta') = \cos\xi \quad (143f)$$

This concludes the derivation of the diffracted field contribution of the ITD. In order to make this expression easy to apply, we wish to asymptotically reduce it to obtain a closed form expression.

5 The Asymptotic Expansion of the Diffracted Field Contribution of the Incremental Theory of Diffraction

Although the ITD diffracted field expression in (140) is valid, it is useful for only a small set of problems in this form. To apply this to a wider class of problems, we wish to obtain a closed form expression that will leave only the integration along the edge. This is accomplished here by asymptotically reducing (140) for high frequencies. This section is a derivation of this closed form result.

We begin by asymptotically reducing the integral in the ξ plane. It is a simple task to show that (140) has saddle points located at $\xi_s = \pi$ for the contour Γ_1 and $\xi_s = -\pi$ for the contour Γ_2. The dyadic $\overline{\overline{F}}_\infty(\xi,\theta')$ in (142) can be simplified if it is assumed that (143) is smooth and slowly varying near the saddle points, this means

$$F_{\beta'r}(\xi_s,\theta') = \sin(\theta'-\beta) \quad (144a)$$

$$F_{\psi'r}(\xi_s,\theta') = 0 \quad (144b)$$

$$F_{\beta'\beta}(\xi_s,\theta') = -\cos(\theta'-\beta) \quad (144c)$$

$$F_{\psi'\beta}(\xi_s,\theta') = 0 \quad (144d)$$

$$F_{\beta'\psi}(\xi_s, \theta') = 0 \tag{144e}$$

$$F_{\psi'\psi}(\xi_s, \theta') = -1. \tag{144f}$$

Therefore, (140) is given approximately by

$$d\vec{E}^d(l) \sim dl\ \vec{E}^i(Q') \cdot \frac{k}{2\pi} \int_{C_{\theta'}} \overline{\overline{K}}_\infty(\theta') \sin\theta' e^{-jkr\cos\beta\cos\theta'} d\theta' \tag{145}$$

where

$$\overline{\overline{K}}_\infty(\theta') = -\hat{\beta}'\hat{r}\sin(\theta'-\beta)\, W_s(\theta') + \hat{\beta}'\hat{\beta}\cos(\theta'-\beta)\, W_s(\theta') + \hat{\psi}'\hat{\psi}\, W_h(\theta') \tag{146}$$

and

$$W_{s,h}(\theta') = \frac{-1}{2\pi j} \int_{\Gamma_d} G_{s,h}(\xi) e^{jkr\sin\beta\sin\theta'\cos\xi}\, d\xi. \tag{147}$$

Next, if we substitute (112) into (147) and let $\kappa = kr\sin\beta\sin\theta'$ and $R_{s,h} = \mp 1$, (147) becomes

$$\begin{aligned} W_{s,h}(\theta') &= \frac{1}{4\pi jn} \int_{\Gamma_1} \cot\left(\frac{\xi+\Psi^-}{2n}\right) e^{j\kappa\cos\xi}\, d\xi \\ &+ \frac{1}{4\pi jn} \int_{\Gamma_2} \cot\left(\frac{\xi+\Psi^-}{2n}\right) e^{j\kappa\cos\xi}\, d\xi \\ &+ \frac{R_{s,h}}{4\pi jn} \int_{\Gamma_1} \cot\left(\frac{\xi+\Psi^+}{2n}\right) e^{j\kappa\cos\xi}\, d\xi \\ &+ \frac{R_{s,h}}{4\pi jn} \int_{\Gamma_2} \cot\left(\frac{\xi+\Psi^+}{2n}\right) e^{j\kappa\cos\xi}\, d\xi. \end{aligned} \tag{148}$$

These integrals have been evaluated by Pathak and Kouyoumjian [31] assuming $\kappa \gg 1$ by using the Pauli-Clemmow modified method of steepest descent which results in

$$W_{s,h}(\theta') \sim \frac{e^{-j\pi/4}}{\sqrt{2\pi k}}\, \widetilde{D}_{s,h}(Q')\, \frac{e^{-jkr\sin\beta\sin\theta'}}{\sqrt{r\sin\beta\sin\theta'}} \tag{149}$$

where

$$\begin{aligned} \widetilde{D}_{s,h}(Q') = \frac{1}{2n} \Bigg[&\left\{ \cot\left(\frac{\pi+\Psi^-}{2n}\right) F\left[kLa^+(\Psi^-)\right] \right. \\ &\left. + \cot\left(\frac{\pi-\Psi^-}{2n}\right) F\left[kLa^-(\Psi^-)\right] \right\} \\ \mp &\left\{ \cot\left(\frac{\pi+\Psi^+}{2n}\right) F\left[kLa^+(\Psi^+)\right] \right. \\ &\left. + \cot\left(\frac{\pi-\Psi^+}{2n}\right) F\left[kLa^-(\Psi^+)\right] \right\} \Bigg] \end{aligned} \tag{150}$$

and $L = r\sin\beta\sin\theta'$. The functions $F[x]$ and $a^{\pm}(\gamma)$ are defined in (6) and (7), respectively. Thus, substituting (146) and (149) into (145) and simplifying, we obtain the integral

$$d\vec{E}^d(l) \sim dl\ \vec{E}^i(Q') \cdot \int_{C_{\theta'}} \overline{\overline{P}}_\infty(\theta') e^{-jkr\cos(\theta'-\beta)} d\theta' \tag{151}$$

where

$$\begin{aligned}\overline{\overline{P}}_\infty(\theta') &= -\hat{\beta}'\hat{r}\frac{e^{-j\pi/4}}{2\pi}\sqrt{\frac{k\sin\theta'}{2\pi r\sin\beta}}\sin(\theta'-\beta)\,\widetilde{D}_s(Q') \\ &\quad +\hat{\beta}'\hat{\beta}\frac{e^{-j\pi/4}}{2\pi}\sqrt{\frac{k\sin\theta'}{2\pi r\sin\beta}}\cos(\theta'-\beta)\,\widetilde{D}_s(Q') \\ &\quad +\hat{\psi}'\hat{\psi}\frac{e^{-j\pi/4}}{2\pi}\sqrt{\frac{k\sin\theta'}{2\pi r\sin\beta}}\,\widetilde{D}_h(Q')\end{aligned} \tag{152}$$

and $\widetilde{D}_{s,h}(Q')$ is given in (150).

Finally, the integral in the θ' plane must be asymptotically reduced. First, the contour of integration $C_{\theta'}$ is deformed to its steepest descent path $S_{\theta'}$ as shown in Figure 12. Also, it is a simple task to show that the integral in (151) has one saddle point located at $\theta'_s = \beta$. The classical method of steepest descent can be used if we assume that $\overline{\overline{P}}_\infty(\theta')$ is a smooth and slowly varying function near the saddle point θ'_s. Therefore, we obtain a closed form asymptotic expression using the method of steepest descent [32] and assuming $kr \gg 1$,

$$\vec{E}^d(P) = \int_{C_e} d\vec{E}^d(l) \tag{153}$$

where C_e is the contour along the actual edge and

$$d\vec{E}^d(l) \sim \vec{E}^i(Q') \cdot \left\{\hat{\beta}'\hat{\beta}\,\widetilde{D}_s(Q') + \hat{\psi}'\hat{\psi}\,\widetilde{D}_h(Q')\right\}\frac{e^{-jkr}}{2\pi r}\,dl \tag{154}$$

is the diffracted field contribution of the ITD. In doing so, the distance parameter becomes $L = r\sin^2\beta$. This is the same result obtained by Tiberio and Maci [15, 16, 17]. For the remainder of this work, the geometries of interest will be restricted to curved edges of flat plates. In this case, we can set $n = 2$ and simplify (150) to

$$\widetilde{D}_{s,h}(Q') = \frac{1}{2}\left\{\frac{F\left[kLa(\Psi^-)\right]}{\cos\left(\frac{\Psi^-}{2}\right)} \mp \frac{F\left[kLa(\Psi^+)\right]}{\cos\left(\frac{\Psi^+}{2}\right)}\right\} \tag{155}$$

where

$$a(\Psi^{\mp}) = 2\cos^2\left(\frac{\Psi^{\mp}}{2}\right). \tag{156}$$

This result is now in a very simple form consisting of only the integral along the edge of the wedge.

SECTION 5

The Radiation by a Source on a Flat Plate with a Curved Edge

A wide class of problems studied in electromagnetics is the radiation of a source on a flat plate. Caustics of the UTD diffracted field will occur if the edge of the plate is curved. The UTD fields must be corrected to account for the caustics to accurately determine the field radiated by the source in those regions. A caustic corrected UTD solution that can be used to determine the field diffracted by the curved edge of a flat plate with a source located on it is derived in this chapter.

1 Problem Formulation

Two main topics must be addressed when formulating a caustic corrected UTD solution for determining the field near the caustics of waves diffracted by curved edges. First, the canonical geometry must be chosen to be the simplest structure containing the phenomena of interest. The method of solution must also be determined. This section is a discussion of the canonical geometry and the method used to obtain a solution for the radiation by a source on a flat plate with a curved edge.

The phenomena of interest here is the coalescence of three diffraction points. Therefore, the canonical geometry to be used should contain no more than three diffraction points. Although a disk is often used as a canonical geometry, it has either two or four diffraction points depending on which region the observation point is in. However, this geometry would unnecessarily complicate the solution because

there is one more diffraction point than is needed for studying this phenomena. This occurs because the disk is finite in extent. The simplest geometry that contains the phenomena of interest is the curved edge of a semi-infinite flat plate. Once the CC-UTD has been developed for this geometry, the solution can be applied to the disk due to the high frequency localization property of electromagnetic fields.

It is also important to consider the mathematics involved with the geometry in order to obtain a tractable solution. The scope of the solution is narrowed for the purposes of this work. The procedure used to obtain a solution here can be used to obtain a more general solution. However, to study the phenomena of interest, it is assumed that the edge of the plate is symmetric, the source lies along the axis of symmetry and the far-zone observation point is also in the plane of symmetry of the edge of the plate. This geometry is chosen so that the diffraction points are symmetrically located and equally spaced. A procedure similar to the one developed here can be used to obtain a solution if the diffraction points are not equally spaced.

The ITD developed by Tiberio and Maci [15, 16, 17] will be used in this work to obtain a caustic corrected UTD solution. The ITD contains three different components as discussed in Section 1 of Chapter 4. The first term is a Physical Optics surface integral. This integral can be formulated by using the spectral domain form of the scalar free space Green's function, interchanging the spectral and spatial integrals and performing the spatial integrals. This results in a double spectral integral form of the PO integral. Upon doing so, it can be seen that the PO integral contains three double integral stationary phase points and a branch point of order $-\frac{3}{2}$. Although it should be theoretically possible to obtain a uniform asymptotic expansion for this type of integral, it is not possible using existing theories. Also, since the phase function would have to be mapped to a fourth order polynomial that is a function of two variables, the canonical integral would have an extremely complicated form. In fact, this integral would be no simpler to compute than the original PO integral. This defeats the purpose of the asymptotic expansion. Therefore, we wish to make some approximations in order to obtain simpler integrals.

As discussed in Section 1 of Chapter 4, the PO surface integral minus its edge contribution is approximately the Geometrical Optics field. This approximation is valid as long as the reflection point is not near the edge when the diffraction points coalesce. This is the same as saying that the caustic boundaries can not be close to the incident or reflection shadow boundaries. This will be assumed here. Therefore, the only remaining contribution of the ITD is the diffracted field component. The total ITD field will be approximated by the GO field and the diffracted field contribution of the ITD integrated along the edge of the plate. The diffracted field contribution of the ITD is derived in Chapter 4.

Only one single integral appears in this solution. The resulting formulation is simple enough in form to allow for the uniform asymptotic expansion of the diffracted field integral equation. The canonical integrals used in this expansion are standard and well tabulated functions. This is an attractive feature of any asymptotic expansion.

2 Diffraction Integral Formulation

An integral equation must be formulated that can be asymptotically expanded to obtain a caustic corrected UTD solution. The ITD will be used in this work to obtain this diffraction integral. This section is a derivation of the diffracted field integral equation used to obtain a caustic corrected UTD solution.

Some assumptions must be made to obtain a usable diffracted field integral equation. First, as discussed in Section 1, the incident and reflection shadow boundaries can not be close to the caustic boundaries caused by the curvature of the edge since only the diffracted field contribution of the ITD is to be asymptotically expanded here. Next, recalling that the ITD diffracted field in Chapter 4 was obtained by asymptotically expanding a double spectral integral assuming that $kr\sin^2\beta \gg 1$, this must also be enforced here. Finally, it will be assumed that the curvature of the edge is symmetric and the source location and the observation direction lie in this plane of symmetry as discussed in Section 1. This geometry is shown in Figure 13.

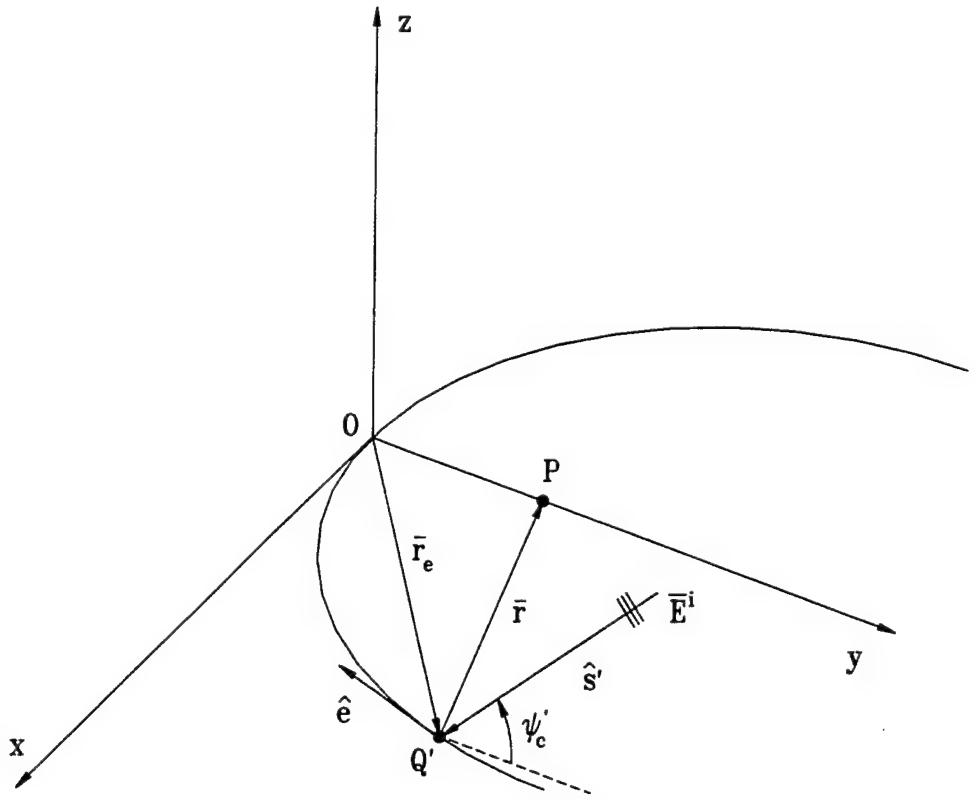

Figure 13: Canonical geometry for the diffraction by a curved edge.

In order to use the ITD formulation, it is important to note that the ITD result is reciprocal. Since the ITD was formulated for plane wave incidence and a near-zone observation point, this can be assumed here and then reciprocity used to obtain the radiated field. The ITD diffracted field as derived in Chapter 4 is

$$\vec{E}^d(P) = \int_{C_e} d\vec{E}^d(l) \tag{157}$$

where C_e is the edge contour and

$$d\vec{E}^d(l) \sim \vec{E}^i(Q') \cdot \left\{ \hat{\beta}'\hat{\beta}\, \widetilde{D}_s(Q') + \hat{\psi}'\hat{\psi}\, \widetilde{D}_h(Q') \right\} \frac{e^{-jkr}}{2\pi r}\, dl \tag{158}$$

is the electric field diffracted by an infinitesimal length of the edge of the wedge. The half-plane diffraction coefficients given by

$$\widetilde{D}_{s,h}(Q') = \frac{1}{2} \left\{ \frac{F\left[kLa(\Psi^-)\right]}{\cos\left(\frac{\Psi^-}{2}\right)} \mp \frac{F\left[kLa(\Psi^+)\right]}{\cos\left(\frac{\Psi^+}{2}\right)} \right\} \tag{159}$$

are to be used since only flat plates are being considered. Also, the angle parameter $a(\Psi^{\mp})$ is given by

$$a(\Psi^{\mp}) = 2\cos^2\left(\frac{\Psi^{\mp}}{2}\right) \tag{160}$$

where $\Psi^{\mp} = \psi \mp \psi'$, the distance parameter is $L = r\sin^2\beta$ and $F[x]$ is the UTD Fresnel transition function defined in (6).

We begin by noting that $\psi = 0$ for all the diffraction points on the edge since the observation point is located on the plate. Therefore, $\hat{\psi}$ is a constant and $\widetilde{D}_s(Q') \equiv 0$ for all the diffraction points on the edge. Using these facts, (157) reduces to

$$\vec{E}^d(P) = \hat{\psi}\frac{1}{2\pi} \int_{C_e} \left[\vec{E}^i(0) \cdot \hat{\psi}'\right] \frac{\widetilde{D}_h(Q')}{r}\, e^{jk\left[-\hat{s}'\cdot\vec{r}_e - r\right]}\, dl \tag{161}$$

where $\vec{E}^i(0) = \hat{\psi}'_c\, E^i_{\psi_c} + \hat{\beta}'_c\, E^i_{\beta_c}$. Also, from (4b) of Chapter 2 we know

$$\hat{\psi}' = \frac{\hat{e} \times \hat{s}'}{\sin\beta'} \tag{162}$$

which makes (161)

$$\begin{aligned} \vec{E}^d(P) \;=\; & \hat{\psi} E^i_{\psi_c} \frac{1}{2\pi} \int_{C_e} \left\{ \hat{\psi}'_c \cdot [\hat{e} \times \hat{s}'] \right\} \frac{\widetilde{D}_h(Q')}{r\sin\beta'}\, e^{jk\left[-\hat{s}'\cdot\vec{r}_e - r\right]}\, dl \\ + \; & \hat{\psi} E^i_{\beta_c} \frac{1}{2\pi} \int_{C_e} \left\{ \hat{\beta}'_c \cdot [\hat{e} \times \hat{s}'] \right\} \frac{\widetilde{D}_h(Q')}{r\sin\beta'}\, e^{jk\left[-\hat{s}'\cdot\vec{r}_e - r\right]}\, dl. \end{aligned} \tag{163}$$

Using a vector identity and noting that $\hat{s}'$ is orthogonal to $\hat{\psi}'_c$ and $\hat{\beta}'_c$,

$$\hat{\psi}'_c \cdot [\hat{e} \times \hat{s}'] = \hat{e} \cdot \left[\hat{s}' \times \hat{\psi}'_c\right] = \hat{e} \cdot \hat{\beta}'_c = -\hat{e} \cdot \hat{x} \tag{164}$$

$$\hat{\beta}'_c \cdot [\hat{e} \times \hat{s}'] = \hat{e} \cdot \left[\hat{s}' \times \hat{\beta}'_c\right] = -\hat{e} \cdot \hat{\psi}'_c . \tag{165}$$

The contribution corresponding to (165) integrates to zero since it is an odd function of arc length. It is now advantageous to change the variable of integration to be along the x direction which converts (163) to,

$$\vec{E}^d(P) = \hat{\psi} E^i_{\psi_c} \frac{1}{2\pi} \int_{-\infty}^{\infty} [-\hat{e} \cdot \hat{x}] \frac{\widetilde{D}_h(Q')}{r \sin \beta'} e^{jk[-\hat{s}' \cdot \vec{r}_e - r]} \frac{dl}{dx_e} dx_e \tag{166}$$

where the Jacobian of the transformation is

$$\frac{dl}{dx_e} = \frac{-1}{\hat{e} \cdot \hat{x}} \tag{167}$$

from (761) of Appendix D. Finally,

$$\vec{E}^d(P) = \hat{\psi} E^i_{\psi_c} \frac{1}{2\pi} \int_{-\infty}^{\infty} \mathcal{F}(x_e) e^{jkh(x_e)} dx_e \tag{168}$$

where

$$h(x_e) = -\hat{s}' \cdot \vec{r}_e - r \tag{169}$$

and

$$\mathcal{F}(x_e) = \frac{\widetilde{D}_h(Q')}{r \sin \beta'}. \tag{170}$$

This completes the derivation of the diffracted field integral equation. This integral must now be asymptotically expanded to obtain closed form results for both the lit and the shadow sides of the caustic.

3 The Uniform Asymptotic Expansion of the Diffracted Field Integral Equation in the Caustic Lit Region

Although the diffracted field integral equation derived in Section 2 can be numerically integrated to predict the field diffracted by a curved edge, it is advantageous to obtain

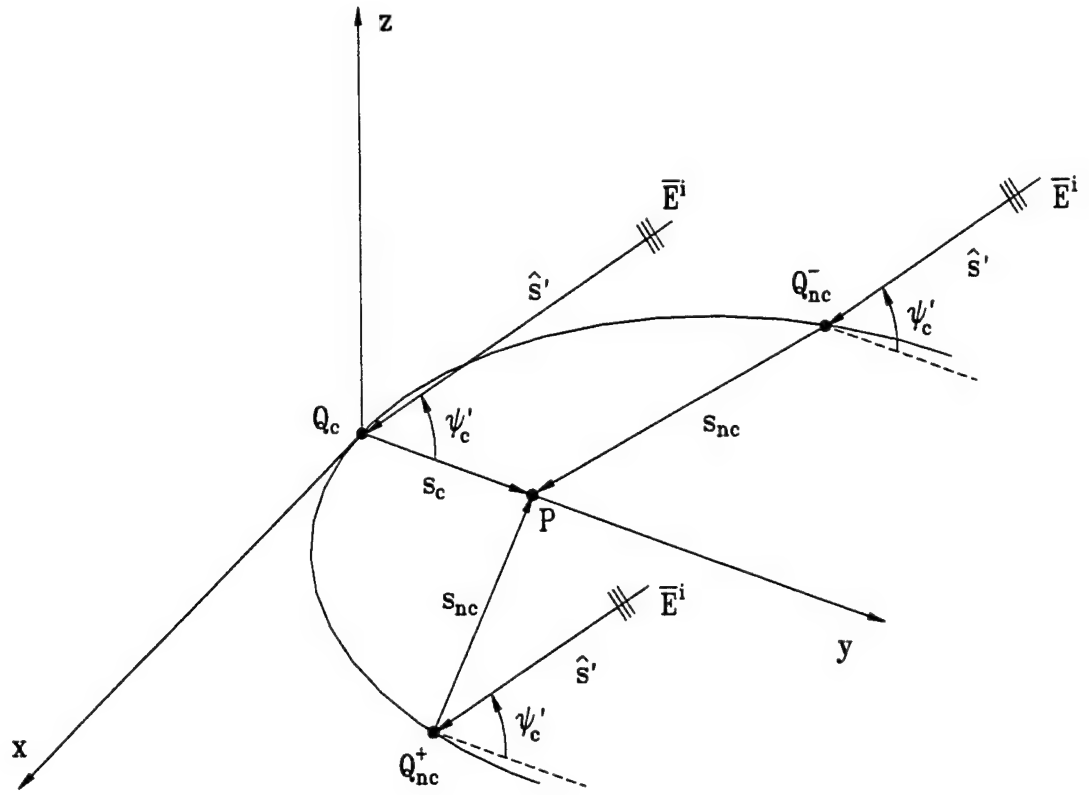

Figure 14: Reciprocal ray geometry for the diffraction by a curved edge in the caustic lit region.

closed form expressions. One way to accomplish this is to asymptotically expand the integral at high frequencies. This section is devoted to the asymptotic expansion of the diffracted field integral equation for the lit side of the caustic.

In the caustic lit region, there are assumed to be three symmetrically located diffraction points as shown in Figure 14. This ray structure occurs because of the assumed symmetry of the edge, source location and radiation direction. A uniform asymptotic expansion must be used when these diffraction points are nearly coincident. The uniform asymptotic expansion derived in Section 2 of Appendix B can be utilized with these assumptions in mind.

First, $m = 0$ in (614) of Appendix B because the integrand of the integral in (168) does not contain a zero at the central stationary phase point. Also, as explained in Section 1 of Appendix B, if the integral has three real stationary phase points then $\mu = -\eta$ where $\mu = \text{sgn}\{h^{\text{IV}}(x_c)\}$ and $\eta = \text{sgn}\{h^{\text{II}}(x_c)\}$. Finally, it is assumed

that $k \gg 1$ and $\mathcal{F}(x_e)$ is a smooth and slowly varying function of x_e about the central stationary phase point. From (657) of Appendix B the diffracted field integral equation in (168) can be approximated as

$$\begin{aligned}
\vec{E}^d(P) &= \hat{\psi}\, E^i_{\psi_c} \frac{1}{2\pi} \int_{-\infty}^{\infty} \mathcal{F}(x_e) e^{jkh(x_e)}\, dx_e \\
&\sim \hat{\psi}\, E^i_{\psi_c} \frac{\mathcal{F}(x_c)}{2\pi} \left| \sqrt{\frac{2\pi}{kh^{II}(x_c)}} \right| e^{j\eta\pi/4} e^{jkh(x_c)} T_c(\xi, 0) \\
&+ \hat{\psi}\, 2\, E^i_{\psi_c} \frac{\mathcal{F}(x_{nc})}{2\pi} \left| \sqrt{\frac{2\pi}{kh^{II}(x_{nc})}} \right| e^{-j\eta\pi/4} e^{jkh(x_{nc})} T_{nc}(\xi, \eta, 0) \qquad (171)
\end{aligned}$$

where the argument of the transition functions is

$$\xi = \left| \sqrt{2k[h(x_{nc}) - h(x_c)]} \right| e^{-j3\eta\pi/4} \qquad (172)$$

from (626) of Appendix B. It is easily shown using (753a) and (764a) of Appendix D that the value of the phase function is

$$h(x_c) = -s_c \qquad (173)$$

at the central stationary phase point and using (756a) and (765a) of Appendix D that the value of the phase function is

$$h(x_{nc}) = -\hat{s}' \cdot \vec{r}_e(Q_{nc}) - s_{nc} \qquad (174)$$

at the non-central stationary phase points. The argument of the transition functions becomes

$$\xi = \left| \sqrt{2k[-\hat{s}' \cdot \vec{r}_e(Q_{nc}) - s_{nc} + s_c]} \right| e^{-j3\eta\pi/4} \qquad (175)$$

using these in (172). Also, from (753c) and (764c) of Appendix D the second derivative of the phase function is

$$h^{II}(x_c) = -\left[\frac{1}{s_c} + \frac{1}{\rho^d(Q_c)} \right] \qquad (176)$$

at the central stationary phase point and from (756c) and (765c) of Appendix D the second derivative of the phase function is

$$h^{II}(x_{nc}) = -\sin^2 \beta_{nc} \left[\frac{1}{s_{nc}} + \frac{1}{\rho^d(Q_{nc})} \right] \left(\frac{-1}{\hat{e} \cdot \hat{x}} \right)^2 \qquad (177)$$

at the non-central stationary phase points. Next, the value of η is

$$\eta = \operatorname{sgn}\{h''(x_c)\} = -\operatorname{sgn}\left\{\frac{\rho^d(Q_c)}{s_c\left[\rho^d(Q_c)+s_c\right]}\right\}. \tag{178}$$

The last items required for the uniform asymptotic expansion are the amplitude functions evaluated at the central

$$\mathcal{F}(x_c) = \frac{\widetilde{D}_h(Q_c)}{s_c} \tag{179}$$

and non-central

$$\mathcal{F}(x_{nc}) = \frac{\widetilde{D}_h(Q_{nc})}{s_{nc}\sin\beta_{nc}} \tag{180}$$

stationary phase points. Finally, substituting (173), (174) and (176) through (180) into (171) and simplifying, we obtain

$$\begin{aligned}
\vec{E}^d(P) \;\sim\; & \vec{E}^i(Q_c)\cdot\overline{\overline{D}}^L(Q_c)\sqrt{\frac{\rho^d(Q_c)}{s_c\left[\rho^d(Q_c)+s_c\right]}}\,e^{-jks_c} \\
+\; & \vec{E}^i(Q_{nc}^+)\cdot\overline{\overline{D}}^L(Q_{nc}^+)\sqrt{\frac{\rho^d(Q_{nc}^+)}{s_{nc}\left[\rho^d(Q_{nc}^+)+s_{nc}\right]}}\,e^{-jks_{nc}} \\
+\; & \vec{E}^i(Q_{nc}^-)\cdot\overline{\overline{D}}^L(Q_{nc}^-)\sqrt{\frac{\rho^d(Q_{nc}^-)}{s_{nc}\left[\rho^d(Q_{nc}^-)+s_{nc}\right]}}\,e^{-jks_{nc}}
\end{aligned} \tag{181}$$

as the asymptotic form of the diffracted field on the lit side of the caustic. The caustic distances $\rho^d(Q_{nc}^+)$ and $\rho^d(Q_{nc}^-)$ are equal because of the symmetry of the geometry. Therefore, $\rho^d(Q_{nc}) = \rho^d(Q_{nc}^+) = \rho^d(Q_{nc}^-)$ will be used for the remainder of this chapter. The dyadic diffraction coefficients for the central and non-central diffraction points are

$$\overline{\overline{D}}^L(Q_c) = -\hat{\psi}'\hat{\psi}\,D_h(Q_c)\,T_c(\xi,0) \tag{182}$$

and

$$\overline{\overline{D}}^L(Q_{nc}) = -\hat{\psi}'\hat{\psi}\,D_h(Q_{nc})\,T_{nc}(\xi,\eta,0), \tag{183}$$

respectively. The diffraction coefficient $D_h(Q_e)$ is identical to the UTD half-plane diffraction coefficient. Also, the caustic correction transition functions $T_c(\xi,0)$ and $T_{nc}(\xi,\eta,0)$ are those defined in (655) and (656) of Appendix B, respectively.

Two important facts can be observed about the result in (181). It was observed that the uniform asymptotic expansion consists of the non-uniform expansions for the

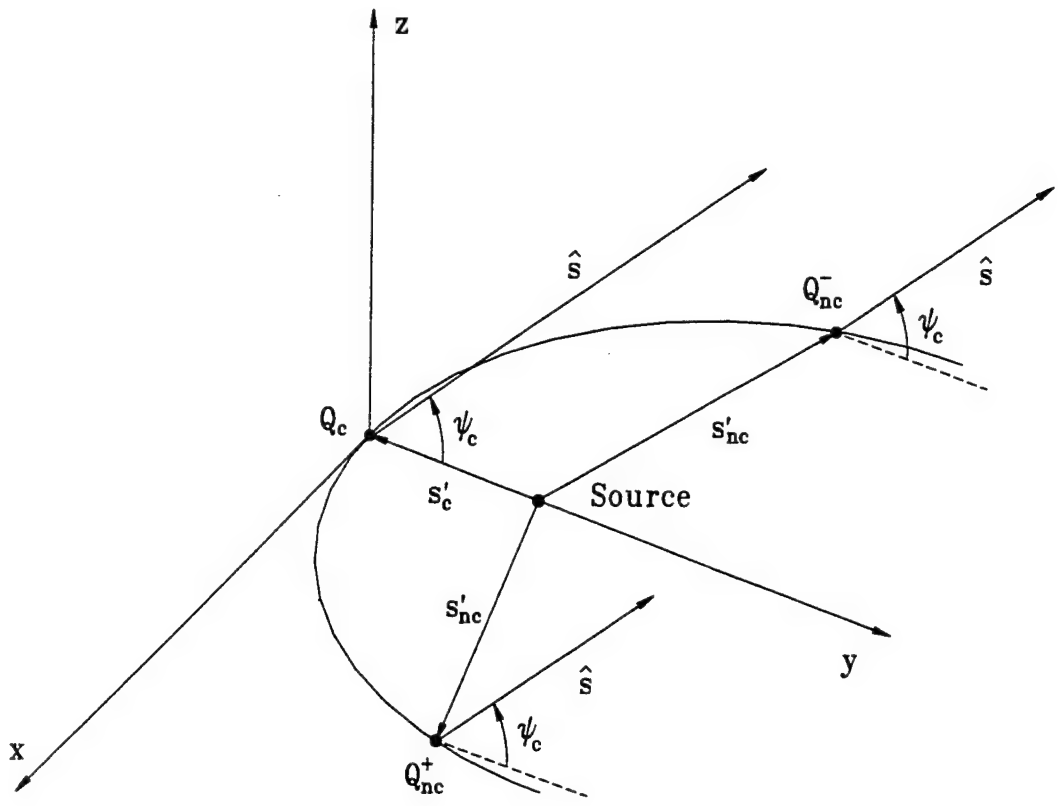

Figure 15: Caustic lit region diffracted ray geometry for the radiation by a source on a flat plate with a curved edge.

central and non-central stationary phase points multiplied by the transition functions $T_c(\xi, 0)$ and $T_{nc}(\xi, \eta, 0)$, respectively. This is also true for the diffracted field as expected. Also, since the non-uniform contributions and the transition functions form a reciprocal result we can use this fact for the case where the source is located on the plate.

We are now in a position to use reciprocity to obtain the field radiated by a source on the flat plate. The radiated field ray structure shown in Figure 15. To obtain the reciprocal set of diffracted field expressions, we begin by noting that the factor $\frac{e^{-jkR_c}}{R_c}$, where R_c is the distance from the central diffraction to the far-zone point, has been suppressed in the plane wave incidence case. This factor must be reintroduced in order to obtain the standard ray optical form. Also, s and ψ must be interchanged with s' and ψ', respectively. Next, the amplitude spreading factor must be rewritten

as

$$\sqrt{\frac{\rho^d}{s[\rho^d+s]}} = \frac{\sqrt{\rho^d}}{s'} \tag{184}$$

where the caustic distance is now determined using (10) of Chapter 2. The field radiated by a source on a flat plate can be rewritten as

$$\begin{aligned}
\vec{E}^d(P) \;\sim\; & \left\{\vec{E}^i(0)\,\frac{e^{-jks'_c}}{s'_c}\right\}\cdot\overline{\overline{D}}^L(Q_c)\sqrt{\rho^d(Q_c)}\,\frac{e^{-jkR_c}}{R_c} \\
+\; & \left\{\vec{E}^i(0)\,\frac{e^{-jks'_{nc}}}{s'_{nc}}\right\}\cdot\overline{\overline{D}}^L(Q^+_{nc})\sqrt{\rho^d(Q_{nc})} \\
& \qquad\times\frac{e^{-jk[R_c-\hat{s}\cdot\vec{r}_e(Q_{nc})]}}{R_c} \\
+\; & \left\{\vec{E}^i(0)\,\frac{e^{-jks'_{nc}}}{s'_{nc}}\right\}\cdot\overline{\overline{D}}^L(Q^-_{nc})\sqrt{\rho^d(Q_{nc})} \\
& \qquad\times\frac{e^{-jk[R_c-\hat{s}\cdot\vec{r}_e(Q_{nc})]}}{R_c}
\end{aligned} \tag{185}$$

where the far-zone approximation

$$R_{nc} \approx \begin{cases} R_c - \hat{s}\cdot\vec{r}_e(Q_{nc}) & \text{; for phase terms} \\ R_c & \text{; for amplitude terms} \end{cases} \tag{186}$$

can be used to rewrite the diffracted field expression in the standard form. Also, R_{nc} is the distance from the non-central diffraction points to the far-zone point. Therefore, the field radiated by a source on a flat plate is

$$\begin{aligned}
\vec{E}^d(P) \;\sim\; & \vec{E}^i(Q_c)\cdot\overline{\overline{D}}^L(Q_c)\sqrt{\rho^d(Q_c)}\,\frac{e^{-jkR_c}}{R_c} \\
+\; & \vec{E}^i(Q^+_{nc})\cdot\overline{\overline{D}}^L(Q^+_{nc})\sqrt{\rho^d(Q_{nc})}\,\frac{e^{-jkR_{nc}}}{R_{nc}} \\
+\; & \vec{E}^i(Q^-_{nc})\cdot\overline{\overline{D}}^L(Q^-_{nc})\sqrt{\rho^d(Q_{nc})}\,\frac{e^{-jkR_{nc}}}{R_{nc}}
\end{aligned} \tag{187}$$

which is again consistent with the UTD diffracted field expressions. The dyadic diffraction coefficients used here are those given in (182) and (183) except the reciprocal forms of ξ and $D_h(Q_e)$ must be used. Substituting (184) into (178) we find that

$$\eta = -\operatorname{sgn}\left\{\rho^d(Q_c)\right\} \tag{188}$$

where $\rho^d(Q_c)$ is found using (10) of Chapter 2 and

$$\xi = \left|\sqrt{2k[\hat{s}\cdot\vec{r}_e(Q_{nc}) - s'_{nc} + s'_c]}\right| e^{-j3\eta\pi/4} \tag{189}$$

for use in the caustic correction transition functions. Next, using reciprocity and recalling that the source is located on the face of the plate, $\Psi^{\mp} = \mp\psi$. Substituting this into the hard polarized half-plane diffraction coefficient we obtain,

$$D_h(Q_e) = \frac{-e^{-j\pi/4}}{2\sqrt{2\pi k}\sin\beta}\sec\left(\frac{\psi}{2}\right) F[kLa(\psi)] \tag{190}$$

where

$$L = s'\sin^2\beta, \tag{191}$$

$$a(\psi) = 2\cos^2\left(\frac{\psi}{2}\right) \tag{192}$$

and a factor of $\frac{1}{2}$ has been included because the incident and reflection shadow boundaries overlap.

4 The Uniform Asymptotic Expansion of the Diffracted Field Integral Equation in the Caustic Shadow Region

The field in the caustic shadow region must also be determined in order to obtain a uniform asymptotic expression for the diffraction by a curved edge. This asymptotic expansion must be performed in a way that is consistent with the expansion on the lit side in order to obtain a uniform result. This section is devoted to the asymptotic expansion of the diffracted field integral equation for the shadow side of the caustic.

It is assumed that only one diffraction point exists in the caustic shadow region as shown in Figure 16. This occurs because the two non-central diffraction points have coalesced and disappeared. The uniform asymptotic expansion derived in Section 3 of Appendix B can be utilized with these assumptions in mind.

First, $m = 0$ in (614) of Appendix B because the integrand of the integral in (168) does not contain a zero at the central stationary phase point. As explained in Section 1 of Appendix B, if the integral has one real stationary phase point and two

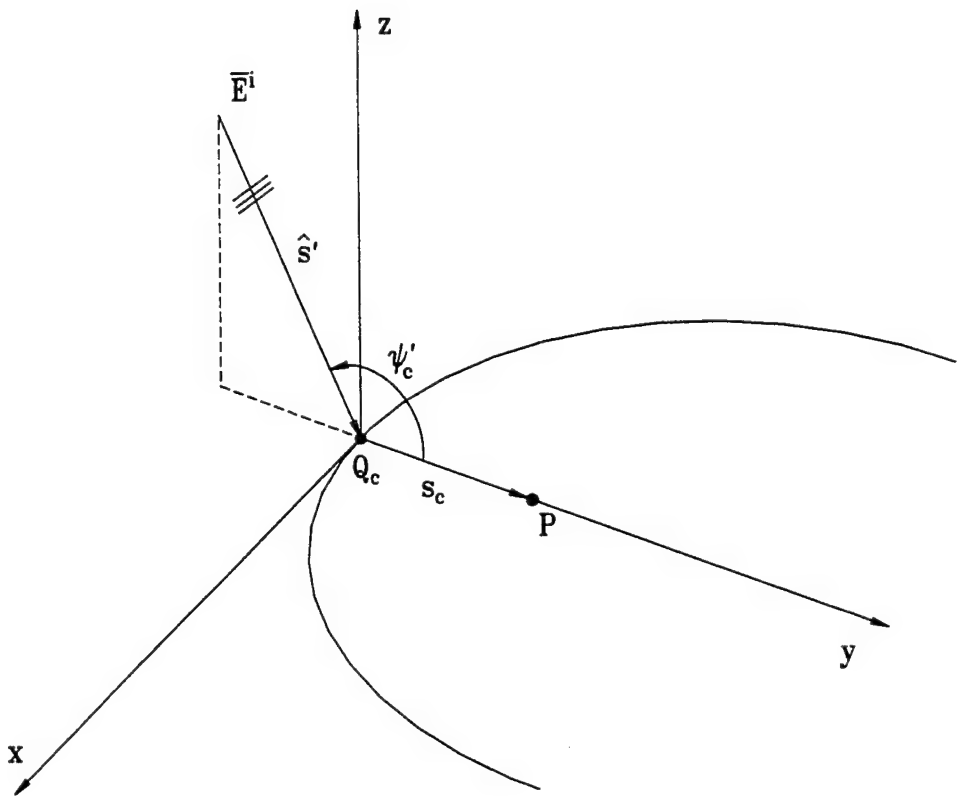

Figure 16: Reciprocal ray geometry for the diffraction by a curved edge in the caustic shadow region.

complex conjugate stationary phase points, then $\mu = \eta$ where $\mu = \text{sgn}\{h^{\text{IV}}(x_c)\}$ and $\eta = \text{sgn}\{h^{\text{II}}(x_c)\}$. Finally, it is assumed that $k \gg 1$ and $\mathcal{F}(x_e)$ is a smooth and slowly varying function of x_e about the central stationary phase point. From (673) of Appendix B the diffracted field integral equation in (168) can be approximated as

$$\begin{aligned}
\vec{E}^d(P) &= \widehat{\psi}\, E^i_{\psi_c} \frac{1}{2\pi} \int_{-\infty}^{\infty} \mathcal{F}(x_e) e^{jkh(x_e)} dx_e \\
&\sim \widehat{\psi}\, E^i_{\psi_c} \frac{\mathcal{F}(x_c)}{2\pi} \left| \sqrt{\frac{2\pi}{kh^{\text{II}}(x_c)}} \right| e^{j\eta\pi/4} e^{jkh(x_c)} T_s(\xi, 0) \\
&+ \widehat{\psi}\, E^i_{\psi_c} \frac{1}{2\pi} \frac{\sqrt{2\pi}}{2|kh^{\text{II}}(x_c)|^{3/2}} e^{j3\eta\pi/4} e^{jkh(x_c)} \\
&\qquad \times \left\{ \mathcal{F}^{\text{II}}(x_c) + \frac{1}{4} C(x_c) \mathcal{F}(x_c) \right\} T_s(\xi, 2)
\end{aligned} \tag{193}$$

where the function $C(x_c)$ is defined as

$$C(x_c) = \frac{3|kh^{\text{II}}(x_c)|}{|\xi|^2} - \frac{h^{\text{IV}}(x_c)}{h^{\text{II}}(x_c)} \tag{194}$$

and the argument of the caustic correction transition functions is

$$\xi = \left| \sqrt{2k[h(x_{nc}) - h(x_c)]} \right| e^{-j\eta\pi/4} \tag{195}$$

from (626) of Appendix B. It is easily shown using (753a) and (764a) of Appendix D that the value of the phase function is

$$h(x_c) = -s_c \tag{196}$$

at the central stationary phase point and using (756a) and (765a) of Appendix D that the value of the phase function is

$$h(x_{nc}) = -\widehat{s}' \cdot \vec{r}_e(Q_{nc}) - s_{nc} \tag{197}$$

at the non-central stationary phase points. The argument of the transition functions becomes

$$\xi = \left| \sqrt{2k[-\widehat{s}' \cdot \vec{r}_e(Q_{nc}) - s_{nc} + s_c]} \right| e^{-j\eta\pi/4} \ . \tag{198}$$

using these in (195). Also, from (753c) and (764c) of Appendix D the second derivative of the phase function is

$$h^{\text{II}}(x_c) = -\left[\frac{1}{s_c} + \frac{1}{\rho^d(Q_c)} \right] \tag{199}$$

at the central stationary phase point which makes

$$\eta = \text{sgn}\left\{h^{II}(x_c)\right\} = -\,\text{sgn}\left\{\frac{\rho^d(Q_c)}{s_c\left[\rho^d(Q_c)+s_c\right]}\right\}. \tag{200}$$

The next item required for the uniform asymptotic expansion is

$$\mathcal{F}(x_c) = \frac{\widetilde{D}_h(Q_c)}{s_c} \tag{201}$$

which is the amplitude function of the integral evaluated at the central diffraction point. It is now advantageous to write $\mathcal{C}(x_c)$ in terms of the derivatives of the phase function with respect to arc length. Therefore, recalling (764c) and (766) from Appendix D we find that

$$\mathcal{C}(x_c) = \mathcal{C}(l_c) - 4\kappa_g^2(Q_c) \tag{202}$$

where

$$\mathcal{C}(l_c) = \frac{3|kh^{II}(l_c)|}{|\xi|^2} - \frac{h^{IV}(l_c)}{h^{II}(l_c)} \tag{203}$$

and $h^{II}(l_c)$ and $h^{IV}(l_c)$ are given in (753c) and (753e) of Appendix D, respectively. The final quantity required for the use of the uniform asymptotic expansion is the second derivative of the amplitude function of the integral with respect to x_e. Differentiating (170) twice with respect to x_e and evaluating the second derivative at the central diffraction point, we obtain

$$\mathcal{F}^{II}(x_c) = \frac{1}{s_c}\left.\frac{d^2\widetilde{D}_h(Q')}{dx_e^2}\right|_{Q_c} - \frac{\widetilde{D}_h(Q_c)}{s_c^2}\left\{\left.\frac{d^2r}{dx_e^2}\right|_{Q_c} + s_c\left.\frac{d^2\sin\beta'}{dx_e^2}\right|_{Q_c}\right\} \tag{204}$$

where (767a), (767b), (779a), (779b), (810b) and (811) have been used to simplify the result. Finally, substituting (196) and (199) through (204) into (193) and simplifying, we obtain

$$\begin{aligned}\vec{E}^d(P) \;\sim\; & \vec{E}^i(Q_c)\cdot\overline{\overline{D}}^S(Q_c)\sqrt{\frac{\rho^d(Q_c)}{s_c\left[\rho^d(Q_c)+s_c\right]}}\,e^{-jks_c} \\ +\; & \vec{E}^i(Q_c)\cdot\overline{\overline{D}}^S(Q_c)\sqrt{\frac{\rho^d(Q_c)}{s_c\left[\rho^d(Q_c)+s_c\right]}}\,e^{-jks_c}\end{aligned} \tag{205}$$

as the asymptotic form of the diffracted field on the shadow side of the caustic. The dyadic diffraction coefficients at the central diffraction point are

$$\overline{\overline{D}}^S(Q_c) = -\hat{\psi}'\hat{\psi}\,D_h(Q_c)\,T_s(\xi,0) \tag{206}$$

and

$$\overline{\overline{\mathcal{D}}}^{s}(Q_c) = -\hat{\psi}'\hat{\psi}\,\mathcal{D}_h(Q_c)\,T_s(\xi,2)\,, \tag{207}$$

where the caustic shadow region caustic correction transition functions $T_s(\xi,0)$ and $T_s(\xi,2)$ are defined in (674) of Appendix B. Also, $D_h(Q_c)$ in (206) is the UTD half-plane diffraction coefficient for the hard polarization. The diffraction coefficient $\mathcal{D}_h(Q_c)$ in (207) is given by

$$\mathcal{D}_h(Q_c) = \frac{1}{2jk}\left\{\frac{-e^{-j\pi/4}}{\sqrt{2\pi k}}\,s_c\,\mathcal{F}^{\text{II}}(x_c) + \frac{1}{4}\mathcal{C}(x_c)D_h(Q_c)\right\}\frac{s_c\,\rho^d(Q_c)}{\rho^d(Q_c)+s_c} \tag{208}$$

where $\mathcal{C}(x_c)$ and $\mathcal{F}^{\text{II}}(x_c)$ are defined in (202) and (204), respectively. This expression can now be written in terms of the derivatives with respect to arc length as

$$\begin{aligned}\mathcal{D}_h(Q_c) \;=\; & \frac{1}{2jk}\left\{\frac{-e^{-j\pi/4}}{\sqrt{2\pi k}}\,s_c\,\mathcal{F}^{\text{II}}(l_c) + \frac{1}{4}\mathcal{C}(l_c)D_h(Q_c)\right. \\ & \left. -\kappa_g^2(Q_c)D_h(Q_c)\right\}\frac{s_c\,\rho^d(Q_c)}{\rho^d(Q_c)+s_c}\end{aligned} \tag{209}$$

where

$$\mathcal{F}^{\text{II}}(l_c) = \frac{1}{s_c}\left.\frac{d^2\widetilde{D}_h(Q')}{dl^2}\right|_{Q_c} - \frac{\widetilde{D}_h(Q_c)}{s_c^2}\left\{\left.\frac{d^2\tau}{dl^2}\right|_{Q_c} + s_c\left.\frac{d^2\sin\beta'}{dl^2}\right|_{Q_c}\right\} \tag{210}$$

and $\mathcal{C}(l_c)$ is given in (203). Next, by substituting (767c), (779c) and (812) into (210) we obtain

$$\begin{aligned}\frac{-e^{-j\pi/4}}{\sqrt{2\pi k}}\,s_c\,\mathcal{F}^{\text{II}}(l_c) \;=\; & \frac{d^2D_h(Q_c)}{dl^2} \\ & - D_h(Q_c)\left\{\frac{1}{s_c^2}\left[1-\frac{s_c\cos\psi_c}{\rho_g(Q_c)}\right] - \kappa_g^2(Q_c)\cos^2\psi_c'\right\}\end{aligned} \tag{211}$$

where $D_h(Q_c)$ is the hard polarized UTD half-plane diffraction coefficient and $\frac{d^2D_h(Q_c)}{dl^2}$ is given in (812) of Appendix D. Therefore, substituting (211) into (209) we obtain

$$\begin{aligned}\mathcal{D}_h(Q_c) \;=\; & \frac{1}{2jk}\left\{\frac{d^2D_h(Q_c)}{dl^2} - D_h(Q_c)\left(\frac{1}{s_c^2}\left[1-\frac{s_c\cos\psi_c}{\rho_g(Q_c)}\right]\right.\right. \\ & \left.\left. +\kappa_g^2(Q_c)\sin^2\psi_c' - \frac{1}{4}\mathcal{C}(l_c)\right)\right\}\frac{s_c\,\rho^d(Q_c)}{\rho^d(Q_c)+s_c}\end{aligned} \tag{212}$$

which is the new curvature dependant diffraction coefficient.

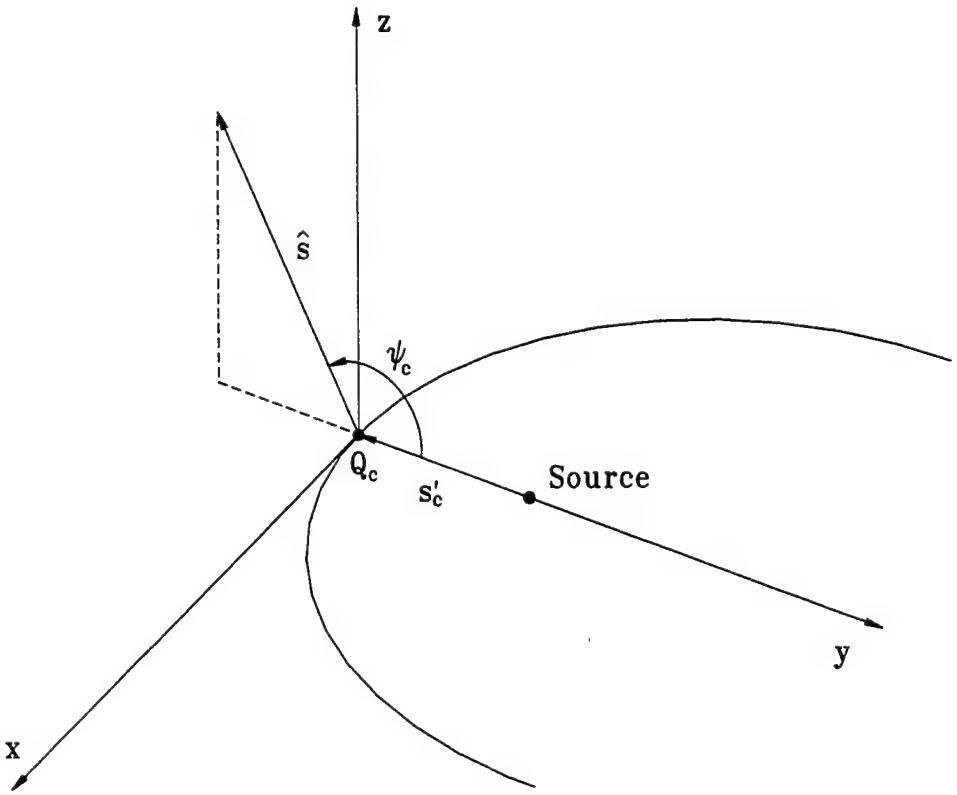

Figure 17: Ray geometry for the diffraction by a curved edge in the caustic shadow region.

We are now in a position to use reciprocity to obtain the field radiated by a source on the flat plate. The radiated field ray structure shown in Figure 17. To obtain the reciprocal set of diffracted field expressions, we begin by noting that the factor $\frac{e^{-jkR_c}}{R_c}$, where R_c is the distance from the central diffraction to the far-zone point, has been suppressed in the plane wave incidence case. This factor must be reintroduced in order to obtain the standard ray optical form. Also, s must be interchanged with s'. Using (184), we can rewrite (205) as

$$\begin{aligned} \vec{E}^d(P) \;\sim\; & \left\{\vec{E}^i(0)\frac{e^{-jks'_c}}{s'_c}\right\}\cdot\overline{\overline{D}}^S(Q_c)\sqrt{\rho^d(Q_c)}\,\frac{e^{-jkR_c}}{R_c} \\ + \; & \left\{\vec{E}^i(0)\frac{e^{-jks'_c}}{s'_c}\right\}\cdot\overline{\overline{D}}^S(Q_c)\sqrt{\rho^d(Q_c)}\,\frac{e^{-jkR_c}}{R_c} \end{aligned} \tag{213}$$

where the caustic distance $\rho^d(Q_c)$ is given by (10) in Chapter 2. Recognizing that the incident field is now a spherical wave

$$\begin{aligned} \vec{E}^d(P) \;\sim\; & \vec{E}^i(Q_c)\cdot\overline{\overline{D}}^S(Q_c)\sqrt{\rho^d(Q_c)}\,\frac{e^{-jkR_c}}{R_c} \\ + \; & \vec{E}^i(Q_c)\cdot\overline{\overline{D}}^S(Q_c)\sqrt{\rho^d(Q_c)}\,\frac{e^{-jkR_c}}{R_c} \end{aligned} \tag{214}$$

which is again consistent with the UTD diffracted field expressions. The dyadic diffraction coefficients used here are those given in (206) and (207) except the reciprocal forms of ξ, $D_h(Q_c)$ and $\mathcal{D}_h(Q_c)$ must be used. Substituting (184) into (200) we find that

$$\eta = -\operatorname{sgn}\left\{\rho^d(Q_c)\right\} \tag{215}$$

where $\rho^d(Q_c)$ is found using (10) of Chapter 2 and

$$\xi = \left|\sqrt{2k[\hat{s}\cdot\vec{r}_e(Q_{nc}) - s'_{nc} + s'_c]}\right| e^{-j\eta\pi/4} \tag{216}$$

for use in the caustic correction transition functions. Next, using reciprocity and recalling that the source is located on the face of the plate, $\Psi^{\mp} = \mp\psi$. Substituting this into the hard polarized half-plane diffraction coefficient we obtain,

$$D_h(Q_c) = \frac{-e^{-j\pi/4}}{2\sqrt{2\pi k}}\sec\left(\frac{\psi_c}{2}\right)F[ks'_c a(\psi_c)] \tag{217}$$

where

$$a(\psi_c) = 2\cos^2\left(\frac{\psi_c}{2}\right) \tag{218}$$

and a factor of $\frac{1}{2}$ has been included because the incident and reflection shadow boundaries overlap. Finally, it is necessary to determine the reciprocal form of $\mathcal{D}_h(Q_c)$ given in (212). By interchanging ψ_c with ψ_c', s_c with s_c' and recalling that the source is located on the face of the plate we obtain

$$\begin{aligned}\mathcal{D}_h(Q_c) &= \frac{\rho^d(Q_c)}{2jk}\left\{\frac{d^2D_h(Q_c)}{dl^2} - D_h(Q_c)\left(\frac{1}{(s_c')^2}\left[1-\frac{s_c'}{\rho_g(Q_c)}\right]\right.\right. \\ &\qquad \left.\left. + \kappa_g^2(Q_c)\sin^2\psi_c - \frac{1}{4}\mathcal{C}(l_c)\right)\right\}\end{aligned} \tag{219}$$

where $\rho^d(Q_c)$ is found using (10) of Chapter 2 and $D_h(Q_c)$ is given in (217). Also, $\mathcal{C}(l_c)$ is given in (203) where the reciprocal forms of $h^{\text{II}}(l_c)$ and $h^{\text{IV}}(l_c)$ are

$$h^{\text{II}}(l_c) = \frac{-1}{\rho^d(Q_c)} \tag{220}$$

from (753c) of Appendix D and

$$\begin{aligned}h^{\text{IV}}(l_c) &= \left[\kappa_g^{\text{II}}(Q_c) - \kappa_g^3(Q_c)\right](1+\cos\psi_c) + \frac{\kappa_g^2(Q_c)}{s_c'} \\ &\qquad + \frac{1}{(s_c')^3}\left[1-\frac{s_c'}{\rho_g(Q_c)}\right]^2\end{aligned} \tag{221}$$

from (753e); respectively, where again $\rho^d(Q_c)$ is found using (10) of Chapter 2. Finally, substituting (818) into (814) of Appendix D we find that

$$D_h^{(I)}(Q_c) = \frac{\cos\psi_c(1-\cos\psi_c)}{2\rho_g^2(Q_c)}\, D_h^{(II)}(Q_c) \tag{222}$$

where

$$D_h^{(II)}(Q_c) = \frac{-e^{-j\pi/4}}{2\sqrt{2\pi k}}\sec\left(\frac{\psi_c}{2}\right) F_s[ks_c'a(\psi_c)] \tag{223}$$

and $a(\psi_c)$ is given in (218). Also, a factor of $\frac{1}{2}$ has been included in (223) because the incident and reflection shadow boundaries overlap. Substituting (217), (222) and (223) into (812) of Appendix D we obtain

$$\frac{d^2D_h(Q_c)}{dl^2} = \left\{\frac{\cos\psi_c(1-\cos\psi_c)}{2\rho_g^2(Q_c)}\right\} D_h^{(II)}(Q_c)$$

$$+ \left\{ \frac{1}{2(s_c')^2} \left[1 - \frac{s_c'}{\rho_g(Q_c)} \right] - \frac{1}{(s_c')^2} \left[1 - \frac{s_c'}{\rho_g(Q_c)} \right]^2 \right\}$$
$$\times \left[D_h(Q_c) - D_h^{(II)}(Q_c) \right] \tag{224}$$

which is the last item required for the curvature dependant diffraction coefficient in (219). These equations can now be used to calculate the diffracted field on the shadow side of the caustic.

SECTION 6

Numerical Calculation of the Field Radiated by a Short Monopole on a Flat Plate with a Curved Edge

It is important to numerically confirm that the caustic corrected UTD (CC-UTD) solution derived in Chapter 5 is accurate. To do so, two geometries are considered in this chapter. First, the radiation by a monopole mounted on a flat plate with a curved edge defined by a parabolic equation is determined. This CC-UTD solution is then compared to the classical UTD solution. The other geometry considered is the radiation by a monopole on an elliptic disk. The CC-UTD solution is compared to the classical UTD solution and a Moment Method (MM) solution. This chapter is devoted to the numerical confirmation of the CC-UTD solution of Chapter 5.

1 Radiation of a Short Monopole on a Flat Plate with an Edge Defined by a Parabolic Equation

The first geometry to be studied is the radiation by a monopole on a flat plate with an edge defined by a parabolic equation. To conform to the assumptions of the derivation of the CC-UTD in Chapter 5 it is important that the monopole is mounted along the symmetry axis of the parabolic edge. Also, the radiation pattern must be taken in the plane of symmetry of the parabolic edge. This geometry is shown in Figure 18. This section consists of two parts. First, the parameters required for the CC-UTD

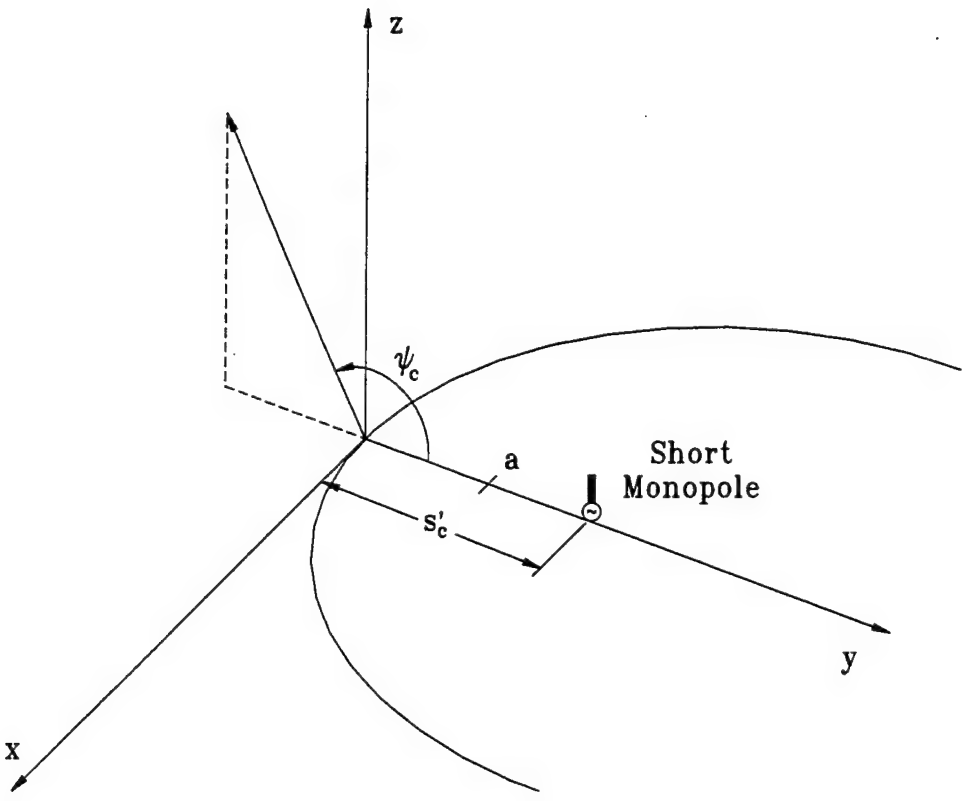

Figure 18: Geometry for the radiation of a short monopole on a flat plate with a curved edge defined by a parabolic equation.

and the UTD solutions are determined. Next, the radiated field is calculated and compared.

1.1 Parabolic Edge Radiated Field Parameters

In order to determine the geometric parameters required for the use of the CC-UTD and the UTD, the edge of the plate will be defined as

$$x_e^2 = 4ay_e \tag{225}$$

where a is the focal length of the parabola. First, the diffraction points can be determined by enforcing the fact that $\cos\beta = \cos\beta'$. In doing so, the central diffraction point is found to be located at

$$y_c = 0 \tag{226}$$

and the non-central diffraction points are found to be located at

$$y_{nc} = \begin{cases} y_o + \varepsilon_c\sqrt{(s_c')^2 - (y_o)^2}\,\cot\psi_c & ;\text{ if } s_c' > a \\ y_o - j\varepsilon_c\sqrt{(y_o)^2 - (s_c')^2}\,\cot\psi_c & ;\text{ if } s_c' < a \end{cases} \tag{227}$$

where $y_o = s_c' - 2a$, $\varepsilon_c = \text{sgn}\{\sin\psi_c\}$ and the monopole location s_c' is fixed. Using this result it is easy to determine the caustic lit and caustic shadow regions. If $y_{nc} > 0$ the far-zone point is in the caustic lit region and if $y_{nc} < 0$ the far-zone point is in the caustic shadow region. Also, the distance from the monopole to the non-central diffraction point is

$$s_{nc}' = \frac{y_{nc} - y_o}{\cos\psi_c}\,. \tag{228}$$

The next quantities needed are the curvature and the second derivative of the curvature at the diffraction points. The curvature of the edge is defined as [33]

$$\kappa_g(Q') = \frac{|y_e''|}{[1 + (y_e')^2]^{3/2}} \tag{229}$$

where using (225) it is easy to show that

$$\kappa_g(Q') = \frac{1}{2a}\left(\frac{a}{a + y_e}\right)^{3/2} \tag{230}$$

for a point on the parabolic edge. Next, evaluating (230) at the central and non-central diffraction points we obtain

$$\kappa_g(Q_c) = \frac{1}{2a} \tag{231}$$

and

$$\kappa_g(Q_{nc}) = \frac{1}{2a}\left(\frac{a}{a+y_{nc}}\right)^{3/2}, \tag{232}$$

respectively. Also, differentiating (230) twice with respect to x_e and evaluating it at the central diffraction point we obtain

$$\kappa_g^{II}(Q_c) = -3\kappa_g^3(Q_c) = \frac{-3}{(2a)^3}\,. \tag{233}$$

It is now necessary to determine the diffraction angles ψ and β at each of the diffraction points. The value of ψ at the central diffraction point is ψ_c, the angle used to specify the pattern and $\beta_c = \beta_c' = \frac{\pi}{2}$. The angle $\beta_{nc} = \beta_{nc}'$ at the non-central diffraction points is found using $\cos\beta_{nc} = \hat{s}_c \cdot \hat{e}$ which results in

$$\sin\beta_{nc} = \sqrt{\frac{a + y_{nc}\sin^2\psi_c}{a+y_{nc}}}\,. \tag{234}$$

The angle ψ at the non-central diffraction points is found to be

$$\cos\psi_{nc} = \frac{2a\cos\psi_c}{\sin\beta_{nc}\sqrt{(2a)^2 + 4ay_{nc}}}\,. \tag{235}$$

Next, it is important to determine the distance to the second caustic of the central and non-central diffraction points. To do so, we recall (10) from Chapter 2 to find

$$\rho^d(Q_c) = \frac{2as_c'}{2a - s_c'(1+\cos\psi_c)} \tag{236}$$

as the caustic distance at the central diffraction point, and

$$\rho^d(Q_{nc}) = \frac{(a+y_{nc})\,s_{nc}'\sin^2\beta_{nc}}{(a+y_{nc})\sin^2\beta_{nc} - a} \tag{237}$$

as the second caustic distance at the non-central diffraction points. Also noting that

$$\hat{s}_c \cdot \vec{r}_e(Q_{nc}) = y_{nc}\cos\psi_c, \tag{238}$$

we are able to determine the argument of the caustic correction transition functions and the far-zone approximation for the non-central diffraction points. Finally, it is necessary to determine the Geometrical Optics (GO) field and the incident field at each of the diffraction points. It is commonly known that the field radiated by a short monopole on an infinite ground plane is [35, 36]

$$\vec{E}(P) = -\hat{\theta} E_o \sin\theta \, \frac{e^{-jkR}}{R} \, \mathrm{U}\left[\frac{\pi}{2} - \theta\right] \tag{239}$$

where

$$E_o = \frac{Z_c I_o k d}{2\pi j} = -j60 I_o k d \tag{240}$$

and R is the distance from the monopole to the far-zone observation point. Also, Z_c is the impedance of free space, I_o is the current on the monopole and d is the length of the monopole. Using (239) we find that

$$\vec{E}^i(Q_c) = \hat{\psi}' E_o \frac{e^{-jks'_c}}{s'_c} \tag{241}$$

is the field incident at the central diffraction point and

$$\vec{E}^i(Q_{nc}) = \hat{\psi}' E_o \frac{e^{-jks'_{nc}}}{s'_{nc}} \tag{242}$$

is the field incident at the non-central diffraction points. Next, using the far-zone approximation

$$R \approx \begin{cases} R_c - s'_c \cos\psi_c & \text{; for phase terms} \\ R_c & \text{; for amplitude terms} \end{cases} \tag{243}$$

in (239), the GO field is given by

$$\vec{E}^{GO}(P) = \hat{\psi}_c E_o \cos\psi_c \, e^{jks'_c \cos\psi_c} \frac{e^{-jkR_c}}{R_c} \, \mathrm{U}[\pi - \psi_c]. \tag{244}$$

Now that we have the GO field and the necessary diffracted field parameters, the diffracted field can be calculated using the expressions derived in Chapter 5. Using (4a) of Chapter 2 we find

$$\hat{\psi} = \frac{-\hat{\beta}_c (x_{nc} \sin\psi_c) + \hat{\psi}_c (2a)}{\sin\beta_{nc} \sqrt{(2a)^2 + 4a y_{nc}}} \tag{245}$$

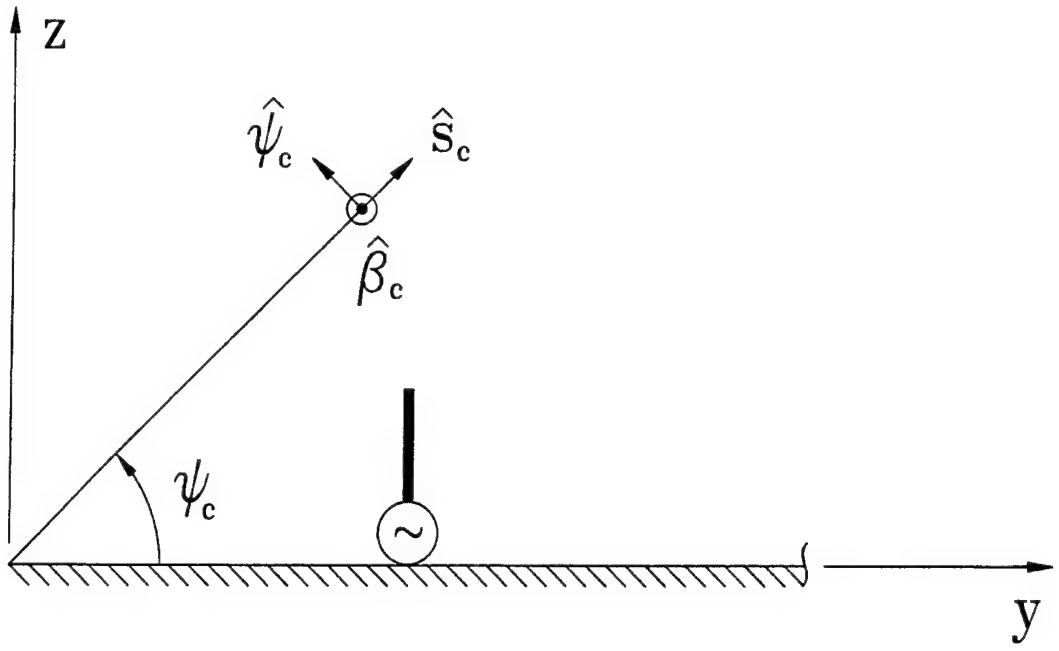

Figure 19: Polarization unit vector directions for the radiation by a short monopole on a flat plate with a parabolic edge.

at the non-central diffraction points. These polarization vectors are shown in Figure 19. The $\hat{\beta}_c$ components of each of the non-central diffraction points will cancel leaving only the $\hat{\psi}_c$ components since the non-central diffraction points are symmetrically located. Therefore, the diffracted field in the caustic lit region (i.e., $y_{nc} > 0$) is

$$\begin{aligned}\vec{E}^d(P) \;\sim\; & \hat{\psi}_c \left\{ -E_o \frac{e^{-jks'_c}}{s'_c} \right\} D_h(Q_c)\, T_c(\xi, 0) \sqrt{\rho^d(Q_c)}\, \frac{e^{-jkR_c}}{R_c} \\ & + \hat{\psi}_c\, 2 \left\{ E_o \frac{-2a}{\sin\beta_{nc}\sqrt{(2a)^2 + 4ay_{nc}}} \frac{e^{-jks'_{nc}}}{s'_{nc}} \right\} \\ & \times D_h(Q_{nc})\, T_{nc}(\xi, \eta, 0) \sqrt{\rho^d(Q_{nc})}\, e^{jky_{nc}\cos\psi_c}\, \frac{e^{-jkR_c}}{R_c} \end{aligned} \tag{246}$$

where (187) has been used in conjunction with the diffracted field parameters found previously in this subsection. Also, the diffraction coefficient is given by (190) through (192) of Chapter 5, the argument of the caustic correction transition functions is

$$\xi = \left| \sqrt{2k[y_{nc}\cos\psi_c - s'_{nc} + s'_c]} \right| e^{-j3\eta\pi/4} \tag{247}$$

from (189) and η is given in (188) of Chapter 5. Next, the diffracted field in the caustic shadow region (i.e., $y_{nc} < 0$) is

$$\begin{aligned}\vec{E}^d(P) \;\sim\; & \hat{\psi}_c \left\{ -E_o \frac{e^{-jks'_c}}{s'_c} \right\} D_h(Q_c)\, T_s(\xi, 0) \sqrt{\rho^d(Q_c)}\, \frac{e^{-jkR_c}}{R_c} \\ + \; & \hat{\psi}_c \left\{ -E_o \frac{e^{-jks'_c}}{s'_c} \right\} \mathcal{D}_h(Q_c)\, T_s(\xi, 2) \sqrt{\rho^d(Q_c)}\, \frac{e^{-jkR_c}}{R_c} \end{aligned} \tag{248}$$

where (214) has been used in conjunction with the diffracted field parameters found previously in this subsection. Also, the diffraction coefficient $D_h(Q_c)$ is given by (217) and (218) of Chapter 5 and $\mathcal{D}_h(Q_c)$ is given by (203), (217) through (221), (223) and (224) of Chapter 5. The argument of the caustic correction transition functions is

$$\xi = \left| \sqrt{2k[y_{nc} \cos\psi_c - s'_{nc} + s'_c]} \right| e^{-j\eta\pi/4} \tag{249}$$

from (216) and η is given in (215) of Chapter 5. These formulas now form a complete CC-UTD solution. The sum of the GO field and the diffracted field corresponding to either the caustic lit region or the caustic shadow region give the total radiated field.

1.2 Numerical Calculation of the Field Radiated by a Short Monopole on a Flat Plate with a Curved Edge Defined by a Parabolic Equation

The numerical calculation of the radiated field expressions derived in Subsection 1.1 confirms the uniformity of the CC-UTD. This also leads to some insight into the physical phenomenology involved in this problem and the CC-UTD formulation. The CC-UTD formulation is compared to the classical UTD solution to illustrate their differences. This subsection is devoted to the numerical calculation of the field radiated by a short monopole on a flat plate with a parabolic edge.

From (227) it is easily seen that if $s'_c < a$ the non-central diffraction points have a complex y location. This means that there is no caustic lit region for this case and the classical UTD solution is valid. Also, if $s'_c \approx a$ there are an infinite number of diffraction points when the observation is taken along the face of the plate since the edge is defined by a parabolic equation. This type of ray structure has not been considered here. Therefore, only the case where $s'_c > a$ will be considered in this

subsection. The quantity to be plotted throughout this subsection is

$$E\,(\mathrm{dB}) = 20\log_{10}\left|\hat{\psi}_c \cdot \vec{E}(P)\right| \tag{250}$$

where $\vec{E}(P)$ is the radiated field component. The factor $E_o \frac{e^{-jkR_c}}{R_c}$ is common to all of the ray optical expressions and will be suppressed in all the calculations in this subsection.

For the sake of discussion, the central ray diffracted field is the first term in (246) when P is in the caustic lit region or the first term of (248) when P is in the caustic shadow region. These terms are labeled this way because they are the same except the caustic correction transition functions differ on the lit and shadow sides of the caustic. The non-central ray diffracted field is the second term in (246) in the caustic lit region. Finally, the curvature dependant central ray diffracted field is the second term in (248). Although this diffracted field has a similar form as the central ray diffracted field, it has a different curvature dependant diffraction coefficient and a different caustic correction transition function.

The first case considered here consists of a flat plate with a parabolic edge with a focal length of $a = 3\lambda$ and a monopole location of $s_c' = 5\lambda$ as shown in Figure 18. We begin by looking at the GO field and the central ray, the curvature dependant central ray and the non-central ray diffracted fields as shown in Figure 20. Several interesting facts about the CC-UTD can be seen from this plot.

First, as discussed in Chapter 5, the Incident Shadow Boundary (ISB) and the Reflection Shadow Boundary (RSB) overlap and occur at $\psi_c = \pi$. The Caustic Boundaries (CB) occur when the amplitude spreading factor of the diffracted field expressions becomes singular. Therefore, equating the denominator of (236) to zero,

$$\cos\psi_{\mathrm{CB}} = \left\{\frac{2a}{s_c'} - 1\right\} \tag{251}$$

are the locations of the CB's. The CB's occur at $\psi_{\mathrm{CB}} = 78.4630^\circ,\ 281.5370^\circ$ for the dimensions chosen here. These values are shown in Figure 20. It is also easy to see how the solutions on the lit and shadow sides of the caustic differ. The central ray and curvature dependant central ray diffracted fields are each bounded in the caustic

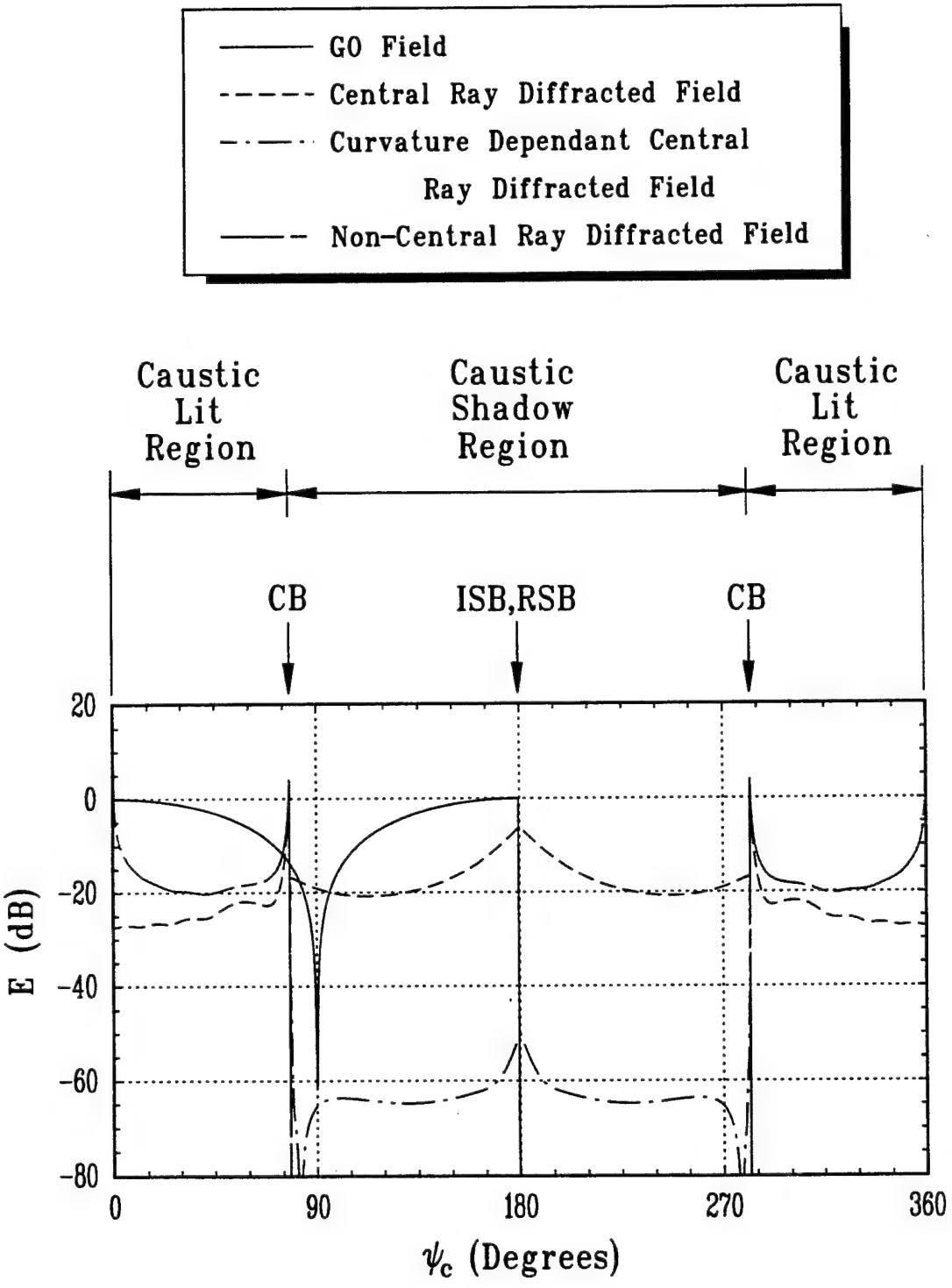

Figure 20: Diffracted field components for a plate with a focal length of $a = 3\lambda$ and a monopole location of $s'_c = 5\lambda$.

shadow region. In this region, the curvature dependant central ray diffracted field can be viewed as a correction to the central ray diffracted field. However, the central ray and non-central ray diffracted field contributions are each singular in the caustic lit region. The central ray diffracted field contribution has a singularity that opposes the singularity in the non-central ray diffracted field. These singularities cancel and the proper field is obtained in the caustic lit region when these two contributions are added to obtain the total diffracted field.

Another interesting effect that appears in Figure 20 is that the non-central diffracted field is infinite along the face of the plate. To explain this phenomena; (227), (228) and (234) can be used to obtain

$$s'_{nc}\sin^2\beta_{nc} = \frac{(s'_c-2a)\sin\psi_c+\varepsilon_c\sqrt{(s'_c)^2-(y_o)^2}\,\cos\psi_c}{(s'_c-a)\sin\psi_c+\varepsilon_c\sqrt{(s'_c)^2-(y_o)^2}\,\cos\psi_c} \times\sqrt{(s'_c)^2-(y_o)^2}\,|\sin\psi_c| \tag{252}$$

which is proportional to the large parameter used in the asymptotic expansion of the double spectral integral form of the ITD diffracted field. Next, we find that

$$\lim_{\psi_c\to 0,2\pi}\frac{(s'_c-2a)\sin\psi_c+\varepsilon_c\sqrt{(s'_c)^2-(y_o)^2}\,\cos\psi_c}{(s'_c-a)\sin\psi_c+\varepsilon_c\sqrt{(s'_c)^2-(y_o)^2}\,\cos\psi_c}=1 \tag{253}$$

which makes

$$ks'_{nc}\sin^2\beta_{nc}\approx 2k\sqrt{a\,(s'_c-a)}\,|\sin\psi_c| \tag{254}$$

as the observation point approaches the face of the plate. This result clearly shows that the large parameter used in the asymptotic expansion of the double spectral integral form of the ITD diffracted field becomes very small near the face of the plate. Therefore, this asymptotic expansion is invalid in these directions. This is not a failure of the ITD or the CC-UTD, it is simply an effect that has been neglected. Also, $\sin\beta_{nc}\to 0$ near the face of the plate since $\sin^2\beta_{nc}$ approaches zero faster than s'_{nc} approaches infinity. When $\sin\beta_{nc}\to 0$ the plate will support waves that travel along its edge. These waves are commonly called edge waves. This geometry can support edge waves because in is semi-infinite in extent. Edge waves will not be supported by most practical geometries and therefore are not a major problem.

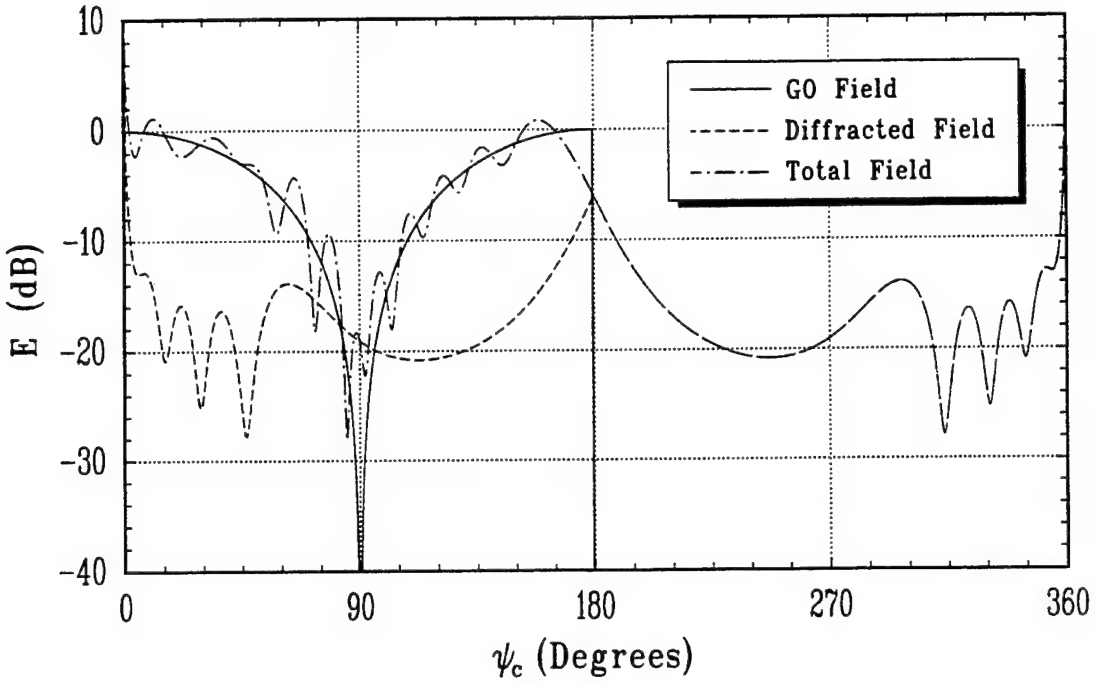

Figure 21: Radiated field components for a plate with a focal length of $a = 3\lambda$ and a monopole location of $s'_c = 5\lambda$.

The diffracted field components can now be added to obtain the total diffracted field. The GO, diffracted and total fields are shown in Figure 21. This figure clearly shows that the diffracted field is not only bounded near the caustic, but it is also smooth and continuous. Therefore, the CC-UTD is uniform across the caustics of the diffracted field. It is also clear that the diffracted field retains a discontinuity along the incident and reflection shadow boundary. Adding the GO field and the diffracted field, we see that the total radiated field is smooth and continuous everywhere.

Finally, Figure 22 shows a comparison between the CC-UTD solution and the UTD solution. This figure shows that the CC-UTD solution corrects for the caustics of the UTD solution. It also shows that the CC-UTD solution smoothly reduces to the UTD solution away from the caustics. This is one of the requirements of a uniform solution.

As another example, Figure 23 shows a comparison between the CC-UTD solution and the UTD solution for a plate with a focal length of $a = 3.5\lambda$ and a monopole location of $s'_c = 10\lambda$. This figure shows that the CC-UTD solution corrects for the

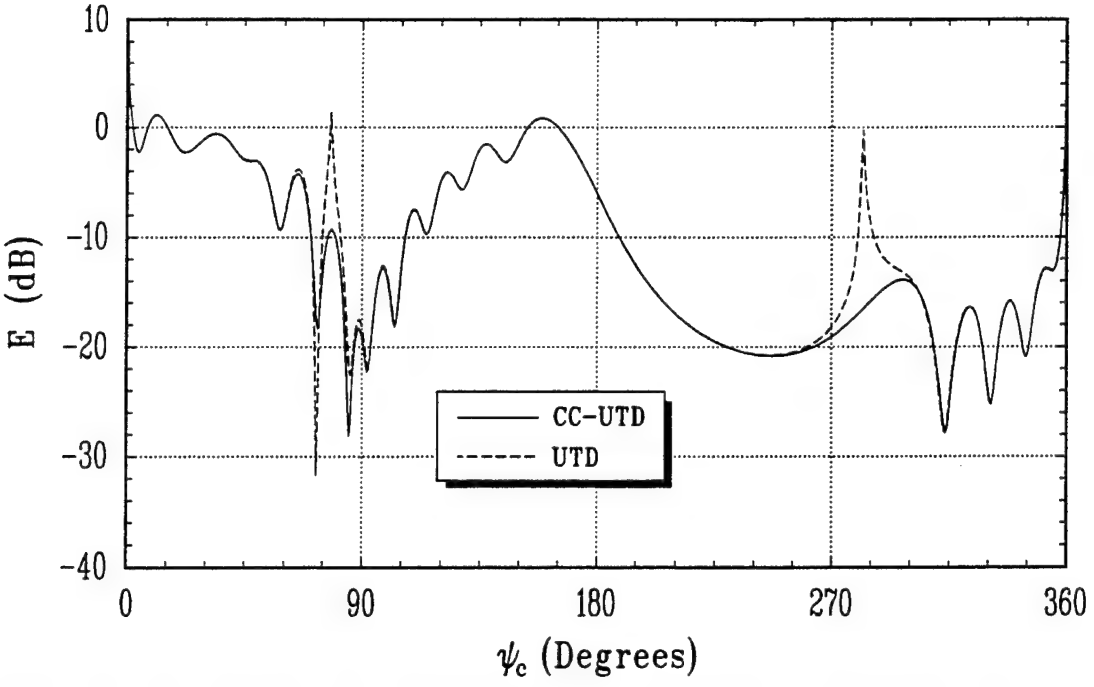

Figure 22: Total radiated field comparison for a plate with a focal length of $a = 3\lambda$ and a monopole location of $s_c' = 5\lambda$.

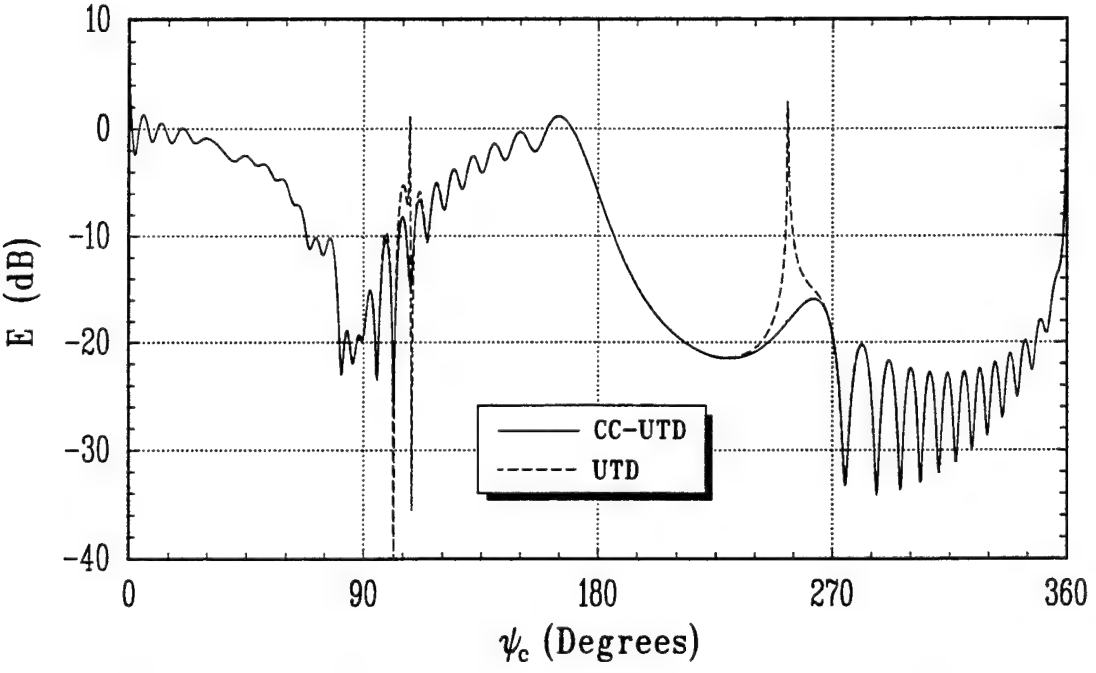

Figure 23: Total radiated field comparison for a plate with a focal length of $a = 3.5\lambda$ and a monopole location of $s_c' = 10\lambda$.

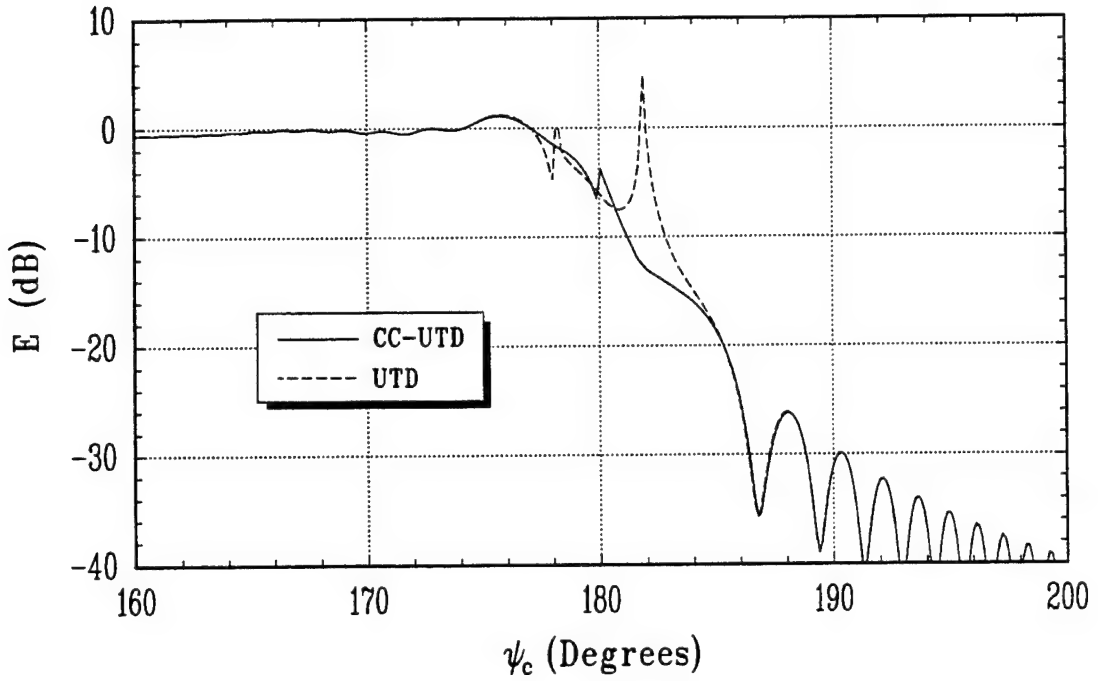

Figure 24: Total radiated field comparison for a plate with a focal length of $a = 0.05\lambda$ and a monopole location of $s_c' = 200\lambda$.

caustics of the UTD solution. It also shows that the CC-UTD solution smoothly reduces to the UTD solution away from the caustics.

Finally, Figure 24 shows a comparison between the CC-UTD solution and the UTD solution for a plate with a focal length of $a = 0.05\lambda$ and a monopole location of $s_c' = 200\lambda$. The dimensions of this geometry have been exaggerated in order to illustrate the breakdown of the CC-UTD solution. This breakdown occurs when the caustic boundaries are near the GO shadow boundary; therefore, only this region is plotted. The CC-UTD and UTD solutions are seen to agree very well away from this region and unnecessary to show for this discussion.

The discontinuity along the GO shadow boundary is a result of the fact that the caustic correction transition functions are multiplied by the Fresnel transition function. This product does not properly correct the fields when the caustic boundaries are near the GO shadow boundary. This is a gradual breakdown in that the fields slowly become less accurate as these boundaries approach each other. However, this

will not impact many practical problems due to the extremely exaggerated dimensions necessary for this breakdown to occur.

2 Gain Normalization of a Uniform Geometrical Theory of Diffraction Solution

The UTD is a good method for determining the field radiated by a monopole on a flat plate. However, the UTD field solution must be normalized to obtain the gain of that antenna. This section is devoted to the discussion of two simple procedures that can be used to find the gain of a short monopole mounted on a structure using the UTD.

This discussion begins with the definition of gain. It is assumed that the antenna is lossless for the purposes of this work. This means the directive gain is the quantity of interest. The directive gain of an antenna is defined as [35, 36]

$$D_g = \frac{4\pi U(r,\theta,\phi)}{P_{rad}} \tag{255}$$

where the root-mean-squared (r.m.s.) radiation intensity is

$$U(r,\theta,\phi) = \frac{r^2}{Z_c}\left|\vec{E}(r,\theta,\phi)\right|^2 \tag{256}$$

and P_{rad} is the total r.m.s. power radiated by the antenna. The directive gain can now be rewritten as

$$D_g = \frac{4\pi\left|\vec{E}_F(r,\theta,\phi)\right|^2}{Z_c\,P_{rad}} = \frac{\left|\vec{E}_F(r,\theta,\phi)\right|^2}{30P_{rad}} \tag{257}$$

where

$$\vec{E}_F(r,\theta,\phi) = \lim_{r\to\infty} re^{jkr}\vec{E}(r,\theta,\phi) \tag{258}$$

is the far-zone electric field. The directive gain can also be converted to decibels using

$$D_g\,(\text{dB}) = 10\log_{10}[D_g] \tag{259}$$

since it is a power ratio.

The UTD solution for a monopole mounted on a flat plate uses the field radiated by a monopole on an infinite ground plane as its starting point. The diffracted field

is then included to account for the fact that the plate is finite in extent. Therefore, the total UTD field is proportional to the field of the monopole on an infinite ground plane. It is commonly known that the field radiated by a short monopole on an infinite ground plane is given by (239) and (240) of Subsection 1.1. It is necessary to determine the current on the monopole, I_o, and the total r.m.s. power radiated in order to obtain the gain of this type of antenna using the UTD.

The first method for determining the directive gain of a short monopole mounted on a structure comes from basic antenna theory. It is easily shown that the total r.m.s. power radiated by a short monopole is [35, 36]

$$P_{rad} = \frac{2Z_c|I_o|^2(kd)^2}{3\pi} = 80|I_o|^2(kd)^2 \tag{260}$$

where I_o is the current on the monopole and d is the length of the monopole. The directive gain in (257) can now be rewritten as

$$D_g = \frac{3}{2}\left|\frac{\vec{E}_F(r,\theta,\phi)}{E_o}\right|^2 \tag{261}$$

where $\vec{E}_F(r,\theta,\phi)$ is the far-zone electric field given in (258) and E_o is given in (240). It is important to note that this expression is valid only if the length of the monopole is very short.

The closed form expression for the total r.m.s. power radiated by the monopole becomes less accurate as the length of the monopole increases. This occurs because the function used to model the current on the monopole becomes less accurate. In these cases, numerical techniques are typically used to obtain a more accurate model of the current. The Method of Moments is a numerical technique that is used to solve for the current induced on the surface of an antenna. This is accomplished by making the geometry consist of a wire segment attached to the structure. It is then assumed that the radiation in due to a voltage excitation located at the point where the wire attaches to the plate. This excitation voltage, V_o, is a known input into the MM solution. The currents induced on the antenna are then obtained using the Method of Moments. The current on the monopole, I_o, has now been solved for and the total r.m.s. power radiated is

$$P_{rad} = \mathrm{Re}\{V_o\, I_o^*\}\ . \tag{262}$$

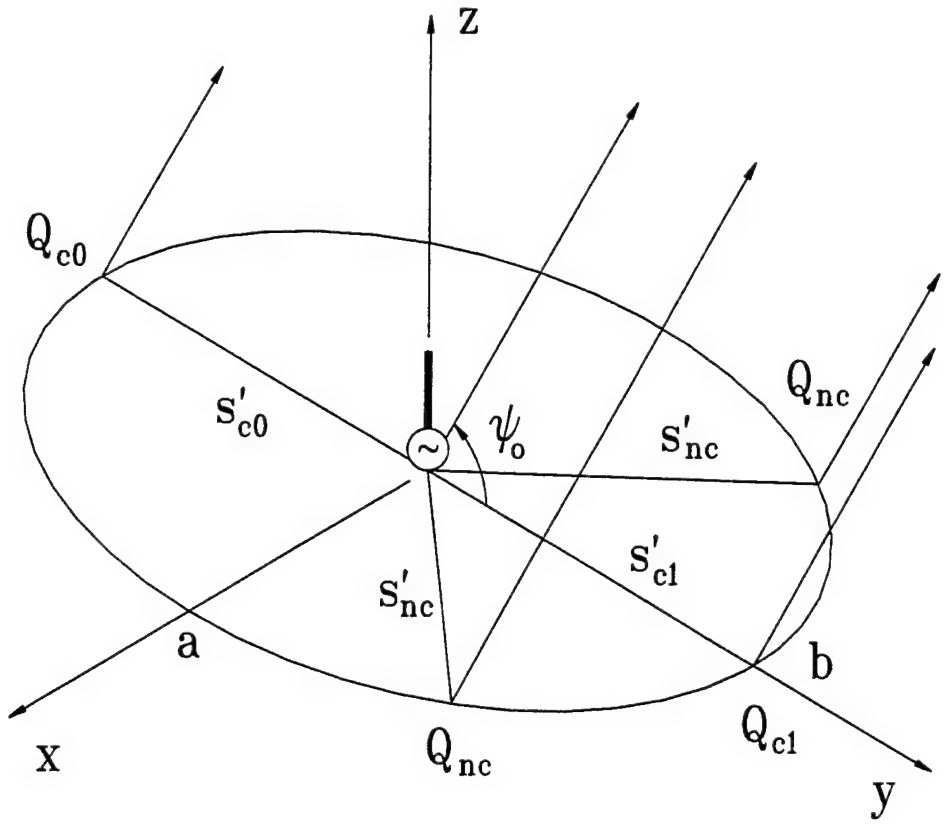

Figure 25: Ray geometry for the radiation of a short monopole on an elliptic disk.

Therefore, if the current on the wire is obtained using the Method of Moments, it can be used in conjunction with the UTD solution to obtain the far-zone electric field in (258). The gain can then be obtained using (257) and the total r.m.s. power generated by the MM solution.

3 Radiation of a Short Monopole on an Elliptic Disk

The other geometry to be studied in this chapter is the radiation by a monopole on an elliptic disk. To conform to the assumptions of the derivation of the CC-UTD in Chapter 5 it is important that the monopole is mounted in the center of the disk and the radiation pattern must be taken in the plane of symmetry of the ellipse. This geometry is shown in Figure 25. This section consists of two parts. First, the parameters required for the CC-UTD and the UTD solutions are determined. Next,

the radiated field is calculated using the CC-UTD and the UTD. These results are compared to a MM solution.

3.1 Elliptic Disk Radiated Field Parameters

It is important to accurately define the edge of the elliptic disk in order to determine the diffraction parameters required to use the CC-UTD and the UTD. An ellipse is defined by

$$\left(\frac{x_e}{a}\right)^2 + \left(\frac{y_e}{b}\right)^2 = 1 \tag{263}$$

where a and b are the principle axes of the ellipse in the x and y directions, respectively. The x and y coordinates of a point of the edge of the elliptic disk can now be related by

$$x_e = a\cos v \tag{264a}$$

$$y_e = b\sin v \tag{264b}$$

where v is the only variable. The diffraction points on the edge of the disk can be determined by recalling that $\cos\beta = \cos\beta'$ at these points. In doing so, we find that $v_{c0} = \frac{3\pi}{2}$, $v_{c1} = \frac{\pi}{2}$ and

$$\sin v_{nc} = \begin{cases} \varepsilon_v\sqrt{\dfrac{-C_0}{C_2}} & ;\text{ if } C_0 > -C_2 \\ \\ -j\varepsilon_v\sqrt{\dfrac{C_0}{C_2}} & ;\text{ if } C_0 < -C_2 \end{cases} \tag{265}$$

are the diffraction points as shown in Figure 25. Also, $\varepsilon_v = \text{sgn}\{(b^2 - a^2)\cos\psi_o\}$ and

$$C_0 = (ab\cos\psi_o)^2 \tag{266a}$$

$$C_2 = b^2\left(b^2 - a^2\right)\cos^2\psi_o - \left(b^2 - a^2\right)^2 \tag{266b}$$

are used to determine the locations of the non-central diffraction points. Now that the diffraction points have been found, it is easy to see that if $|\sin v_{nc}| < 1$ the far-zone point is in the caustic lit region and all other cases correspond to the caustic

shadow region. Next, the distances from the monopole to the diffraction points are easily shown to be

$$s'_{nc} = \begin{cases} \left|\sqrt{a^2 + (b^2 - a^2)\sin^2 v_{nc}}\right| & ; \text{if } (a^2 - b^2)\sin^2 v_{nc} < a^2 \\ -j\left|\sqrt{a^2 + (b^2 - a^2)\sin^2 v_{nc}}\right| & ; \text{if } (a^2 - b^2)\sin^2 v_{nc} > a^2 \end{cases} \tag{267}$$

and $s'_{c0} = s'_{c1} = b$. The curvature of the edge at any point is found to be

$$\begin{aligned} \kappa_g(Q') &= \frac{a^4 b}{[a^4 + (b^2 - a^2)\, x_e^2]^{3/2}} \\ &= \frac{ab}{[(a\sin v)^2 + (b\cos v)^2]^{3/2}} \end{aligned} \tag{268}$$

from (229). Evaluating (268) at Q_{c0}, Q_{c1} and Q_{nc} we obtain

$$\kappa_g(Q_{c0}) = \kappa_g(Q_{c1}) = \frac{b}{a^2} \tag{269}$$

and

$$\kappa_g(Q_{nc}) = \frac{ab}{\left[b^2 + (a^2 - b^2)\sin^2 v_{nc}\right]^{3/2}}, \tag{270}$$

respectively. Also, differentiating (268) twice and evaluating the second derivative at Q_{c0} and Q_{c1} we get

$$\kappa_g^{II}(Q_{c0}) = \kappa_g^{II}(Q_{c1}) = \frac{3b(a^2 - b^2)}{a^6} \tag{271}$$

which is used in the calculation of the curvature dependant diffraction coefficients in the caustic shadow regions. Using the fact that $\beta = \beta'$ at the diffraction points,

$$\beta_{c0} = \beta_{c1} = \frac{\pi}{2} \tag{272}$$

and

$$\sin\beta_{nc} = \sqrt{\frac{(b\sin\psi_o)^2 + \left(a^2 - b^2\sin^2\psi_o\right)\sin^2 v_{nc}}{b^2 + (a^2 - b^2)\sin^2 v_{nc}}} \tag{273}$$

are the oblique incidence angles at the diffraction points. The incidence angles at the diffraction points are $\psi'_{c0} = \psi'_{c1} = \psi'_{nc} = 0$ since the monopole is located on the disk and

$$\psi_{c0} = \psi_o, \tag{274}$$

$$\psi_{c1} = \begin{cases} \pi - \psi_o & ; \text{if } \psi_o < \pi \\ 3\pi - \psi_o & ; \text{if } \psi_o > \pi \end{cases} \tag{275}$$

and

$$\cos\psi_{nc} = \frac{-a\sin v_{nc}\cos\psi_o}{\sin\beta_{nc}\sqrt{b^2 + (a^2 - b^2)\sin^2 v_{nc}}} \tag{276}$$

are the angles from the diffraction points to the far-zone observation point. The caustic distances can now be determined using (10) of Chapter 2 and are given by

$$\rho^d(Q_{c0}) = \frac{a^2 b}{a^2 - b^2(1 + \cos\psi_o)}, \tag{277}$$

$$\rho^d(Q_{c1}) = \frac{a^2 b}{a^2 - b^2(1 - \cos\psi_o)} \tag{278}$$

and

$$\rho^d(Q_{nc}) = \frac{B^4(v_{nc}) s'_{nc}\sin^2\beta_{nc}}{B^4(v_{nc})\sin^2\beta_{nc} - a^2b^2 + a^2 b s'_{nc}\cos\psi_o\sin v_{nc}} \tag{279}$$

where

$$B(v_{nc}) = \sqrt{b^2 + (a^2 - b^2)\sin^2 v_{nc}}\,. \tag{280}$$

The GO field is found using (239) to be

$$\vec{E}^{GO}(P) = \hat{\psi}_o\, E_o \cos\psi_o \frac{e^{-jkR}}{R}\,\mathrm{U}[\pi - \psi_o] \tag{281}$$

where

$$E_o = \frac{Z_c I_o k d}{2\pi j} = -j60 I_o k d\,. \tag{282}$$

Also, (239) can be used to determine the incident field at each of the diffraction points as

$$\vec{E}^i(Q_{c0}) = \vec{E}^i(Q_{c1}) = \hat{\psi}'\, E_o \frac{e^{-jkb}}{b} \tag{283}$$

at the two central diffraction points and

$$\vec{E}^i(Q_{nc}) = \hat{\psi}'\, E_o \frac{e^{-jks'_{nc}}}{s'_{nc}} \tag{284}$$

at the two non-central diffraction points. The far-zone approximation of the distance from a diffraction point to the far-zone observation point, R_d, is

$$R_d \approx \begin{cases} R - b\sin v_d\cos\psi_o & ; \text{for phase terms} \\ R & ; \text{for amplitude terms} \end{cases} \tag{285}$$

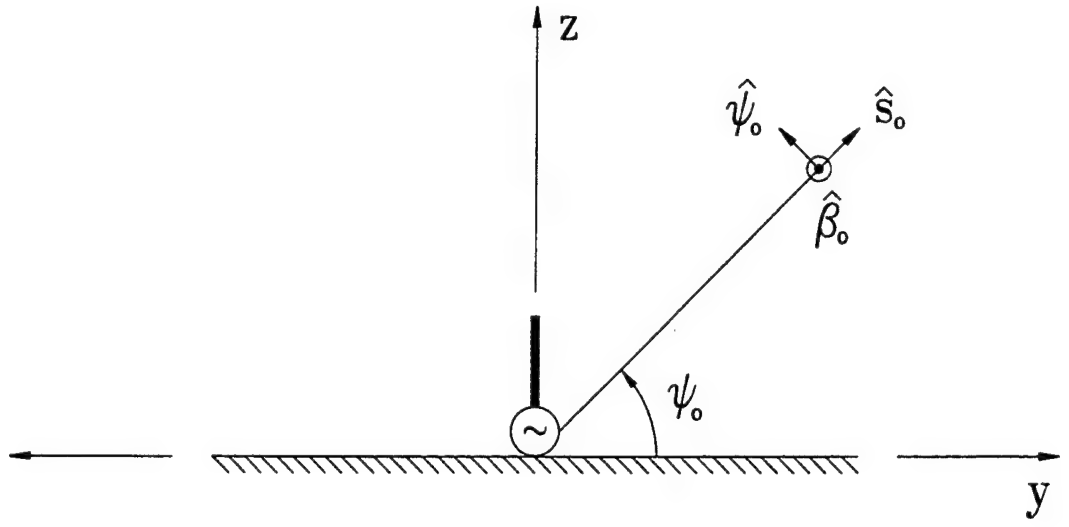

Figure 26: Polarization unit vector directions for the radiation by a short monopole on an elliptic disk.

where R is the distance from the center of the elliptic disk to the far-zone point and v_d is the value of v corresponding to the diffraction point that is to be referenced to the center of the disk. It is now necessary to determine the various components of the ray fixed coordinate $\hat{\psi}$ in terms of the global coordinate system. In doing so, we find that $\hat{\psi}_{c0} = \hat{\psi}_o$ and $\hat{\psi}_{c1} = -\hat{\psi}_o$ at the central diffraction points along with

$$\hat{\psi} = \frac{-\hat{\beta}_o (b \sin\psi_o \cos v_{nc}) - \hat{\psi}_o (a \sin v_{nc})}{\sin\beta_{nc}\sqrt{b^2 + (a^2 - b^2)\sin^2 v_{nc}}} \tag{286}$$

at the non-central diffraction points which have been found using (4a) of Chapter 2. These polarization vectors are shown in Figure 26. Now, since the non-central diffraction points are symmetrically located about the x-axis, the $\hat{\beta}_o$ component of each of the non-central diffraction points cancel to leave only the $\hat{\psi}_o$ components as expected. Therefore, the diffracted field in the caustic lit region is

$$\begin{aligned}
\vec{E}^d(P) \;\sim\; & \hat{\psi}_o \left\{ -E_o \frac{e^{-jkb}}{b} \right\} D_h(Q_{c0})\, T_c(\xi_0, 0) \sqrt{\rho^d(Q_{c0})}\, e^{-jkb\cos\psi_o}\, \frac{e^{-jkR}}{R} \\
+ \; & \hat{\psi}_o \left\{ E_o \frac{e^{-jkb}}{b} \right\} D_h(Q_{c1})\, T_c(\xi_1, 0) \sqrt{\rho^d(Q_{c1})}\, e^{jkb\cos\psi_o}\, \frac{e^{-jkR}}{R} \\
+ \; & \hat{\psi}_o 2 \left\{ E_o \frac{a \sin v_{nc}}{\sin\beta_{nc}\sqrt{b^2 + (a^2 - b^2)\sin^2 v_{nc}}} \frac{e^{-jks'_{nc}}}{s'_{nc}} \right\}
\end{aligned}$$

$$\times D_h(Q_{nc})\, T_{nc}(\xi_{nc}, \eta, 0)\sqrt{\rho^d(Q_{nc})}\, e^{jkb\sin v_{nc}\cos\psi_o}\, \frac{e^{-jkR}}{R} \qquad (287)$$

where (187) of Chapter 5 has been used with the diffracted field parameters found in this subsection. Also, the diffraction coefficient is given in (190) through (192) of Chapter 5. The arguments of the caustic correction transition functions must be carefully determined since the non-central diffraction points coalesce at both Q_{c0} and Q_{c1}. Using (189) of Chapter 5 we find that

$$\xi_0 = \left|\sqrt{2k[(\sin v_{nc} + 1)\, b\cos\psi_o - s'_{nc} + b]}\right| e^{-j3\eta\pi/4} \qquad (288)$$

is the argument of the caustic correction transition functions for determining the diffracted field near the caustics of Q_{c0} and

$$\xi_1 = \left|\sqrt{2k[(\sin v_{nc} - 1)\, b\cos\psi_o - s'_{nc} + b]}\right| e^{-j3\eta\pi/4} \qquad (289)$$

is the argument of the caustic correction transition functions for determining the diffracted field near the caustics of Q_{c1}. Next, the argument of the caustic correction transition functions for the non-central diffracted field is

$$\xi_{nc} = \begin{cases} \xi_0 & ;\text{if } -1 < \sin v_{nc} < 0 \\ \xi_1 & ;\text{if } 0 < \sin v_{nc} < 1 \end{cases} \qquad (290)$$

which has been chosen to account for the fact that the non-central diffraction points coalesce to both Q_{c0} and Q_{c1}. Also, from (188) in Chapter 5

$$\eta = -\operatorname{sgn}\left\{\rho^d(Q_{c0})\right\} = -\operatorname{sgn}\left\{\rho^d(Q_{c1})\right\} \qquad (291)$$

where $\rho^d(Q_{c0})$ and $\rho^d(Q_{c1})$ are given by (277) and (278), respectively. Finally, the diffracted field in the caustic shadow region is

$$\begin{aligned}
\vec{E}^d(P) \;\sim\; & \hat{\psi}_o\left\{-E_o\frac{e^{-jkb}}{b}\right\} D_h(Q_{c0})\, T_s(\xi_0, 0)\sqrt{\rho^d(Q_{c0})}\, e^{-jkb\cos\psi_o}\, \frac{e^{-jkR}}{R} \\
+\; & \hat{\psi}_o\left\{-E_o\frac{e^{-jkb}}{b}\right\} \mathcal{D}_h(Q_{c0})\, T_s(\xi_0, 2)\sqrt{\rho^d(Q_{c0})}\, e^{-jkb\cos\psi_o}\, \frac{e^{-jkR}}{R} \\
+\; & \hat{\psi}_o\left\{E_o\frac{e^{-jkb}}{b}\right\} D_h(Q_{c1})\, T_s(\xi_1, 0)\sqrt{\rho^d(Q_{c1})}\, e^{jkb\cos\psi_o}\, \frac{e^{-jkR}}{R} \\
+\; & \hat{\psi}_o\left\{E_o\frac{e^{-jkb}}{b}\right\} \mathcal{D}_h(Q_{c1})\, T_s(\xi_1, 2)\sqrt{\rho^d(Q_{c1})}\, e^{jkb\cos\psi_o}\, \frac{e^{-jkR}}{R}
\end{aligned} \qquad (292)$$

from (214) of Chapter 5 and the diffracted field parameters found previously in this subsection. Also, the diffraction coefficient $D_h(Q_c)$ is given by (217) and (218) of Chapter 5 and $\mathcal{D}_h(Q_c)$ is given by (203), (217) through (221), (223) and (224) of Chapter 5. The argument of the caustic correction transition functions for determining the diffracted field near the caustics of Q_{c0} is

$$\xi_0 = \left|\sqrt{2k[(\sin v_{nc} + 1)\, b \cos\psi_o - s'_{nc} + b]}\right| e^{-j\eta_0 \pi/4} \tag{293}$$

and the argument of the caustic correction transition functions for determining the diffracted field near the caustics of Q_{c1} is

$$\xi_1 = \left|\sqrt{2k[(\sin v_{nc} - 1)\, b \cos\psi_o - s'_{nc} + b]}\right| e^{-j\eta_1 \pi/4} \tag{294}$$

where $\eta_0 = -\operatorname{sgn}\left\{\rho^d(Q_{c0})\right\}$ and $\eta_1 = -\operatorname{sgn}\left\{\rho^d(Q_{c1})\right\}$. It is important to note that it is possible for $\{(\sin v_{nc} \pm 1)\, b \cos\psi_o - s'_{nc} + b\}$ to be complex in the caustic shadow region. Although this case should be analyzed using uniform steepest descent techniques, it is treated here heuristically. The caustic correction transition functions are not critical when this occurs because it is usually in the deep caustic shadow region. Therefore, $|(\sin v_{nc} \pm 1)\, b \cos\psi_o - s'_{nc} + b|$ can be used because it will produce a transition function argument that is piece-wise continuous in magnitude. The ramifications of this approximation will be discussed in the next subsection when these expressions are calculated numerically. These formulas now form a complete CC-UTD solution for the radiation by a monopole on an elliptic disk. The sum of the GO field and the diffracted field corresponding to the caustic lit region or the caustic shadow region give the total radiated field.

3.2 Numerical Calculation of the Field Radiated by a Short Monopole on an Elliptic Disk

The numerical calculation of the expressions derived in Subsection 3.1 confirms the uniformity of the CC-UTD developed in Chapter 5. This subsection contains a comparison between the CC-UTD, the UTD and a MM solution. The field radiated by a short monopole on an elliptic disk is calculated in this subsection to illustrate the practical use and accuracy of the CC-UTD developed in Chapter 5.

The directive gain of this antenna will be plotted throughout this subsection. The CC-UTD and the UTD field solutions are converted to directive gain using (261) derived in Section 2. Also, the MM solution is generated throughout the subsection using the general program developed by Nehrbass, Gupta and Newman [37]. This MM solution calculates the gain of the antenna using the second method discussed in Section 2. It should be noted that the gain calculations using the CC-UTD and the UTD are entirely independent of the gain calculations using the MM. This results in an unbiased comparison of the resulting solutions.

First, as discussed in Chapter 5, the Incident Shadow Boundaries (ISB) and the Reflection Shadow Boundaries (RSB) overlap and occur at $\psi_o = 0, \pi$. The Caustic Boundaries (CB) occur when the amplitude spreading factors of the diffracted field expressions become singular. Therefore, equating the denominators of (277) and (278) to zero we obtain

$$\cos\psi_{\text{CB0}} = \left\{\left(\frac{a}{b}\right)^2 - 1\right\} \tag{295}$$

and

$$\cos\psi_{\text{CB1}} = \left\{1 - \left(\frac{a}{b}\right)^2\right\} \tag{296}$$

as the locations of the CB's of Q_{c0} and Q_{c1}, respectively. It is clearly seen from these expressions that if $a > \sqrt{2}\,b$ none of the diffraction points will merge. This means that there are no caustics for the geometries satisfying this condition.

The first pattern cut is taken by making $a = 2$ m and $b = 5$ m at a frequency of 200 MHz. The directive gain in the y-z plane for this antenna is calculated using the CC-UTD, the UTD and the Method of Moments and the results are shown in Figure 27. It is clearly seen that caustics will occur in this plane because $a < \sqrt{2}\,b$. The CB's of Q_{c0} occur at $\psi_{\text{CB0}} = 147.14^\circ, 212.86^\circ$ and the CB's of Q_{c1} occur at $\psi_{\text{CB1}} = 32.86^\circ, 327.14^\circ$ for the dimensions chosen here. These boundaries are clearly seen in Figure 27. One of the advantages of the CC-UTD is that it is a fast way to compute the radiation pattern. For this geometry, the MM solution required 29 minutes and 19.24 seconds to compute on a Silicon Graphics Indigo/R4K workstation. However, the CC-UTD and the UTD solutions were run concurrently on the same computer and required only 1.23 seconds. It is seen from this figure that the CC-UTD

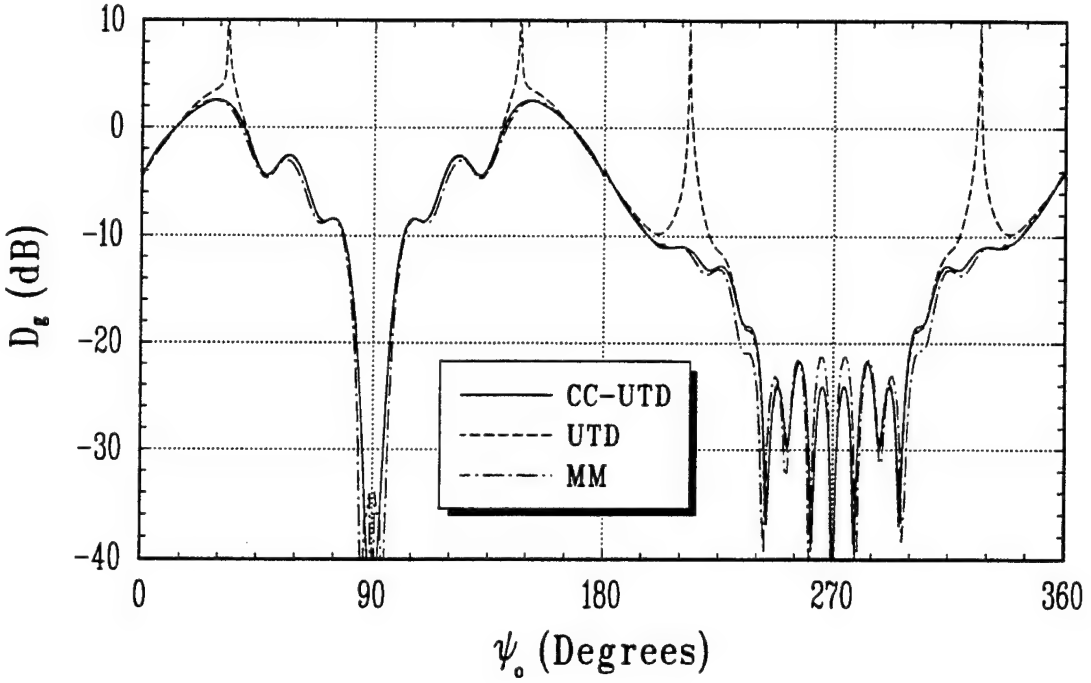

Figure 27: Directive gain comparison in the y-z plane for a short monopole mounted on an elliptic disk with $a = 2$ m and $b = 5$ m at a frequency of 200 MHz.

is bounded and uniform across the caustics. It also smoothly reduces to the classical UTD away from the caustics. It can also be seen that the CC-UTD and the MM solutions differ only by about 2 dB in the back lobe region. It can also be seen that there are small discontinuities along the GO shadow boundaries. This occurs because double diffractions have been neglected in this calculation.

As discussed at the end of Subsection 3.1, $\{(\sin v_{nc} \pm 1)\, b \cos\psi_o - s'_{nc} + b\}$ in the arguments of the caustic correction transition functions may become complex in the caustic shadow region. The angles for which this occurs are

$$\cos\psi_\xi = \pm\sqrt{1 - \left(\frac{a}{b}\right)^2} \tag{297}$$

by making $C_2 = 0$. These points are $\psi_\xi = 23.58°$, $156.42°$, $203.58°$ and $336.42°$ for this geometry and can be seen in Figure 27. It is seen from Figure 27 that this has a negligible effect in the main lobe region and only a small effect in the back lobe region. The field in these regions are piece-wise continuous as discussed in the

previous subsection. In general, this has little noticeable effect for most practical geometries.

The numerical integration of the classical Method of Equivalent Currents (MEC) solution and the more recent ITD formulation is now performed to illustrate the differences between them. It is important to note that only the integration of the diffracted field contribution of the ITD is performed numerically and the remaining integral contributions are taken to be the GO fields. Although this is not a complete ITD solution, it is consistent with the formulations in this work and with the assumptions of the MEC. This will result in an unbiased comparison of the two integral formulations.

The MEC used here is the same as the one used by Greer and Burnside [11]. The equivalent currents used by Greer and Burnside are the equivalent currents of Ryan and Peters [4, 5] with two modifications. First, as discussed by Knott and Senior [9], the substitution of $\sin^2\beta = \sin\beta\sin\beta'$ is made to enforce reciprocity. Second, the GTD diffraction coefficients are replaced with the UTD diffraction coefficients for normal incidence. These equivalent currents are then substituted into the radiation integral and numerically integrated. The comparison between the CC-UTD, MEC and MM solutions is shown in Figure 28. It is seen from this figure that the MEC solution does a good job of correcting for the caustics. However, there is a difference of about 2 dB between the MEC and MM solutions in the back lobe caustic regions. This occurs partly because the equivalent currents used will not produce the complete UTD solution when the method of stationary phase is applied to the integral. Since the UTD diffraction coefficients for normal incidence are used, the stationary phase evaluation of the radiation integral can not produce a UTD solution with the proper distance parameters for obliquely diffracted rays.

Next, the diffracted field contribution of the ITD is numerically integrated and added to the GO field. The comparison between the CC-UTD, ITD and MM solutions is shown in Figure 29. It is seen from this figure that either high frequency solution does a good job of correcting for the caustics. This figure also illustrates that the

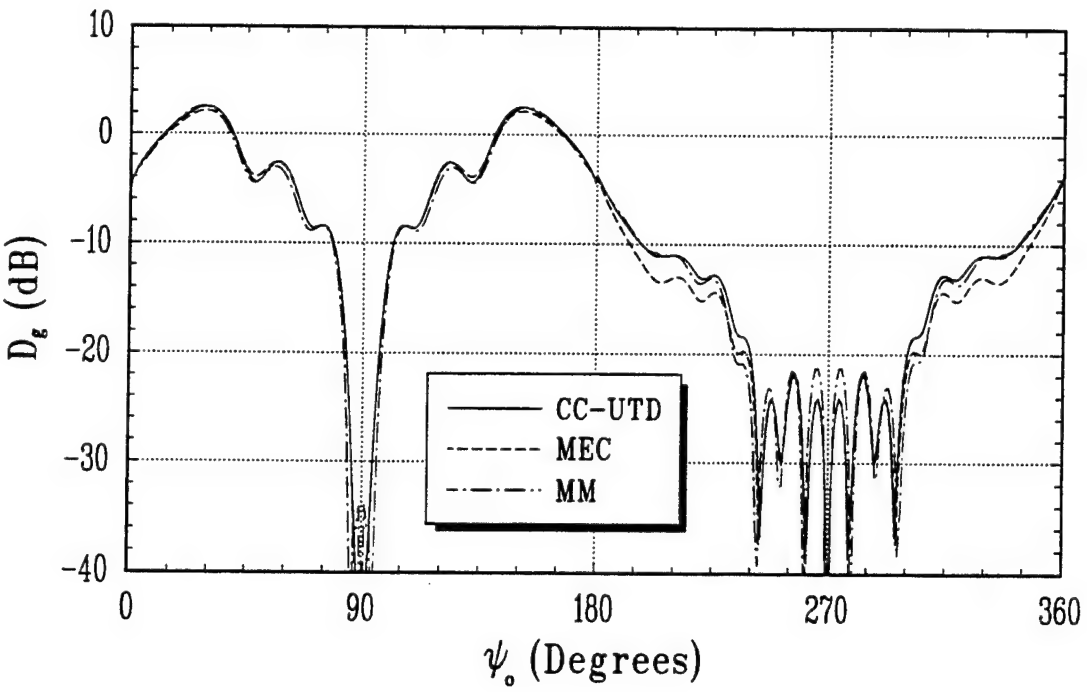

Figure 28: Directive gain comparison between the CC-UTD, MEC and MM for the y-z plane pattern of a short monopole on an elliptic disk with $a = 2$ m and $b = 5$ m at a frequency of 200 MHz.

CC-UTD solution is a good approximation of the original ITD diffracted field integral equation.

To obtain the other principle plane radiation pattern for this disk, the values of a and b are interchanged due to the definition of the angle ψ_o. Therefore, the other plane of this disk is obtained by making $a = 5$ m and $b = 2$ m at a frequency of 200 MHz. The directive gain in the y-z plane for this antenna is calculated using the CC-UTD, the UTD and the Method of Moments and the results are shown in Figure 30. It is clearly seen that no caustics will occur in this plane because $a > \sqrt{2}\,b$. Therefore, the caustic corrections should have little effect and the CC-UTD and the UTD solutions should be essentially identical. The computer run times for this example are the same as those of the previous example. It is seen from this figure that the CC-UTD is essentially the same as the UTD and in good agreement with the MM. Again, there are small discontinuities along the GO shadow boundaries because double diffractions have been neglected in this calculation.

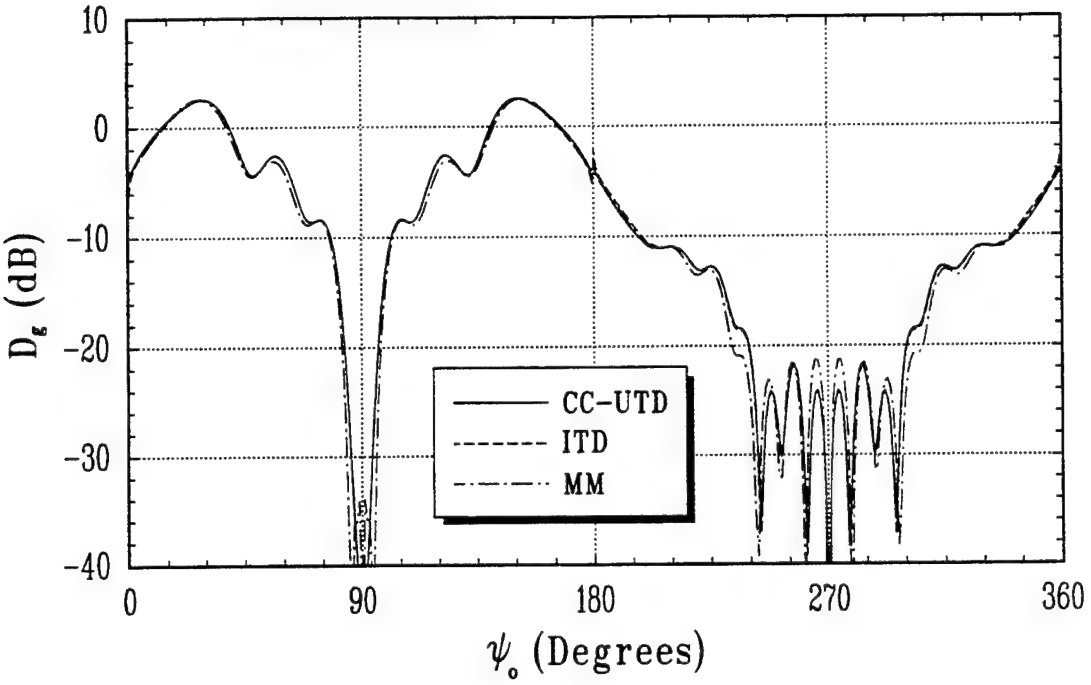

Figure 29: Directive gain comparison between the CC-UTD, ITD and MM for the y-z plane pattern of a short monopole on an elliptic disk with $a = 2$ m and $b = 5$ m at a frequency of 200 MHz.

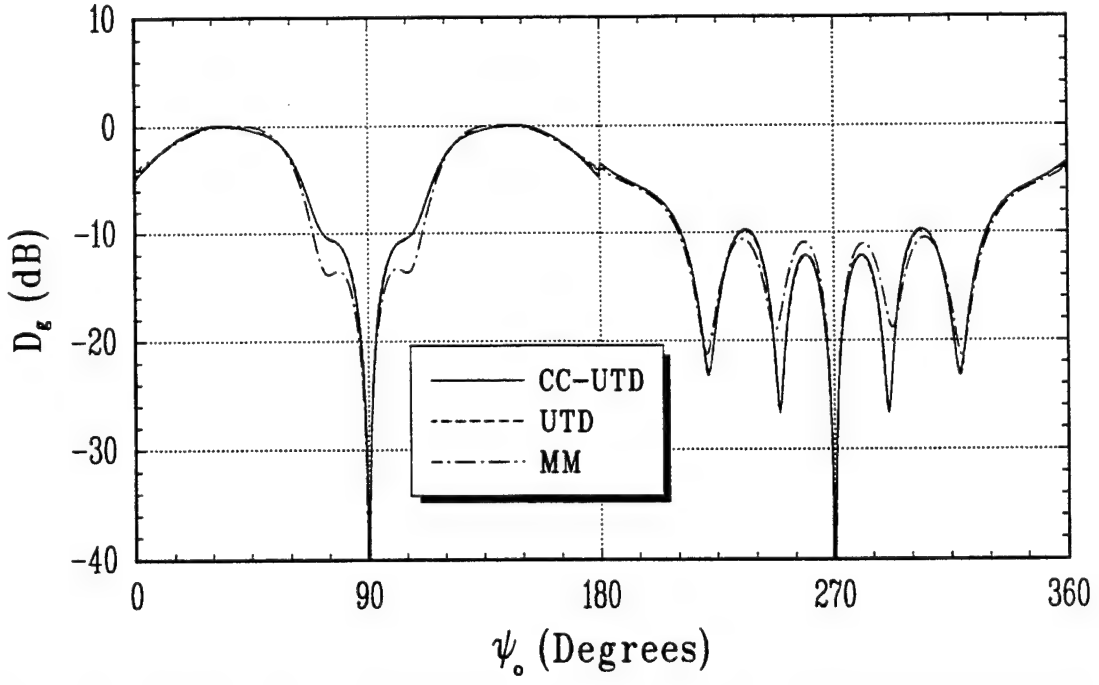

Figure 30: Directive gain comparison in the y-z plane for a short monopole mounted on an elliptic disk with $a = 5$ m and $b = 2$ m at a frequency of 200 MHz.

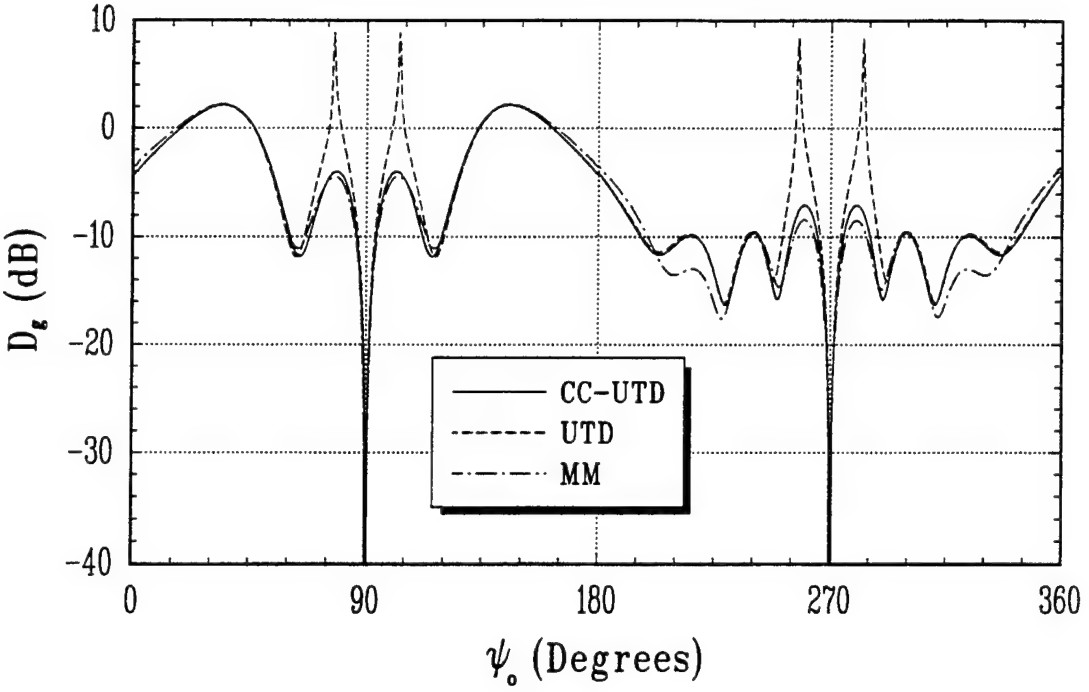

Figure 31: Directive gain comparison in the y-z plane for a short monopole mounted on an elliptic disk with $a = 1.5$ m and $b = 1.7$ m at a frequency of 300 MHz.

The next pattern cut is taken by making $a = 1.5$ m and $b = 1.7$ m at a frequency of 300 MHz. The directive gain in the y-z plane for this antenna is calculated using the CC-UTD, the UTD and the Method of Moments and the results are shown in Figure 31. It is clearly seen that caustics will occur in this plane because $a < \sqrt{2}\,b$. The CB's of Q_{c0} occur at $\psi_{CB0} = 102.79°$, $257.21°$ and the CB's of Q_{c1} occur at $\psi_{CB1} = 77.21°$, $282.79°$ for the dimensions chosen here. These boundaries are clearly seen in Figure 31. For this geometry, the MM solution required 30 minutes and 28.58 seconds to compute and the CC-UTD and UTD solutions required only 1.19 seconds. It is seen from this figure that the CC-UTD, the UTD and the MM are in good agreement. Again, there are small discontinuities along the GO shadow boundaries because double diffractions have been neglected in this calculation.

The other plane of this disk is obtained by making $a = 1.7$ m and $b = 1.5$ m at a frequency of 300 MHz. The directive gain in the y-z plane for this antenna is calculated using the CC-UTD, the UTD and the Method of Moments and the results are shown in Figure 32. It is clearly seen that caustics will also occur in

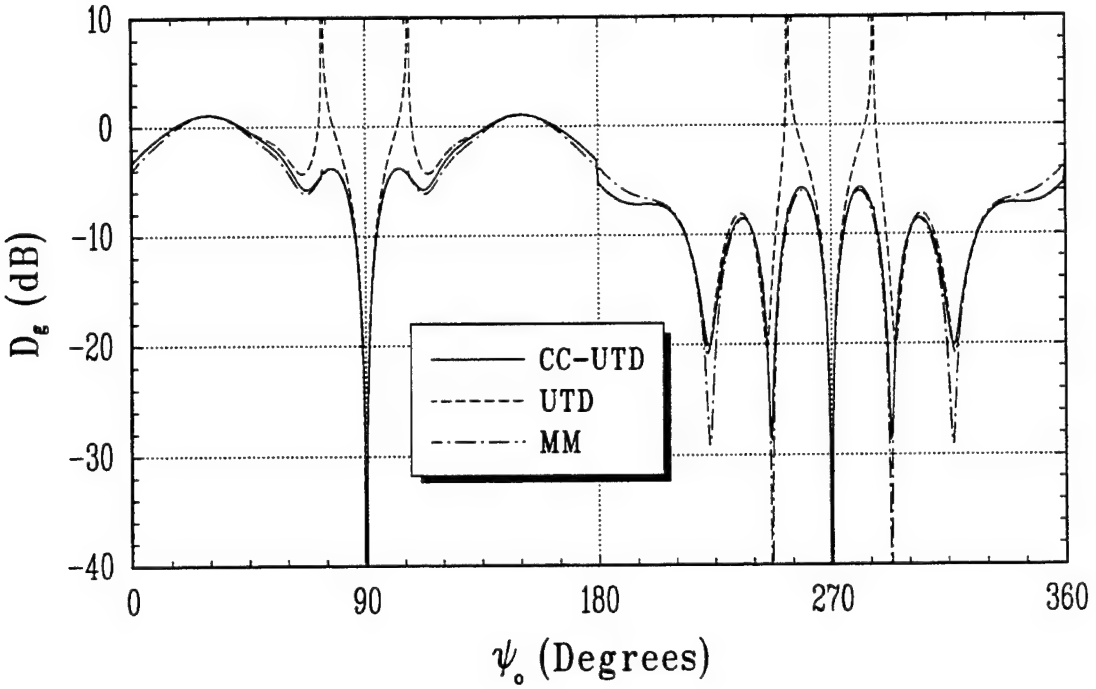

Figure 32: Directive gain comparison in the y-z plane for a short monopole mounted on an elliptic disk with $a = 1.7$ m and $b = 1.5$ m at a frequency of 300 MHz.

this plane because $a < \sqrt{2}\,b$. The CB's of Q_{c0} occur at $\psi_{CB0} = 73.47°$, $286.53°$ and the CB's of Q_{c1} occur at $\psi_{CB1} = 106.53°$, $253.47°$ for the dimensions chosen here. These boundaries are clearly seen in Figure 32. The computer run times for this example are the same as those of the previous example. It is seen from this figure that the CC-UTD, the UTD and the MM are in good agreement. Again, there are small discontinuities along the GO shadow boundaries because double diffractions have been neglected in this calculation.

The next pattern cut is taken by making $a = 2.0$ m and $b = 1.414$ m at a frequency of 300 MHz. The directive gain in the y-z plane for this antenna is calculated using the CC-UTD, the UTD and the Method of Moments and the results are shown in Figure 33. It is clearly seen that caustics will not occur in this plane because $a > \sqrt{2}\,b$. However, for this geometry $a \approx \sqrt{2}b$ which means that the diffraction point become very close together but do not coalesce. This means that although the UTD solution is not singular in this plane, it will predict incorrect directive gain when this occurs. This effect can be clearly seen in Figure 33. For this geometry, the MM solution required 44

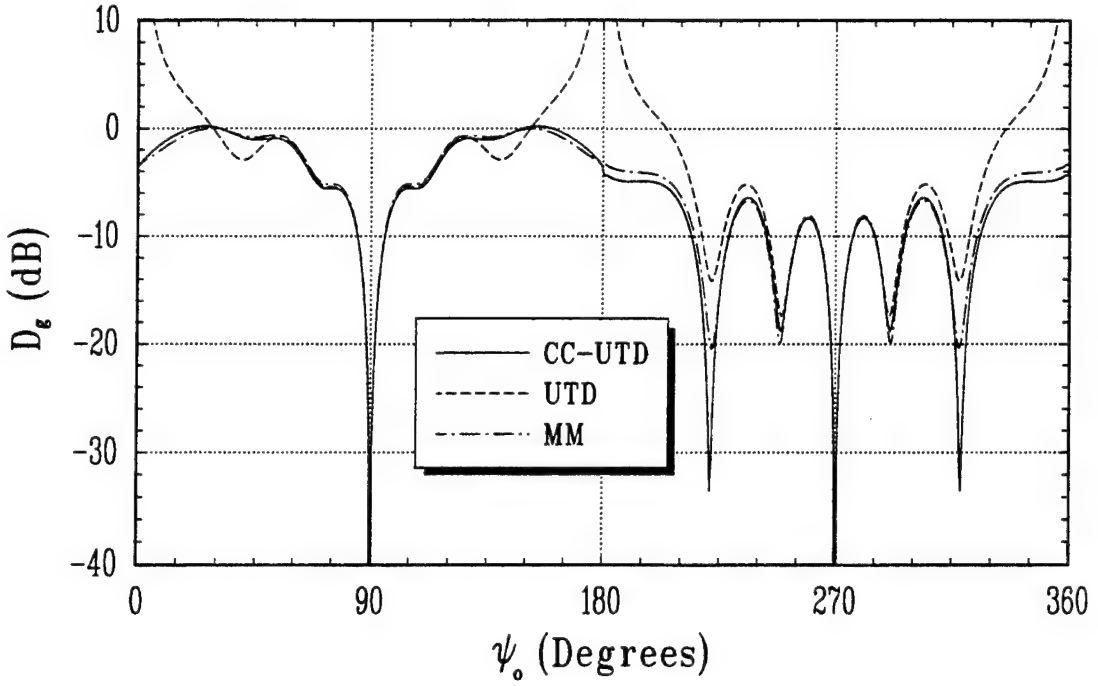

Figure 33: Directive gain comparison in the y-z plane for a short monopole mounted on an elliptic disk with $a = 2$ m and $b = 1.414$ m at a frequency of 300 MHz.

minutes and 22.67 seconds to compute and the CC-UTD and UTD solutions required only 1.23 seconds. It is seen from this figure that the CC-UTD and the MM are in good agreement. It should be noted that the discontinuities along the GO shadow boundaries are not caused by the absence of double diffraction terms, but are caused by the breakdown of the CC-UTD. It was assumed in the derivation of the CC-UTD that the GO shadow boundaries can not be close to the caustic boundaries. This breakdown is not catastrophic for this case which means the caustic lit region expressions in the CC-UTD are well behaved when this occurs.

The next pattern cut is taken by making $a = 2.0$ m and $b = 1.415$ m at a frequency of 300 MHz. The directive gain in the y-z plane for this antenna is calculated using the CC-UTD, the UTD and the Method of Moments and the results are shown in Figure 34. It is clearly seen that caustics will occur in this plane because $a < \sqrt{2}\,b$. However, for this geometry $a \approx \sqrt{2}b$ and the diffraction point coalesce on either side of the GO shadow boundaries. The CB's of Q_{c0} occur at $\psi_{CB0} = 3.8207°$, $356.1793°$ and the CB's of Q_{c1} occur at $\psi_{CB1} = 176.1793°$, $183.8207°$ for the dimensions chosen

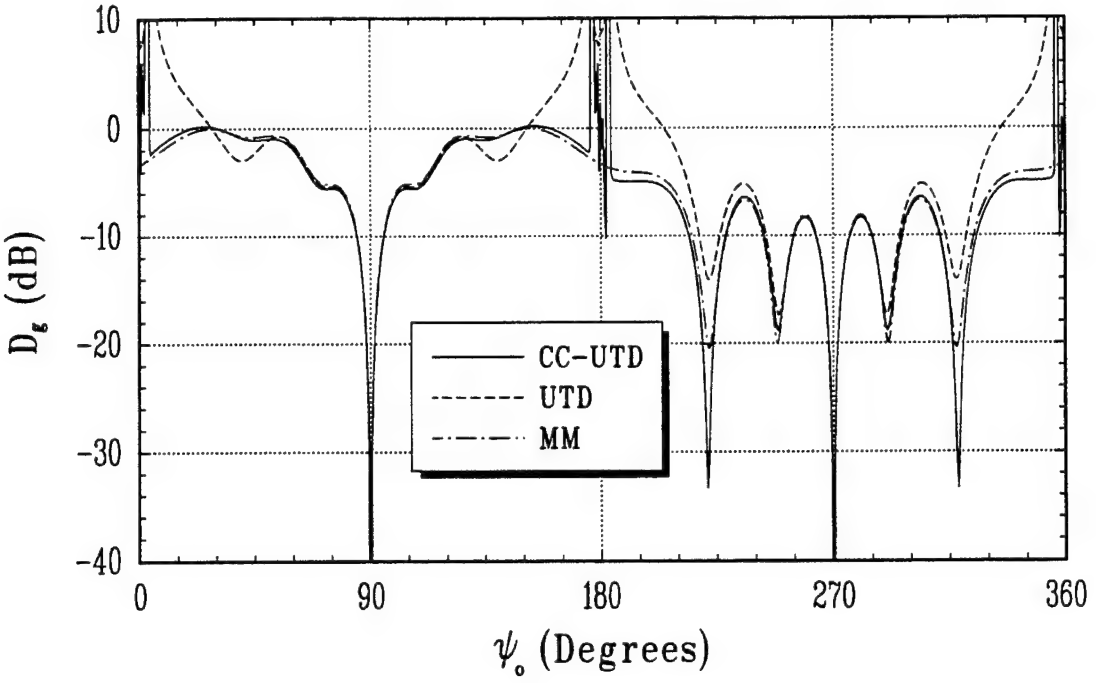

Figure 34: Directive gain comparison in the y-z plane for a short monopole mounted on an elliptic disk with $a = 2$ m and $b = 1.415$ m at a frequency of 300 MHz.

here. It is clear from Figure 34 that the breakdown of the CC-UTD is catastrophic for this case. This means the caustic shadow region expressions in the CC-UTD are not well behaved when this occurs.

The breakdown of the CC-UTD solution on the lit side of the caustic can be attributed to one main fact. The product of the caustic correction transition functions and the Fresnel transition function do not correctly account for the phenomena that is occurring. That is, this product is incorrect when the diffraction points coalesce near the GO shadow boundaries. This produces a non-catastrophic result because each transition function will correct its own particular phenomena, but when these phenomena are near, the result is slightly off. On the other hand, the caustic shadow region expressions of the CC-UTD breakdown for two reasons. The first is the product of the caustic correction transition functions and the Fresnel transition function do not correctly account for the phenomena that is occurring. This is similar to the caustic lit region. However, it was seen that the caustic shadow region field predicted by the CC-UTD was catastrophic. This occurs because the curvature dependent diffraction

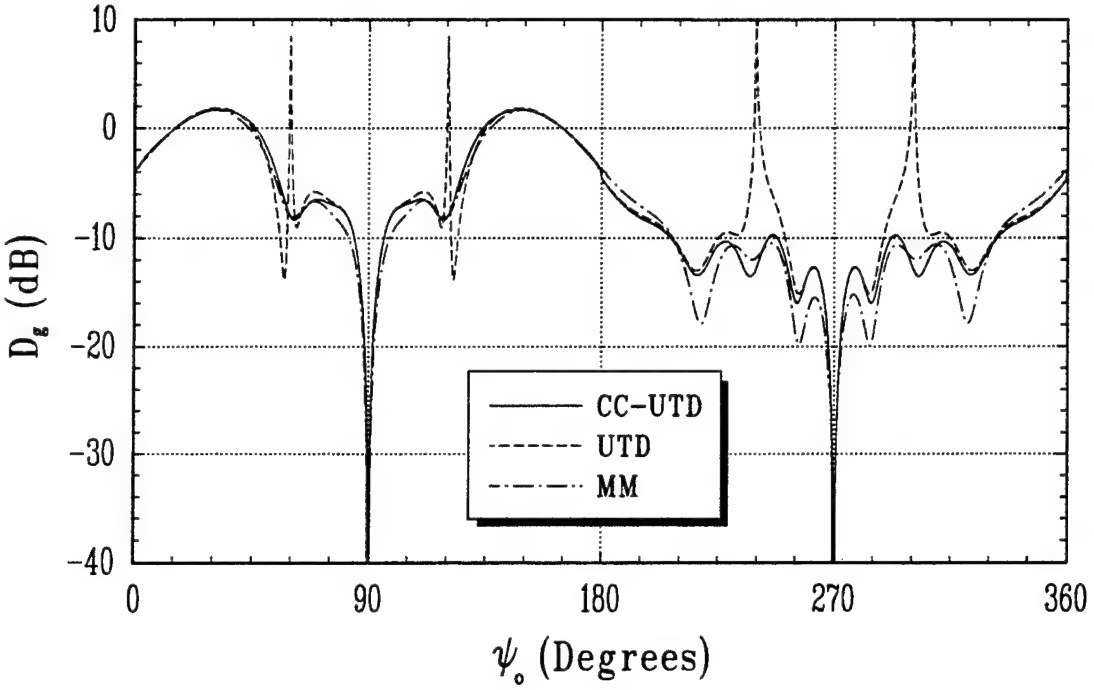

Figure 35: Directive gain comparison in the y-z plane for a short monopole mounted on an elliptic disk with $a = \sqrt{2}$ m and $b = 2$ m at a frequency of 300 MHz.

coefficient used in the caustic shadow region was obtained by differentiating the ITD half-plane diffraction coefficient. This differentiation is valid only if the function is well behaved near the point of differentiation. This is not true in this case because we are near the GO shadow boundaries.

The final pattern cut is obtained by making $a = \sqrt{2}$ m and $b = 2.0$ m at a frequency of 300 MHz. This will correspond to the other plane of both of the previous examples since the field variation as a function of a is minimal in this plane. The directive gain in the y-z plane for this antenna is calculated using the CC-UTD, the UTD and the Method of Moments and the results are shown in Figure 35. It is clearly seen that caustics will also occur in this plane because $a < \sqrt{2}\,b$. The CB's of Q_{c0} occur at $\psi_{CB0} = 120°, 240°$ and the CB's of Q_{c1} occur at $\psi_{CB1} = 60°, 300°$ for the dimensions chosen here. These boundaries are clearly seen in Figure 35. The computer run times for this example are the same as those of the previous example. It is seen from this figure that the CC-UTD, the UTD and the MM are in good agreement. Again, there

are small discontinuities along the GO shadow boundaries because double diffractions have been neglected in this calculation.

SECTION 7

Scattering by a Flat Plate with a Curved Edge

The near-zone scattering by an object with a curved edge is of great importance in many high frequency electromagnetic problems. Although the Uniform Geometrical Theory of Diffraction gives accurate results away from the caustics of the curved edge, it fails near and at the caustics. This chapter is devoted to the derivation of a caustic corrected UTD solution for the near-zone diffraction by a curved edge. This formulation is similar to that in Chapter 5 except the near-zone point is no longer restricted to lie on the face of the plate. This results in a more general caustic corrected UTD solution.

1 Problem Formulation

In Chapter 5, a caustic corrected UTD solution was derived for determining the field diffracted by a curved edge. In that derivation, the source location was restricted to lie on the face of the plate. In addition to being a useful solution in its own right, it illustrates the basic procedures used to obtain a CC-UTD solution for this type of problem. To generalize the applicability of the CC-UTD solution, the near-zone point will no longer be located on the face of the plate. The basic procedure used in Chapter 5 will be used here to obtain a CC-UTD solution for this more general case.

Two main topics must be addressed when formulating a caustic corrected UTD solution for determining the field near the caustics of waves diffracted by curved edges.

First, the canonical geometry must be chosen to be the simplest structure containing the phenomena of interest. The method of solution must also be determined. This section is a discussion of the canonical geometry and the method of solution for the scattering by a flat plate with a curved edge.

The phenomena of interest here is the coalescence of three diffraction points. Therefore, the canonical geometry to be used should contain no more than three diffraction points. Although a disk is often used as a canonical geometry, it has either two or four diffraction points depending on which region the observation point is in. However, this geometry would unnecessarily complicate the solution because there is one more diffraction point than is needed for studying this phenomena. This occurs because the disk is finite in extent. The simplest geometry that contains the phenomena of interest is the curved edge of a semi-infinite flat plate. Once the CC-UTD has been developed for this geometry, the solution can be applied to the disk due to the high frequency localization property of electromagnetic fields.

It is also important to consider the mathematics involved with the geometry in order to obtain a tractable solution. The scope of the solution is narrowed for the purposes of this work. The procedure used to obtain a solution here can be used to obtain a more general solution. However, to study the phenomena of interest, it is assumed that the edge of the plate is symmetric, the source direction lies in the plane of symmetry and the near-zone observation point is also in the plane of symmetry of the edge of the plate. This geometry is chosen so that the diffraction points are symmetrically located and equally spaced. A procedure similar to the one developed here can be used to obtain a solution if the diffraction points are not equally spaced.

The ITD developed by Tiberio and Maci [15, 16, 17] will be used in this work to obtain a caustic corrected UTD solution. The ITD contains three different components as discussed in Section 1 of Chapter 4. The first term is a Physical Optics surface integral. This integral can be formulated by using the spectral domain form of the scalar free space Green's function, interchanging the spectral and spatial integrals and performing the spatial integrals. This results in a double spectral integral form of the PO integral. Upon doing so, it can be seen that the PO integral contains three

double integral stationary phase points and a branch point of order $-\frac{3}{2}$. Although it should be theoretically possible to obtain a uniform asymptotic expansion for this type of integral, it is not possible using existing theories. Also, since the phase function would have to be mapped to a fourth order polynomial that is a function of two variables, the canonical integral would have an extremely complicated form. In fact, this integral would be no simpler to compute than the original PO integral. This defeats the purpose of the asymptotic expansion. Therefore, we wish to make some approximations in order to obtain simpler integrals.

As discussed in Section 1 of Chapter 4, the PO surface integral minus its edge contribution is approximately the Geometrical Optics field. This approximation is valid as long as the reflection point is not near the edge when the diffraction points coalesce. This is the same as saying that the caustic boundaries can not be close to the incident or reflection shadow boundaries. This will be assumed here. Therefore, the only remaining contribution of the ITD is the diffracted field component. The total ITD field will be approximated by the GO field and the diffracted field contribution of the ITD integrated along the edge of the plate. The diffracted field contribution of the ITD is derived in Chapter 4.

Only single integrals appear in this solution. The resulting formulation is simple enough in form to allow for the uniform asymptotic expansion of the diffracted field integral equations. The canonical integrals used in this expansion are standard and well tabulated functions. This is an attractive feature of any asymptotic expansion.

2 Diffraction Integral Formulation

A set of integral equations must be formulated so that they can be asymptotically expanded to obtain a caustic corrected UTD solution. The ITD will be used in this work to obtain these diffraction integrals. This section is a derivation of the diffracted field integral equations used to obtain a caustic corrected UTD solution.

Some assumptions must be made to obtain a usable set of diffracted field integral equations. First, as discussed in Section 1, the incident and reflection shadow boundaries can not be close to the caustic boundaries caused by the curvature of the

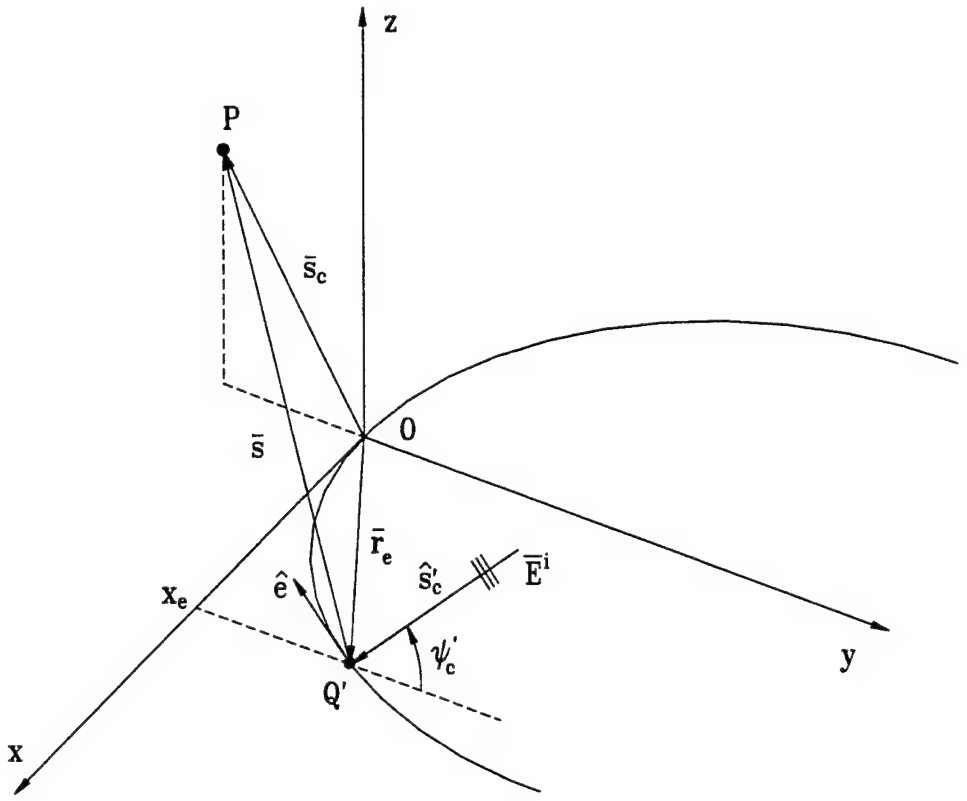

Figure 36: Scattering geometry for the diffraction by a curved edge.

edge since only the diffracted field contribution of the ITD is to be asymptotically expanded here. Next, recalling that the ITD diffracted field in Chapter 4 was obtained by asymptotically expanding a double spectral integral assuming that $kr\sin^2\beta \gg 1$, this must also be enforced here. Finally, it will be assumed that the curvature of the edge is symmetric and the source direction and the observation location lie in this plane of symmetry as discussed in Section 1. This geometry is shown in Figure 36.

The diffraction integrals used to obtain a caustic corrected UTD solution are determined using the ITD. The diffracted field contribution of the ITD is

$$\vec{E}^d(P) = \int_{C_e} d\vec{E}^d(l) \tag{298}$$

where C_e is the edge contour and

$$d\vec{E}^d(l) \sim \vec{E}^i(Q') \cdot \left\{ \hat{\beta}'\hat{\beta}\,\widetilde{D}_s(Q') + \hat{\psi}'\hat{\psi}\,\widetilde{D}_h(Q') \right\} \frac{e^{-jkr}}{2\pi r}\, dl \tag{299}$$

is the electric field diffracted by an infinitesimal length of the edge of a wedge. The half-plane diffraction coefficients given by

$$\widetilde{D}_{s,h}(Q') = \frac{1}{2}\left\{\frac{F\left[kLa(\Psi^-)\right]}{\cos\left(\frac{\Psi^-}{2}\right)} \mp \frac{F\left[kLa(\Psi^+)\right]}{\cos\left(\frac{\Psi^+}{2}\right)}\right\} \tag{300}$$

are used since only flat plates are being considered. Also, the angle parameter $a(\Psi^{\mp})$ is given by

$$a(\Psi^{\mp}) = 2\cos^2\left(\frac{\Psi^{\mp}}{2}\right) \tag{301}$$

where $\Psi^{\mp} = \psi \mp \psi'$, the distance parameter is $L = r\sin^2\beta$ and $F[x]$ is the UTD Fresnel transition function defined in (6). It will be advantageous to define the total diffracted field as the sum of a soft polarization diffracted field and a hard polarization diffracted field

$$\vec{E}^d(P) = \vec{E}^d_s(P) + \vec{E}^d_h(P) \tag{302}$$

where

$$\vec{E}^d_s(P) = \int_{-\infty}^{\infty} d\vec{E}^d_s(x_e) \tag{303}$$

is the soft polarization diffracted field contribution and

$$\vec{E}^d_h(P) = \int_{-\infty}^{\infty} d\vec{E}^d_h(x_e) \tag{304}$$

is the hard polarization diffracted field contribution. The soft polarized incremental diffracted electric field is

$$d\vec{E}^d_s(x_e) = \vec{E}^i(Q')\cdot\hat{\beta}'\hat{\beta}\,\widetilde{D}_s(Q')\,\frac{e^{-jkr}}{2\pi r}\left(\frac{dl}{dx_e}\right)dx_e \tag{305}$$

and the hard polarized incremental diffracted electric field is

$$d\vec{E}^d_h(x_e) = \vec{E}^i(Q')\cdot\hat{\psi}'\hat{\psi}\,\widetilde{D}_h(Q')\,\frac{e^{-jkr}}{2\pi r}\left(\frac{dl}{dx_e}\right)dx_e \tag{306}$$

where the variable of integration is changed from arc length to the x direction. Also, the incident field at any point on the edge is

$$\vec{E}^i(Q') = \vec{E}^i(0)\,e^{-jk\hat{s}'_c\cdot\vec{r}_e} \tag{307}$$

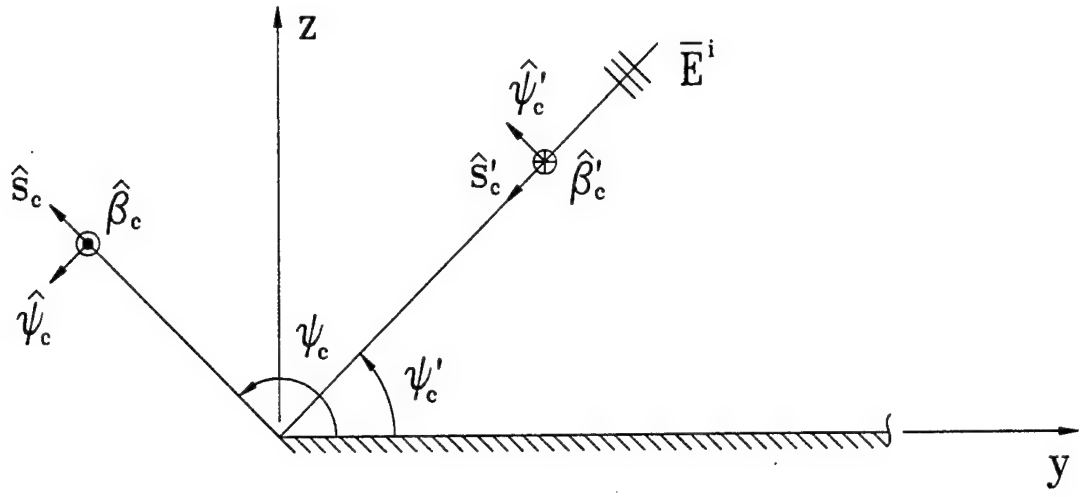

Figure 37: Polarization unit vectors for the diffraction by a curved edge.

where

$$\vec{E}^i(0) = \hat{\beta}'_c E^i_{\beta_c} + \hat{\psi}'_c E^i_{\psi_c} \tag{308}$$

and the polarization unit vectors for the incident field are shown in Figure 37. It is now necessary to write the incident ray fixed unit vectors $\hat{\beta}'$ and $\hat{\psi}'$ in terms of the fixed incident unit vector directions $\hat{\beta}'_c$ and $\hat{\psi}'_c$ and the diffracted ray fixed unit vectors $\hat{\beta}$ and $\hat{\psi}$ in terms of the fixed observation unit vectors $\hat{s}_c$, $\hat{\beta}_c$ and $\hat{\psi}_c$. These unit vectors are shown in Figure 37. The definition of the x_e and y_e coordinates of a point on the edge is necessary in order to determine these unit vector transformations. The y_e coordinate of a point on the edge is related to the x_e coordinate by

$$\begin{aligned} y_e &= \sum_{p=1}^{\infty} \frac{a_{2p}}{(2p)!} x_e^{2p} \\ &= \frac{1}{2!} a_2 x_e^2 + \frac{1}{4!} a_4 x_e^4 + \frac{1}{6!} a_6 x_e^6 + \sum_{p=4}^{\infty} \frac{a_{2p}}{(2p)!} x_e^{2p} \end{aligned} \tag{309}$$

since the edge was assumed to be symmetric about the y-axis. The vectors $\vec{r}_e$ and $\hat{e}$ shown in Figure 36 can now be determined since the edge of the plate has been defined. First, the position vector $\vec{r}_e$ is defined as

$$\vec{r}_e = \hat{x}\, x_e + \hat{y}\, y_e = \sum_{q=0}^{\infty} \frac{\vec{r}_e^{(q)}(Q_c)}{q!} x_e^q \tag{310}$$

where the derivatives of the position vector are taken with respect to x_e. The position vector can be written as

$$\begin{aligned}\vec{r}_e &= \hat{x}\{x_e\} + \hat{y}\left\{\frac{1}{2!}\kappa_g(Q_c)\,x_e^2 + \frac{1}{4!}\left[\kappa_g^{\rm II}(Q_c) + 3\kappa_g^3(Q_c)\right]\,x_e^4\right. \\ &\quad \left. + \frac{1}{6!}\left[\kappa_g^{\rm IV}(Q_c) + 34\kappa_g^2(Q_c)\kappa_g^{\rm II}(Q_c) + 45\kappa_g^5(Q_c)\right]\,x_e^6\right\} \\ &\quad + \sum_{q=7}^{\infty}\frac{\vec{r}_e^{\,(q)}(Q_c)}{q!}\,x_e^q \end{aligned} \tag{311}$$

using (724), (758) and (763) from Appendix D. The first three coefficients in (309) are

$$a_2 = \kappa_g(Q_c)\,, \tag{312}$$

$$a_4 = \kappa_g^{\rm II}(Q_c) + 3\kappa_g^3(Q_c) \tag{313}$$

and

$$a_6 = \kappa_g^{\rm IV}(Q_c) + 34\kappa_g^2(Q_c)\kappa_g^{\rm II}(Q_c) + 45\kappa_g^5(Q_c) \tag{314}$$

which are found by comparing (309) and (311). It is important to note that $\kappa_g^{\rm II}(Q_c)$ and $\kappa_g^{\rm IV}(Q_c)$ are the second and fourth derivatives of the curvature with respect to arc length, respectively. The edge vector is given by

$$\hat{e} = \frac{-\hat{x} - \hat{y}\,\frac{dy_e}{dx_e}}{\sqrt{1 + \left(\frac{dy_e}{dx_e}\right)^2}} = \frac{\vec{e}}{\left(\frac{dl}{dx_e}\right)} \tag{315}$$

from the definition of the unit edge vector and

$$\vec{e} = -\hat{x} - \hat{y}\,\frac{dy_e}{dx_e} \tag{316}$$

is the edge vector. The rotation of the incident ray fixed unit vectors $\hat{\beta}'$ and $\hat{\psi}'$ into the fixed incident vectors $\hat{\beta}'_c$ and $\hat{\psi}'_c$ can now be performed. The incident ray fixed unit vector $\hat{\psi}'$ is

$$\hat{\psi}' = \frac{\hat{e} \times \hat{s}'_c}{\sin\beta'} = \frac{\vec{e} \times \hat{s}'_c}{\left(\frac{dl}{dx_e}\right)\sin\beta'} \tag{317}$$

using the definition of $\hat{\psi}'$ given in (4b) of Chapter 2 and the unit edge vector definition in (315). Decomposing the edge vector into

$$\vec{e} = \hat{s}'_c\,(\vec{e}\cdot\hat{s}'_c) + \hat{\beta}'_c\,\left(\vec{e}\cdot\hat{\beta}'_c\right) + \hat{\psi}'_c\,\left(\vec{e}\cdot\hat{\psi}'_c\right) \tag{318}$$

and taking the cross product we obtain

$$\hat{\psi}' = \hat{\beta}'_c \left\{ - \frac{\vec{e} \cdot \hat{\psi}'_c}{\left(\frac{dl}{dx_e}\right) \sin \beta'} \right\} + \hat{\psi}'_c \left\{ \frac{\vec{e} \cdot \hat{\beta}'_c}{\left(\frac{dl}{dx_e}\right) \sin \beta'} \right\} \tag{319}$$

as $\hat{\psi}'$ in terms of the incident wave unit vector directions. Next, the unit vector $\hat{\beta}'$ is defined as

$$\hat{\beta}' = \hat{s}'_c \times \hat{\psi}' \tag{320}$$

using (4d) in Chapter 2 which leads to

$$\hat{\beta}' = \hat{\beta}'_c \left\{ \frac{\vec{e} \cdot \hat{\beta}'_c}{\left(\frac{dl}{dx_e}\right) \sin \beta'} \right\} + \hat{\psi}'_c \left\{ \frac{\vec{e} \cdot \hat{\psi}'_c}{\left(\frac{dl}{dx_e}\right) \sin \beta'} \right\} \tag{321}$$

as the vector $\hat{\beta}'$ in terms of the incident wave unit vector directions. The decomposition of the diffracted ray fixed unit vectors $\hat{\beta}$ and $\hat{\psi}$ into the fixed observation unit vectors $\hat{s}_c$, $\hat{\beta}_c$ and $\hat{\psi}_c$ can now be performed. The unit vector $\hat{\psi}$ is defined as

$$\hat{\psi} = \frac{\hat{s} \times \hat{e}}{\sin \beta} \tag{322}$$

using (4a) of Chapter 2. We can now write $\hat{\psi}$ as

$$\hat{\psi} = \frac{s_c \left(\hat{s}_c \times \vec{e}\right)}{\left(\frac{dl}{dx_e}\right) r \sin \beta} - \frac{\vec{r}_e \times \vec{e}}{\left(\frac{dl}{dx_e}\right) r \sin \beta} \tag{323}$$

using (315) and

$$\hat{s} = \frac{\hat{s}_c \, s_c - \vec{r}_e}{r} \tag{324}$$

which can be obtained from Figure 36. It is now necessary to decompose the vectors

$$\vec{e} = \hat{s}_c \left(\vec{e} \cdot \hat{s}_c\right) + \hat{\beta}_c \left(\vec{e} \cdot \hat{\beta}_c\right) + \hat{\psi}_c \left(\vec{e} \cdot \hat{\psi}_c\right) \tag{325}$$

and

$$\vec{r}_e \times \vec{e} = \hat{s}_c \left\{\hat{s}_c \cdot \left(\vec{r}_e \times \vec{e}\right)\right\} + \hat{\psi}_c \left\{\hat{\psi}_c \cdot \left(\vec{r}_e \times \vec{e}\right)\right\} \tag{326}$$

into their $\hat{s}_c$, $\hat{\beta}_c$ and $\hat{\psi}_c$ components. This allows us to take the cross products in (323) to obtain

$$\begin{aligned} \hat{\psi} \;=\; & \hat{s}_c \left\{ - \frac{\left[\hat{s}_c \cdot \left(\vec{r}_e \times \vec{e}\right)\right]}{\left(\frac{dl}{dx_e}\right) r \sin \beta} \right\} + \hat{\beta}_c \left\{ \frac{s_c \left(\vec{e} \cdot \hat{\psi}_c\right)}{\left(\frac{dl}{dx_e}\right) r \sin \beta} \right\} \\ + \; & \hat{\psi}_c \left\{ - \frac{s_c \left(\vec{e} \cdot \hat{\beta}_c\right)}{\left(\frac{dl}{dx_e}\right) r \sin \beta} - \frac{\left[\hat{\psi}_c \cdot \left(\vec{r}_e \times \vec{e}\right)\right]}{\left(\frac{dl}{dx_e}\right) r \sin \beta} \right\} \end{aligned} \tag{327}$$

as the unit vector $\hat{\psi}$ in terms of its $\hat{s}_c$, $\hat{\beta}_c$ and $\hat{\psi}_c$ components. Finally, the unit vector $\hat{\beta}$ is

$$\hat{\beta} = \hat{s} \times \hat{\psi} = \frac{s_c \left(\hat{s}_c \times \hat{\psi}\right)}{r} - \frac{\vec{r}_e \times \hat{\psi}}{r} \tag{328}$$

using the definition (4c) of Chapter 2 and $\hat{s}$ given by (324). By decomposing the position vector $\vec{r}_e$ as

$$\vec{r}_e = \hat{s}_c \left(\vec{r}_e \cdot \hat{s}_c\right) + \hat{\beta}_c \left(\vec{r}_e \cdot \hat{\beta}_c\right) + \hat{\psi}_c \left(\vec{r}_e \cdot \hat{\psi}_c\right) \tag{329}$$

we can perform the cross products in (328) to obtain

$$\begin{aligned}
\hat{\beta} \;=\; & \hat{s}_c \left\{ - \frac{s_c \left(\vec{e} \cdot \hat{\beta}_c\right) \left(\vec{r}_e \cdot \hat{\beta}_c\right)}{\left(\frac{dl}{dx_e}\right) r^2 \sin\beta} - \frac{\left[\hat{\psi}_c \cdot \left(\vec{r}_e \times \vec{e}\right)\right] \left(\vec{r}_e \cdot \hat{\beta}_c\right)}{\left(\frac{dl}{dx_e}\right) r^2 \sin\beta} \right. \\
& \qquad \left. - \frac{s_c \left(\vec{e} \cdot \hat{\psi}_c\right) \left(\vec{r}_e \cdot \hat{\psi}_c\right)}{\left(\frac{dl}{dx_e}\right) r^2 \sin\beta} \right\} \\
+ \; & \hat{\beta}_c \left\{ - \frac{s_c^2 \left(\vec{e} \cdot \hat{\beta}_c\right)}{\left(\frac{dl}{dx_e}\right) r^2 \sin\beta} - \frac{s_c \left[\hat{\psi}_c \cdot \left(\vec{r}_e \times \vec{e}\right)\right]}{\left(\frac{dl}{dx_e}\right) r^2 \sin\beta} + \frac{s_c \left(\vec{e} \cdot \hat{\beta}_c\right) \left(\vec{r}_e \cdot \hat{s}_c\right)}{\left(\frac{dl}{dx_e}\right) r^2 \sin\beta} \right. \\
& \qquad \left. + \frac{\left[\hat{\psi}_c \cdot \left(\vec{r}_e \times \vec{e}\right)\right] \left(\vec{r}_e \cdot \hat{s}_c\right)}{\left(\frac{dl}{dx_e}\right) r^2 \sin\beta} - \frac{\left[\hat{s}_c \cdot \left(\vec{r}_e \times \vec{e}\right)\right] \left(\vec{r}_e \cdot \hat{\psi}_c\right)}{\left(\frac{dl}{dx_e}\right) r^2 \sin\beta} \right\} \\
+ \; & \hat{\psi}_c \left\{ - \frac{s_c^2 \left(\vec{e} \cdot \hat{\psi}_c\right)}{\left(\frac{dl}{dx_e}\right) r^2 \sin\beta} + \frac{s_c \left(\vec{e} \cdot \hat{\psi}_c\right) \left(\vec{r}_e \cdot \hat{s}_c\right)}{\left(\frac{dl}{dx_e}\right) r^2 \sin\beta} \right. \\
& \qquad \left. + \frac{\left[\hat{s}_c \cdot \left(\vec{r}_e \times \vec{e}\right)\right] \left(\vec{r}_e \cdot \hat{\beta}_c\right)}{\left(\frac{dl}{dx_e}\right) r^2 \sin\beta} \right\}
\end{aligned} \tag{330}$$

as the unit vector $\hat{\beta}$ in terms of its $\hat{s}_c$, $\hat{\beta}_c$ and $\hat{\psi}_c$ components.

The soft and hard incremental diffracted electric fields can now be determined since the ray fixed unit vectors have been decomposed into the global incident and scatter unit vector directions. The soft polarization incremental diffracted electric field is

$$\begin{aligned}
d\vec{E}_s^d(x_e) \;=\; & \vec{E}^i(Q') \cdot \hat{\beta}' \hat{\beta}\, \widetilde{D}_s(Q') \frac{e^{-jkr}}{2\pi r} \left(\frac{dl}{dx_e}\right) dx_e \\
=\; & \hat{s}_c \left\{ \hat{s}_c \cdot \left[\vec{E}^i(0) \cdot \hat{\beta}' \hat{\beta}\right] \right\} \left(\frac{dl}{dx_e}\right) \frac{\widetilde{D}_s(Q')}{2\pi r} e^{jkh(x_e)}\, dx_e \\
+\; & \hat{\beta}_c \left\{ \hat{\beta}_c \cdot \left[\vec{E}^i(0) \cdot \hat{\beta}' \hat{\beta}\right] \right\} \left(\frac{dl}{dx_e}\right) \frac{\widetilde{D}_s(Q')}{2\pi r} e^{jkh(x_e)}\, dx_e
\end{aligned}$$

$$+ \quad \hat{\psi}_c \left\{ \hat{\psi}_c \cdot \left[\vec{E}^i(0) \cdot \hat{\beta}' \hat{\beta} \right] \right\} \left(\frac{dl}{dx_e} \right) \frac{\widetilde{D}_s(Q')}{2\pi r} \, e^{jkh(x_e)} \, dx_e \tag{331}$$

where

$$h(x_e) = -\hat{s}'_c \cdot \vec{r}_e - r \tag{332}$$

is the phase function of the diffraction integrals. It is important to determine the order of the zeros of the amplitude functions to obtain the correct asymptotic expressions for the diffracted fields. It is therefore necessary to determine the various dot products in the unit vectors $\hat{\beta}'$, $\hat{\psi}'$, $\hat{\beta}$ and $\hat{\psi}$. At this point, these dot products are only determined to find the order of the zeros of the amplitude functions because we wish to retain the vector nature of the solution. We begin by noting that

$$\hat{s}'_c = -\hat{y} \cos\psi'_c - \hat{z} \sin\psi'_c \tag{333a}$$

$$\hat{\beta}'_c = -\hat{x} \tag{333b}$$

$$\hat{\psi}'_c = -\hat{y} \sin\psi'_c + \hat{z} \cos\psi'_c \tag{333c}$$

are the incident wave unit vectors and

$$\hat{s}_c = \hat{y} \cos\psi_c + \hat{z} \sin\psi_c \tag{334a}$$

$$\hat{\beta}_c = \hat{x} \tag{334b}$$

$$\hat{\psi}_c = -\hat{y} \sin\psi_c + \hat{z} \cos\psi_c \tag{334c}$$

are the scattered wave unit vectors. Next, using (310) and (316) we find that

$$\vec{r}_e \times \vec{e} = \hat{z} \left(y_e - x_e \frac{dy_e}{dx_e} \right) \tag{335}$$

where y_e is given in (309). Therefore, the necessary dot products are found to be

$$\vec{e} \cdot \hat{\beta}'_c = 1 \tag{336a}$$

$$\vec{e} \cdot \hat{\psi}'_c = \frac{dy_e}{dx_e} \sin\psi'_c \propto x_e \tag{336b}$$

$$\vec{e} \cdot \hat{\beta}_c = -1 \tag{336c}$$

$$\vec{e} \cdot \hat{\psi}_c = \frac{dy_e}{dx_e} \sin\psi_c \propto x_e \tag{336d}$$

$$\vec{r}_e \cdot \hat{s}_c = y_e \cos\psi_c \propto x_e^2 \tag{336e}$$

$$\vec{r}_e \cdot \hat{\beta}_c = x_e \tag{336f}$$

$$\vec{r}_e \cdot \hat{\psi}_c = -y_e \sin\psi_c \propto x_e^2 \tag{336g}$$

$$\hat{s}_c \cdot (\vec{r}_e \times \vec{e}) = \left(y_e - x_e \frac{dy_e}{dx_e}\right) \sin\psi_c \propto x_e^2 \tag{336h}$$

$$\hat{\psi}_c \cdot (\vec{r}_e \times \vec{e}) = \left(y_e - x_e \frac{dy_e}{dx_e}\right) \cos\psi_c \propto x_e^2 \tag{336i}$$

using (309) to determine how each quantity is proportional to ($\propto$) x_e. Therefore, using (308), (321) and (330) we find that

$$\begin{aligned}
\hat{s}_c \cdot \left[\vec{E}^i(0) \cdot \hat{\beta}' \hat{\beta}\right] &= x_e \left\{ -E^i_{\beta_c} \frac{s_c \left(\vec{e}\cdot\hat{\beta}_c\right)\left(\vec{r}_e\cdot\hat{\beta}_c\right)\left(\vec{e}\cdot\hat{\beta}'_c\right)}{x_e \left(\frac{dl}{dx_e}\right)^2 r^2 \sin\beta \sin\beta'} \right\} \\
&+ x_e^2 \left\{ -E^i_{\psi_c} \frac{s_c \left(\vec{e}\cdot\hat{\beta}_c\right)\left(\vec{r}_e\cdot\hat{\beta}_c\right)\left(\vec{e}\cdot\hat{\psi}'_c\right)}{x_e^2 \left(\frac{dl}{dx_e}\right)^2 r^2 \sin\beta \sin\beta'} \right\} \\
&+ x_e^3 \left\{ -E^i_{\beta_c} \frac{\left[\hat{\psi}_c \cdot (\vec{r}_e \times \vec{e})\right]\left(\vec{r}_e\cdot\hat{\beta}_c\right)\left(\vec{e}\cdot\hat{\beta}'_c\right)}{x_e^3 \left(\frac{dl}{dx_e}\right)^2 r^2 \sin\beta \sin\beta'} \right. \\
&\qquad \left. -E^i_{\beta_c} \frac{s_c \left(\vec{e}\cdot\hat{\psi}_c\right)\left(\vec{r}_e\cdot\hat{\psi}_c\right)\left(\vec{e}\cdot\hat{\beta}'_c\right)}{x_e^3 \left(\frac{dl}{dx_e}\right)^2 r^2 \sin\beta \sin\beta'} \right\} \\
&+ x_e^4 \left\{ -E^i_{\psi_c} \frac{\left[\hat{\psi}_c \cdot (\vec{r}_e \times \vec{e})\right]\left(\vec{r}_e\cdot\hat{\beta}_c\right)\left(\vec{e}\cdot\hat{\psi}'_c\right)}{x_e^4 \left(\frac{dl}{dx_e}\right)^2 r^2 \sin\beta \sin\beta'} \right. \\
&\qquad \left. -E^i_{\psi_c} \frac{s_c \left(\vec{e}\cdot\hat{\psi}_c\right)\left(\vec{r}_e\cdot\hat{\psi}_c\right)\left(\vec{e}\cdot\hat{\psi}'_c\right)}{x_e^4 \left(\frac{dl}{dx_e}\right)^2 r^2 \sin\beta \sin\beta'} \right\}
\end{aligned} \tag{337}$$

where (336) has been used to determine the order of the zeros. Similarly, we find that

$$\begin{aligned}
\hat{\beta}_c \cdot \left[\vec{E}^i(0) \cdot \hat{\beta}' \hat{\beta}\right] &= \left\{ -E^i_{\beta_c} \frac{s_c^2 \left(\vec{e}\cdot\hat{\beta}_c\right)\left(\vec{e}\cdot\hat{\beta}'_c\right)}{\left(\frac{dl}{dx_e}\right)^2 r^2 \sin\beta \sin\beta'} \right\} \\
&+ x_e \left\{ -E^i_{\psi_c} \frac{s_c^2 \left(\vec{e}\cdot\hat{\beta}_c\right)\left(\vec{e}\cdot\hat{\psi}'_c\right)}{x_e \left(\frac{dl}{dx_e}\right)^2 r^2 \sin\beta \sin\beta'} \right\} \\
&+ x_e^3 \left\{ -E^i_{\psi_c} \frac{s_c \left[\hat{\psi}_c \cdot (\vec{r}_e \times \vec{e})\right]\left(\vec{e}\cdot\hat{\psi}'_c\right)}{x_e^3 \left(\frac{dl}{dx_e}\right)^2 r^2 \sin\beta \sin\beta'} \right. \\
&\qquad \left. +E^i_{\psi_c} \frac{s_c \left(\vec{e}\cdot\hat{\beta}_c\right)\left(\vec{r}_e\cdot\hat{s}_c\right)\left(\vec{e}\cdot\hat{\psi}'_c\right)}{x_e^3 \left(\frac{dl}{dx_e}\right)^2 r^2 \sin\beta \sin\beta'} \right\}
\end{aligned}$$

$$
\begin{aligned}
&+ \quad x_e^4 \left\{ E^i_{\beta_c} \frac{\left[\widehat{\psi}_c \cdot (\vec{r}_e \times \vec{e})\right] (\vec{r}_e \cdot \widehat{s}_c) \left(\vec{e} \cdot \widehat{\beta}'_c\right)}{x_e^4 \left(\frac{dl}{dx_e}\right)^2 r^2 \sin\beta \sin\beta'} \right. \\
&\qquad -E^i_{\beta_c} \frac{[\widehat{s}_c \cdot (\vec{r}_e \times \vec{e})] \left(\vec{r}_e \cdot \widehat{\psi}_c\right) \left(\vec{e} \cdot \widehat{\beta}'_c\right)}{x_e^4 \left(\frac{dl}{dx_e}\right)^2 r^2 \sin\beta \sin\beta'} \\
&\qquad \left. -E^i_{\beta_c} \frac{s_c \left\{\left[\widehat{\psi}_c \cdot (\vec{r}_e \times \vec{e})\right] - \left(\vec{e} \cdot \widehat{\beta}_c\right) (\vec{r}_e \cdot \widehat{s}_c)\right\} \left(\vec{e} \cdot \widehat{\beta}'_c\right)}{x_e^4 \left(\frac{dl}{dx_e}\right)^2 r^2 \sin\beta \sin\beta'} \right\} \\
&+ \quad x_e^5 \left\{ E^i_{\psi_c} \frac{\left[\widehat{\psi}_c \cdot (\vec{r}_e \times \vec{e})\right] (\vec{r}_e \cdot \widehat{s}_c) \left(\vec{e} \cdot \widehat{\psi}'_c\right)}{x_e^5 \left(\frac{dl}{dx_e}\right)^2 r^2 \sin\beta \sin\beta'} \right. \\
&\qquad \left. -E^i_{\psi_c} \frac{[\widehat{s}_c \cdot (\vec{r}_e \times \vec{e})] \left(\vec{r}_e \cdot \widehat{\psi}_c\right) \left(\vec{e} \cdot \widehat{\psi}'_c\right)}{x_e^5 \left(\frac{dl}{dx_e}\right)^2 r^2 \sin\beta \sin\beta'} \right\}
\end{aligned} \tag{338}
$$

and

$$
\begin{aligned}
\widehat{\psi}_c \cdot \left[\vec{E}^i(0) \cdot \widehat{\beta}' \widehat{\beta}\right] \quad = \quad & x_e \left\{ -E^i_{\beta_c} \frac{s_c^2 \left(\vec{e} \cdot \widehat{\psi}_c\right) \left(\vec{e} \cdot \widehat{\beta}'_c\right)}{x_e \left(\frac{dl}{dx_e}\right)^2 r^2 \sin\beta \sin\beta'} \right\} \\
& + \quad x_e^2 \left\{ -E^i_{\psi_c} \frac{s_c^2 \left(\vec{e} \cdot \widehat{\psi}_c\right) \left(\vec{e} \cdot \widehat{\psi}'_c\right)}{x_e^2 \left(\frac{dl}{dx_e}\right)^2 r^2 \sin\beta \sin\beta'} \right\} \\
& + \quad x_e^3 \left\{ E^i_{\beta_c} \frac{s_c \left(\vec{e} \cdot \widehat{\psi}_c\right) (\vec{r}_e \cdot \widehat{s}_c) \left(\vec{e} \cdot \widehat{\beta}'_c\right)}{x_e^3 \left(\frac{dl}{dx_e}\right)^2 r^2 \sin\beta \sin\beta'} \right. \\
& \qquad \left. + E^i_{\beta_c} \frac{[\widehat{s}_c \cdot (\vec{r}_e \times \vec{e})] \left(\vec{r}_e \cdot \widehat{\beta}_c\right) \left(\vec{e} \cdot \widehat{\beta}'_c\right)}{x_e^3 \left(\frac{dl}{dx_e}\right)^2 r^2 \sin\beta \sin\beta'} \right\} \\
& + \quad x_e^4 \left\{ E^i_{\psi_c} \frac{s_c \left(\vec{e} \cdot \widehat{\psi}_c\right) (\vec{r}_e \cdot \widehat{s}_c) \left(\vec{e} \cdot \widehat{\psi}'_c\right)}{x_e^4 \left(\frac{dl}{dx_e}\right)^2 r^2 \sin\beta \sin\beta'} \right. \\
& \qquad \left. + E^i_{\psi_c} \frac{[\widehat{s}_c \cdot (\vec{r}_e \times \vec{e})] \left(\vec{r}_e \cdot \widehat{\beta}_c\right) \left(\vec{e} \cdot \widehat{\psi}'_c\right)}{x_e^4 \left(\frac{dl}{dx_e}\right)^2 r^2 \sin\beta \sin\beta'} \right\}
\end{aligned} \tag{339}
$$

which are found using (308), (321) and (330) in conjunction with (336) to determine the order of the zeros. These can now be substituted into (303) and (331) and integrated. It is important to note that the terms that are proportional to odd powers of x_e will integrate to zero. Therefore, the soft polarized diffracted field is

$$
\vec{E}^d_s(P) \quad = \quad \widehat{s}_c \{\mathcal{I}^s_2(P) + \mathcal{I}^s_4(P)\} + \widehat{\beta}_c \{\mathcal{J}^s_0(P) + \mathcal{J}^s_4(P)\}
$$

$$+ \quad \hat{\psi}_c \{\mathcal{K}_2^s(P) + \mathcal{K}_4^s(P)\} \tag{340}$$

where the soft polarized diffraction integrals are

$$\mathcal{I}_2^s(P) = -E_{\psi_c}^i \frac{s_c \left(\vec{e} \cdot \hat{\beta}_c\right)}{2\pi} \int_{-\infty}^{\infty} x_e^2 \, \tilde{A}_2^s(x_e) \, e^{jkh(x_e)} dx_e \tag{341}$$

$$\mathcal{I}_4^s(P) = -E_{\psi_c}^i \frac{1}{2\pi} \int_{-\infty}^{\infty} x_e^4 \, \tilde{A}_4^s(x_e) \, e^{jkh(x_e)} dx_e \tag{342}$$

$$\mathcal{J}_0^s(P) = -E_{\beta_c}^i \frac{s_c^2 \left(\vec{e} \cdot \hat{\beta}_c\right) \left(\vec{e} \cdot \hat{\beta}'_c\right)}{2\pi} \int_{-\infty}^{\infty} \tilde{B}_0^s(x_e) \, e^{jkh(x_e)} dx_e \tag{343}$$

$$\mathcal{J}_4^s(P) = E_{\beta_c}^i \frac{\left(\vec{e} \cdot \hat{\beta}'_c\right)}{2\pi} \int_{-\infty}^{\infty} x_e^4 \, \tilde{B}_4^s(x_e) \, e^{jkh(x_e)} dx_e \tag{344}$$

$$\mathcal{K}_2^s(P) = -E_{\psi_c}^i \frac{s_c^2}{2\pi} \int_{-\infty}^{\infty} x_e^2 \, \tilde{C}_2^s(x_e) \, e^{jkh(x_e)} dx_e \tag{345}$$

$$\mathcal{K}_4^s(P) = E_{\psi_c}^i \frac{1}{2\pi} \int_{-\infty}^{\infty} x_e^4 \, \tilde{C}_4^s(x_e) \, e^{jkh(x_e)} dx_e \tag{346}$$

and

$$\tilde{A}_2^s(x_e) = \frac{\left(\vec{r}_e \cdot \hat{\beta}_c\right) \left(\vec{e} \cdot \hat{\psi}'_c\right)}{x_e^2} \frac{\widetilde{D}_s(Q')}{\left(\frac{dl}{dx_e}\right) r^3 \sin\beta \sin\beta'} \tag{347}$$

$$\begin{aligned} \tilde{A}_4^s(x_e) = & \frac{\left[\hat{\psi}_c \cdot (\vec{r}_e \times \vec{e})\right] \left(\vec{r}_e \cdot \hat{\beta}_c\right) \left(\vec{e} \cdot \hat{\psi}'_c\right)}{x_e^4} \frac{\widetilde{D}_s(Q')}{\left(\frac{dl}{dx_e}\right) r^3 \sin\beta \sin\beta'} \\ & + \frac{s_c \left(\vec{e} \cdot \hat{\psi}_c\right) \left(\vec{r}_e \cdot \hat{\psi}_c\right) \left(\vec{e} \cdot \hat{\psi}'_c\right)}{x_e^4} \frac{\widetilde{D}_s(Q')}{\left(\frac{dl}{dx_e}\right) r^3 \sin\beta \sin\beta'} \end{aligned} \tag{348}$$

$$\tilde{B}_0^s(x_e) = \frac{\widetilde{D}_s(Q')}{\left(\frac{dl}{dx_e}\right) r^3 \sin\beta \sin\beta'} \tag{349}$$

$$\begin{aligned} \tilde{B}_4^s(x_e) = & \frac{\left[\hat{\psi}_c \cdot (\vec{r}_e \times \vec{e})\right] (\vec{r}_e \cdot \hat{s}_c)}{x_e^4} \frac{\widetilde{D}_s(Q')}{\left(\frac{dl}{dx_e}\right) r^3 \sin\beta \sin\beta'} \\ & + \frac{-\left[\hat{s}_c \cdot (\vec{r}_e \times \vec{e})\right] \left(\vec{r}_e \cdot \hat{\psi}_c\right)}{x_e^4} \frac{\widetilde{D}_s(Q')}{\left(\frac{dl}{dx_e}\right) r^3 \sin\beta \sin\beta'} \\ & + \frac{-s_c \left\{\left[\hat{\psi}_c \cdot (\vec{r}_e \times \vec{e})\right] - \left(\vec{e} \cdot \hat{\beta}_c\right) (\vec{r}_e \cdot \hat{s}_c)\right\}}{x_e^4} \\ & \times \frac{\widetilde{D}_s(Q')}{\left(\frac{dl}{dx_e}\right) r^3 \sin\beta \sin\beta'} \end{aligned} \tag{350}$$

$$\tilde{C}_2^s(x_e) = \frac{\left(\vec{e}\cdot\hat{\psi}_c\right)\left(\vec{e}\cdot\hat{\psi}'_c\right)}{x_e^2}\,\frac{\widetilde{D}_s(Q')}{\left(\frac{dl}{dx_e}\right)r^3\sin\beta\sin\beta'} \tag{351}$$

$$\begin{aligned}\tilde{C}_4^s(x_e) &= \frac{s_c\left(\vec{e}\cdot\hat{\psi}_c\right)\left(\vec{r}_e\cdot\hat{s}_c\right)\left(\vec{e}\cdot\hat{\psi}'_c\right)}{x_e^4}\,\frac{\widetilde{D}_s(Q')}{\left(\frac{dl}{dx_e}\right)r^3\sin\beta\sin\beta'} \\ &+ \frac{[\hat{s}_c\cdot(\vec{r}_e\times\vec{e})]\left(\vec{r}_e\cdot\hat{\beta}_c\right)\left(\vec{e}\cdot\hat{\psi}'_c\right)}{x_e^4}\,\frac{\widetilde{D}_s(Q')}{\left(\frac{dl}{dx_e}\right)r^3\sin\beta\sin\beta'}\end{aligned} \tag{352}$$

are the amplitude functions of these diffraction integrals. This same procedure is now used to determine the hard polarized diffracted field. The hard polarization incremental diffracted electric field is given by

$$\begin{aligned}d\vec{E}_h^d(x_e) &= \vec{E}^i(Q')\cdot\hat{\psi}'\hat{\psi}\,\widetilde{D}_h(Q')\frac{e^{-jkr}}{2\pi r}\left(\frac{dl}{dx_e}\right)dx_e \\ &= \hat{s}_c\left\{\hat{s}_c\cdot\left[\vec{E}^i(0)\cdot\hat{\psi}'\hat{\psi}\right]\right\}\left(\frac{dl}{dx_e}\right)\frac{\widetilde{D}_h(Q')}{2\pi r}\,e^{jkh(x_e)}\,dx_e \\ &+ \hat{\beta}_c\left\{\hat{\beta}_c\cdot\left[\vec{E}^i(0)\cdot\hat{\psi}'\hat{\psi}\right]\right\}\left(\frac{dl}{dx_e}\right)\frac{\widetilde{D}_h(Q')}{2\pi r}\,e^{jkh(x_e)}\,dx_e \\ &+ \hat{\psi}_c\left\{\hat{\psi}_c\cdot\left[\vec{E}^i(0)\cdot\hat{\psi}'\hat{\psi}\right]\right\}\left(\frac{dl}{dx_e}\right)\frac{\widetilde{D}_h(Q')}{2\pi r}\,e^{jkh(x_e)}\,dx_e\end{aligned} \tag{353}$$

where $h(x_e)$ is the phase function of the diffraction integrals as given in (332). Therefore, using (308), (319) and (327) we find that

$$\begin{aligned}\hat{s}_c\cdot\left[\vec{E}^i(0)\cdot\hat{\psi}'\hat{\psi}\right] &= x_e^2\left\{-E^i_{\psi_c}\frac{[\hat{s}_c\cdot(\vec{r}_e\times\vec{e})]\left(\vec{e}\cdot\hat{\beta}'_c\right)}{x_e^2\left(\frac{dl}{dx_e}\right)^2 r\sin\beta\sin\beta'}\right\} \\ &+ x_e^3\left\{E^i_{\beta_c}\frac{[\hat{s}_c\cdot(\vec{r}_e\times\vec{e})]\left(\vec{e}\cdot\hat{\psi}'_c\right)}{x_e^3\left(\frac{dl}{dx_e}\right)^2 r\sin\beta\sin\beta'}\right\}\end{aligned} \tag{354}$$

where (336) has been used to determine the order of the zeros. Similarly, we find that

$$\begin{aligned}\hat{\beta}_c\cdot\left[\vec{E}^i(0)\cdot\hat{\psi}'\hat{\psi}\right] &= x_e\left\{E^i_{\psi_c}\frac{s_c\left(\vec{e}\cdot\hat{\psi}_c\right)\left(\vec{e}\cdot\hat{\beta}'_c\right)}{x_e\left(\frac{dl}{dx_e}\right)^2 r\sin\beta\sin\beta'}\right\} \\ &+ x_e^2\left\{-E^i_{\beta_c}\frac{s_c\left(\vec{e}\cdot\hat{\psi}_c\right)\left(\vec{e}\cdot\hat{\psi}'_c\right)}{x_e^2\left(\frac{dl}{dx_e}\right)^2 r\sin\beta\sin\beta'}\right\}\end{aligned} \tag{355}$$

and

$$\hat{\psi}_c\cdot\left[\vec{E}^i(0)\cdot\hat{\psi}'\hat{\psi}\right] = \left\{-E^i_{\psi_c}\frac{s_c\left(\vec{e}\cdot\hat{\beta}_c\right)\left(\vec{e}\cdot\hat{\beta}'_c\right)}{\left(\frac{dl}{dx_e}\right)^2 r\sin\beta\sin\beta'}\right\}$$

$$+ \quad x_e \left\{ E^i_{\beta_c} \frac{s_c \left(\vec{e}\cdot\hat{\beta}_c\right)\left(\vec{e}\cdot\hat{\psi}'_c\right)}{x_e \left(\frac{dl}{dx_e}\right)^2 r \sin\beta \sin\beta'} \right\}$$

$$+ \quad x_e^2 \left\{ -E^i_{\psi_c} \frac{\left[\hat{\psi}_c \cdot (\vec{r}_e \times \vec{e})\right]\left(\vec{e}\cdot\hat{\beta}'_c\right)}{x_e^2 \left(\frac{dl}{dx_e}\right)^2 r \sin\beta \sin\beta'} \right\}$$

$$+ \quad x_e^3 \left\{ E^i_{\beta_c} \frac{\left[\hat{\psi}_c \cdot (\vec{r}_e \times \vec{e})\right]\left(\vec{e}\cdot\hat{\psi}'_c\right)}{x_e^3 \left(\frac{dl}{dx_e}\right)^2 r \sin\beta \sin\beta'} \right\} \tag{356}$$

which are found using (308), (319) and (327) in conjunction with (336) to determine the order of the zeros. These can now be substituted into (304) and (353) and integrated. It is important to note that the terms that are proportional to odd powers of x_e will integrate to zero. Therefore, the hard polarized diffracted field is

$$\vec{E}^d_h(P) = \hat{s}_c \mathcal{I}^h_2(P) + \hat{\beta}_c \mathcal{J}^h_2(P) + \hat{\psi}_c \left\{ \mathcal{K}^h_0(P) + \mathcal{K}^h_2(P) \right\} \tag{357}$$

where the hard polarized diffraction integrals are

$$\mathcal{I}^h_2(P) = -E^i_{\psi_c} \frac{\left(\vec{e}\cdot\hat{\beta}'_c\right)}{2\pi} \int_{-\infty}^{\infty} x_e^2 \, \tilde{A}^h_2(x_e) \, e^{jkh(x_e)} dx_e \tag{358}$$

$$\mathcal{J}^h_2(P) = -E^i_{\beta_c} \frac{s_c}{2\pi} \int_{-\infty}^{\infty} x_e^2 \, \tilde{B}^h_2(x_e) \, e^{jkh(x_e)} dx_e \tag{359}$$

$$\mathcal{K}^h_0(P) = -E^i_{\psi_c} \frac{s_c \left(\vec{e}\cdot\hat{\beta}_c\right)\left(\vec{e}\cdot\hat{\beta}'_c\right)}{2\pi} \int_{-\infty}^{\infty} \tilde{C}^h_0(x_e) \, e^{jkh(x_e)} dx_e \tag{360}$$

$$\mathcal{K}^h_2(P) = -E^i_{\psi_c} \frac{\left(\vec{e}\cdot\hat{\beta}'_c\right)}{2\pi} \int_{-\infty}^{\infty} x_e^2 \, \tilde{C}^h_2(x_e) \, e^{jkh(x_e)} dx_e \tag{361}$$

and

$$\tilde{A}^h_2(x_e) = \frac{\left[\hat{s}_c \cdot (\vec{r}_e \times \vec{e})\right]}{x_e^2} \frac{\widetilde{D}_h(Q')}{\left(\frac{dl}{dx_e}\right) r^2 \sin\beta \sin\beta'} \tag{362}$$

$$\tilde{B}^h_2(x_e) = \frac{\left(\vec{e}\cdot\hat{\psi}_c\right)\left(\vec{e}\cdot\hat{\psi}'_c\right)}{x_e^2} \frac{\widetilde{D}_h(Q')}{\left(\frac{dl}{dx_e}\right) r^2 \sin\beta \sin\beta'} \tag{363}$$

$$\tilde{C}^h_0(x_e) = \frac{\widetilde{D}_h(Q')}{\left(\frac{dl}{dx_e}\right) r^2 \sin\beta \sin\beta'} \tag{364}$$

$$\tilde{C}^h_2(x_e) = \frac{\left[\hat{\psi}_c \cdot (\vec{r}_e \times \vec{e})\right]}{x_e^2} \frac{\widetilde{D}_h(Q')}{\left(\frac{dl}{dx_e}\right) r^2 \sin\beta \sin\beta'} \tag{365}$$

are the amplitude functions of these diffraction integrals. The soft and hard polarized diffracted field integral equations must be asymptotically reduced on the lit and shadow sides of the caustic in order to obtain a caustic corrected UTD solution.

3 The Uniform Asymptotic Expansion of the Diffracted Field Integral Equations in the Caustic Lit Region

Although the diffracted field integral equations derived in Section 2 can be numerically integrated to predict the field diffracted by a curved edge, it is advantageous to obtain closed form expressions. One way to accomplish this is to asymptotically expand the integrals at high frequencies. This section is devoted to the asymptotic expansion of the diffracted field integral equations for the lit side of the caustic.

In the caustic lit region, there are assumed to be three symmetrically located diffraction points as shown in Figure 38. This occurs because of the assumed symmetry of the edge, source direction and observation location. The uniform asymptotic expansion derived in Section 2 of Appendix B can be utilized when these diffraction points are nearly coincident with these assumptions in mind.

As explained in Section 1 of Appendix B, if an integral has three real stationary phase points then $\mu = -\eta$ where $\mu = \text{sgn}\{h^{\text{IV}}(x_c)\}$ and $\eta = \text{sgn}\{h^{\text{II}}(x_c)\}$. It is also easily shown using (753a) and (764a) of Appendix D that the value of the phase function is

$$h(x_c) = -s_c \tag{366}$$

at the central stationary phase point and using (756a) and (765a) of Appendix D that the value of the phase function is

$$h(x_{nc}) = -\hat{s}'_c \cdot \vec{r}_e(Q_{nc}) - s_{nc} \tag{367}$$

at the non-central stationary phase points. The argument of the transition functions becomes

$$\xi = \left|\sqrt{2k[-\hat{s}'_c \cdot \vec{r}_e(Q_{nc}) - s_{nc} + s_c]}\right| e^{-j3\eta\pi/4} \tag{368}$$

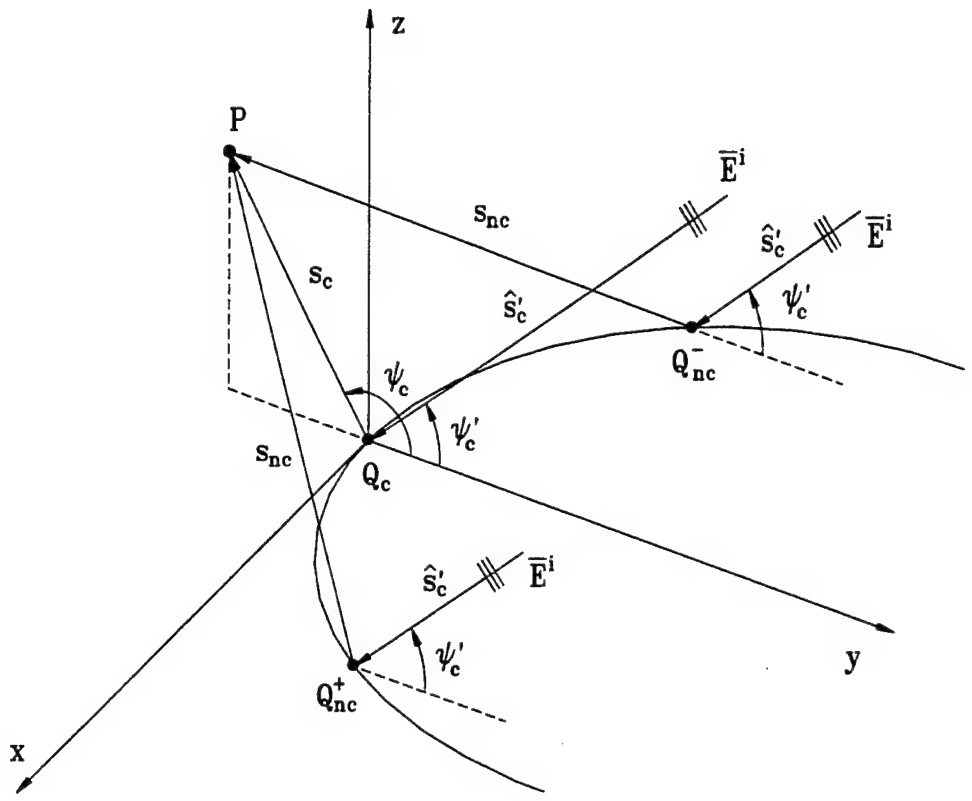

Figure 38: Caustic lit region diffracted ray geometry for the scattering by a flat plate with a curved edge.

using these in (626) in Appendix B and the fact that $\mu = -\eta$. Also, from (753c) and (764c) of Appendix D the second derivative of the phase function is

$$h^{II}(x_c) = -\left[\frac{1}{s_c} + \frac{1}{\rho^d(Q_c)}\right] \tag{369}$$

at the central stationary phase point and

$$\eta = \operatorname{sgn}\{h^{II}(x_c)\} = -\operatorname{sgn}\left\{\frac{\rho^d(Q_c)}{s_c[\rho^d(Q_c) + s_c]}\right\} \tag{370}$$

is the value of η. From (756c) and (765c) of Appendix D the second derivative of the phase function is

$$h^{II}(x_{nc}) = -\sin^2\beta_{nc}\left[\frac{1}{s_{nc}} + \frac{1}{\rho^d(Q_{nc})}\right]\left(\left.\frac{dl}{dx_e}\right|_{Q_{nc}}\right)^2 \tag{371}$$

at the non-central stationary phase points. The only remaining quantities to be determined are the values of the amplitude functions of the integrals evaluated at the central and non-central stationary phase points.

The first six derivatives of y_e are required in order to evaluate the amplitude functions of the diffraction integrals at the central stationary phase point. This is accomplished by differentiating the Taylor series form of y_e given in (309) and evaluating them at $x_e = x_c = 0$ to obtain

$$y_e|_{Q_c} = 0 \tag{372a}$$

$$\left.\frac{dy_e}{dx_e}\right|_{Q_c} = 0 \tag{372b}$$

$$\left.\frac{d^2y_e}{dx_e^2}\right|_{Q_c} = a_2 = \kappa_g(Q_c) \tag{372c}$$

$$\left.\frac{d^3y_e}{dx_e^3}\right|_{Q_c} = 0 \tag{372d}$$

$$\left.\frac{d^4y_e}{dx_e^4}\right|_{Q_c} = a_4 = \kappa_g^{II}(Q_c) + 3\kappa_g^3(Q_c) \tag{372e}$$

$$\left.\frac{d^5y_e}{dx_e^5}\right|_{Q_c} = 0 \tag{372f}$$

$$\left.\frac{d^6y_e}{dx_e^6}\right|_{Q_c} = a_6 = \kappa_g^{IV}(Q_c) + 34\kappa_g^2(Q_c)\kappa_g^{II}(Q_c) + 45\kappa_g^5(Q_c) \tag{372g}$$

which are also the coefficients of each term in the series using the definition of the Taylor series. Next, the common factor

$$\tilde{\mathcal{F}}_s(x_e) = \frac{\widetilde{D}_s(Q')}{\left(\frac{dl}{dx_e}\right) r^3 \sin\beta \sin\beta'} \tag{373}$$

can be observed in the amplitude functions of the soft polarization diffraction integrals of (347) through (352). This can be evaluated at the central stationary phase point as

$$\tilde{\mathcal{F}}_s(x_c) = \frac{1}{s_c^3}\, \widetilde{D}_s(Q_c) \tag{374}$$

using (767a), (776a) and (779a) of Appendix D. The remaining portions of the amplitude functions are found by substituting (336) into (347) through (352) and taking the limit as $x_e \to 0$. This results in

$$\tilde{A}_2^s(x_c) = \frac{\sin\psi_c'}{s_c^3\, \rho_g(Q_c)}\, \widetilde{D}_s(Q_c) \tag{375}$$

$$\tilde{A}_4^s(x_c) = \frac{-\left\{\rho_g(Q_c)\cos\psi_c + s_c \sin^2\psi_c\right\} \sin\psi_c'}{2 s_c^3\, \rho_g^3(Q_c)}\, \widetilde{D}_s(Q_c) \tag{376}$$

$$\tilde{B}_0^s(x_c) = \frac{1}{s_c^3}\, \widetilde{D}_s(Q_c) \tag{377}$$

$$\tilde{B}_4^s(x_c) = \frac{s_c\left[\kappa_g^{\text{II}}(Q_c) + 3\kappa_g^3(Q_c)\right] - 3\kappa_g^2(Q_c)}{12 s_c^3}\, \widetilde{D}_s(Q_c) \tag{378}$$

$$\tilde{C}_2^s(x_c) = \frac{\sin\psi_c \sin\psi_c'}{s_c^3\, \rho_g^2(Q_c)}\, \widetilde{D}_s(Q_c) \tag{379}$$

$$\tilde{C}_4^s(x_c) = \frac{-\left\{\rho_g(Q_c) - s_c\cos\psi_c\right\} \sin\psi_c \sin\psi_c'}{2 s_c^3\, \rho_g^3(Q_c)}\, \widetilde{D}_s(Q_c) \tag{380}$$

where repeated use of l'Hôpital's rule and (372) have been used to determine these limits. Similarly, the common factor

$$\tilde{\mathcal{F}}_h(x_e) = \frac{\widetilde{D}_h(Q')}{\left(\frac{dl}{dx_e}\right) r^2 \sin\beta \sin\beta'} \tag{381}$$

can be observed in the amplitude functions of the hard polarization diffraction integrals of (362) through (365). This can be evaluated at the central stationary phase point as

$$\tilde{\mathcal{F}}_h(x_c) = \frac{1}{s_c^2}\, \widetilde{D}_h(Q_c) \tag{382}$$

using (767a), (776a) and (779a) of Appendix D. The remaining portions of the amplitude functions are found by substituting (336) into (362) through (365) and taking the limit as $x_e \to 0$. This results in

$$\tilde{A}_2^h(x_c) = \frac{-\sin\psi_c}{2\,s_c^2\,\rho_g(Q_c)}\,\widetilde{D}_h(Q_c) \tag{383}$$

$$\tilde{B}_2^h(x_c) = \frac{\sin\psi_c \sin\psi_c'}{s_c^2\,\rho_g^2(Q_c)}\,\widetilde{D}_h(Q_c) \tag{384}$$

$$\tilde{C}_0^h(x_c) = \frac{1}{s_c^2}\,\widetilde{D}_h(Q_c) \tag{385}$$

$$\tilde{C}_2^h(x_c) = \frac{-\cos\psi_c}{2\,s_c^2\,\rho_g(Q_c)}\,\widetilde{D}_h(Q_c) \tag{386}$$

where repeated use of l'Hôpital's rule and (372) have been used to determine these limits. Next, the amplitude functions of the soft and hard polarization diffraction integrals can be evaluated at the non-central diffraction points. A result that is useful in simplifying these expressions is

$$\hat{e}(Q_{nc}) = \frac{\vec{e}(Q_{nc})}{\left(\frac{dl}{dx_e}\Big|_{Q_{nc}}\right)} \tag{387}$$

from (315) which is the unit edge vector evaluated at the non-central stationary phase points. Therefore, the amplitude functions of the soft polarization diffraction integrals of (347) through (352) are

$$x_{nc}^2\,\tilde{A}_2^s(x_{nc}) = \frac{\left[\vec{r}_e(Q_{nc})\cdot\hat{\beta}_c\right]\left[\hat{e}(Q_{nc})\cdot\hat{\psi}_c'\right]}{s_{nc}^3\sin^2\beta_{nc}}\,\widetilde{D}_s(Q_{nc}) \tag{388}$$

$$\begin{aligned} x_{nc}^4\,\tilde{A}_4^s(x_{nc}) &= \frac{s_c\left[\hat{e}(Q_{nc})\cdot\hat{\psi}_c\right]\left[\vec{r}_e(Q_{nc})\cdot\hat{\psi}_c\right]\left[\vec{e}(Q_{nc})\cdot\hat{\psi}_c'\right]}{s_{nc}^3\sin^2\beta_{nc}}\,\widetilde{D}_s(Q_{nc}) \\ &+ \frac{\left\{\hat{\psi}_c\cdot\left[\vec{r}_e(Q_{nc})\times\hat{e}(Q_{nc})\right]\right\}\left[\vec{r}_e(Q_{nc})\cdot\hat{\beta}_c\right]\left[\vec{e}(Q_{nc})\cdot\hat{\psi}_c'\right]}{s_{nc}^3\sin^2\beta_{nc}}\,\widetilde{D}_s(Q_{nc}) \end{aligned} \tag{389}$$

$$\tilde{B}_0^s(x_{nc}) = \frac{1}{\left(\frac{dl}{dx_e}\Big|_{Q_{nc}}\right)s_{nc}^3\sin^2\beta_{nc}}\,\widetilde{D}_s(Q_{nc}) \tag{390}$$

$$\begin{aligned} x_{nc}^4\,\tilde{B}_4^s(x_{nc}) &= \frac{\left\{\hat{\psi}_c\cdot\left[\vec{r}_e(Q_{nc})\times\hat{e}(Q_{nc})\right]\right\}\left[\vec{r}_e(Q_{nc})\cdot\hat{s}_c\right]}{s_{nc}^3\sin^2\beta_{nc}}\,\widetilde{D}_s(Q_{nc}) \\ &+ \frac{-s_c\left(\left\{\hat{\psi}_c\cdot\left[\vec{r}_e(Q_{nc})\times\hat{e}(Q_{nc})\right]\right\} - \left[\hat{e}(Q_{nc})\cdot\hat{\beta}_c\right]\left[\vec{r}_e(Q_{nc})\cdot\hat{s}_c\right]\right)}{s_{nc}^3\sin^2\beta_{nc}}\,\widetilde{D}_s(Q_{nc}) \end{aligned}$$

$$+\frac{-\{\hat{s}_c\cdot[\vec{r}_e(Q_{nc})\times\hat{e}(Q_{nc})]\}\left[\vec{r}_e(Q_{nc})\cdot\hat{\psi}_c\right]}{s_{nc}^3\sin^2\beta_{nc}}\widetilde{D}_s(Q_{nc}) \tag{391}$$

$$x_{nc}^2\,\tilde{C}_2^s(x_{nc}) = \frac{\left[\hat{e}(Q_{nc})\cdot\hat{\psi}_c\right]\left[\vec{e}(Q_{nc})\cdot\hat{\psi}_c'\right]}{s_{nc}^3\sin^2\beta_{nc}}\widetilde{D}_s(Q_{nc}) \tag{392}$$

$$x_{nc}^4\,\tilde{C}_4^s(x_{nc}) = \frac{s_c\left[\hat{e}(Q_{nc})\cdot\hat{\psi}_c\right]\left[\vec{r}_e(Q_{nc})\cdot\hat{s}_c\right]\left[\vec{e}(Q_{nc})\cdot\hat{\psi}_c'\right]}{s_{nc}^3\sin^2\beta_{nc}}\widetilde{D}_s(Q_{nc})$$
$$+\frac{\{\hat{s}_c\cdot[\vec{r}_e(Q_{nc})\times\hat{e}(Q_{nc})]\}\left[\vec{r}_e(Q_{nc})\cdot\hat{\beta}_c\right]\left[\vec{e}(Q_{nc})\cdot\hat{\psi}_c'\right]}{s_{nc}^3\sin^2\beta_{nc}}\widetilde{D}_s(Q_{nc}) \tag{393}$$

at the non-central stationary phase points and the amplitude functions of the hard polarization diffraction integrals of (362) through (365) are

$$x_{nc}^2\,\tilde{A}_2^h(x_{nc}) = \frac{\{\hat{s}_c\cdot[\vec{r}_e(Q_{nc})\times\hat{e}(Q_{nc})]\}}{s_{nc}^2\sin^2\beta_{nc}}\widetilde{D}_h(Q_{nc}) \tag{394}$$

$$x_{nc}^2\,\tilde{B}_2^h(x_{nc}) = \frac{\left[\hat{e}(Q_{nc})\cdot\hat{\psi}_c\right]\left[\vec{e}(Q_{nc})\cdot\hat{\psi}_c'\right]}{s_{nc}^2\sin^2\beta_{nc}}\widetilde{D}_h(Q_{nc}) \tag{395}$$

$$\tilde{C}_0^h(x_{nc}) = \frac{1}{\left(\frac{dl}{dx_e}\Big|_{Q_{nc}}\right)s_{nc}^2\sin^2\beta_{nc}}\widetilde{D}_h(Q_{nc}) \tag{396}$$

$$x_{nc}^2\,\tilde{C}_2^h(x_{nc}) = \frac{\left\{\hat{\psi}_c\cdot[\vec{r}_e(Q_{nc})\times\hat{e}(Q_{nc})]\right\}}{s_{nc}^2\sin^2\beta_{nc}}\widetilde{D}_h(Q_{nc}) \tag{397}$$

at the non-central stationary phase points. This completes the derivation of the quantities required to obtain uniform asymptotic expressions for the diffracted field on the lit side of the caustic. It is now necessary to substitute these quantities into the uniform asymptotic expansion derived in Section 2 of Appendix B and simplify the result to obtain a standard ray optical form.

The uniform asymptotic expansions of the soft and hard polarized diffraction integrals can now be performed since all the necessary quantities have been determined. To make the uniform asymptotic expansions easier to simplify we can recognize that

$$\frac{e^{j\eta\pi/4}}{\sqrt{|h^{II}(x_c)|}} = s_c\sqrt{\frac{\rho^d(Q_c)}{s_c\left[\rho^d(Q_c)+s_c\right]}}\;e^{-j\pi/4} \tag{398}$$

at the central stationary phase point and

$$\frac{e^{-j\eta\pi/4}}{\sqrt{|h^{II}(x_{nc})|}} = \frac{s_{nc}}{\left(\frac{dl}{dx_e}\Big|_{Q_{nc}}\right)\sin\beta_{nc}}\sqrt{\frac{\rho^d(Q_{nc})}{s_{nc}\left[\rho^d(Q_{nc})+s_{nc}\right]}}\;e^{-j\pi/4} \tag{399}$$

at the non-central stationary phase points. The diffraction coefficients and caustic distances at Q_{nc}^{+} and Q_{nc}^{-} are equal because of the assumed symmetry of the geometry. Therefore, $D_{s,h}(Q_{nc}) = D_{s,h}(Q_{nc}^{+}) = D_{s,h}(Q_{nc}^{-})$ and $\rho^d(Q_{nc}) = \rho^d(Q_{nc}^{+}) = \rho^d(Q_{nc}^{-})$ will be used for the remainder of this chapter. We begin here by determining the uniform asymptotic expansions of the soft polarization diffraction integrals of (341) through (346). It is assumed here that the function $\tilde{A}_2^s(x_e)$ is a smooth and slowly varying function of x_e near the stationary phase points and $k \gg 1$. This allows us to use the uniform asymptotic expansion (657) of Appendix B. Therefore, the uniform asymptotic expansion of (341) is

$$
\begin{aligned}
\widehat{s}_c \mathcal{I}_2^s(P) \;\sim\; & \widehat{s}_c \, E_{\psi_c}^i \frac{s_c}{2\pi} \tilde{A}_2^s(x_c) \frac{\sqrt{2\pi}}{k^{3/2}} \left\{ \frac{e^{j\eta\pi/4}}{\sqrt{|h^{\,\mathrm{II}}(x_c)|}} \right\}^3 e^{jkh(x_c)} T_c(\xi, 2) \\
& - \widehat{s}_c \, 2E_{\psi_c}^i \frac{s_c \left[\vec{e}(Q_{nc}) \cdot \widehat{\beta}_c \right]}{2\pi} \left\{ x_{nc}^2 \tilde{A}_2^s(x_{nc}) \right\} \sqrt{\frac{2\pi}{k}} \\
& \times \left\{ \frac{e^{-j\eta\pi/4}}{\sqrt{|h^{\,\mathrm{II}}(x_{nc})|}} \right\} e^{jkh(x_{nc})} T_{nc}(\xi, \eta, 2) \\
\sim\; & \vec{E}^i(Q_c) \cdot \left\{ -\widehat{\psi}' \, \widehat{s}_c \left(\frac{s_c \sin \psi_c'}{jk\rho_g(Q_c)} \right) D_s(Q_c) T_c(\xi, 2) \right\} \\
& \times \left\{ \frac{\rho^d(Q_c)}{s_c \left[\rho^d(Q_c) + s_c \right]} \right\}^{3/2} e^{-jks_c} \\
+ \;\; & \vec{E}^i(Q_{nc}^{+}) \cdot \left\{ -\widehat{\beta}' \, \widehat{s}_c \left(\frac{-s_c \left[\widehat{e}(Q_{nc}) \cdot \widehat{\beta}_c \right] \left[\vec{r}_e(Q_{nc}) \cdot \widehat{\beta}_c \right]}{s_{nc}^2 \sin \beta_{nc}} \right) D_s(Q_{nc}) \right. \\
& \left. \times T_{nc}(\xi, \eta, 2) \right\} \sqrt{\frac{\rho^d(Q_{nc})}{s_{nc} \left[\rho^d(Q_{nc}) + s_{nc} \right]}} \, e^{-jks_{nc}} \\
+ \;\; & \vec{E}^i(Q_{nc}^{-}) \cdot \left\{ -\widehat{\beta}' \, \widehat{s}_c \left(\frac{-s_c \left[\widehat{e}(Q_{nc}) \cdot \widehat{\beta}_c \right] \left[\vec{r}_e(Q_{nc}) \cdot \widehat{\beta}_c \right]}{s_{nc}^2 \sin \beta_{nc}} \right) D_s(Q_{nc}) \right. \\
& \left. \times T_{nc}(\xi, \eta, 2) \right\} \sqrt{\frac{\rho^d(Q_{nc})}{s_{nc} \left[\rho^d(Q_{nc}) + s_{nc} \right]}} \, e^{-jks_{nc}} \qquad (400)
\end{aligned}
$$

where (375), (388), (398) and (399) have been used to simplify the result. It is now assumed that the function $\tilde{A}_4^s(x_e)$ is a smooth and slowly varying function of x_e near the stationary phase points and $k \gg 1$. This allows us to use the uniform asymptotic expansion (657) of Appendix B. Therefore, the uniform asymptotic expansion of (342)

is

$$\begin{aligned}
\widehat{s}_c \mathcal{I}_4^s(P) \;\sim\; & -\widehat{s}_c\, E^i_{\psi_c} \frac{1}{2\pi} \tilde{A}_4^s(x_c) \frac{3\sqrt{2\pi}}{k^{5/2}} \left\{ \frac{e^{j\eta\pi/4}}{\sqrt{|h^{\,\mathrm{II}}(x_c)|}} \right\}^5 e^{jkh(x_c)} T_c(\xi, 4) \\
& -\widehat{s}_c\, 2\, E^i_{\psi_c} \frac{1}{2\pi} \left\{ x_{nc}^4 \tilde{A}_4^s(x_{nc}) \right\} \sqrt{\frac{2\pi}{k}} \left\{ \frac{e^{-j\eta\pi/4}}{\sqrt{|h^{\,\mathrm{II}}(x_{nc})|}} \right\} e^{jkh(x_{nc})} T_{nc}(\xi, \eta, 4) \\
\sim\; & \vec{E}^i(Q_c) \cdot \left\{ -\widehat{\psi}'\, \widehat{s}_c \left(\frac{-3s_c^2 \left\{ \rho_g(Q_c) \cos\psi_c + s_c \sin^2\psi_c \right\} \sin\psi_c'}{2k^2 \rho_g^3(Q_c)} \right) \right. \\
& \left. \times D_s(Q_c)\, T_c(\xi, 4) \right\} \left\{ \frac{\rho^d(Q_c)}{s_c \left[\rho^d(Q_c) + s_c \right]} \right\}^{5/2} e^{-jks_c} \\
+\; & \vec{E}^i(Q_{nc}^+) \cdot \left\{ -\widehat{\beta}'\, \widehat{s}_c \left(\frac{-\left\{ \widehat{\psi}_c \cdot [\vec{r}_e(Q_{nc}) \times \widehat{e}(Q_{nc})] \right\} \left[\vec{r}_e(Q_{nc}) \cdot \widehat{\beta}_c \right]}{s_{nc}^2 \sin\beta_{nc}} \right. \right. \\
& \left. + \frac{-s_c \left[\widehat{e}(Q_{nc}) \cdot \widehat{\psi}_c \right] \left[\vec{r}_e(Q_{nc}) \cdot \widehat{\psi}_c \right]}{s_{nc}^2 \sin\beta_{nc}} \right) \\
& \left. \times D_s(Q_{nc}) T_{nc}(\xi, \eta, 4) \right\} \sqrt{\frac{\rho^d(Q_{nc})}{s_{nc} \left[\rho^d(Q_{nc}) + s_{nc} \right]}}\, e^{-jks_{nc}} \\
+\; & \vec{E}^i(Q_{nc}^-) \cdot \left\{ -\widehat{\beta}'\, \widehat{s}_c \left(\frac{-\left\{ \widehat{\psi}_c \cdot [\vec{r}_e(Q_{nc}) \times \widehat{e}(Q_{nc})] \right\} \left[\vec{r}_e(Q_{nc}) \cdot \widehat{\beta}_c \right]}{s_{nc}^2 \sin\beta_{nc}} \right. \right. \\
& \left. + \frac{-s_c \left[\widehat{e}(Q_{nc}) \cdot \widehat{\psi}_c \right] \left[\vec{r}_e(Q_{nc}) \cdot \widehat{\psi}_c \right]}{s_{nc}^2 \sin\beta_{nc}} \right) \\
& \left. \times D_s(Q_{nc})\, T_{nc}(\xi, \eta, 4) \right\} \sqrt{\frac{\rho^d(Q_{nc})}{s_{nc} \left[\rho^d(Q_{nc}) + s_{nc} \right]}}\, e^{-jks_{nc}} \qquad (401)
\end{aligned}$$

where (376), (389), (398) and (399) have been used to simplify the result. It is now assumed that the function $\tilde{B}_0^s(x_e)$ is a smooth and slowly varying function of x_e near the stationary phase points and $k \gg 1$. This allows us to use the uniform asymptotic expansion (657) of Appendix B. Therefore, the uniform asymptotic expansion of (343) is

$$\begin{aligned}
\widehat{\beta}_c \mathcal{J}_0^s(P) \;\sim\; & \widehat{\beta}_c\, E^i_{\beta_c} \frac{s_c^2}{2\pi} \tilde{B}_0^s(x_c) \sqrt{\frac{2\pi}{k}} \left\{ \frac{e^{j\eta\pi/4}}{\sqrt{|h^{\,\mathrm{II}}(x_c)|}} \right\} e^{jkh(x_c)} T_c(\xi, 0) \\
& -\widehat{\beta}_c\, 2\, E^i_{\beta_c} \frac{s_c^2 \left[\vec{e}(Q_{nc}) \cdot \widehat{\beta}_c \right] \left[\vec{e}(Q_{nc}) \cdot \widehat{\beta}_c' \right]}{2\pi} \tilde{B}_0^s(x_{nc}) \sqrt{\frac{2\pi}{k}} \\
& \times \left\{ \frac{e^{-j\eta\pi/4}}{\sqrt{|h^{\,\mathrm{II}}(x_{nc})|}} \right\} e^{jkh(x_{nc})}\, T_{nc}(\xi, \eta, 0)
\end{aligned}$$

$$
\begin{aligned}
&\sim \vec{E}^i(Q_c)\cdot\left\{-\widehat{\beta}'\,\widehat{\beta}_c D_s(Q_c)T_c(\xi,0)\right\}\sqrt{\frac{\rho^d(Q_c)}{s_c\left[\rho^d(Q_c)+s_c\right]}}\;e^{-jks_c}\\
&+\ \vec{E}^i(Q_{nc}^+)\cdot\left\{-\widehat{\beta}'\,\widehat{\beta}_c\left(\frac{-s_c^2\left[\widehat{e}(Q_{nc})\cdot\widehat{\beta}_c\right]}{s_{nc}^2\sin\beta_{nc}}\right)D_s(Q_{nc})\right.\\
&\qquad\left.\times T_{nc}(\xi,\eta,0)\right\}\sqrt{\frac{\rho^d(Q_{nc})}{s_{nc}\left[\rho^d(Q_{nc})+s_{nc}\right]}}\;e^{-jks_{nc}}\\
&+\ \vec{E}^i(Q_{nc}^-)\cdot\left\{-\widehat{\beta}'\,\widehat{\beta}_c\left(\frac{-s_c^2\left[\widehat{e}(Q_{nc})\cdot\widehat{\beta}_c\right]}{s_{nc}^2\sin\beta_{nc}}\right)D_s(Q_{nc})\right.\\
&\qquad\left.\times T_{nc}(\xi,\eta,0)\right\}\sqrt{\frac{\rho^d(Q_{nc})}{s_{nc}\left[\rho^d(Q_{nc})+s_{nc}\right]}}\;e^{-jks_{nc}}
\end{aligned}
\tag{402}
$$

where (377), (390), (398) and (399) have been used to simplify the result. It is now assumed that the function $\tilde{B}_4^s(x_e)$ is a smooth and slowly varying function of x_e near the stationary phase points and $k \gg 1$. This allows us to use the uniform asymptotic expansion (657) of Appendix B. Therefore, the uniform asymptotic expansion of (344) is

$$
\begin{aligned}
\widehat{\beta}_c\,\mathcal{J}_4^s(P) &\sim \widehat{\beta}_c\,E^i_{\beta_c}\frac{1}{2\pi}\tilde{B}_4^s(x_c)\,\frac{3\sqrt{2\pi}}{k^{5/2}}\left\{\frac{e^{j\eta\pi/4}}{\sqrt{|h^{\,\mathrm{II}}(x_c)|}}\right\}^5 e^{jkh(x_c)}T_c(\xi,4)\\
&\quad-\widehat{\beta}_c\,2\,E^i_{\beta_c}\frac{\left[\vec{e}(Q_{nc})\cdot\widehat{\beta}'_c\right]}{2\pi}\left\{x_{nc}^4\tilde{B}_4^s(x_{nc})\right\}\sqrt{\frac{2\pi}{k}}\\
&\qquad\times\left\{\frac{e^{-j\eta\pi/4}}{\sqrt{|h^{\,\mathrm{II}}(x_{nc})|}}\right\}e^{jkh(x_{nc})}\,T_{nc}(\xi,\eta,4)\\
&\sim \vec{E}^i(Q_c)\cdot\left\{-\widehat{\beta}'\,\widehat{\beta}_c\left(\frac{3s_c^2\kappa_g^2(Q_c)-s_c^3\left[\kappa_g^{\,\mathrm{II}}(Q_c)+3\kappa_g^3(Q_c)\right]}{4k^2}\right)D_s(Q_c)\right.\\
&\qquad\left.\times T_c(\xi,4)\right\}\left\{\frac{\rho^d(Q_c)}{s_c\left[\rho^d(Q_c)+s_c\right]}\right\}^{5/2}e^{-jks_c}\\
&+\ \vec{E}^i(Q_{nc}^+)\cdot\left\{-\widehat{\beta}'\,\widehat{\beta}_c\left(\frac{\left\{\widehat{\psi}_c\cdot\left[\vec{r}_e(Q_{nc})\times\widehat{e}(Q_{nc})\right]\right\}\left[\vec{r}_e(Q_{nc})\cdot\widehat{s}_c\right]}{s_{nc}^2\sin\beta_{nc}}\right.\right.\\
&\qquad+\frac{-s_c\left(\left\{\widehat{\psi}_c\cdot\left[\vec{r}_e(Q_{nc})\times\vec{e}(Q_{nc})\right]\right\}-\left[\widehat{e}(Q_{nc})\cdot\widehat{\beta}_c\right]\left[\vec{r}_e(Q_{nc})\cdot\widehat{s}_c\right]\right)}{s_{nc}^2\sin\beta_{nc}}\\
&\qquad\left.\left.+\frac{-\left\{\widehat{s}_c\cdot\left[\vec{r}_e(Q_{nc})\times\widehat{e}(Q_{nc})\right]\right\}\left[\vec{r}_e(Q_{nc})\cdot\widehat{\psi}_c\right]}{s_{nc}^2\sin\beta_{nc}}\right)D_s(Q_{nc})\right.
\end{aligned}
$$

$$\times T_{nc}(\xi,\eta,4)\Bigg\}\sqrt{\frac{\rho^d(Q_{nc})}{s_{nc}\left[\rho^d(Q_{nc})+s_{nc}\right]}}\;e^{-jks_{nc}}$$

$$+\quad \vec{E}^i(Q_{nc}^-)\cdot\Bigg\{-\widehat{\beta}'\,\widehat{\beta}_c\Bigg(\frac{\left\{\widehat{\psi}_c\cdot[\vec{r}_e(Q_{nc})\times\widehat{e}(Q_{nc})]\right\}[\vec{r}_e(Q_{nc})\cdot\widehat{s}_c]}{s_{nc}^2\sin\beta_{nc}}$$

$$+\frac{-s_c\left(\left\{\widehat{\psi}_c\cdot[\vec{r}_e(Q_{nc})\times\vec{e}(Q_{nc})]\right\}-\left[\widehat{e}(Q_{nc})\cdot\widehat{\beta}_c\right][\vec{r}_e(Q_{nc})\cdot\widehat{s}_c]\right)}{s_{nc}^2\sin\beta_{nc}}$$

$$+\frac{-\{\widehat{s}_c\cdot[\vec{r}_e(Q_{nc})\times\widehat{e}(Q_{nc})]\}\left[\vec{r}_e(Q_{nc})\cdot\widehat{\psi}_c\right]}{s_{nc}^2\sin\beta_{nc}}\Bigg)D_s(Q_{nc})$$

$$\times T_{nc}(\xi,\eta,4)\Bigg\}\sqrt{\frac{\rho^d(Q_{nc})}{s_{nc}\left[\rho^d(Q_{nc})+s_{nc}\right]}}\;e^{-jks_{nc}} \tag{403}$$

where (378), (391), (398) and (399) have been used to simplify the result. It is now assumed that the function $\tilde{C}_2^s(x_e)$ is a smooth and slowly varying function of x_e near the stationary phase points and $k\gg 1$. This allows us to use the uniform asymptotic expansion (657) of Appendix B. Therefore, the uniform asymptotic expansion of (345) is

$$\widehat{\psi}_c\,\mathcal{K}_2^s(P)\;\sim\;-\widehat{\psi}_c\,E_{\psi_c}^i\frac{s_c^2}{2\pi}\tilde{C}_2^s(x_c)\frac{\sqrt{2\pi}}{k^{3/2}}\left\{\frac{e^{j\eta\pi/4}}{\sqrt{|h^{\,\mathrm{II}}(x_c)|}}\right\}^3 e^{jkh(x_c)}T_c(\xi,2)$$

$$-\widehat{\psi}_c\,2E_{\psi_c}^i\frac{s_c^2}{2\pi}\left\{x_{nc}^2\tilde{C}_2^s(x_{nc})\right\}\sqrt{\frac{2\pi}{k}}$$

$$\times\left\{\frac{e^{-j\eta\pi/4}}{\sqrt{|h^{\,\mathrm{II}}(x_{nc})|}}\right\}e^{jkh(x_{nc})}\,T_{nc}(\xi,\eta,2)$$

$$\sim\;\vec{E}^i(Q_c)\cdot\left\{-\widehat{\psi}'\,\widehat{\psi}_c\left(\frac{js_c^2\sin\psi_c\sin\psi_c'}{k\rho_g^2(Q_c)}\right)D_s(Q_c)\,T_c(\xi,2)\right\}$$

$$\times\left\{\frac{\rho^d(Q_c)}{s_c\left[\rho^d(Q_c)+s_c\right]}\right\}^{3/2}e^{-jks_c}$$

$$+\quad\vec{E}^i(Q_{nc}^+)\cdot\left\{-\widehat{\beta}'\,\widehat{\psi}_c\left(\frac{-s_c^2\left[\widehat{e}(Q_{nc})\cdot\widehat{\psi}_c\right]}{s_{nc}^2\sin\beta_{nc}}\right)D_s(Q_{nc})\right.$$

$$\left.\times T_{nc}(\xi,\eta,2)\right\}\sqrt{\frac{\rho^d(Q_{nc})}{s_{nc}\left[\rho^d(Q_{nc})+s_{nc}\right]}}\;e^{-jks_{nc}}$$

$$+\quad\vec{E}^i(Q_{nc}^-)\cdot\left\{-\widehat{\beta}'\,\widehat{\psi}_c\left(\frac{-s_c^2\left[\widehat{e}(Q_{nc})\cdot\widehat{\psi}_c\right]}{s_{nc}^2\sin\beta_{nc}}\right)D_s(Q_{nc})\right.$$

$$\times T_{nc}(\xi,\eta,2)\Bigg\}\sqrt{\frac{\rho^d(Q_{nc})}{s_{nc}\left[\rho^d(Q_{nc})+s_{nc}\right]}}\;e^{-jks_{nc}} \tag{404}$$

where (379), (392), (398) and (399) have been used to simplify the result. It is now assumed that the function $\tilde{C}_4^s(x_e)$ is a smooth and slowly varying function of x_e near the stationary phase points and $k \gg 1$. This allows us to use the uniform asymptotic expansion (657) of Appendix B. Therefore, the uniform asymptotic expansion of (346) is

$$\begin{aligned}
\widehat{\psi}_c\,\mathcal{K}_4^s(P) \;\sim\;& \widehat{\psi}_c\,E^i_{\psi_c}\frac{1}{2\pi}\tilde{C}_4^s(x_c)\,\frac{3\sqrt{2\pi}}{k^{5/2}}\left\{\frac{e^{j\eta\pi/4}}{\sqrt{|h^{\,\mathrm{II}}(x_c)|}}\right\}^5 e^{jkh(x_c)}T_c(\xi,4)\\
&+\widehat{\psi}_c\,2\,E^i_{\psi_c}\,\frac{1}{2\pi}\left\{x_{nc}^4\tilde{C}_4^s(x_{nc})\right\}\sqrt{\frac{2\pi}{k}}\\
&\qquad\times\left\{\frac{e^{-j\eta\pi/4}}{\sqrt{|h^{\,\mathrm{II}}(x_{nc})|}}\right\}e^{jkh(x_{nc})}T_{nc}(\xi,\eta,4)\\
\sim\;& \vec{E}^i(Q_c)\cdot\Bigg\{-\widehat{\psi}'\,\widehat{\psi}_c\left(\frac{3s_c^2\left\{\rho_g(Q_c)-s_c\cos\psi_c\right\}\sin\psi_c\sin\psi_c'}{2k^2\rho_g^3(Q_c)}\right)\\
&\qquad\times D_s(Q_c)\,T_c(\xi,4)\Bigg\}\left\{\frac{\rho^d(Q_c)}{s_c\left[\rho^d(Q_c)+s_c\right]}\right\}^{5/2}e^{-jks_c}\\
+\;& \vec{E}^i(Q_{nc}^+)\cdot\Bigg\{-\widehat{\beta}'\,\widehat{\psi}_c\left(\frac{s_c\left[\widehat{e}\,(Q_{nc})\cdot\widehat{\psi}_c\right]\left[\vec{r}_e(Q_{nc})\cdot\widehat{s}_c\right]}{s_{nc}^2\sin\beta_{nc}}\right.\\
&\qquad\left.+\frac{\left\{\widehat{s}_c\cdot\left[\vec{r}_e(Q_{nc})\times\widehat{e}\,(Q_{nc})\right]\right\}\left[\vec{r}_e(Q_{nc})\cdot\widehat{\beta}_c\right]}{s_{nc}^2\sin\beta_{nc}}\right)D_s(Q_{nc})\\
&\qquad\times T_{nc}(\xi,\eta,4)\Bigg\}\sqrt{\frac{\rho^d(Q_{nc})}{s_{nc}\left[\rho^d(Q_{nc})+s_{nc}\right]}}\;e^{-jks_{nc}}\\
+\;& \vec{E}^i(Q_{nc}^-)\cdot\Bigg\{-\widehat{\beta}'\,\widehat{\psi}_c\left(\frac{s_c\left[\widehat{e}\,(Q_{nc})\cdot\widehat{\psi}_c\right]\left[\vec{r}_e(Q_{nc})\cdot\widehat{s}_c\right]}{s_{nc}^2\sin\beta_{nc}}\right.\\
&\qquad\left.+\frac{\left\{\widehat{s}_c\cdot\left[\vec{r}_e(Q_{nc})\times\widehat{e}\,(Q_{nc})\right]\right\}\left[\vec{r}_e(Q_{nc})\cdot\widehat{\beta}_c\right]}{s_{nc}^2\sin\beta_{nc}}\right)D_s(Q_{nc})\\
&\qquad\times T_{nc}(\xi,\eta,4)\Bigg\}\sqrt{\frac{\rho^d(Q_{nc})}{s_{nc}\left[\rho^d(Q_{nc})+s_{nc}\right]}}\;e^{-jks_{nc}}
\end{aligned} \tag{405}$$

where (380), (393), (398) and (399) have been used to simplify the result. Next, it is necessary to determine the uniform asymptotic expansions of the hard polarization diffraction integrals of (358) through (361). It is assumed here that the function

$\tilde{A}_2^h(x_e)$ is a smooth and slowly varying function of x_e near the stationary phase points and $k \gg 1$. This allows us to use the uniform asymptotic expansion (657) of Appendix B. Therefore, the uniform asymptotic expansion of (358) is

$$\begin{aligned}
\widehat{s}_c\,\mathcal{I}_2^h(P) \;\sim\; & -\widehat{s}_c\,E^i_{\psi_c}\frac{1}{2\pi}\tilde{A}_2^h(x_c)\,\frac{\sqrt{2\pi}}{k^{3/2}}\left\{\frac{e^{j\eta\pi/4}}{\sqrt{|h^{\,\mathrm{II}}(x_c)|}}\right\}^3 e^{jkh(x_c)}T_c(\xi,2) \\
& -\widehat{s}_c\,2E^i_{\psi_c}\frac{\left[\vec{e}(Q_{nc})\cdot\widehat{\beta}'_c\right]}{2\pi}\left\{x_{nc}^2\tilde{A}_2^h(x_{nc})\right\}\sqrt{\frac{2\pi}{k}} \\
& \times\left\{\frac{e^{-j\eta\pi/4}}{\sqrt{|h^{\,\mathrm{II}}(x_{nc})|}}\right\} e^{jkh(x_{nc})}\,T_{nc}(\xi,\eta,2) \\
\sim\; & \vec{E}^i(Q_c)\cdot\left\{-\widehat{\psi}'\,\widehat{s}_c\left(\frac{s_c\sin\psi_c}{2jk\rho_g(Q_c)}\right)D_h(Q_c)\,T_c(\xi,2)\right\} \\
& \times\left\{\frac{\rho^d(Q_c)}{s_c\,[\rho^d(Q_c)+s_c]}\right\}^{3/2} e^{-jks_c} \\
+\;\; & \vec{E}^i(Q_{nc}^+)\cdot\left\{-\widehat{\psi}'\,\widehat{s}_c\left(\frac{-\{\widehat{s}_c\cdot[\vec{r}_e(Q_{nc})\times\widehat{e}(Q_{nc})]\}}{s_{nc}\sin\beta_{nc}}\right)D_h(Q_{nc})\right. \\
& \left.\times T_{nc}(\xi,\eta,2)\right\}\sqrt{\frac{\rho^d(Q_{nc})}{s_{nc}\,[\rho^d(Q_{nc})+s_{nc}]}}\;e^{-jks_{nc}} \\
+\;\; & \vec{E}^i(Q_{nc}^-)\cdot\left\{-\widehat{\psi}'\,\widehat{s}_c\left(\frac{-\{\widehat{s}_c\cdot[\vec{r}_e(Q_{nc})\times\widehat{e}(Q_{nc})]\}}{s_{nc}\sin\beta_{nc}}\right)D_h(Q_{nc})\right. \\
& \left.\times T_{nc}(\xi,\eta,2)\right\}\sqrt{\frac{\rho^d(Q_{nc})}{s_{nc}\,[\rho^d(Q_{nc})+s_{nc}]}}\;e^{-jks_{nc}} \qquad (406)
\end{aligned}$$

where (383), (394), (398) and (399) have been used to simplify the result. It is now assumed that the function $\tilde{B}_2^h(x_e)$ is a smooth and slowly varying function of x_e near the stationary phase points and $k \gg 1$. This allows us to use the uniform asymptotic expansion (657) of Appendix B. Therefore, the uniform asymptotic expansion of (359) is

$$\begin{aligned}
\widehat{\beta}_c\,\mathcal{J}_2^h(P) \;\sim\; & -\widehat{\beta}_c\,E^i_{\beta_c}\frac{s_c}{2\pi}\tilde{B}_2^h(x_c)\,\frac{\sqrt{2\pi}}{k^{3/2}}\left\{\frac{e^{j\eta\pi/4}}{\sqrt{|h^{\,\mathrm{II}}(x_c)|}}\right\}^3 e^{jkh(x_c)}T_c(\xi,2) \\
& -\widehat{\beta}_c\,2\,E^i_{\beta_c}\frac{s_c}{2\pi}\left\{x_{nc}^2\tilde{B}_2^h(x_{nc})\right\}\sqrt{\frac{2\pi}{k}} \\
& \times\left\{\frac{e^{-j\eta\pi/4}}{\sqrt{|h^{\,\mathrm{II}}(x_{nc})|}}\right\} e^{jkh(x_{nc})}\,T_{nc}(\xi,\eta,2)
\end{aligned}$$

$$
\begin{aligned}
&\sim \vec{E}^{i}(Q_c)\cdot\left\{-\widehat{\beta}'\,\widehat{\beta}_c\left(\frac{js_c^2\sin\psi_c\sin\psi_c'}{k\rho_g^2(Q_c)}\right)D_h(Q_c)\,T_c(\xi,2)\right\}\\
&\qquad\times\left\{\frac{\rho^d(Q_c)}{s_c\,[\rho^d(Q_c)+s_c]}\right\}^{3/2}e^{-jks_c}\\
&+\ \vec{E}^{i}(Q_{nc}^{+})\cdot\left\{-\widehat{\psi}'\,\widehat{\beta}_c\left(\frac{s_c\left[\widehat{e}(Q_{nc})\cdot\widehat{\psi}_c\right]}{s_{nc}\sin\beta_{nc}}\right)D_h(Q_{nc})\right.\\
&\qquad\left.\times T_{nc}(\xi,\eta,2)\right\}\sqrt{\frac{\rho^d(Q_{nc})}{s_{nc}\,[\rho^d(Q_{nc})+s_{nc}]}}\,e^{-jks_{nc}}\\
&+\ \vec{E}^{i}(Q_{nc}^{-})\cdot\left\{-\widehat{\psi}'\,\widehat{\beta}_c\left(\frac{s_c\left[\widehat{e}(Q_{nc})\cdot\widehat{\psi}_c\right]}{s_{nc}\sin\beta_{nc}}\right)D_h(Q_{nc})\right.\\
&\qquad\left.\times T_{nc}(\xi,\eta,2)\right\}\sqrt{\frac{\rho^d(Q_{nc})}{s_{nc}\,[\rho^d(Q_{nc})+s_{nc}]}}\,e^{-jks_{nc}}
\end{aligned}
\tag{407}
$$

where (384), (395), (398) and (399) have been used to simplify the result. It is now assumed that the function $\tilde{C}_0^h(x_e)$ is a smooth and slowly varying function of x_e near the stationary phase points and $k \gg 1$. This allows us to use the uniform asymptotic expansion (657) of Appendix B. Therefore, the uniform asymptotic expansion of (360) is

$$
\begin{aligned}
\widehat{\psi}_c\,K_0^h(P) &\sim \widehat{\psi}_c\,E_{\psi_c}^{i}\frac{s_c}{2\pi}\,\tilde{C}_0^h(x_c)\sqrt{\frac{2\pi}{k}}\left\{\frac{e^{j\eta\pi/4}}{\sqrt{|h^{II}(x_c)|}}\right\}e^{jkh(x_c)}T_c(\xi,0)\\
&\quad-\widehat{\psi}_c\,2\,E_{\psi_c}^{i}\frac{s_c\left[\vec{e}(Q_{nc})\cdot\widehat{\beta}_c\right]\left[\vec{e}(Q_{nc})\cdot\widehat{\beta}_c'\right]}{2\pi}\,\tilde{C}_0^h(x_{nc})\sqrt{\frac{2\pi}{k}}\\
&\qquad\times\left\{\frac{e^{-j\eta\pi/4}}{\sqrt{|h^{II}(x_{nc})|}}\right\}e^{jkh(x_{nc})}T_{nc}(\xi,\eta,0)\\
&\sim \vec{E}^{i}(Q_c)\cdot\left\{-\widehat{\psi}'\,\widehat{\psi}_c\,D_h(Q_c)\,T_c(\xi,0)\right\}\sqrt{\frac{\rho^d(Q_c)}{s_c\,[\rho^d(Q_c)+s_c]}}\,e^{-jks_c}\\
&+\ \vec{E}^{i}(Q_{nc}^{+})\cdot\left\{-\widehat{\psi}'\,\widehat{\psi}_c\left(\frac{-s_c\left[\widehat{e}(Q_{nc})\cdot\widehat{\beta}_c\right]}{s_{nc}\sin\beta_{nc}}\right)D_h(Q_{nc})\right.\\
&\qquad\left.\times T_{nc}(\xi,\eta,0)\right\}\sqrt{\frac{\rho^d(Q_{nc})}{s_{nc}\,[\rho^d(Q_{nc})+s_{nc}]}}\,e^{-jks_{nc}}\\
&+\ \vec{E}^{i}(Q_{nc}^{-})\cdot\left\{-\widehat{\psi}'\,\widehat{\psi}_c\left(\frac{-s_c\left[\widehat{e}(Q_{nc})\cdot\widehat{\beta}_c\right]}{s_{nc}\sin\beta_{nc}}\right)D_h(Q_{nc})\right.
\end{aligned}
$$

$$\times T_{nc}(\xi,\eta,0)\Bigg\}\sqrt{\frac{\rho^d(Q_{nc})}{s_{nc}\left[\rho^d(Q_{nc})+s_{nc}\right]}}\;e^{-jks_{nc}} \tag{408}$$

where (385), (396), (398) and (399) have been used to simplify the result. It is now assumed that the function $\tilde{C}_2^h(x_e)$ is a smooth and slowly varying function of x_e near the stationary phase points and $k \gg 1$. This allows us to use the uniform asymptotic expansion (657) of Appendix B. Therefore, the uniform asymptotic expansion of (361) is

$$\begin{aligned}
\hat{\psi}_c\,\mathcal{K}_2^h(P) \;\sim\; & -\hat{\psi}_c\,E^i_{\psi_c}\frac{1}{2\pi}\tilde{C}_2^h(x_c)\,\frac{\sqrt{2\pi}}{k^{3/2}}\left\{\frac{e^{j\eta\pi/4}}{\sqrt{|h^{\,\mathrm{II}}(x_c)|}}\right\}^3 e^{jkh(x_c)}T_c(\xi,2)\\
& -\hat{\psi}_c\,2\,E^i_{\psi_c}\frac{\left[\vec{e}(Q_{nc})\cdot\hat{\beta}'_c\right]}{2\pi}\left\{x_{nc}^2\tilde{C}_2^h(x_{nc})\right\}\sqrt{\frac{2\pi}{k}}\\
& \times\left\{\frac{e^{-j\eta\pi/4}}{\sqrt{|h^{\,\mathrm{II}}(x_{nc})|}}\right\}e^{jkh(x_{nc})}\,T_{nc}(\xi,\eta,2)\\
\sim\; & \vec{E}^i(Q_c)\cdot\left\{-\hat{\psi}'\hat{\psi}_c\left(\frac{s_c\cos\psi_c}{2jk\rho_g(Q_c)}\right)D_h(Q_c)\,T_c(\xi,2)\right\}\\
& \times\left\{\frac{\rho^d(Q_c)}{s_c\left[\rho^d(Q_c)+s_c\right]}\right\}^{3/2}e^{-jks_c}\\
+\;\; & \vec{E}^i(Q^+_{nc})\cdot\left\{-\hat{\psi}'\hat{\psi}_c\left(\frac{-\left\{\hat{\psi}_c\cdot[\vec{r}_e(Q_{nc})\times\hat{e}(Q_{nc})]\right\}}{s_{nc}\sin\beta_{nc}}\right)D_h(Q_{nc})\right.\\
& \left.\times T_{nc}(\xi,\eta,2)\right\}\sqrt{\frac{\rho^d(Q_{nc})}{s_{nc}\left[\rho^d(Q_{nc})+s_{nc}\right]}}\;e^{-jks_{nc}}\\
+\;\; & \vec{E}^i(Q^-_{nc})\cdot\left\{-\hat{\psi}'\hat{\psi}_c\left(\frac{-\left\{\hat{\psi}_c\cdot[\vec{r}_e(Q_{nc})\times\hat{e}(Q_{nc})]\right\}}{s_{nc}\sin\beta_{nc}}\right)D_h(Q_{nc})\right.\\
& \left.\times T_{nc}(\xi,\eta,2)\right\}\sqrt{\frac{\rho^d(Q_{nc})}{s_{nc}\left[\rho^d(Q_{nc})+s_{nc}\right]}}\;e^{-jks_{nc}}
\end{aligned} \tag{409}$$

where (386), (397), (398) and (399) have been used to simplify the result. This completes the uniform asymptotic expansion of the diffracted field integral equations on the lit side of the caustic. However, it is advantageous to rewrite these results in a more convenient and standard form. Therefore, adding (400) through (409) and regrouping the terms we obtain

$$\vec{E}^d(P) \;\sim\; \vec{E}^i(Q_c)\cdot\overline{\overline{D}}^L(Q_c)\sqrt{\frac{\rho^d(Q_c)}{s_c\left[\rho^d(Q_c)+s_c\right]}}\;e^{-jks_c}$$

$$
\begin{aligned}
&+ \vec{E}^i(Q_c)\cdot\overline{\overline{D}}_1^L(Q_c)\left\{\frac{\rho^d(Q_c)}{s_c\left[\rho^d(Q_c)+s_c\right]}\right\}^{3/2} e^{-jks_c}\\
&+ \vec{E}^i(Q_c)\cdot\overline{\overline{D}}_2^L(Q_c)\left\{\frac{\rho^d(Q_c)}{s_c\left[\rho^d(Q_c)+s_c\right]}\right\}^{5/2} e^{-jks_c}\\
&+ \vec{E}^i(Q_{nc}^+)\cdot\overline{\overline{D}}^L(Q_{nc}^+)\sqrt{\frac{\rho^d(Q_{nc})}{s_{nc}\left[\rho^d(Q_{nc})+s_{nc}\right]}}\, e^{-jks_{nc}}\\
&+ \vec{E}^i(Q_{nc}^-)\cdot\overline{\overline{D}}^L(Q_{nc}^-)\sqrt{\frac{\rho^d(Q_{nc})}{s_{nc}\left[\rho^d(Q_{nc})+s_{nc}\right]}}\, e^{-jks_{nc}} \qquad (410)
\end{aligned}
$$

which is in a dyadic form similar to the UTD. The first three terms of this expression represent the field diffracted by the central diffraction point and the dyadic diffraction coefficients are

$$
\overline{\overline{D}}^L(Q_c) = -\hat{\beta}'\hat{\beta}_c\, D_s(Q_c)\, T_c(\xi,0) - \hat{\psi}'\hat{\psi}_c\, D_h(Q_c)\, T_c(\xi,0)\,, \qquad (411)
$$

$$
\begin{aligned}
\overline{\overline{D}}_1^L(Q_c) \;=\; & -\hat{\psi}'\hat{s}_c\left(\frac{s_c\sin\psi_c'}{jk\rho_g(Q_c)}\right) D_s(Q_c)\, T_c(\xi,2)\\
& -\hat{\psi}'\hat{\psi}_c\left(\frac{js_c^2\sin\psi_c\sin\psi_c'}{k\rho_g^2(Q_c)}\right) D_s(Q_c)\, T_c(\xi,2)\\
& -\hat{\psi}'\hat{s}_c\left(\frac{s_c\sin\psi_c}{2jk\rho_g(Q_c)}\right) D_h(Q_c)\, T_c(\xi,2)\\
& -\hat{\beta}'\hat{\beta}_c\left(\frac{js_c^2\sin\psi_c\sin\psi_c'}{k\rho_g^2(Q_c)}\right) D_h(Q_c)\, T_c(\xi,2)\\
& -\hat{\psi}'\hat{\psi}_c\left(\frac{s_c\cos\psi_c}{2jk\rho_g(Q_c)}\right) D_h(Q_c)\, T_c(\xi,2) \qquad (412)
\end{aligned}
$$

and

$$
\begin{aligned}
\overline{\overline{D}}_2^L(Q_c) \;=\; & -\hat{\psi}'\hat{s}_c\left(\frac{-3s_c^2\left\{\rho_g(Q_c)\cos\psi_c + s_c\sin^2\psi_c\right\}\sin\psi_c'}{2k^2\rho_g^3(Q_c)}\right) D_s(Q_c)\, T_c(\xi,4)\\
& -\hat{\beta}'\hat{\beta}_c\left(\frac{3s_c^2\kappa_g^2(Q_c) - s_c^3\left[\kappa_g^{\mathrm{II}}(Q_c) + 3\kappa_g^3(Q_c)\right]}{4k^2}\right) D_s(Q_c)\, T_c(\xi,4)\\
& -\hat{\psi}'\hat{\psi}_c\left(\frac{3s_c^2\left\{\rho_g(Q_c) - s_c\cos\psi_c\right\}\sin\psi_c\sin\psi_c'}{2k^2\rho_g^3(Q_c)}\right)\\
& \qquad \times D_s(Q_c)\, T_c(\xi,4) \qquad (413)
\end{aligned}
$$

where $D_{s,h}(Q_c)$ are the UTD half-plane diffraction coefficients and $T_c(\xi,m)$ are the caustic correction transition functions given by (655) of Appendix B. Also, the last

two terms of (410) correspond to the two non-central diffraction points. The dyadic diffraction coefficient for these terms is

$$\overline{\overline{D}}^{L}(Q_{nc}) = -\hat{\beta}'\,\vec{\mathbf{B}}_u(\xi)\,D_s(Q_{nc}) - \hat{\psi}'\,\vec{\Psi}_u(\xi)\,D_h(Q_{nc}) \tag{414}$$

where $D_{s,h}(Q_{nc})$ are the UTD half-plane diffraction coefficients. Also, the uniform polarization vectors $\vec{\mathbf{B}}_u(\xi)$ and $\vec{\Psi}_u(\xi)$ are given by

$$\begin{aligned}
\vec{\mathbf{B}}_u(\xi) \;=\; & \hat{s}_c \left\{ \frac{-s_c \left[\hat{e}(Q_{nc})\cdot\hat{\beta}_c\right]\left[\vec{r}_e(Q_{nc})\cdot\hat{\beta}_c\right]}{s_{nc}^2 \sin\beta_{nc}}\, T_{nc}(\xi,\eta,2) \right. \\
& \quad + \frac{-\left\{\hat{\psi}_c\cdot\left[\vec{r}_e(Q_{nc})\times\hat{e}(Q_{nc})\right]\right\}\left[\vec{r}_e(Q_{nc})\cdot\hat{\beta}_c\right]}{s_{nc}^2 \sin\beta_{nc}}\, T_{nc}(\xi,\eta,4) \\
& \quad \left. + \frac{-s_c \left[\hat{e}(Q_{nc})\cdot\hat{\psi}_c\right]\left[\vec{r}_e(Q_{nc})\cdot\hat{\psi}_c\right]}{s_{nc}^2 \sin\beta_{nc}}\, T_{nc}(\xi,\eta,4) \right\} \\
& + \hat{\beta}_c \left\{ \frac{-s_c^2 \left[\hat{e}(Q_{nc})\cdot\hat{\beta}_c\right]}{s_{nc}^2 \sin\beta_{nc}}\, T_{nc}(\xi,\eta,0) \right. \\
& \quad + \frac{-s_c \left\{\hat{\psi}_c\cdot\left[\vec{r}_e(Q_{nc})\times\hat{e}(Q_{nc})\right]\right\}}{s_{nc}^2 \sin\beta_{nc}}\, T_{nc}(\xi,\eta,4) \\
& \quad + \frac{s_c \left[\hat{e}(Q_{nc})\cdot\hat{\beta}_c\right]\left[\vec{r}_e(Q_{nc})\cdot\hat{s}_c\right]}{s_{nc}^2 \sin\beta_{nc}}\, T_{nc}(\xi,\eta,4) \\
& \quad + \frac{\left\{\hat{\psi}_c\cdot\left[\vec{r}_e(Q_{nc})\times\hat{e}(Q_{nc})\right]\right\}\left[\vec{r}_e(Q_{nc})\cdot\hat{s}_c\right]}{s_{nc}^2 \sin\beta_{nc}}\, T_{nc}(\xi,\eta,4) \\
& \quad \left. + \frac{-\left\{\hat{s}_c\cdot\left[\vec{r}_e(Q_{nc})\times\hat{e}(Q_{nc})\right]\right\}\left[\vec{r}_e(Q_{nc})\cdot\hat{\psi}_c\right]}{s_{nc}^2 \sin\beta_{nc}}\, T_{nc}(\xi,\eta,4) \right\} \\
& + \hat{\psi}_c \left\{ \frac{-s_c^2 \left[\hat{e}(Q_{nc})\cdot\hat{\psi}_c\right]}{s_{nc}^2 \sin\beta_{nc}}\, T_{nc}(\xi,\eta,2) \right. \\
& \quad + \frac{s_c \left[\hat{e}(Q_{nc})\cdot\hat{\psi}_c\right]\left[\vec{r}_e(Q_{nc})\cdot\hat{s}_c\right]}{s_{nc}^2 \sin\beta_{nc}}\, T_{nc}(\xi,\eta,4) \\
& \quad \left. + \frac{\left\{\hat{s}_c\cdot\left[\vec{r}_e(Q_{nc})\times\hat{e}(Q_{nc})\right]\right\}\left[\vec{r}_e(Q_{nc})\cdot\hat{\beta}_c\right]}{s_{nc}^2 \sin\beta_{nc}}\, T_{nc}(\xi,\eta,4) \right\}
\end{aligned} \tag{415}$$

and

$$\begin{aligned}
\vec{\Psi}_u(\xi) \;=\; & \hat{s}_c \left\{ \frac{-\left\{\hat{s}_c\cdot\left[\vec{r}_e(Q_{nc})\times\hat{e}(Q_{nc})\right]\right\}}{s_{nc}\sin\beta_{nc}}\, T_{nc}(\xi,\eta,2) \right\} \\
& + \hat{\beta}_c \left\{ \frac{s_c \left[\hat{e}(Q_{nc})\cdot\hat{\psi}_c\right]}{s_{nc}\sin\beta_{nc}}\, T_{nc}(\xi,\eta,2) \right\}
\end{aligned}$$

$$+ \quad \widehat{\psi}_c \left\{ \frac{-s_c \left[\widehat{e}(Q_{nc}) \cdot \widehat{\beta}_c \right]}{s_{nc} \sin \beta_{nc}} T_{nc}(\xi, \eta, 0) \right.$$

$$\left. + \frac{-\left\{ \widehat{\psi}_c \cdot [\vec{r}_e(Q_{nc}) \times \widehat{e}(Q_{nc})] \right\}}{s_{nc} \sin \beta_{nc}} T_{nc}(\xi, \eta, 2) \right\} ; \qquad (416)$$

respectively, where $T_{nc}(\xi, \eta, m)$ are the caustic correction transition functions given by (656) of Appendix B. These uniform polarization vectors are used because the variation of the caustic correction transition functions prevents us from recombining the components of the typical $\widehat{\beta}$ and $\widehat{\psi}$ polarization vectors. However, in this form

$$\lim_{|\xi| \to \infty} \vec{\mathbf{B}}_u(\xi) = \widehat{\beta} \qquad (417)$$

and

$$\lim_{|\xi| \to \infty} \vec{\Psi}_u(\xi) = \widehat{\psi} \qquad (418)$$

which means that the uniform polarization vectors reduce to the standard polarization unit vectors away from the caustics and are modified near the caustics to obtain the proper field value.

4 The Uniform Asymptotic Expansion of the Diffracted Field Integral Equations in the Caustic Shadow Region

The field in the caustic shadow region must also be determined in order to obtain a uniform asymptotic expression for the diffraction by a curved edge. This asymptotic expansion must be performed in a way that is consistent with the expansion on the lit side in order to obtain a uniform result. This section is devoted to the asymptotic expansion of the diffracted field integral equations for the shadow side of the caustic.

It is assumed that only one diffraction point exists in the caustic shadow region as shown in Figure 39. This occurs because the two non-central diffraction points have coalesced and disappeared. The uniform asymptotic expansion derived in Section 3 of Appendix B can be utilized with these assumptions in mind.

As explained in Section 1 of Appendix B, if an integral has one real stationary phase point and two complex conjugate stationary phase points then $\mu = \eta$ where $\mu =$

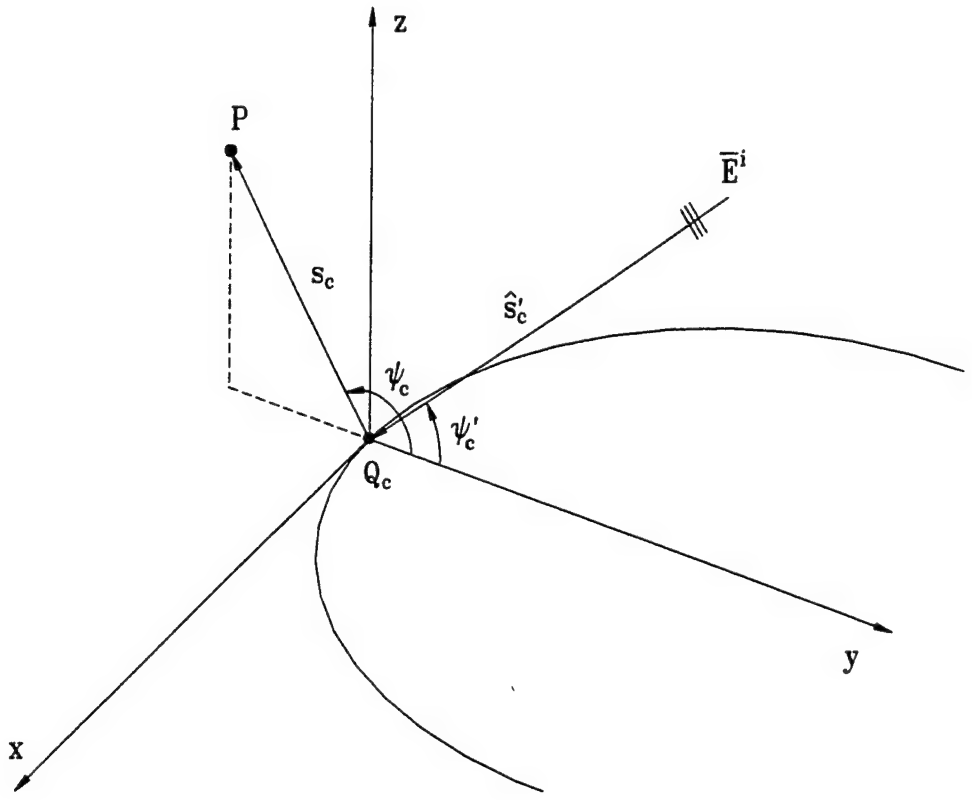

Figure 39: Ray geometry for the diffraction by a curved edge in the caustic shadow region.

$\text{sgn}\{h^{\text{IV}}(x_c)\}$ and $\eta = \text{sgn}\{h^{\text{II}}(x_c)\}$. It is also easily shown using (753a) and (764a) of Appendix D that the value of the phase function is

$$h(x_c) = -s_c \tag{419}$$

at the central stationary phase point and using (756a) and (765a) of Appendix D that the value of the phase function is

$$h(x_{nc}) = -\hat{s}'_c \cdot \vec{r}_e(Q_{nc}) - s_{nc} \tag{420}$$

at the non-central stationary phase points. The argument of the transition functions becomes

$$\xi = \left|\sqrt{2k[-\hat{s}'_c \cdot \vec{r}_e(Q_{nc}) - s_{nc} + s_c]}\right| e^{-j\eta\pi/4} \tag{421}$$

using these in (626) in Appendix B and the fact that $\mu = \eta$. Also, from (753c) and (764c) of Appendix D the second derivative of the phase function is

$$h^{\text{II}}(x_c) = -\left[\frac{1}{s_c} + \frac{1}{\rho^d(Q_c)}\right] \tag{422}$$

at the central stationary phase point and

$$\eta = \text{sgn}\{h^{\text{II}}(x_c)\} = -\text{sgn}\left\{\frac{\rho^d(Q_c)}{s_c[\rho^d(Q_c) + s_c]}\right\} \tag{423}$$

is the value of η. The values of the amplitude functions of the diffraction integrals where determined in Section 3 and are found in (375) through (380) for the soft polarization diffraction integrals and (383) through (386) for the hard polarization diffraction integrals. The only remaining quantities to be determined are the values of the the second derivatives of the amplitude functions of the integrals with respect to x_e evaluated at the central stationary phase point.

It is now necessary to determine the second derivatives of the amplitude functions of the diffraction integrals with respect to x_e. These derivatives will be divided into different elements in order to use the chain rule. First, the values of the vector products in (336) evaluated at the central stationary phase point is

$$\left.\frac{\vec{e} \cdot \hat{\psi}'_c}{x_e}\right|_{Q_c} = \kappa_g(Q_c) \sin\psi'_c \tag{424a}$$

$$\left.\frac{\vec{e}\cdot\widehat{\psi}_c}{x_e}\right|_{Q_c} = \kappa_g(Q_c)\sin\psi_c \tag{424b}$$

$$\left.\frac{\vec{r}_e\cdot\widehat{s}_c}{x_e^2}\right|_{Q_c} = \frac{1}{2}\kappa_g(Q_c)\cos\psi_c \tag{424c}$$

$$\left.\frac{\vec{r}_e\cdot\widehat{\psi}_c}{x_e^2}\right|_{Q_c} = -\frac{1}{2}\kappa_g(Q_c)\sin\psi_c \tag{424d}$$

$$\left.\frac{\widehat{s}_c\cdot(\vec{r}_e\times\vec{e})}{x_e^2}\right|_{Q_c} = -\frac{1}{2}\kappa_g(Q_c)\sin\psi_c \tag{424e}$$

$$\left.\frac{\widehat{\psi}_c\cdot(\vec{r}_e\times\vec{e})}{x_e^2}\right|_{Q_c} = -\frac{1}{2}\kappa_g(Q_c)\cos\psi_c \tag{424f}$$

$$\left.\frac{\widehat{\psi}_c\cdot(\vec{r}_e\times\vec{e})-\left(\vec{e}\cdot\widehat{\beta}_c\right)(\vec{r}_e\cdot\widehat{s}_c)}{x_e^4}\right|_{Q_c} =$$

$$= -\frac{1}{12}\left[\kappa_g^{\rm II}(Q_c)+3\kappa_g^3(Q_c)\right]\cos\psi_c \tag{424g}$$

where l'Hôpital's rule and (372) have been used to determine these values. It is also necessary to determine the second derivatives of these quantities with respect to x_e. Differentiating twice with respect to x_e we obtain

$$\left.\frac{d^2}{dx_e^2}\left\{\frac{\vec{e}\cdot\widehat{\psi}_c'}{x_e}\right\}\right|_{Q_c} = \frac{1}{3}\left[\kappa_g^{\rm II}(Q_c)+3\kappa_g^3(Q_c)\right]\sin\psi_c' \tag{425a}$$

$$\left.\frac{d^2}{dx_e^2}\left\{\frac{\vec{e}\cdot\widehat{\psi}_c}{x_e}\right\}\right|_{Q_c} = \frac{1}{3}\left[\kappa_g^{\rm II}(Q_c)+3\kappa_g^3(Q_c)\right]\sin\psi_c \tag{425b}$$

$$\left.\frac{d^2}{dx_e^2}\left\{\frac{\vec{r}_e\cdot\widehat{s}_c}{x_e^2}\right\}\right|_{Q_c} = \frac{1}{12}\left[\kappa_g^{\rm II}(Q_c)+3\kappa_g^3(Q_c)\right]\cos\psi_c \tag{425c}$$

$$\left.\frac{d^2}{dx_e^2}\left\{\frac{\vec{r}_e\cdot\widehat{\psi}_c}{x_e^2}\right\}\right|_{Q_c} = -\frac{1}{12}\left[\kappa_g^{\rm II}(Q_c)+3\kappa_g^3(Q_c)\right]\sin\psi_c \tag{425d}$$

$$\left.\frac{d^2}{dx_e^2}\left\{\frac{\widehat{s}_c\cdot(\vec{r}_e\times\vec{e})}{x_e^2}\right\}\right|_{Q_c} = -\frac{1}{4}\left[\kappa_g^{\rm II}(Q_c)+3\kappa_g^3(Q_c)\right]\sin\psi_c \tag{425e}$$

$$\left.\frac{d^2}{dx_e^2}\left\{\frac{\widehat{\psi}_c\cdot(\vec{r}_e\times\vec{e})}{x_e^2}\right\}\right|_{Q_c} = -\frac{1}{4}\left[\kappa_g^{\rm II}(Q_c)+3\kappa_g^3(Q_c)\right]\cos\psi_c \tag{425f}$$

$$\left.\frac{d^2}{dx_e^2}\left\{\frac{\widehat{\psi}_c\cdot(\vec{r}_e\times\vec{e})-\left(\vec{e}\cdot\widehat{\beta}_c\right)(\vec{r}_e\cdot\widehat{s}_c)}{x_e^4}\right\}\right|_{Q_c} =$$

$$= -\frac{1}{90}\left[\kappa_g^{\rm IV}(Q_c)+34\kappa_g^2(Q_c)\kappa_g^{\rm II}(Q_c)+45\kappa_g^5(Q_c)\right]\cos\psi_c \tag{425g}$$

where the Taylor series form of y_e of (309) is used to determine the series form of the function to be differentiated. The common factor

$$\tilde{\mathcal{F}}_s(x_e) = \frac{\widetilde{D}_s(Q')}{\left(\frac{dl}{dx_e}\right) r^3 \sin\beta \sin\beta'} = \frac{\widetilde{D}_s(Q')}{\mathcal{P}_s(Q')} \tag{426}$$

where

$$\mathcal{P}_s(Q') = \left(\frac{dl}{dx_e}\right) r^3 \sin\beta \sin\beta' \tag{427}$$

is now differentiated twice with respect to x_e to obtain

$$\begin{aligned} \mathcal{F}_s^{\text{II}}(Q_c) &= \frac{-e^{-j\pi/4}}{\sqrt{2\pi k}} \tilde{\mathcal{F}}_s^{\text{II}}(x_c) \\ &= \frac{1}{s_c^3} \frac{d^2 D_s(Q_c)}{dl^2} - \frac{1}{s_c^6} \mathcal{P}_s^{\text{II}}(Q_c)\, D_s(Q_c) \end{aligned} \tag{428}$$

where

$$\begin{aligned} \mathcal{P}_s^{\text{II}}(Q_c) &= s_c\, \kappa_g^2(Q_c) \left\{ s_c^2 \left(\sin^2\psi_c' - \cos^2\psi_c \right) + 2\rho_g^2(Q_c) \right. \\ &\qquad \left. - s_c\, \rho_g(Q_c) \cos\psi_c \right\} \end{aligned} \tag{429}$$

for the soft polarization integrals. Also, the common factor

$$\tilde{\mathcal{F}}_h(x_e) = \frac{\widetilde{D}_h(Q')}{\left(\frac{dl}{dx_e}\right) r^2 \sin\beta \sin\beta'} = \frac{\widetilde{D}_h(Q')}{\mathcal{P}_h(Q')} \tag{430}$$

where

$$\mathcal{P}_h(Q') = \left(\frac{dl}{dx_e}\right) r^2 \sin\beta \sin\beta' \tag{431}$$

is now differentiated twice with respect to x_e to obtain

$$\begin{aligned} \mathcal{F}_h^{\text{II}}(Q_c) &= \frac{-e^{-j\pi/4}}{\sqrt{2\pi k}} \tilde{\mathcal{F}}_h^{\text{II}}(x_c) \\ &= \frac{1}{s_c^2} \frac{d^2 D_h(Q_c)}{dl^2} - \frac{1}{s_c^4} \mathcal{P}_h^{\text{II}}(Q_c)\, D_h(Q_c) \end{aligned} \tag{432}$$

where

$$\mathcal{P}_h^{\text{II}}(Q_c) = \kappa_g^2(Q_c) \left\{ s_c^2 \left(\sin^2\psi_c' - \cos^2\psi_c \right) + \rho_g^2(Q_c) \right\} \tag{433}$$

for the hard polarization integrals. The amplitude functions of the soft polarization integrals of (347) through (352) are now differentiated twice with respect to x_e to

obtain

$$\frac{d^2A_2^s(Q_c)}{dl^2} = \frac{-e^{-j\pi/4}}{\sqrt{2\pi k}}\frac{d^2\tilde{A}_2^s(x_e)}{dx_e^2}\bigg|_{Q_c}$$

$$= \frac{\left[\kappa_g^{\rm II}(Q_c)+3\kappa_g^3(Q_c)\right]\sin\psi_c'}{3s_c^3}D_s(Q_c)$$

$$+\kappa_g(Q_c)\sin\psi_c'\,\mathcal{F}_s^{\rm II}(Q_c) \tag{434a}$$

$$\frac{d^2A_4^s(Q_c)}{dl^2} = \frac{-e^{-j\pi/4}}{\sqrt{2\pi k}}\frac{d^2\tilde{A}_4^s(x_e)}{dx_e^2}\bigg|_{Q_c}$$

$$= \frac{-5\left\{\rho_g(Q_c)\cos\psi_c+s_c\sin^2\psi_c\right\}}{12s_c^3\rho_g^2(Q_c)}\left[\kappa_g^{\rm II}(Q_c)+3\kappa_g^3(Q_c)\right]$$

$$\times\sin\psi_c'\,D_s(Q_c)$$

$$+\frac{-\left\{\rho_g(Q_c)\cos\psi_c+s_c\sin^2\psi_c\right\}\sin\psi_c'}{2\rho_g^3(Q_c)}\mathcal{F}_s^{\rm II}(Q_c) \tag{434b}$$

$$\frac{d^2B_0^s(Q_c)}{dl^2} = \frac{-e^{-j\pi/4}}{\sqrt{2\pi k}}\frac{d^2\tilde{B}_0^s(x_e)}{dx_e^2}\bigg|_{Q_c} = \mathcal{F}_s^{\rm II}(Q_c) \tag{434c}$$

$$\frac{d^2B_4^s(Q_c)}{dl^2} = \frac{-e^{-j\pi/4}}{\sqrt{2\pi k}}\frac{d^2\tilde{B}_4^s(x_e)}{dx_e^2}\bigg|_{Q_c}$$

$$= \frac{\left[\kappa_g^{\rm IV}(Q_c)+34\kappa_g^2(Q_c)\kappa_g^{\rm II}(Q_c)+45\kappa_g^5(Q_c)\right]}{90s_c^2}\cos\psi_c\,D_s(Q_c)$$

$$+\frac{-\kappa_g(Q_c)\left[\kappa_g^{\rm II}(Q_c)+3\kappa_g^3(Q_c)\right]\sin^2\psi_c}{6s_c^3}D_s(Q_c)$$

$$+\frac{1}{12}\Big\{s_c\left[\kappa_g^{\rm II}(Q_c)+3\kappa_g^3(Q_c)\right]\cos\psi_c$$

$$-3\kappa_g^2(Q_c)\sin^2\psi_c\Big\}\,\mathcal{F}_s^{\rm II}(Q_c) \tag{434d}$$

$$\frac{d^2C_2^s(Q_c)}{dl^2} = \frac{-e^{-j\pi/4}}{\sqrt{2\pi k}}\frac{d^2\tilde{C}_2^s(x_e)}{dx_e^2}\bigg|_{Q_c}$$

$$= \frac{2\kappa_g(Q_c)\left[\kappa_g^{\rm II}(Q_c)+3\kappa_g^3(Q_c)\right]}{3s_c^3}D_s(Q_c)$$

$$+\kappa_g^2(Q_c)\sin\psi_c\sin\psi_c'\,\mathcal{F}_s^{\rm II}(Q_c) \tag{434e}$$

$$\frac{d^2C_4^s(Q_c)}{dl^2} = \frac{-e^{-j\pi/4}}{\sqrt{2\pi k}}\frac{d^2\tilde{C}_4^s(x_e)}{dx_e^2}\bigg|_{Q_c}$$

$$= \frac{5\kappa_g^2(Q_c)\left\{s_c\cos\psi_c-\rho_g(Q_c)\right\}}{12s_c^3}\left[\kappa_g^{\rm II}(Q_c)+3\kappa_g^3(Q_c)\right]$$

$$\times\sin\psi_c\sin\psi_c'\,D_s(Q_c)$$

$$+\frac{1}{2}\kappa_g^3(Q_c)\left\{s_c\cos\psi_c-\rho_g(Q_c)\right\}$$

$$\times \sin\psi_c \sin\psi_c' \mathcal{F}_s^{\text{II}}(Q_c) \tag{434f}$$

at the central stationary phase point where $\mathcal{F}_s^{\text{II}}(Q_c)$ is given in (428) and (429), $D_s(Q_c)$ is the soft polarization UTD half-plane diffraction coefficient and $\frac{d^2 D_s(Q_c)}{dl^2}$ is given by (812) through (818) of Appendix D. The amplitude functions of the hard polarization integrals of (362) through (365) are now differentiated twice with respect to x_e to obtain

$$\begin{aligned}
\frac{d^2 A_2^h(Q_c)}{dl^2} &= \frac{-e^{-j\pi/4}}{\sqrt{2\pi k}} \frac{d^2 \tilde{A}_2^h(x_e)}{dx_e^2}\bigg|_{Q_c} \\
&= \frac{-\left[\kappa_g^{\text{II}}(Q_c) + 3\kappa_g^3(Q_c)\right] \sin\psi_c}{4s_c^2} D_h(Q_c) \\
&\quad - \frac{1}{2}\kappa_g(Q_c) \sin\psi_c \mathcal{F}_h^{\text{II}}(Q_c) \qquad (435a) \\
\frac{d^2 B_2^h(Q_c)}{dl^2} &= \frac{-e^{-j\pi/4}}{\sqrt{2\pi k}} \frac{d^2 \tilde{B}_2^h(x_e)}{dx_e^2}\bigg|_{Q_c} \\
&= \frac{2\kappa_g(Q_c)\left[\kappa_g^{\text{II}}(Q_c) + 3\kappa_g^3(Q_c)\right]}{3s_c^2} D_h(Q_c) \\
&\quad + \kappa_g^2(Q_c) \sin\psi_c \sin\psi_c' \mathcal{F}_h^{\text{II}}(Q_c) \qquad (435b) \\
\frac{d^2 C_0^h(Q_c)}{dl^2} &= \frac{-e^{-j\pi/4}}{\sqrt{2\pi k}} \frac{d^2 \tilde{C}_0^h(x_e)}{dx_e^2}\bigg|_{Q_c} = \mathcal{F}_h^{\text{II}}(Q_c) \qquad (435c) \\
\frac{d^2 C_2^h(Q_c)}{dl^2} &= \frac{-e^{-j\pi/4}}{\sqrt{2\pi k}} \frac{d^2 \tilde{C}_2^h(x_e)}{dx_e^2}\bigg|_{Q_c} \\
&= \frac{-\left[\kappa_g^{\text{II}}(Q_c) + 3\kappa_g^3(Q_c)\right] \cos\psi_c}{4s_c^2} D_h(Q_c) \\
&\quad - \frac{1}{2}\kappa_g(Q_c) \cos\psi_c \mathcal{F}_h^{\text{II}}(Q_c) \qquad (435d)
\end{aligned}$$

at the central stationary phase point where $\mathcal{F}_h^{\text{II}}(Q_c)$ is given in (432) and (433), $D_h(Q_c)$ is the hard polarization UTD half-plane diffraction coefficient and $\frac{d^2 D_h(Q_c)}{dl^2}$ is given by (812) through (818) of Appendix D. This completes the derivation of the quantities required to obtain uniform asymptotic expressions for the diffracted field on the shadow side of the caustic. It is now necessary to substitute these quantities into the uniform asymptotic expansion derived in Section 3 of Appendix B and simplifying the result to obtain a standard ray optical form.

The uniform asymptotic expansions of the soft and hard polarized diffraction integrals can now be performed since all the necessary quantities have been determined. To make the uniform asymptotic expansions easier to simplify we can recognize that

$$\frac{e^{j\eta\pi/4}}{\sqrt{|h^{II}(x_c)|}} = s_c\sqrt{\frac{\rho^d(Q_c)}{s_c\,[\rho^d(Q_c)+s_c]}}\;\; e^{-j\pi/4} \tag{436}$$

at the central stationary phase point. We begin here by determining the uniform asymptotic expansions of the soft polarization diffraction integrals of (341) through (346). It is assumed here that the function $\tilde{A}_2^s(x_e)$ is a smooth and slowly varying function of x_e near the stationary phase point and $k \gg 1$. This allows us to use the uniform asymptotic expansion (673) of Appendix B. Therefore, the uniform asymptotic expansion of (341) is

$$\begin{aligned}
\widehat{s}_c\,\mathcal{I}_2^s(P) \;\sim\;& \widehat{s}_c\,E^i_{\psi_c}\,\frac{s_c}{2\pi}\tilde{A}_2^s(x_c)\,\frac{\sqrt{2\pi}}{k^{3/2}}\left\{\frac{e^{j\eta\pi/4}}{\sqrt{|h^{II}(x_c)|}}\right\}^3 e^{jkh(x_c)}\,T_s(\xi,2)\\
&+\widehat{s}_c\,E^i_{\psi_c}\,\frac{s_c}{2\pi}\,\frac{3\sqrt{2\pi}}{2k^{5/2}}\left\{\frac{e^{j\eta\pi/4}}{\sqrt{|h^{II}(x_c)|}}\right\}^5 e^{jkh(x_c)}\,T_s(\xi,4)\\
&\times\left\{\left.\frac{d^2\tilde{A}_2^s(x_e)}{dx_e^2}\right|_{Q_c}+\frac{5}{12}\left[C(l_c)-4\kappa_g^2(Q_c)\right]\tilde{A}_2^s(x_c)\right\}\\
\sim\;& \vec{E}^i(Q_c)\cdot\left\{-\widehat{\psi}'\widehat{s}_c\left(\frac{s_c\sin\psi_c'}{jk\rho_g(Q_c)}\right)D_s(Q_c)\,T_s(\xi,2)\right\}\\
&\times\left\{\frac{\rho^d(Q_c)}{s_c\,[\rho^d(Q_c)+s_c]}\right\}^{3/2} e^{-jks_c}\\
+\;& \vec{E}^i(Q_c)\cdot\left\{-\widehat{\psi}'\widehat{s}_c\left(\frac{-3s_c^6}{2k^2}\,\frac{d^2A_2^s(Q_c)}{dl^2}+\frac{-5s_c^3\sin\psi_c'}{8k^2\rho_g(Q_c)}\right.\right.\\
&\left.\left.\times\left[C(l_c)-4\kappa_g^2(Q_c)\right]D_s(Q_c)\right)T_s(\xi,4)\right\}\\
&\times\left\{\frac{\rho^d(Q_c)}{s_c\,[\rho^d(Q_c)+s_c]}\right\}^{5/2} e^{-jks_c}
\end{aligned} \tag{437}$$

where (375), (434) and (436) have been used to simplify the result. Also, the function $C(l_c)$ is given by

$$C(l_c) = \frac{3|kh^{II}(l_c)|}{|\xi|^2} - \frac{h^{IV}(l_c)}{h^{II}(l_c)} \tag{438}$$

where

$$h^{II}(l_c) = -\left[\frac{1}{s_c}+\frac{1}{\rho^d(Q_c)}\right] \tag{439}$$

is the second derivative of the phase function given by (753c) of Appendix D and

$$h^{\rm IV}(l_c) = \left[\kappa_g^{\rm II}(Q_c) - \kappa_g^3(Q_c)\right]\left[\cos\psi_c + \cos\psi_c'\right] + \frac{\kappa_g^2(Q_c)}{s_c} + \frac{3}{s_c^3}\left[1 - \frac{s_c\cos\psi_c}{\rho_g(Q_c)}\right]^2 \tag{440}$$

is the fourth derivative of the phase function given by (753e) of Appendix D. It is now assumed that the function $\tilde{A}_4^s(x_e)$ is a smooth and slowly varying function of x_e near the stationary phase point and $k \gg 1$. This allows us to use the uniform asymptotic expansion (673) of Appendix B. Therefore, the uniform asymptotic expansion of (342) is

$$\begin{aligned}
\widehat{s}_c\,\mathcal{I}_4^s(P) \sim\ & -\widehat{s}_c\,E_{\psi_c}^i\,\frac{1}{2\pi}\tilde{A}_4^s(x_c)\,\frac{3\sqrt{2\pi}}{k^{5/2}}\left\{\frac{e^{j\eta\pi/4}}{\sqrt{|h^{\rm II}(x_c)|}}\right\}^5 e^{jkh(x_c)}\,T_s(\xi,4) \\
& -\widehat{s}_c\,E_{\psi_c}^i\,\frac{1}{2\pi}\,\frac{15\sqrt{2\pi}}{2k^{7/2}}\left\{\frac{e^{j\eta\pi/4}}{\sqrt{|h^{\rm II}(x_c)|}}\right\}^7 e^{jkh(x_c)}\,T_s(\xi,6) \\
& \times\left\{\left.\frac{d^2\tilde{A}_4^s(x_e)}{dx_e^2}\right|_{Q_c} + \frac{7}{12}\left[C(l_c) - 4\kappa_g^2(Q_c)\right]\tilde{A}_4^s(x_c)\right\} \\
\sim\ & \vec{E}^i(Q_c)\cdot\left\{-\widehat{\psi}'\widehat{s}_c\left(\frac{-3s_c^2\left\{\rho_g(Q_c)\cos\psi_c + s_c\sin^2\psi_c\right\}\sin\psi_c'}{2k^2\rho_g^3(Q_c)}\right)\right. \\
& \left.\times D_s(Q_c)\,T_s(\xi,4)\right\}\left\{\frac{\rho^d(Q_c)}{s_c\left[\rho^d(Q_c)+s_c\right]}\right\}^{5/2} e^{-jks_c} \\
+\ & \vec{E}^i(Q_c)\cdot\left\{-\widehat{\psi}'\widehat{s}_c\left(\frac{15s_c^7}{2jk^3}\,\frac{d^2A_4^s(Q_c)}{dl^2}\right.\right. \\
& +\frac{j35s_c^4\left\{\rho_g(Q_c)\cos\psi_c + s_c\sin^2\psi_c\right\}\sin\psi_c'}{16k^3\rho_g^3(Q_c)} \\
& \left.\left.\times\left[C(l_c) - 4\kappa_g^2(Q_c)\right]D_s(Q_c)\right)T_s(\xi,6)\right\} \\
& \times\left\{\frac{\rho^d(Q_c)}{s_c\left[\rho^d(Q_c)+s_c\right]}\right\}^{7/2} e^{-jks_c}
\end{aligned} \tag{441}$$

where (376), (434) and (436) have been used to simplify the result. It is now assumed that the function $\tilde{B}_0^s(x_e)$ is a smooth and slowly varying function of x_e near the stationary phase point and $k \gg 1$. This allows us to use the uniform asymptotic expansion (673) of Appendix B. Therefore, the uniform asymptotic expansion of (343)

is

$$\begin{aligned}
\widehat{\beta}_c\,\mathcal{J}_0^s(P) \;\sim\;& \widehat{\beta}_c\,E^i_{\beta_c}\,\frac{s_c^2}{2\pi}\,\tilde{B}_0^s(x_c)\sqrt{\frac{2\pi}{k}}\left\{\frac{e^{j\eta\pi/4}}{\sqrt{|h^{\,\mathrm{II}}(x_c)|}}\right\}e^{jkh(x_c)}\,T_s(\xi,0)\\
&+\widehat{\beta}_c\,E^i_{\beta_c}\,\frac{s_c^2}{2\pi}\,\frac{\sqrt{2\pi}}{2k^{3/2}}\left\{\frac{e^{j\eta\pi/4}}{\sqrt{|h^{\,\mathrm{II}}(x_c)|}}\right\}^3 e^{jkh(x_c)}\,T_s(\xi,2)\\
&\times\left\{\left.\frac{d^2\tilde{B}_0^s(x_e)}{dx_e^2}\right|_{Q_c}+\frac{1}{4}\left[C(l_c)-4\kappa_g^2(Q_c)\right]\tilde{B}_0^s(x_c)\right\}\\
\sim\;& \vec{E}^i(Q_c)\cdot\left\{-\widehat{\beta}'\widehat{\beta}_c\,D_s(Q_c)\,T_s(\xi,0)\right\}\sqrt{\frac{\rho^d(Q_c)}{s_c\left[\rho^d(Q_c)+s_c\right]}}\;e^{-jks_c}\\
+\;& \vec{E}^i(Q_c)\cdot\left\{-\widehat{\beta}'\widehat{\beta}_c\left(\frac{s_c^5}{2jk}\,\frac{d^2B_0^s(Q_c)}{dl^2}+\frac{s_c^2}{8jk}\right.\right.\\
&\left.\left.\times\left[C(l_c)-4\kappa_g^2(Q_c)\right]D_s(Q_c)\right)T_s(\xi,2)\right\}\\
&\times\left\{\frac{\rho^d(Q_c)}{s_c\left[\rho^d(Q_c)+s_c\right]}\right\}^{3/2}e^{-jks_c}
\end{aligned}\tag{442}$$

where (377), (434) and (436) have been used to simplify the result. It is now assumed that the function $\tilde{B}_4^s(x_e)$ is a smooth and slowly varying function of x_e near the stationary phase point and $k \gg 1$. This allows us to use the uniform asymptotic expansion (673) of Appendix B. Therefore, the uniform asymptotic expansion of (344) is

$$\begin{aligned}
\widehat{\beta}_c\,\mathcal{J}_4^s(P) \;\sim\;& \widehat{\beta}_c\,E^i_{\beta_c}\,\frac{1}{2\pi}\,\tilde{B}_4^s(x_c)\,\frac{3\sqrt{2\pi}}{k^{5/2}}\left\{\frac{e^{j\eta\pi/4}}{\sqrt{|h^{\,\mathrm{II}}(x_c)|}}\right\}^5 e^{jkh(x_c)}\,T_s(\xi,4)\\
&+\widehat{\beta}_c\,E^i_{\beta_c}\,\frac{1}{2\pi}\,\frac{15\sqrt{2\pi}}{2k^{7/2}}\left\{\frac{e^{j\eta\pi/4}}{\sqrt{|h^{\,\mathrm{II}}(x_c)|}}\right\}^7 e^{jkh(x_c)}\,T_s(\xi,6)\\
&\times\left\{\left.\frac{d^2\tilde{B}_4^s(x_e)}{dx_e^2}\right|_{Q_c}+\frac{7}{12}\left[C(l_c)-4\kappa_g^2(Q_c)\right]\tilde{B}_4^s(x_c)\right\}\\
\sim\;& \vec{E}^i(Q_c)\cdot\left\{-\widehat{\beta}'\widehat{\beta}_c\left(\frac{3s_c^2\kappa_g^2(Q_c)-s_c^3\left[\kappa_g^{\,\mathrm{II}}(Q_c)+3\kappa_g^3(Q_c)\right]}{4k^2}\right)\right.\\
&\left.\times D_s(Q_c)\,T_s(\xi,4)\right\}\left\{\frac{\rho^d(Q_c)}{s_c\left[\rho^d(Q_c)+s_c\right]}\right\}^{5/2}e^{-jks_c}\\
+\;& \vec{E}^i(Q_c)\cdot\left\{-\widehat{\beta}'\widehat{\beta}_c\left(\frac{15js_c^7}{2k^3}\,\frac{d^2B_4^s(Q_c)}{dl^2}\right.\right.
\end{aligned}$$

$$+\frac{35s_c^2\left\{3s_c^2\kappa_g^2(Q_c)-s_c^3\left[\kappa_g^{\rm II}(Q_c)+3\kappa_g^3(Q_c)\right]\right\}}{96jk^3}$$
$$\times\left[C(l_c)-4\kappa_g^2(Q_c)\right]D_s(Q_c)\Big)\,T_s(\xi,6)\Big\}$$
$$\times\left\{\frac{\rho^d(Q_c)}{s_c\left[\rho^d(Q_c)+s_c\right]}\right\}^{7/2}e^{-jks_c} \qquad (443)$$

where (378), (434) and (436) have been used to simplify the result. It is now assumed that the function $\tilde{C}_2^s(x_e)$ is a smooth and slowly varying function of x_e near the stationary phase point and $k \gg 1$. This allows us to use the uniform asymptotic expansion (673) of Appendix B. Therefore, the uniform asymptotic expansion of (345) is

$$\begin{aligned}
\widehat{\psi}_c\,\mathcal{K}_2^s(P) \;\sim\; & -\widehat{\psi}_c\,E^i_{\psi_c}\,\frac{s_c^2}{2\pi}\tilde{C}_2^s(x_c)\,\frac{\sqrt{2\pi}}{k^{3/2}}\left\{\frac{e^{j\eta\pi/4}}{\sqrt{|h^{\rm II}(x_c)|}}\right\}^3 e^{jkh(x_c)}\,T_s(\xi,2)\\
& -\widehat{\psi}_c\,E^i_{\psi_c}\,\frac{s_c^2}{2\pi}\,\frac{3\sqrt{2\pi}}{2k^{5/2}}\left\{\frac{e^{j\eta\pi/4}}{\sqrt{|h^{\rm II}(x_c)|}}\right\}^5 e^{jkh(x_c)}\,T_s(\xi,4)\\
& \quad\times\left\{\left.\frac{d^2\tilde{C}_2^s(x_e)}{dx_e^2}\right|_{Q_c}+\frac{5}{12}\left[C(l_c)-4\kappa_g^2(Q_c)\right]\tilde{C}_2^s(x_c)\right\}\\
\sim\; & \vec{E}^i(Q_c)\cdot\left\{-\widehat{\psi}'\widehat{\psi}_c\left(\frac{js_c^2\sin\psi_c\sin\psi_c'}{k\rho_g^2(Q_c)}\right)D_s(Q_c)\,T_s(\xi,2)\right\}\\
& \quad\times\left\{\frac{\rho^d(Q_c)}{s_c\left[\rho^d(Q_c)+s_c\right]}\right\}^{3/2}e^{-jks_c}\\
+\;\; & \vec{E}^i(Q_c)\cdot\left\{-\widehat{\psi}'\widehat{\psi}_c\left(\frac{3s_c^7}{2k^2}\,\frac{d^2C_2^s(Q_c)}{dl^2}+\frac{5\sin\psi_c\sin\psi_c'}{8k^2s_c^3\rho_g^2(Q_c)}\right.\right.\\
& \quad\left.\left.\times\left[C(l_c)-4\kappa_g^2(Q_c)\right]D_s(Q_c)\right)T_s(\xi,4)\right\}\\
& \quad\times\left\{\frac{\rho^d(Q_c)}{s_c\left[\rho^d(Q_c)+s_c\right]}\right\}^{5/2}e^{-jks_c} \qquad (444)
\end{aligned}$$

where (379), (434) and (436) have been used to simplify the result. It is now assumed that the function $\tilde{C}_4^s(x_e)$ is a smooth and slowly varying function of x_e near the stationary phase point and $k \gg 1$. This allows us to use the uniform asymptotic expansion (673) of Appendix B. Therefore, the uniform asymptotic expansion of (346)

is

$$\begin{aligned}
\widehat{\psi}_c \mathcal{K}_4^s(P) \;\sim\; & \widehat{\psi}_c E_{\psi_c}^i \frac{1}{2\pi} \tilde{C}_4^s(x_c) \frac{3\sqrt{2\pi}}{k^{5/2}} \left\{ \frac{e^{j\eta\pi/4}}{\sqrt{|h^{\,\mathrm{II}}(x_c)|}} \right\}^5 e^{jkh(x_c)} T_s(\xi,4) \\
& + \widehat{\psi}_c E_{\psi_c}^i \frac{1}{2\pi} \frac{15\sqrt{2\pi}}{2k^{7/2}} \left\{ \frac{e^{j\eta\pi/4}}{\sqrt{|h^{\,\mathrm{II}}(x_c)|}} \right\}^7 e^{jkh(x_c)} T_s(\xi,6) \\
& \times \left\{ \left. \frac{d^2 \tilde{C}_4^s(x_e)}{dx_e^2} \right|_{Q_c} + \frac{7}{12} \left[C(l_c) - 4\kappa_g^2(Q_c) \right] \tilde{C}_4^s(x_c) \right\} \\
\sim\; & \vec{E}^i(Q_c) \cdot \left\{ -\widehat{\psi}' \widehat{\psi}_c \left(\frac{3s_c^2 \left\{ \rho_g(Q_c) - s_c \cos\psi_c \right\} \sin\psi_c \sin\psi_c'}{2k^2 \rho_g^3(Q_c)} \right) \right. \\
& \left. \times D_s(Q_c) T_s(\xi,4) \right\} \left\{ \frac{\rho^d(Q_c)}{s_c \left[\rho^d(Q_c) + s_c \right]} \right\}^{5/2} e^{-jks_c} \\
+\; & \vec{E}^i(Q_c) \cdot \left\{ -\widehat{\psi}' \widehat{\psi}_c \left(\frac{15js_c^7}{2k^3} \frac{d^2 C_4^s(Q_c)}{dl^2} \right. \right. \\
& + \frac{35s_c^4 \left\{ \rho_g(Q_c) - s_c \cos\psi_c \right\} \sin\psi_c \sin\psi_c'}{16jk^3 \rho_g^3(Q_c)} \\
& \left. \left. \times \left[C(l_c) - 4\kappa_g^2(Q_c) \right] D_s(Q_c) \right) T_s(\xi,6) \right\} \\
& \times \left\{ \frac{\rho^d(Q_c)}{s_c \left[\rho^d(Q_c) + s_c \right]} \right\}^{7/2} e^{-jks_c}
\end{aligned} \tag{445}$$

where (380), (434) and (436) have been used to simplify the result. Next, it is necessary to determine the uniform asymptotic expansions of the hard polarization diffraction integrals of (358) through (361). It is assumed here that the function $\tilde{A}_2^h(x_e)$ is a smooth and slowly varying function of x_e near the stationary phase point and $k \gg 1$. This allows us to use the uniform asymptotic expansion (657) of Appendix B. Therefore, the uniform asymptotic expansion of (358) is

$$\begin{aligned}
\widehat{s}_c \mathcal{I}_2^h(P) \;\sim\; & -\widehat{s}_c E_{\psi_c}^i \frac{1}{2\pi} \tilde{A}_2^h(x_c) \frac{\sqrt{2\pi}}{k^{3/2}} \left\{ \frac{e^{j\eta\pi/4}}{\sqrt{|h^{\,\mathrm{II}}(x_c)|}} \right\}^3 e^{jkh(x_c)} T_s(\xi,2) \\
& - \widehat{s}_c E_{\psi_c}^i \frac{1}{2\pi} \frac{3\sqrt{2\pi}}{2k^{5/2}} \left\{ \frac{e^{j\eta\pi/4}}{\sqrt{|h^{\,\mathrm{II}}(x_c)|}} \right\}^5 e^{jkh(x_c)} T_s(\xi,4) \\
& \times \left\{ \left. \frac{d^2 \tilde{A}_2^h(x_e)}{dx_e^2} \right|_{Q_c} + \frac{5}{12} \left[C(l_c) - 4\kappa_g^2(Q_c) \right] \tilde{A}_2^h(x_c) \right\} \\
\sim\; & \vec{E}^i(Q_c) \cdot \left\{ -\widehat{\psi}' \widehat{s}_c \left(\frac{s_c \sin\psi_c}{2jk\rho_g(Q_c)} \right) D_h(Q_c) T_s(\xi,2) \right\}
\end{aligned}$$

$$\times \left\{ \frac{\rho^d(Q_c)}{s_c\left[\rho^d(Q_c)+s_c\right]} \right\}^{3/2} e^{-jks_c}$$

$$+ \quad \vec{E}^i(Q_c)\cdot\left\{ -\widehat{\psi}'\widehat{s}_c \left(\frac{3s_c^5}{2k^2}\,\frac{d^2A_2^h(Q_c)}{dl^2} + \frac{-15s_c^3\sin\psi_c}{48k^2\rho_g(Q_c)} \right.\right.$$

$$\left.\left. \times \left[C(l_c) - 4\kappa_g^2(Q_c) \right] D_h(Q_c) \right) T_s(\xi,4) \right\}$$

$$\times \left\{ \frac{\rho^d(Q_c)}{s_c\left[\rho^d(Q_c)+s_c\right]} \right\}^{5/2} e^{-jks_c} \tag{446}$$

where (383), (435) and (436) have been used to simplify the result. It is now assumed that the function $\tilde{B}_2^h(x_e)$ is a smooth and slowly varying function of x_e near the stationary phase point and $k \gg 1$. This allows us to use the uniform asymptotic expansion (673) of Appendix B. Therefore, the uniform asymptotic expansion of (359) is

$$\widehat{\beta}_c\,\mathcal{J}_2^h(P) \;\sim\; -\widehat{\beta}_c\,E^i_{\beta_c}\,\frac{s_c}{2\pi}\,\tilde{B}_2^h(x_c)\,\frac{\sqrt{2\pi}}{k^{3/2}} \left\{ \frac{e^{j\eta\pi/4}}{\sqrt{|h^{\,\mathrm{II}}(x_c)|}} \right\}^3 e^{jkh(x_c)}\,T_s(\xi,2)$$

$$-\widehat{\beta}_c\,E^i_{\beta_c}\,\frac{s_c}{2\pi}\,\frac{3\sqrt{2\pi}}{2k^{5/2}} \left\{ \frac{e^{j\eta\pi/4}}{\sqrt{|h^{\,\mathrm{II}}(x_c)|}} \right\}^5 e^{jkh(x_c)}\,T_s(\xi,4)$$

$$\times \left\{ \left.\frac{d^2\tilde{B}_2^h(x_e)}{dx_e^2}\right|_{Q_c} + \frac{5}{12}\left[C(l_c) - 4\kappa_g^2(Q_c) \right]\tilde{B}_2^h(x_c) \right\}$$

$$\sim \quad \vec{E}^i(Q_c)\cdot\left\{ -\widehat{\beta}'\widehat{\beta}_c \left(\frac{js_c^2\sin\psi_c\sin\psi_c'}{k\rho_g^2(Q_c)} \right) D_h(Q_c)\,T_s(\xi,2) \right\}$$

$$\times \left\{ \frac{\rho^d(Q_c)}{s_c\left[\rho^d(Q_c)+s_c\right]} \right\}^{3/2} e^{-jks_c}$$

$$+ \quad \vec{E}^i(Q_c)\cdot\left\{ -\widehat{\beta}'\widehat{\beta}_c \left(\frac{3s_c^6}{2k^2}\,\frac{d^2B_2^h(Q_c)}{dl^2} + \frac{5s_c^4\sin\psi_c\sin\psi_c'}{8k^2\rho_g^2(Q_c)} \right.\right.$$

$$\left.\left. \times \left[C(l_c) - 4\kappa_g^2(Q_c) \right] D_h(Q_c) \right) T_s(\xi,4) \right\}$$

$$\times \left\{ \frac{\rho^d(Q_c)}{s_c\left[\rho^d(Q_c)+s_c\right]} \right\}^{5/2} e^{-jks_c} \tag{447}$$

where (384), (435) and (436) have been used to simplify the result. It is now assumed that the function $\tilde{C}_0^h(x_e)$ is a smooth and slowly varying function of x_e near the stationary phase point and $k \gg 1$. This allows us to use the uniform asymptotic expansion (673) of Appendix B. Therefore, the uniform asymptotic expansion of (360)

is

$$\begin{aligned}
\widehat{\psi}_c \mathcal{K}_0^h(P) \;\sim\; & \widehat{\psi}_c E^i_{\psi_c} \frac{s_c}{2\pi} \tilde{C}_0^h(x_c) \sqrt{\frac{2\pi}{k}} \left\{ \frac{e^{j\eta\pi/4}}{\sqrt{|h^{\,\mathrm{II}}(x_c)|}} \right\} e^{jkh(x_c)} T_s(\xi, 0) \\
& + \widehat{\psi}_c E^i_{\psi_c} \frac{s_c}{2\pi} \frac{\sqrt{2\pi}}{2k^{3/2}} \left\{ \frac{e^{j\eta\pi/4}}{\sqrt{|h^{\,\mathrm{II}}(x_c)|}} \right\}^3 e^{jkh(x_c)} T_s(\xi, 2) \\
& \times \left\{ \left. \frac{d^2 \tilde{C}_0^h(x_e)}{dx_e^2} \right|_{Q_c} + \frac{1}{4} \left[\mathcal{C}(l_c) - 4\kappa_g^2(Q_c) \right] \tilde{C}_0^h(x_c) \right\} \\
\sim\; & \vec{E}^i(Q_c) \cdot \left\{ -\widehat{\psi}' \widehat{\psi}_c D_h(Q_c) T_s(\xi, 0) \right\} \sqrt{\frac{\rho^d(Q_c)}{s_c \left[\rho^d(Q_c) + s_c \right]}} \; e^{-jks_c} \\
+\; & \vec{E}^i(Q_c) \cdot \left\{ -\widehat{\psi}' \widehat{\psi}_c \left(\frac{s_c^4}{2jk} \frac{d^2 C_0^h(Q_c)}{dl^2} + \frac{s_c^2}{8jk} \right. \right. \\
& \left. \left. \times \left[\mathcal{C}(l_c) - 4\kappa_g^2(Q_c) \right] D_h(Q_c) \right) T_s(\xi, 2) \right\} \\
& \times \left\{ \frac{\rho^d(Q_c)}{s_c \left[\rho^d(Q_c) + s_c \right]} \right\}^{3/2} e^{-jks_c}
\end{aligned} \tag{448}$$

where (385), (435) and (436) have been used to simplify the result. It is now assumed that the function $\tilde{C}_2^h(x_e)$ is a smooth and slowly varying function of x_e near the stationary phase point and $k \gg 1$. This allows us to use the uniform asymptotic expansion (673) of Appendix B. Therefore, the uniform asymptotic expansion of (361) is

$$\begin{aligned}
\widehat{\psi}_c \mathcal{K}_2^h(P) \;\sim\; & -\widehat{\psi}_c E^i_{\psi_c} \frac{1}{2\pi} \tilde{C}_2^h(x_c) \frac{\sqrt{2\pi}}{k^{3/2}} \left\{ \frac{e^{j\eta\pi/4}}{\sqrt{|h^{\,\mathrm{II}}(x_c)|}} \right\}^3 e^{jkh(x_c)} T_s(\xi, 2) \\
& - \widehat{\psi}_c E^i_{\psi_c} \frac{1}{2\pi} \frac{3\sqrt{2\pi}}{2k^{5/2}} \left\{ \frac{e^{j\eta\pi/4}}{\sqrt{|h^{\,\mathrm{II}}(x_c)|}} \right\}^5 e^{jkh(x_c)} T_s(\xi, 4) \\
& \times \left\{ \left. \frac{d^2 \tilde{C}_2^h(x_e)}{dx_e^2} \right|_{Q_c} + \frac{5}{12} \left[\mathcal{C}(l_c) - 4\kappa_g^2(Q_c) \right] \tilde{C}_2^h(x_c) \right\} \\
\sim\; & \vec{E}^i(Q_c) \cdot \left\{ -\widehat{\psi}' \widehat{\psi}_c \left(\frac{s_c \cos\psi_c}{2jk\rho_g(Q_c)} \right) D_h(Q_c) T_s(\xi, 2) \right\} \\
& \times \left\{ \frac{\rho^d(Q_c)}{s_c \left[\rho^d(Q_c) + s_c \right]} \right\}^{3/2} e^{-jks_c} \\
+\; & \vec{E}^i(Q_c) \cdot \left\{ -\widehat{\psi}' \widehat{\psi}_c \left(\frac{3s_c^5}{2k^2} \frac{d^2 C_2^h(Q_c)}{dl^2} + \frac{-5s_c^3 \cos\psi_c}{16k^2 \rho_g(Q_c)} \right. \right.
\end{aligned}$$

$$\times \left[C(l_c) - 4\kappa_g^2(Q_c)\right] D_h(Q_c)\Big) T_s(\xi,4)\Big\}$$
$$\times \left\{\frac{\rho^d(Q_c)}{s_c\left[\rho^d(Q_c)+s_c\right]}\right\}^{5/2} e^{-jks_c} \tag{449}$$

where (386), (435) and (436) have been used to simplify the result. This completes the uniform asymptotic expansion of the diffracted field integral equations on the shadow side of the caustic. However, it is advantageous to rewrite these results in a more convenient and standard form. Therefore, adding (437) through (449) and regrouping the terms we obtain

$$\begin{aligned}
\vec{E}^d(P) \;\sim\; & \vec{E}^i(Q_c)\cdot\overline{\overline{D}}^S(Q_c)\sqrt{\frac{\rho^d(Q_c)}{s_c\left[\rho^d(Q_c)+s_c\right]}}\, e^{-jks_c} \\
+\; & \vec{E}^i(Q_c)\cdot\overline{\overline{D}}_1^S(Q_c)\left\{\frac{\rho^d(Q_c)}{s_c\left[\rho^d(Q_c)+s_c\right]}\right\}^{3/2} e^{-jks_c} \\
+\; & \vec{E}^i(Q_c)\cdot\overline{\overline{D}}_2^S(Q_c)\left\{\frac{\rho^d(Q_c)}{s_c\left[\rho^d(Q_c)+s_c\right]}\right\}^{5/2} e^{-jks_c} \\
+\; & \vec{E}^i(Q_c)\cdot\overline{\overline{D}}_3^S(Q_c)\left\{\frac{\rho^d(Q_c)}{s_c\left[\rho^d(Q_c)+s_c\right]}\right\}^{7/2} e^{-jks_c}
\end{aligned} \tag{450}$$

which is the caustic shadow region diffracted field in a standard dyadic form. The dyadic diffraction coefficient appearing in the first term of (450) is given by

$$\overline{\overline{D}}^S(Q_c) = -\hat{\beta}'\hat{\beta}_c\, D_s(Q_c)\, T_s(\xi,0) - \hat{\psi}'\hat{\psi}_c\, D_h(Q_c)\, T_s(\xi,0) \tag{451}$$

and corresponds to the UTD dyadic diffraction coefficient multiplied by the caustic correction transition function $T_s(\xi,0)$ which can be found in (674) of Appendix B. The last three terms in (450) correspond to curvature dependant components of the diffracted field and their dyadic diffraction coefficients are given by

$$\begin{aligned}
\overline{\overline{D}}_1^S(Q_c) \;=\; & -\hat{\psi}'\hat{s}_c\left(\frac{s_c\sin\psi_c'}{jk\rho_g(Q_c)}\right) D_s(Q_c)\, T_s(\xi,2) \\
& -\hat{\psi}'\hat{\psi}_c\left(\frac{js_c^2\sin\psi_c\sin\psi_c'}{k\rho_g^2(Q_c)}\right) D_s(Q_c)\, T_s(\xi,2) \\
& -\hat{\psi}'\hat{s}_c\left(\frac{s_c\sin\psi_c}{2jk\rho_g(Q_c)}\right) D_h(Q_c)\, T_s(\xi,2) \\
& -\hat{\beta}'\hat{\beta}_c\left(\frac{js_c^2\sin\psi_c\sin\psi_c'}{k\rho_g^2(Q_c)}\right) D_h(Q_c)\, T_s(\xi,2)
\end{aligned}$$

$$
\begin{aligned}
&-\widehat{\psi}'\widehat{\psi}_c\left(\frac{s_c\cos\psi_c}{2jk\rho_g(Q_c)}\right)D_h(Q_c)\,T_s(\xi,2)\\
&-\widehat{\beta}'\widehat{\beta}_c\left(\frac{s_c^5}{2jk}\,\frac{d^2B_0^s(Q_c)}{dl^2}+\frac{s_c^2}{8jk}\right.\\
&\qquad\left.\times\left[C(l_c)-4\kappa_g^2(Q_c)\right]D_s(Q_c)\right)T_s(\xi,2)\\
&-\widehat{\psi}'\widehat{\psi}_c\left(\frac{s_c^4}{2jk}\,\frac{d^2C_0^h(Q_c)}{dl^2}+\frac{s_c^2}{8jk}\right.\\
&\qquad\left.\times\left[C(l_c)-4\kappa_g^2(Q_c)\right]D_h(Q_c)\right)T_s(\xi,2)\,, \qquad (452)
\end{aligned}
$$

$$
\begin{aligned}
\overline{\overline{D}}_2^S(Q_c) \;=\;& -\widehat{\psi}'\widehat{s}_c\left(\frac{-3s_c^2\left\{\rho_g(Q_c)\cos\psi_c+s_c\sin^2\psi_c\right\}\sin\psi_c'}{2k^2\rho_g^3(Q_c)}\right)D_s(Q_c)\,T_s(\xi,4)\\
&-\widehat{\beta}'\widehat{\beta}_c\left(\frac{3s_c^2\kappa_g^2(Q_c)-s_c^3\left[\kappa_g^{\rm II}(Q_c)+3\kappa_g^3(Q_c)\right]}{4k^2}\right)D_s(Q_c)\,T_s(\xi,4)\\
&-\widehat{\psi}'\widehat{\psi}_c\left(\frac{3s_c^2\left\{\rho_g(Q_c)-s_c\cos\psi_c\right\}\sin\psi_c\sin\psi_c'}{2k^2\rho_g^3(Q_c)}\right)D_s(Q_c)\,T_s(\xi,4)\\
&-\widehat{\psi}'\widehat{s}_c\left(\frac{-3s_c^6}{2k^2}\,\frac{d^2A_2^s(Q_c)}{dl^2}+\frac{-5s_c^3\sin\psi_c'}{8k^2\rho_g(Q_c)}\right.\\
&\qquad\left.\times\left[C(l_c)-4\kappa_g^2(Q_c)\right]D_s(Q_c)\right)T_s(\xi,4)\\
&-\widehat{\psi}'\widehat{\psi}_c\left(\frac{3s_c^7}{2k^2}\,\frac{d^2C_2^s(Q_c)}{dl^2}+\frac{5\sin\psi_c\sin\psi_c'}{8k^2s_c^3\rho_g^2(Q_c)}\right.\\
&\qquad\left.\times\left[C(l_c)-4\kappa_g^2(Q_c)\right]D_s(Q_c)\right)T_s(\xi,4)\\
&-\widehat{\psi}'\widehat{s}_c\left(\frac{3s_c^5}{2k^2}\,\frac{d^2A_2^h(Q_c)}{dl^2}+\frac{-15s_c^3\sin\psi_c}{48k^2\rho_g(Q_c)}\right.\\
&\qquad\left.\times\left[C(l_c)-4\kappa_g^2(Q_c)\right]D_h(Q_c)\right)T_s(\xi,4)\\
&-\widehat{\beta}'\widehat{\beta}_c\left(\frac{3s_c^6}{2k^2}\,\frac{d^2B_2^h(Q_c)}{dl^2}+\frac{5s_c^4\sin\psi_c\sin\psi_c'}{8k^2\rho_g^2(Q_c)}\right.\\
&\qquad\left.\times\left[C(l_c)-4\kappa_g^2(Q_c)\right]D_h(Q_c)\right)T_s(\xi,4)\\
&-\widehat{\psi}'\widehat{\psi}_c\left(\frac{3s_c^5}{2k^2}\,\frac{d^2C_2^h(Q_c)}{dl^2}+\frac{-5s_c^3\cos\psi_c}{16k^2\rho_g(Q_c)}\right.\\
&\qquad\left.\times\left[C(l_c)-4\kappa_g^2(Q_c)\right]D_h(Q_c)\right)T_s(\xi,4) \qquad (453)
\end{aligned}
$$

and

$$\begin{aligned}
\overline{\overline{D}}_3^s(Q_c) &= -\widehat{\psi}'\widehat{s}_c\left(\frac{15s_c^7}{2jk^3}\,\frac{d^2A_4^s(Q_c)}{dl^2}+\frac{j35s_c^4\left\{\rho_g(Q_c)\cos\psi_c+s_c\sin^2\psi_c\right\}\sin\psi_c'}{16k^3\rho_g^3(Q_c)}\right.\\
&\qquad\left.\times\left[\mathcal{C}(l_c)-4\kappa_g^2(Q_c)\right]D_s(Q_c)\right)T_s(\xi,6)\\
&\quad-\widehat{\beta}'\widehat{\beta}_c\left(\frac{15js_c^7}{2k^3}\,\frac{d^2B_4^s(Q_c)}{dl^2}\right.\\
&\qquad+\frac{35s_c^2\left\{3s_c^2\kappa_g^2(Q_c)-s_c^3\left[\kappa_g^{\rm II}(Q_c)+3\kappa_g^3(Q_c)\right]\right\}}{96jk^3}\\
&\qquad\left.\times\left[\mathcal{C}(l_c)-4\kappa_g^2(Q_c)\right]D_s(Q_c)\right)T_s(\xi,6)\\
&\quad-\widehat{\psi}'\widehat{\psi}_c\left(\frac{15js_c^7}{2k^3}\,\frac{d^2C_4^s(Q_c)}{dl^2}+\frac{35s_c^4\left\{\rho_g(Q_c)-s_c\cos\psi_c\right\}\sin\psi_c\sin\psi_c'}{16jk^3\rho_g^3(Q_c)}\right.\\
&\qquad\left.\times\left[\mathcal{C}(l_c)-4\kappa_g^2(Q_c)\right]D_s(Q_c)\right)T_s(\xi,6) \qquad (454)
\end{aligned}$$

where $D_{s,h}(Q_c)$ are the UTD half-plane diffraction coefficients, $\mathcal{C}(l_c)$ is given in (438) through (440) and the second derivatives of the amplitude functions are given in (434) and (435). Also, the caustic correction transition functions $T_s(\xi,k)$ are defined in (674) of Appendix B. This completes the uniform asymptotic expansion of the diffracted field integral equations for the shadow side of the caustic.

5 Useful Approximate Field Expressions

Although the diffracted field expressions derived in Sections 3 and 4 are written in terms of simple functions, they may seem complicated at first. Therefore, some simple approximations can be helpful in reducing these expressions to something more practical. This section is a discussion of two approximations that can be used to simplify the calculation of the diffracted field expressions.

The first approximation deals simply with the shape of the edge. This approximation will change only the central diffracted field expressions since only the central diffracted field contains explicit information about the shape of the edge. The edge of the plate was first assumed to be in the form of a power series as given in (309). Although this is theoretically precise, this series can be approximated by only the

leading term. This is due to the fact that the central diffracted field is dependant on the local geometry near the diffraction point. Therefore, the diffracted field expressions can be approximated by making

$$a_4 = \kappa_g^{\rm II}(Q_c) + 3\kappa_g^3(Q_c) = 0 \tag{455}$$

and

$$a_6 = \kappa_g^{\rm IV}(Q_c) + 34\kappa_g^2(Q_c)\kappa_g^{\rm II}(Q_c) + 45\kappa_g^5(Q_c) = 0 \tag{456}$$

which is the same as saying $\kappa_g^{\rm II}(Q_c) \approx -3\kappa_g^3(Q_c)$ and $\kappa_g^{\rm IV}(Q_c) \approx 57\kappa_g^5(Q_c)$. These turn out to be excellent approximations as will be shown in the next chapter when the expressions derived in this chapter are calculated.

The second approximation deals with the nature of the diffracted field integral equations. Although the diffracted field expressions derived in Sections 3 and 4 are all required to obtain a completely uniform caustic corrected UTD solution that reduces to the UTD away from the caustic, only two main contributions are required to obtain a good approximation of the field. The integrals in Section 2 containing zeros will produce only non-central diffracted field components to a first order asymptotic approximation. Although the zeros need to be accounted for in order to obtain a uniform asymptotic expansion of these integrals, their contribution to the total diffracted field is small compared to the integrals that do not contain zeros. Therefore, the total diffracted field can be approximated by

$$\vec{E}^d(P) \approx \hat{\beta}_c \mathcal{J}_0^s(P) + \hat{\psi}_c \mathcal{K}_0^h(P) \tag{457}$$

where $\mathcal{J}_0^s(P)$ and $\mathcal{K}_0^h(P)$ are the only two integrals that do not contain zeros. It is important to note that these are the two integrals that compensate for the discontinuities of the GO fields. These integrals have been asymptotically reduced on the lit side of the caustic in Section 3 and can be written as

$$\begin{aligned}\vec{E}^d(P) \;\sim\; & \vec{E}^i(Q_c)\cdot\overline{\overline{D}}^L(Q_c)\sqrt{\frac{\rho^d(Q_c)}{s_c\,[\rho^d(Q_c)+s_c]}}\,e^{-jks_c} \\ + \; & \vec{E}^i(Q_{nc}^+)\cdot\overline{\overline{D}}^L(Q_{nc}^+)\sqrt{\frac{\rho^d(Q_{nc})}{s_{nc}\,[\rho^d(Q_{nc})+s_{nc}]}}\,e^{-jks_{nc}}\end{aligned}$$

$$+ \quad \vec{E}^i(Q_{nc}^-) \cdot \overline{\overline{D}}^L(Q_{nc}^-) \sqrt{\frac{\rho^d(Q_{nc})}{s_{nc}\left[\rho^d(Q_{nc}) + s_{nc}\right]}}\, e^{-jks_{nc}} \tag{458}$$

where

$$\overline{\overline{D}}^L(Q_c) \approx -\hat{\beta}'\hat{\beta}_c\, D_s(Q_c)\, T_c(\xi, 0) - \hat{\psi}'\hat{\psi}_c\, D_h(Q_c)\, T_c(\xi, 0) \tag{459}$$

is the dyadic diffraction coefficient for the central diffracted field and

$$\overline{\overline{D}}^L(Q_{nc}) = -\hat{\beta}'\vec{\mathbf{B}}_u(\xi)\, D_s(Q_{nc}) - \hat{\psi}'\vec{\Psi}_u(\xi)\, D_h(Q_{nc}) \tag{460}$$

is the dyadic diffraction coefficient for the non-central diffracted fields. Also, the uniform polarization vectors $\vec{\mathbf{B}}_u(\xi)$ and $\vec{\Psi}_u(\xi)$ are

$$\vec{\mathbf{B}}_u(\xi) \approx \hat{\beta}_c \left\{ \frac{-s_c^2 \left[\hat{e}(Q_{nc}) \cdot \hat{\beta}_c\right]}{s_{nc}^2 \sin\beta_{nc}}\, T_{nc}(\xi, \eta, 0) \right\} \tag{461}$$

and

$$\vec{\Psi}_u(\xi) \approx \hat{\psi}_c \left\{ \frac{-s_c \left[\hat{e}(Q_{nc}) \cdot \hat{\beta}_c\right]}{s_{nc} \sin\beta_{nc}}\, T_{nc}(\xi, \eta, 0) \right\}, \tag{462}$$

respectively. It is clear that these expressions do not reduce to the standard UTD ray fixed polarization unit vectors $\hat{\beta}$ and $\hat{\psi}$. It should be noted that $\hat{\beta}\, T_{nc}(\xi, \eta, 0)$ and $\hat{\psi}\, T_{nc}(\xi, \eta, 0)$ can not be used in the place of $\vec{\mathbf{B}}_u(\xi)$ and $\vec{\Psi}_u(\xi)$; respectively, because the result will no longer be uniform. These integrals have also been asymptotically reduced on the shadow side of the caustic in Section 4 and can be written as

$$\begin{aligned} \vec{E}^d(P) \quad &\sim \quad \vec{E}^i(Q_c) \cdot \overline{\overline{D}}^S(Q_c) \sqrt{\frac{\rho^d(Q_c)}{s_c\left[\rho^d(Q_c) + s_c\right]}}\, e^{-jks_c} \\ &+ \quad \vec{E}^i(Q_c) \cdot \overline{\overline{D}}^S(Q_c) \left\{ \frac{\rho^d(Q_c)}{s_c\left[\rho^d(Q_c) + s_c\right]} \right\}^{3/2} e^{-jks_c} \end{aligned} \tag{463}$$

where

$$\overline{\overline{D}}^S(Q_c) \approx -\hat{\beta}'\hat{\beta}_c\, D_s(Q_c)\, T_s(\xi, 0) - \hat{\psi}'\hat{\psi}_c\, D_h(Q_c)\, T_s(\xi, 0) \tag{464}$$

is the dyadic diffraction coefficient for the central diffracted field and

$$\begin{aligned} \overline{\overline{D}}^S(Q_c) \quad \approx \quad -\hat{\beta}'\hat{\beta}_c \Bigg(&\frac{s_c^5}{2jk}\, \mathcal{F}_s^{\mathrm{II}}(Q_c) + \frac{s_c^2}{8jk} \\ &\times \left[C(l_c) - 4\kappa_g^2(Q_c)\right] D_s(Q_c) \Bigg)\, T_s(\xi, 2) \end{aligned}$$

$$-\widehat{\psi}'\widehat{\psi}_c\left(\frac{s_c^4}{2jk}\,\mathcal{F}_h^{\mathrm{II}}(Q_c)+\frac{s_c^2}{8jk}\right.$$
$$\left.\times\left[C(l_c)-4\kappa_g^2(Q_c)\right]D_h(Q_c)\right)T_s(\xi,2) \qquad (465)$$

is the dyadic diffraction coefficient for the curvature dependant central diffracted field. This turns out to be good approximation as will be shown in the next chapter when the expressions derived in this chapter are calculated.

SECTION 8

Numerical Calculation of the Field Scattered by a Plane Wave Incident on a Flat Plate with a Curved Edge

It is important to numerically confirm that the caustic corrected UTD (CC-UTD) solution derived in Chapter 7 is accurate. To do so, two geometries are considered in this chapter. First, the scattering by a flat plate with a curved edge defined by a parabolic equation is determined. This CC-UTD solution is then compared to the classical UTD solution. The other geometry considered is the scattering by an elliptic disk. The CC-UTD solution is compared to the classical UTD solution and a Moment Method (MM) solution. This chapter is devoted to the numerical confirmation of the CC-UTD solution of Chapter 7.

1 Scattering a Flat Plate with an Edge Defined by a Parabolic Equation

The first geometry to be studied is the scattering by a flat plate with an edge defined by a parabolic equation. To conform to the assumptions of the derivation of the CC-UTD in Chapter 7 it is important that the plane wave propagates in the plane of symmetry of the parabolic edge. Also, the near-zone observation point must be in the plane of symmetry of the parabolic edge. This geometry is shown in Figure 40. This section consists of two parts. First, the parameters required for the CC-UTD

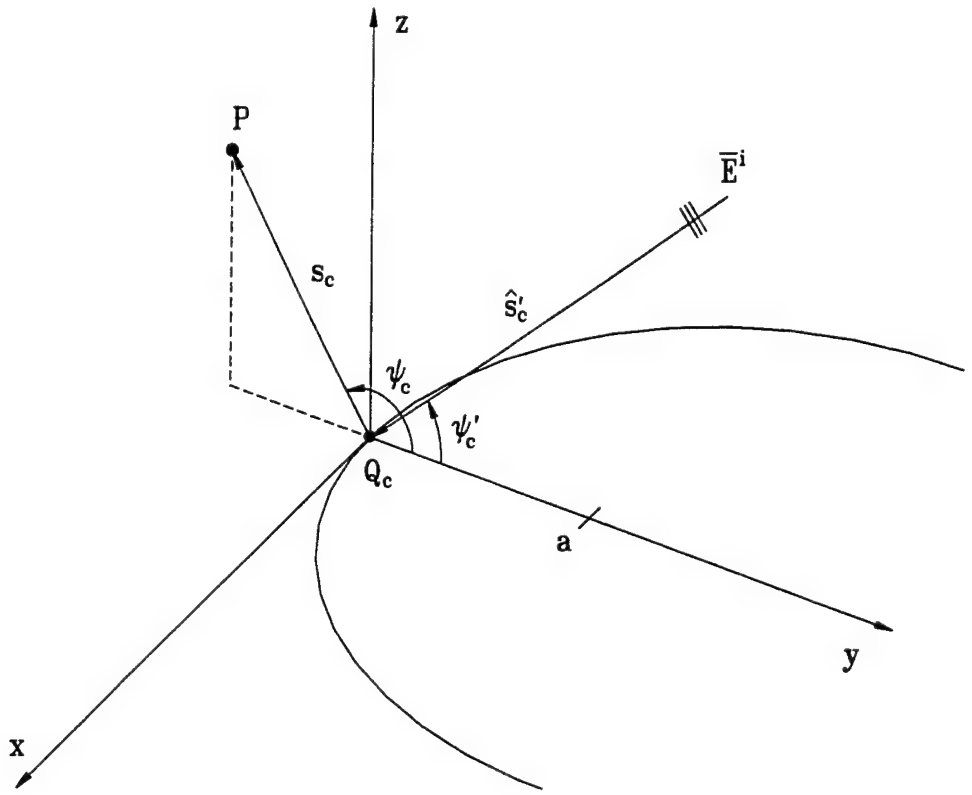

Figure 40: Geometry for the scattering by a flat plate with a curved edge defined by a parabolic equation.

and the UTD solutions are determined. Next, the scattered field is calculated and compared.

1.1 Parabolic Edge Scattered Field Parameters

In order to determine the geometric parameters required for the use of the CC-UTD and the UTD, the edge of the plate will be defined as

$$x_e^2 = 4ay_e \tag{466}$$

where a is the focal length of the parabola. First, the diffraction points can be determined by enforcing the fact that $\cos\beta = \cos\beta'$. In doing so, the central diffraction point is found to be located at

$$y_c = 0 \tag{467}$$

and the non-central diffraction points are found to be located at

$$y_{nc} = \begin{cases} y_o + \varepsilon_c\sqrt{s_c^2 - y_o^2}\,\cot\psi_c' & ;\text{ if } s_c^2 - y_o^2 > 0 \\ y_o - j\varepsilon_c\sqrt{y_o^2 - s_c^2}\,\cot\psi_c' & ;\text{ if } s_c^2 - y_o^2 < 0 \end{cases} \tag{468}$$

where $y_o = s_c\cos\psi_c - 2a$, $\varepsilon_c = \text{sgn}\{\sin\psi_c'\}$ and the observation distance s_c is fixed. Using this result it is easy to determine the caustic lit and caustic shadow regions. If $y_{nc} > 0$ the observation point is in the caustic lit region and if $y_{nc} < 0$ the observation point is in the caustic shadow region. Also, the distance from the non-central diffraction points to the observation point is

$$s_{nc} = \frac{y_{nc} - y_o}{\cos\psi_c'}\,. \tag{469}$$

The next quantities needed are the curvature and the second and fourth derivatives of the curvature at the diffraction points. The curvature of the edge is defined as [33]

$$\kappa_g(Q') = \frac{|y_e''|}{[1 + (y_e')^2]^{3/2}} \tag{470}$$

where using (466) it is easy to show that

$$\kappa_g(Q') = \frac{1}{2a}\left(\frac{a}{a + y_e}\right)^{3/2} \tag{471}$$

for a point on the parabolic edge. Next, evaluating (471) at the central and non-central diffraction points we obtain

$$\kappa_g(Q_c) = \frac{1}{2a} \tag{472}$$

and

$$\kappa_g(Q_{nc}) = \frac{1}{2a}\left(\frac{a}{a+y_{nc}}\right)^{3/2}, \tag{473}$$

respectively. Also, differentiating (471) four times with respect to x_e, evaluating them at the central diffraction point and using (758) and (763) of Appendix D to convert these derivatives we obtain

$$\kappa_g^{\mathrm{II}}(Q_c) = -3\kappa_g^3(Q_c) = \frac{-3}{(2a)^3} \tag{474}$$

as the second derivative and

$$\kappa_g^{\mathrm{IV}}(Q_c) = 57\kappa_g^5(Q_c) = \frac{57}{(2a)^5} \tag{475}$$

as the fourth derivative of the curvature with respect to arc length. It is now necessary to determine the diffraction angles ψ and β at each of the diffraction points. The values of ψ and ψ' at the central diffraction point are ψ_c and ψ_c', respectively. Also, the oblique incidence angles at the central diffraction point are $\beta_c = \beta_c' = \frac{\pi}{2}$. The angle ψ is found using

$$\cos\psi_{nc} = \frac{2a\left(s_c\cos\psi_c + y_{nc}\right)}{s_{nc}\sin\beta_{nc}\sqrt{(2a)^2 + 4ay_{nc}}} \tag{476}$$

and the angle ψ' is found using

$$\cos\psi_{nc}' = \frac{2a\cos\psi_c'}{\sin\beta_{nc}\sqrt{(2a)^2 + 4ay_{nc}}} \tag{477}$$

at the non-central diffraction points. The angle $\beta_{nc} = \beta_{nc}'$ at the non-central diffraction points is

$$\sin\beta_{nc} = \sqrt{\frac{a + y_{nc}\sin^2\psi_c'}{a + y_{nc}}} \tag{478}$$

using $\cos\beta_{nc} = \cos\beta_{nc}' = \hat{s}_c' \cdot \hat{e}$. Next, it is important to determine the distance to the second caustic of the central and non-central diffraction points. To do so, we

recall (10) from Chapter 2 to find

$$\rho^d(Q_c) = \frac{-2a}{\cos\psi_c + \cos\psi_c'} \tag{479}$$

as the caustic distance at the central diffraction point, and

$$\rho^d(Q_{nc}) = -\left(\frac{a + y_{nc}}{a}\right) s_{nc} \sin^2\beta_{nc} \tag{480}$$

as the second caustic distance at the non-central diffraction points. Also noting that

$$\hat{s}_c' \cdot \vec{r}_e(Q_{nc}) = -y_{nc} \cos\psi_c', \tag{481}$$

we are able to determine the argument of the caustic correction transition functions. Finally, it is necessary to determine the Geometrical Optics (GO) field and the incident field at each of the diffraction points. The incident field at the observation point is

$$\vec{E}^i(P) = \left\{\hat{\beta}_c' E^i_{\beta_c} + \hat{\psi}_c' E^i_{\psi_c}\right\} e^{jks_c\cos(\psi_c - \psi_c')} \, \mathrm{U}\left[\pi - |\psi_c - \psi_c'|\right] \tag{482}$$

which is determined using classical GO techniques. The incident wave polarization vectors $\hat{\beta}_c'$ and $\hat{\psi}_c'$ must be transformed into the global polarization unit vectors $\hat{s}_c$, $\hat{\beta}_c$ and $\hat{\psi}_c$ as shown in Figure 41. Using the coordinate transformation

$$\hat{\beta}_c' = -\hat{\beta}_c \tag{483}$$

$$\hat{\psi}_c' = \hat{s}_c \sin(\psi_c - \psi_c') + \hat{\psi}_c \cos(\psi_c - \psi_c') \tag{484}$$

it is found that

$$\begin{aligned}\vec{E}^i(P) = {} & \left\{\hat{s}_c E^i_{\psi_c} \sin(\psi_c - \psi_c') - \hat{\beta}_c E^i_{\beta_c} + \hat{\psi}_c E^i_{\psi_c} \cos(\psi_c - \psi_c')\right\} \\ & \times e^{jks_c\cos(\psi_c - \psi_c')} \, \mathrm{U}\left[\pi - |\psi_c - \psi_c'|\right]\end{aligned} \tag{485}$$

is the incident field at the observation point. Next, the reflected field at the observation point is

$$\vec{E}^r(P) = \left\{\hat{\beta}_r E^i_{\beta_c} R_s + \hat{\psi}_r E^i_{\psi_c} R_h\right\} e^{jks_c\cos(\psi_c + \psi_c')} \, \mathrm{U}\left[\pi - |\psi_c + \psi_c'|\right] \tag{486}$$

where the reflection coefficients are $R_{s,h} = \mp 1$. The reflected wave polarization vectors $\hat{\beta}_r$ and $\hat{\psi}_r$ must be transformed into the global polarization unit vectors $\hat{s}_c$, $\hat{\beta}_c$ and $\hat{\psi}_c$

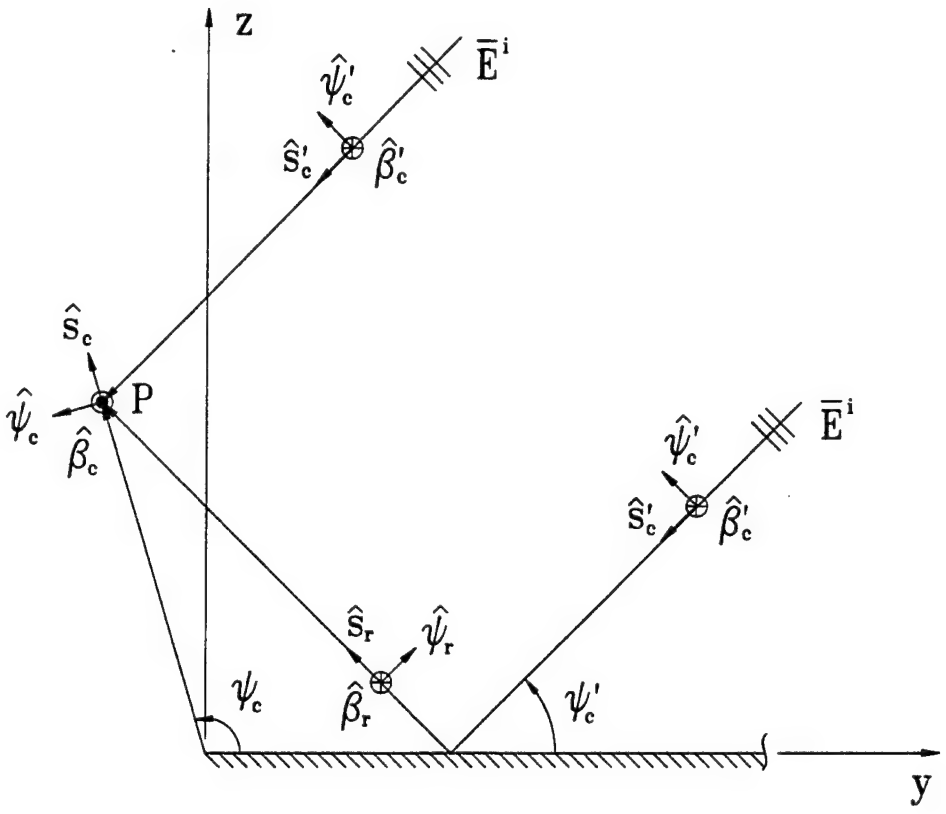

Figure 41: Polarization unit vector definition for the Geometrical Optics fields in the presence of a flat plate with a curved edge defined by a parabolic equation.

as shown in Figure 41. Using the coordinate transformation

$$\widehat{\beta}_r = -\widehat{\beta}_c \tag{487}$$

$$\widehat{\psi}_r = \widehat{s}_c \sin(\psi_c + \psi_c') + \widehat{\psi}_c \cos(\psi_c + \psi_c') \tag{488}$$

it is found that

$$\begin{aligned}\vec{E}^r(P) = &\left\{\widehat{s}_c\, E^i_{\psi_c} \sin(\psi_c + \psi_c') + \widehat{\beta}_c\, E^i_{\beta_c} + \widehat{\psi}_c\, E^i_{\psi_c} \cos(\psi_c + \psi_c')\right\} \\ &\times e^{jks_c \cos(\psi_c + \psi_c')}\, \mathrm{U}\left[\pi - |\psi_c + \psi_c'|\right]\end{aligned} \tag{489}$$

is the reflected field at the observation point. The GO field at the observation point is the sum of the incident field and the reflected field at the observation point. The diffracted field can now be determined using the diffraction parameters found previously.

The incident field at each diffraction point and polarization vectors are required to determine the diffracted field on the lit side of the caustic. The incident field is

$$\vec{E}^i(Q_c) = \widehat{\beta}'_c\, E^i_{\beta_c} + \widehat{\psi}'_c\, E^i_{\psi_c} \tag{490}$$

at the central diffraction point and

$$\vec{E}^i(Q_{nc}) = \left\{\widehat{\beta}'_c\, E^i_{\beta_c} + \widehat{\psi}'_c\, E^i_{\psi_c}\right\} e^{jky_{nc} \cos\psi_c'} \tag{491}$$

at the non-central diffraction points. It is now necessary to rotate the incident ray fixed polarization unit vectors $\widehat{\beta}'$ and $\widehat{\psi}'$ into the global incident polarization unit vectors $\widehat{\beta}'_c$ and $\widehat{\psi}'_c$. The incident wave ray fixed polarization unit vectors at the central diffraction point are $\widehat{\beta}' = \widehat{\beta}'_c$ and $\widehat{\psi}' = \widehat{\psi}'_c$. The incident wave ray fixed polarization unit vectors at the non-central diffraction points are

$$\widehat{\beta}' = \widehat{\beta}'_c \left\{\frac{2a}{\sin\beta_{nc}\sqrt{(2a)^2 + 4ay_{nc}}}\right\} + \widehat{\psi}'_c \left\{\frac{x_{nc} \sin\psi_c'}{\sin\beta_{nc}\sqrt{(2a)^2 + 4ay_{nc}}}\right\} \tag{492}$$

and

$$\widehat{\psi}' = \widehat{\beta}'_c \left\{\frac{-x_{nc} \sin\psi_c'}{\sin\beta_{nc}\sqrt{(2a)^2 + 4ay_{nc}}}\right\} + \widehat{\psi}'_c \left\{\frac{2a}{\sin\beta_{nc}\sqrt{(2a)^2 + 4ay_{nc}}}\right\} \tag{493}$$

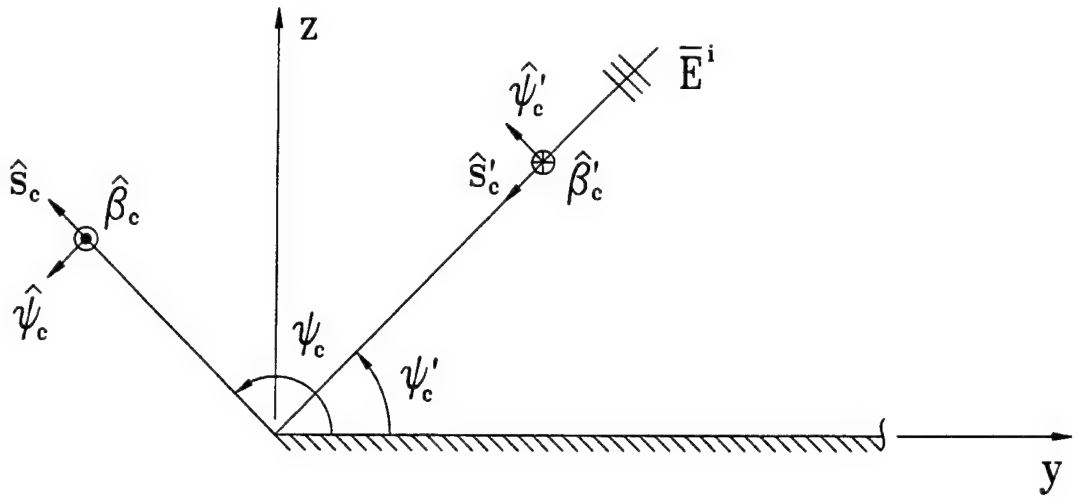

Figure 42: Polarization unit vector definition for the diffraction by a curved edge defined by a parabolic equation.

in terms of the global incident wave polarization unit vectors $\hat{\beta}_c'$ and $\hat{\psi}_c'$ as shown in Figure 42. Also, the modified diffracted ray fixed polarization vectors $\vec{\mathbf{B}}_u(\xi)$ and $\vec{\Psi}_u(\xi)$ as given by (415) and (416) of Chapter 7 are

$$\begin{aligned}
\vec{\mathbf{B}}_u(\xi) &= \hat{s}_c \left\{ \frac{2a\, s_c\, x_{nc}\, T_{nc}(\xi,\eta,2) + (2a\cos\psi_c + s_c \sin^2\psi_c)\, x_{nc}\, y_{nc}\, T_{nc}(\xi,\eta,4)}{s_{nc}^2 \sin\beta_{nc}\sqrt{(2a)^2 + 4ay_{nc}}} \right\} \\
&+ \hat{\beta}_c \left\{ \frac{2a\, s_c^2\, T_{nc}(\xi,\eta,0) - 2a\, y_{nc}^2\, T_{nc}(\xi,\eta,4)}{s_{nc}^2 \sin\beta_{nc}\sqrt{(2a)^2 + 4ay_{nc}}} \right\} \\
&+ \hat{\psi}_c \left\{ \frac{-s_c^2\, x_{nc} \sin\psi_c\, T_{nc}(\xi,\eta,2)}{s_{nc}^2 \sin\beta_{nc}\sqrt{(2a)^2 + 4ay_{nc}}} \right. \\
&\qquad \left. + \frac{(s_c\cos\psi_c - 2a)\, x_{nc}\, y_{nc} \sin\psi_c\, T_{nc}(\xi,\eta,4)}{s_{nc}^2 \sin\beta_{nc}\sqrt{(2a)^2 + 4ay_{nc}}} \right\} \qquad (494)
\end{aligned}$$

and

$$\begin{aligned}
\vec{\Psi}_u(\xi) &= \hat{s}_c \left\{ \frac{2a\, y_{nc} \sin\psi_c\, T_{nc}(\xi,\eta,2)}{s_{nc} \sin\beta_{nc}\sqrt{(2a)^2 + 4ay_{nc}}} \right\} + \hat{\beta}_c \left\{ \frac{s_c\, x_{nc} \sin\psi_c\, T_{nc}(\xi,\eta,2)}{s_{nc} \sin\beta_{nc}\sqrt{(2a)^2 + 4ay_{nc}}} \right\} \\
&+ \hat{\psi}_c \left\{ \frac{2a\, s_c\, T_{nc}(\xi,\eta,0) + 2a\, y_{nc} \cos\psi_c\, T_{nc}(\xi,\eta,2)}{s_{nc} \sin\beta_{nc}\sqrt{(2a)^2 + 4ay_{nc}}} \right\} ; \qquad (495)
\end{aligned}$$

respectively, in terms of the global polarization unit vectors $\widehat{s}_c$, $\widehat{\beta}_c$ and $\widehat{\psi}_c$ as shown in Figure 42. The argument of the caustic correction transition functions is

$$\xi = \left|\sqrt{2k[y_{nc}\cos\psi_c' - s_{nc} + s_c]}\right| e^{-j3\eta\pi/4} \tag{496}$$

from (368) and η given in (370) of Chapter 7. These vectors and the diffraction parameters derived earlier are now used in (410) through (414) of Chapter 7 along with the UTD half-plane diffraction coefficients to determine the diffracted field on the lit side of the caustic.

The diffracted field in the caustic shadow region can be computed using (450) through (454) of Chapter 7. The diffracted field parameters required in order to use this result have been derived previously in this chapter. The only quantity left is the argument of the caustic correction transition functions

$$\xi = \left|\sqrt{2k[y_{nc}\cos\psi_c' - s_{nc} + s_c]}\right| e^{-j\eta\pi/4} \tag{497}$$

from (421) and η given in (423) of Chapter 7. It is important to note that it is possible for $\{y_{nc}\cos\psi_c' - s_{nc} + s_c\}$ to be complex in the caustic shadow region. Although this case should be analyzed using uniform steepest descent techniques, it is treated here heuristically. The caustic correction transition functions are not critical when this occurs because it is usually in the deep caustic shadow region. Therefore, $|\, y_{nc}\cos\psi_c' - s_{nc} + s_c \,|$ can be used because it will produce a transition function argument that is piece-wise continuous in magnitude. The ramifications of this approximation will be discussed in the next subsection when these expressions are calculated numerically. There is no reason to transform the polarization vectors since those used in Chapter 7 are also used here. Therefore, the GO field and the diffracted field add to produce the total field.

1.2 Numerical Calculation of the Field Scattered by a Flat Plate with a Parabolic Edge

The numerical calculation of the field expressions derived in Subsection 1.1 confirms the uniformity of the CC-UTD. This also leads to some insight into the physical

phenomenology involved in this problem and the CC-UTD formulation. The CC-UTD formulation is compared to the classical UTD solution to illustrate their differences. This subsection is devoted to the numerical calculation of the total field in the presence of a flat plate with a parabolic edge.

Various components of the total field are plotted in this subsection in order to discuss the properties of the CC-UTD solution. The quantity to be plotted throughout this subsection for a $\widehat{\beta}_c'$ polarized incident plane wave is

$$E_\beta \text{ (dB)} = 20 \log_{10} \left| \widehat{\beta}_c \cdot \vec{E}(P) \right| \tag{498}$$

for the $\widehat{\beta}_c$ component of the field at the observation point. The CC-UTD does not produce any cross polarization for this incident wave polarization. This is due to the assumed symmetry of the edge, incidence direction and observation location. Also, $\vec{E}(P)$ is the component of the electric field being discussed. Next, the quantities to be plotted throughout this subsection for a $\widehat{\psi}_c'$ polarized incident plane wave are

$$E_s \text{ (dB)} = 20 \log_{10} \left| \widehat{s}_c \cdot \vec{E}(P) \right| \tag{499}$$

for the $\widehat{s}_c$ component and

$$E_\psi \text{ (dB)} = 20 \log_{10} \left| \widehat{\psi}_c \cdot \vec{E}(P) \right| \tag{500}$$

for the $\widehat{\psi}_c$ component of the field at the observation point. However, the CC-UTD does not produce a $\widehat{\beta}_c$ component for this incident wave polarization. This is due to the assumed symmetry of the edge, incidence direction and observation location.

The first case considered here consists of a flat plate with a parabolic edge having a focal length of $a = 3\lambda$, an observation distance of $s_c = 5\lambda$ and an incidence angle of $\psi_c' = 45^\circ$ as shown in Figure 40. The different components of the CC-UTD solution will first be plotted to illustrate some of the properties of the formulation. Only the $\mathcal{J}_o^s(P)$ will be separated into its different components since all of the remaining integrals will have the same characteristics.

For the sake of discussion, the central ray diffracted field is the first term in (402) of Chapter 7 when P is in the caustic lit region or the first term of (442) of Chapter 7

when P is in the caustic shadow region. These terms are labeled this way because they are the same except the caustic correction transition functions differ on the lit and shadow sides of the caustic. The non-central ray diffracted field is the sum of the last two terms in (402) of Chapter 7 in the caustic lit region. Finally, the curvature dependant central ray diffracted field is the second term in (442) of Chapter 7. Although this diffracted field has a similar form as the central ray diffracted field, it has a different curvature dependant diffraction coefficient and a different caustic correction transition function.

We now look at the central ray, curvature dependant central ray and non-central ray diffracted field components of $\mathcal{J}_o^s(P)$ as shown in Figure 43. As explained earlier, this is obtained by making the incident wave purely $\widehat{\beta}_c'$ polarized. Several interesting facts about the CC-UTD can be seen from this plot.

The Incident Shadow Boundary (ISB) is located at $\psi_c = \pi + \psi_c' = 225°$ and the Reflection Shadow Boundary (RSB) is located at $\psi_c = \pi - \psi_c' = 135°$ for a flat plate with a parabolic edge with a focal length of $a = 3\lambda$, an observation distance of $s_c = 5\lambda$ and an incidence angle of $\psi_c' = 45°$. The Caustic Boundaries (CB) occur when the amplitude spreading factor of the diffracted field expressions becomes singular. Therefore, equating $\rho^d(Q_c) + s_c$ to zero we find that

$$\cos\psi_{\text{CB}} = \left\{\frac{2a}{s_c} - \cos\psi_c'\right\} \tag{501}$$

are the locations of the CB's. The CB's are located at $\psi_{\text{CB}} = 60.47°, 299.53°$ for the dimensions chosen here. These values are shown in Figure 43. It is also easy to see how the solutions on the lit and shadow sides of the caustic differ. The central ray and curvature dependant central ray diffracted fields are each bounded in the caustic shadow region. In this region, the curvature dependant central ray diffracted field can be viewed as a correction to the central ray diffracted field. However, the central ray and non-central ray diffracted field contributions are each singular in the caustic lit region. The central ray diffracted field contribution has a singularity that opposes the singularity of the non-central ray diffracted field. These singularities cancel and

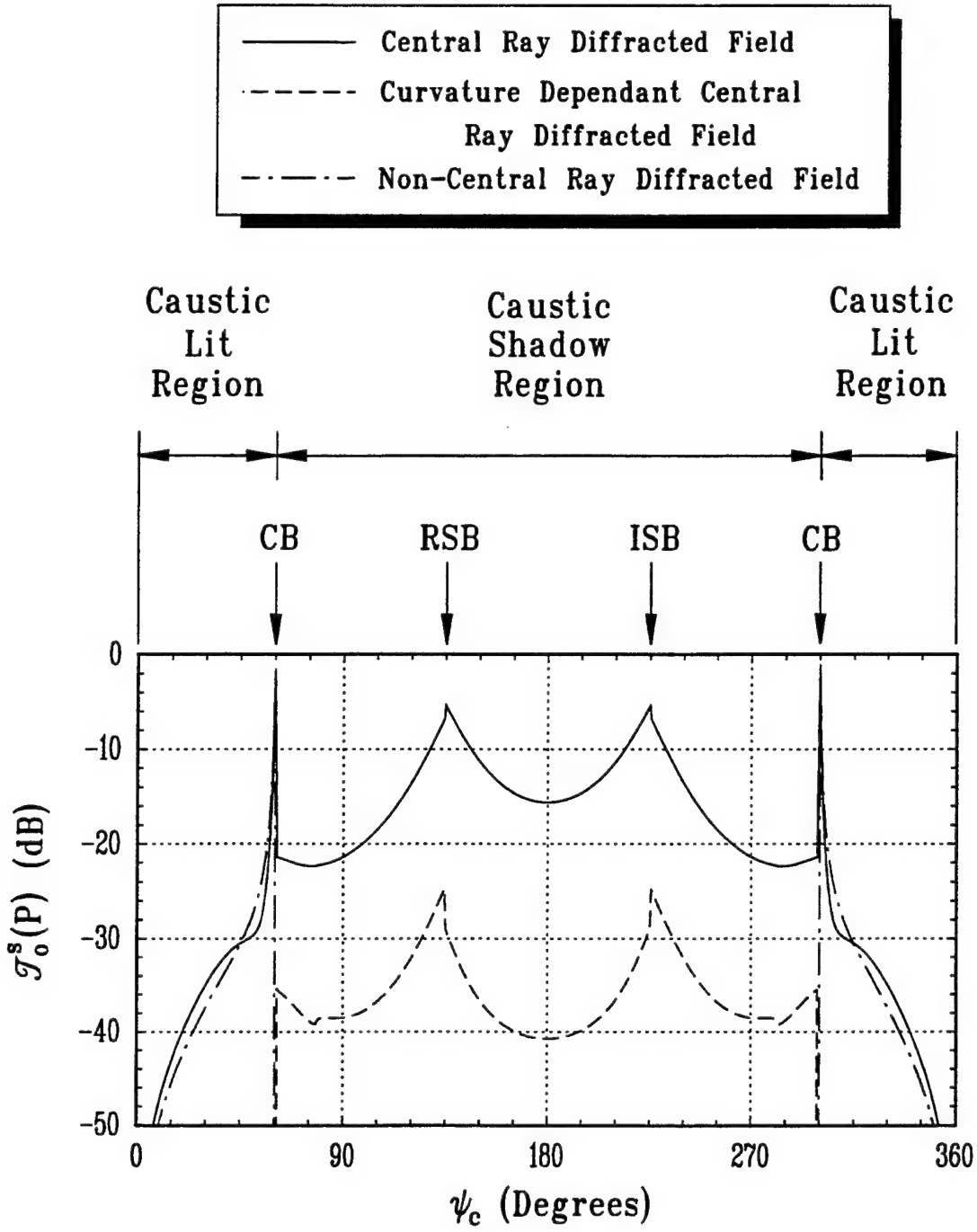

Figure 43: Diffracted field components of $\mathcal{J}_o^s(P)$ for a plate with a focal length of $a = 3\lambda$, an observation distance of $s_c = 5\lambda$ and an incidence angle of $\psi_c' = 45^o$.

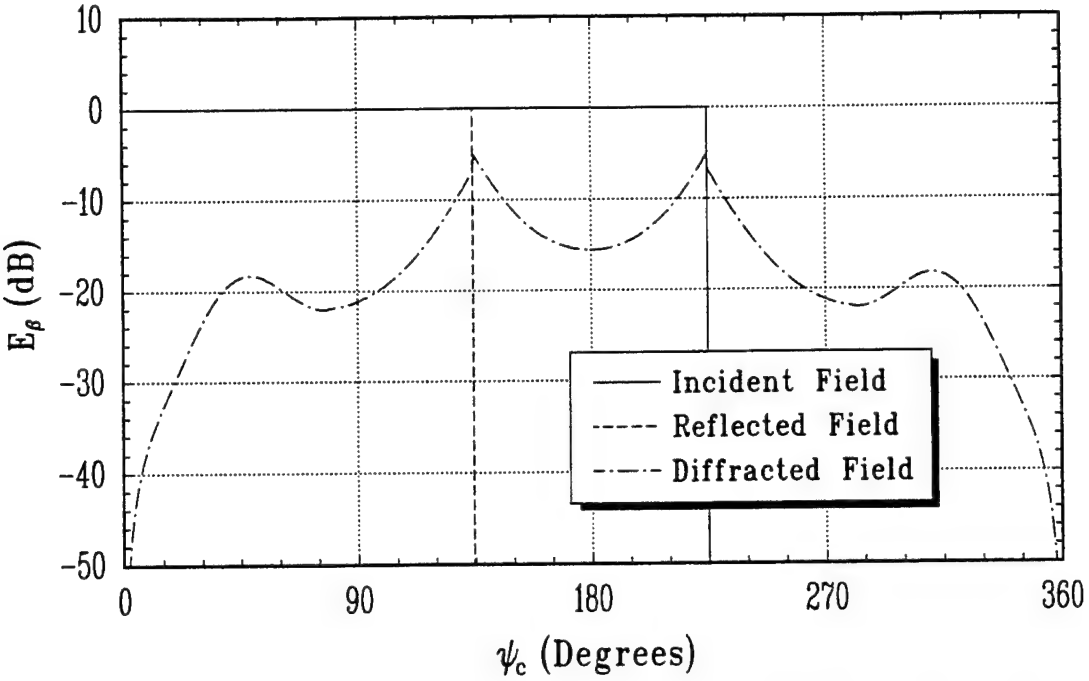

Figure 44: Field components in the $\widehat{\beta}_c$ direction for a plate with a focal length of $a = 3\lambda$, an observation distance of $s_c = 5\lambda$ and an incidence angle of $\psi_c' = 45°$.

the proper field is obtained in the caustic lit region when these two contributions are added to obtain the total diffracted field.

As discussed at the end of Subsection 1.1, $\{y_{nc}\cos\psi_c' - s_{nc} + s_c\}$ in the arguments of the caustic correction transition functions may become complex in the caustic shadow region. The angles for which this occurs are

$$\cos\psi_\xi = \left\{\frac{2a}{s_c} - 1\right\} \tag{502}$$

by making $s_c^2 - y_o^2 = 0$. These points are $\psi_\xi = 78.4630°$ and $281.5370°$ for this geometry and can be seen in Figure 43. It is seen from Figure 43 that this has a negligible effect for the central ray diffracted field but not for the curvature dependant central ray diffracted field. However, the sum of these two field components shows little effect from this anomaly. The field in the caustic shadow region is piece-wise continuous as discussed in the previous subsection.

We can now look at the incident, reflected and total diffracted fields for the $\widehat{\beta}_c$ component as shown in Figure 44. These quantities are obtained by making the

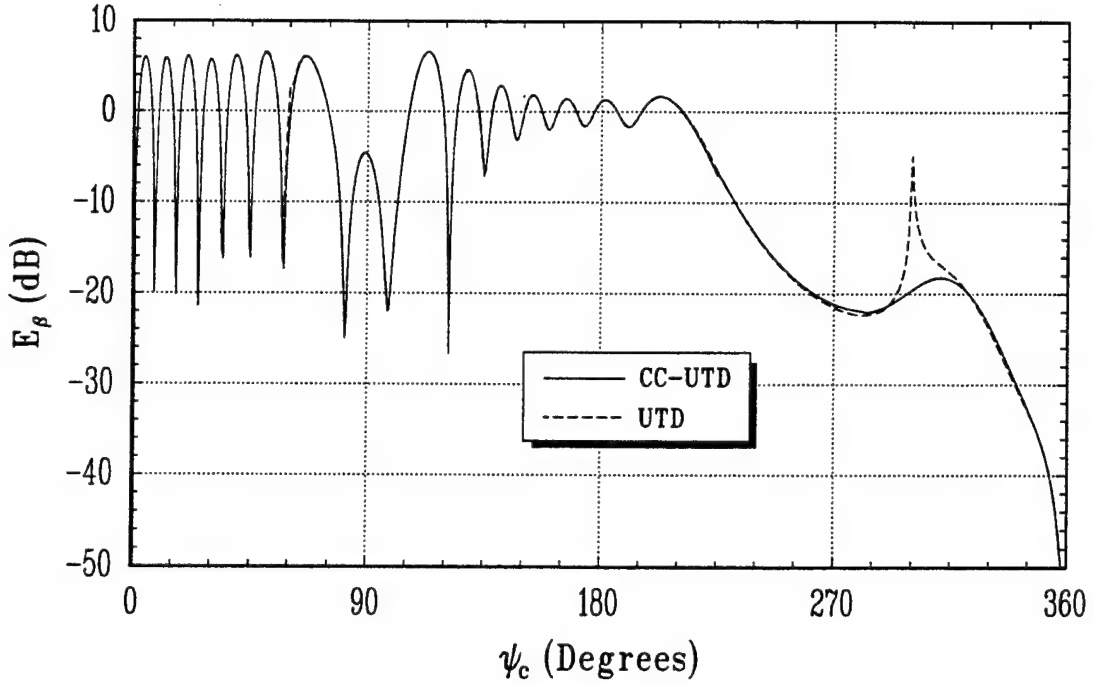

Figure 45: Total field comparison in the $\widehat{\beta}_c$ direction for a plate with a focal length of $a = 3\lambda$, an observation distance of $s_c = 5\lambda$ and an incidence angle of $\psi_c' = 45°$.

incident wave purely $\widehat{\beta}_c'$ polarized. This figure clearly shows that the diffracted field is not only bounded near the caustic, but it is also smooth and continuous. Therefore, the CC-UTD is uniform across the caustics of the diffracted field. It is also clear that the diffracted field retains discontinuities along the incident and reflection shadow boundaries. Also, as explained earlier, there is a negligible effect of the approximation used in the argument of the caustic correction transition functions on the shadow side of the caustic.

Finally, Figure 45 shows a comparison between the CC-UTD and UTD solutions. Adding the incident, reflected and diffracted fields; we see that the total field is smooth and continuous everywhere. This figure shows that the CC-UTD solution corrects for the caustics of the UTD solution. It also shows that the CC-UTD solution smoothly reduces to the UTD solution away from the caustics. This is one of the requirements of a uniform solution. It is clear that the CC-UTD solution retains the proper discontinuities along the incident and reflection shadow boundaries to compensate for the discontinuities of the GO fields.

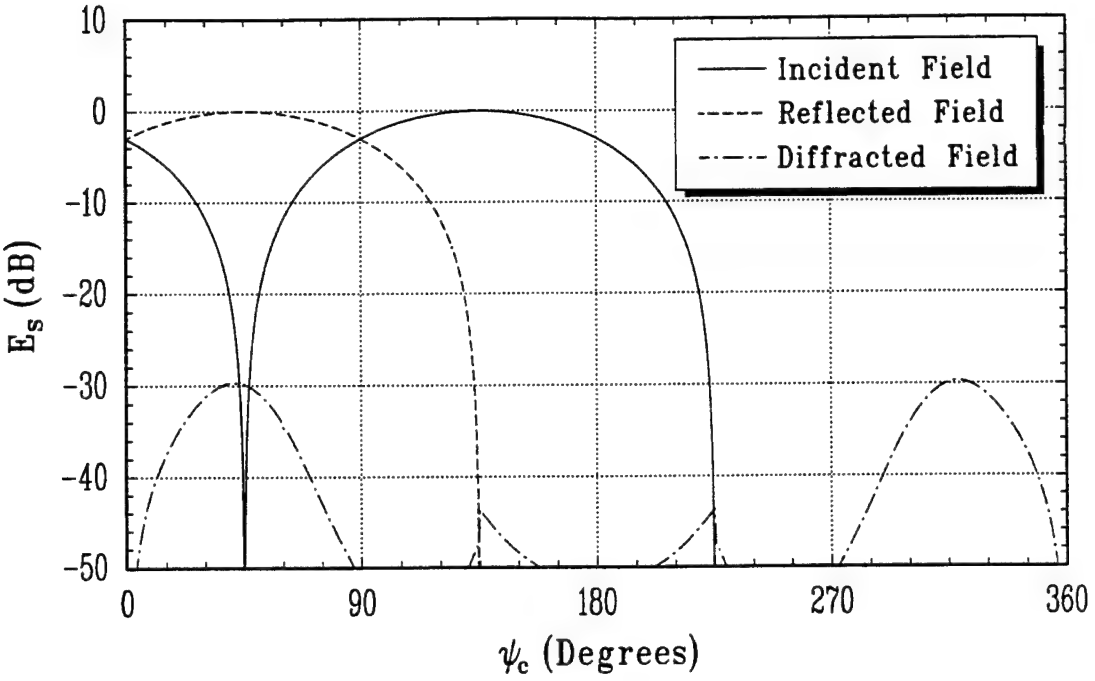

Figure 46: Field components in the $\hat{s}_c$ direction for a plate with a focal length of $a = 3\lambda$, an observation distance of $s_c = 5\lambda$ and an incidence angle of $\psi_c' = 45^o$.

We can now look at the incident, reflected and total diffracted fields for the $\hat{s}_c$ polarization as shown in Figure 46 and the $\hat{\psi}_c$ polarization as shown in Figure 47. These field quantities are obtained by making the incident wave purely $\hat{\psi}_c'$ polarized. These figures clearly show that the diffracted field is not only bounded near the caustic, but it is also smooth and continuous. Therefore, the CC-UTD is uniform across the caustics of the diffracted field. It is also clear that the diffracted field in the $\hat{\psi}_c$ direction retains discontinuities along the incident and reflection shadow boundaries as expected. As explained earlier, there is a negligible effect of the approximation used in the argument of the caustic correction transition functions on the shadow side of the caustic.

Finally, Figures 48 and 49 show a comparison between the CC-UTD and UTD solutions for the $\hat{s}_c$ and $\hat{\psi}_c$ components, respectively. Adding the incident, reflected and diffracted fields; we see that the total field is smooth and continuous everywhere. These figures show that the CC-UTD solution corrects for the caustics of the UTD solution. It also shows that the CC-UTD solution smoothly reduces to the UTD

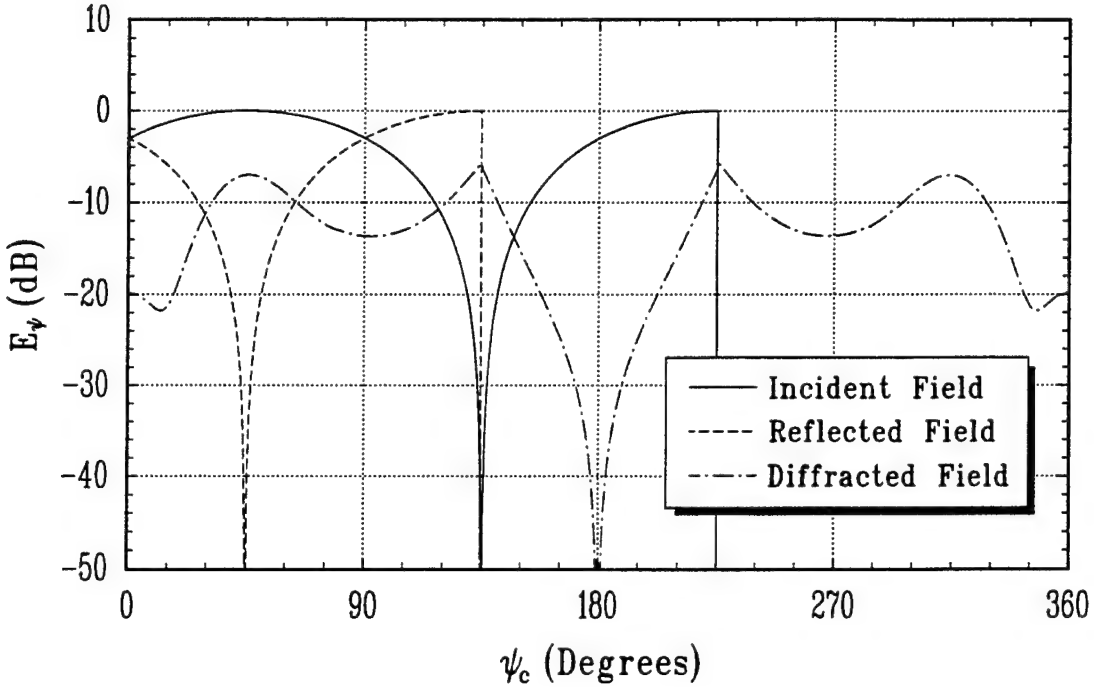

Figure 47: Field components in the $\widehat{\psi}_c$ direction for a plate with a focal length of $a = 3\lambda$, an observation distance of $s_c = 5\lambda$ and an incidence angle of $\psi_c' = 45°$.

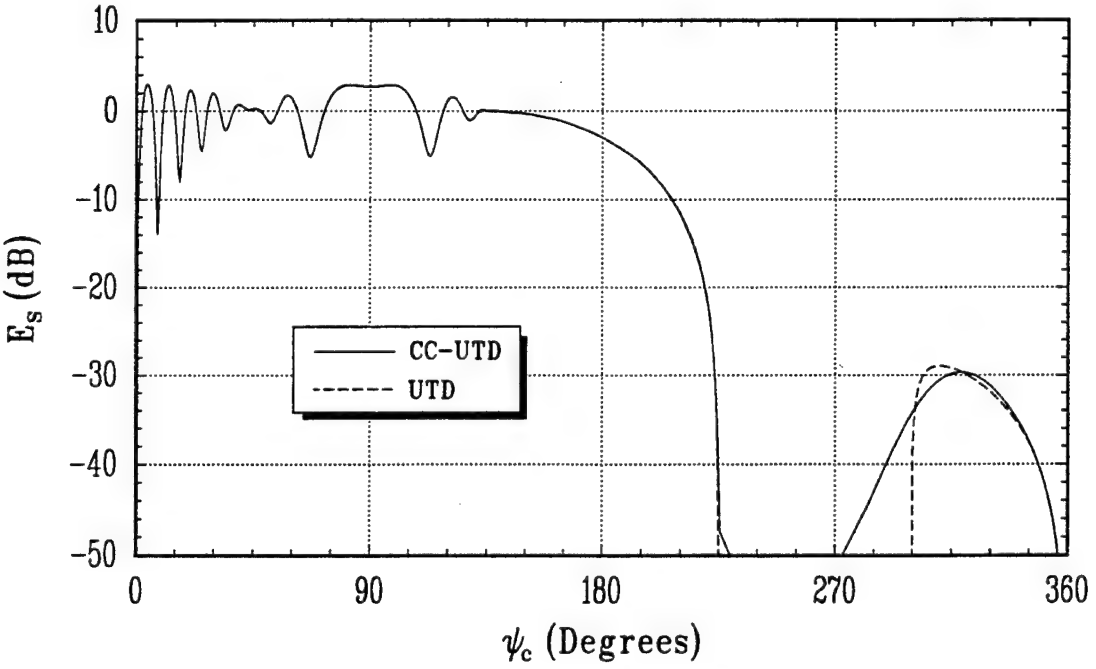

Figure 48: Total field comparison in the $\widehat{s}_c$ direction for a plate with a focal length of $a = 3\lambda$, an observation distance of $s_c = 5\lambda$ and an incidence angle of $\psi_c' = 45°$.

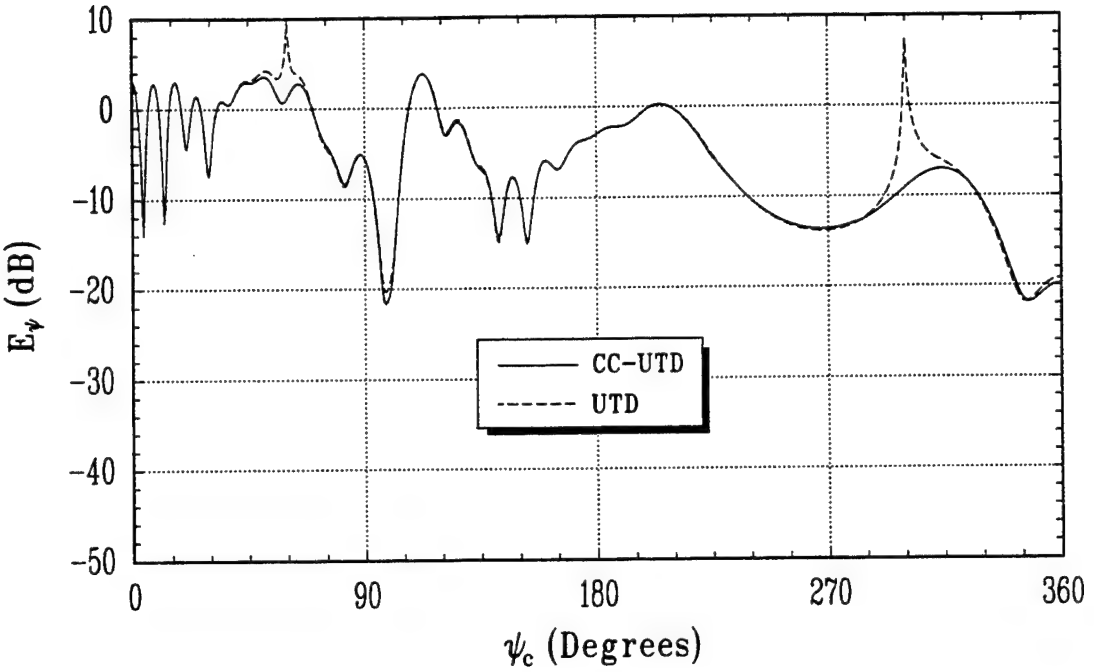

Figure 49: Total field comparison in the $\widehat{\psi}_c$ direction for a plate with a focal length of $a = 3\lambda$, an observation distance of $s_c = 5\lambda$ and an incidence angle of $\psi_c' = 45°$.

solution away from the caustics. This is one of the requirements of a uniform solution. Although these patterns are continuous everywhere, the $\widehat{s}_c$ component is discontinuous in slope along the incident and reflection shadow boundaries. This occurs because the slope diffraction terms where neglected in the asymptotic expansion of the ITD diffracted field of Chapter 4. This is generally a small effect that is usually neglected. This line of thinking is consistent with the UTD.

As another example, the total field is calculated for a plate with a focal length of $a = 4\lambda$, an observation distance of $s_c = 8\lambda$ and an incidence angle of $\psi_c' = 30°$. Figure 50 shows a comparison between the $\widehat{\beta}_c$ components of the CC-UTD and UTD solutions which is obtained by making the incident wave $\widehat{\beta}_c'$ polarized. We see that the total field is smooth and continuous everywhere. This figure shows that the CC-UTD solution corrects for the caustics of the UTD solution. It also shows that the CC-UTD solution smoothly reduces to the UTD solution away from the caustics. It is clear that the CC-UTD solution retains the proper discontinuities along the incident and reflection shadow boundaries to compensate for the discontinuities of the GO fields.

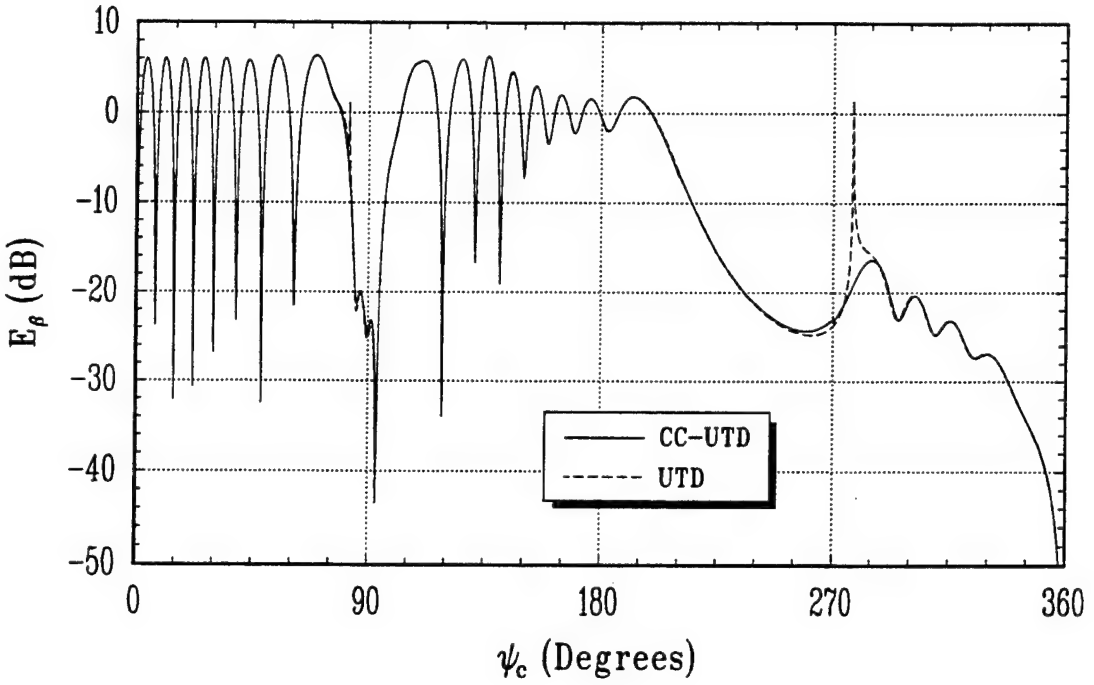

Figure 50: Total field comparison in the $\widehat{\beta}_c$ direction for a plate with a focal length of $a = 4\lambda$, an observation distance of $s_c = 8\lambda$ and an incidence angle of $\psi_c' = 30°$.

Figures 51 and 52 show a comparison between the CC-UTD and UTD solutions for the $\widehat{s}_c$ and $\widehat{\psi}_c$ components, respectively. These components are obtained by making the incident wave $\widehat{\psi}_c'$ polarized. These figures show that the CC-UTD solution corrects for the caustics of the UTD solution. It also shows that the CC-UTD solution smoothly reduces to the UTD solution away from the caustics. Although these patterns are continuous everywhere, the $\widehat{s}_c$ component is discontinuous in slope along the incident and reflection shadow boundaries. This occurs because the slope diffraction terms where neglected in the asymptotic expansion of the ITD diffracted field of Chapter 4. This is generally a small effect that is usually neglected. This line of thinking is consistent with the UTD.

2 Scattering by an Elliptic Disk

The other geometry to be studied in this chapter is the scattering by an elliptic disk. To conform to the assumptions of the derivation of the CC-UTD in Chapter 7 it is important that the incident plane wave impinges on the disk along one of its two

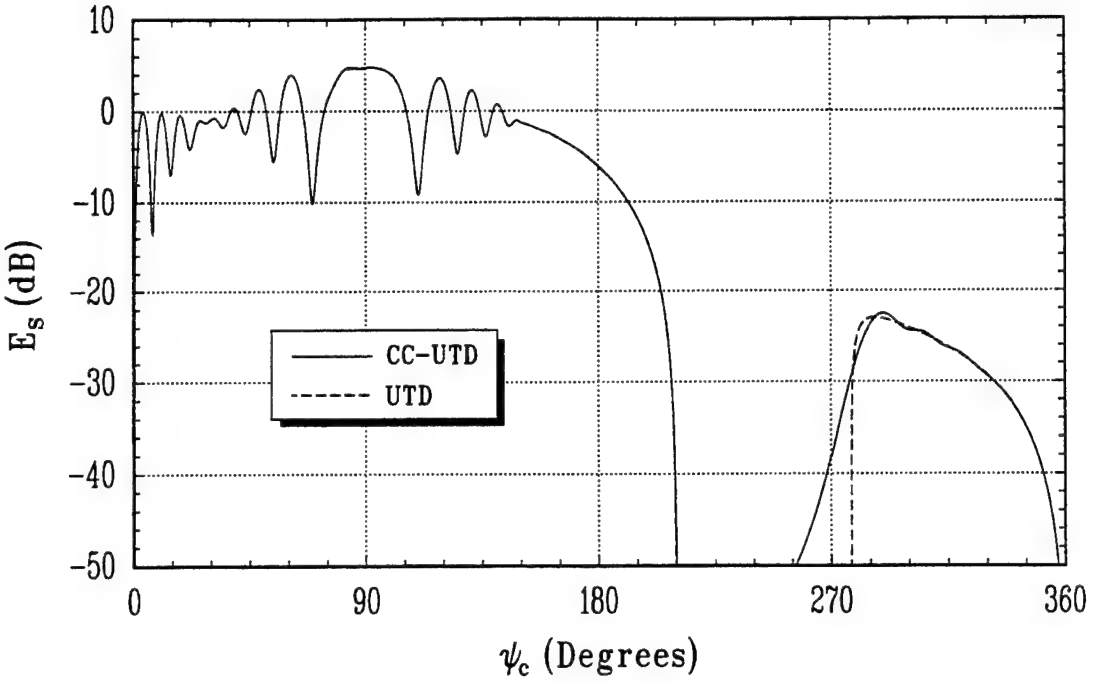

Figure 51: Total field comparison in the $\hat{s}_c$ direction for a plate with a focal length of $a = 4\lambda$, an observation distance of $s_c = 8\lambda$ and an incidence angle of $\psi_c' = 30°$.

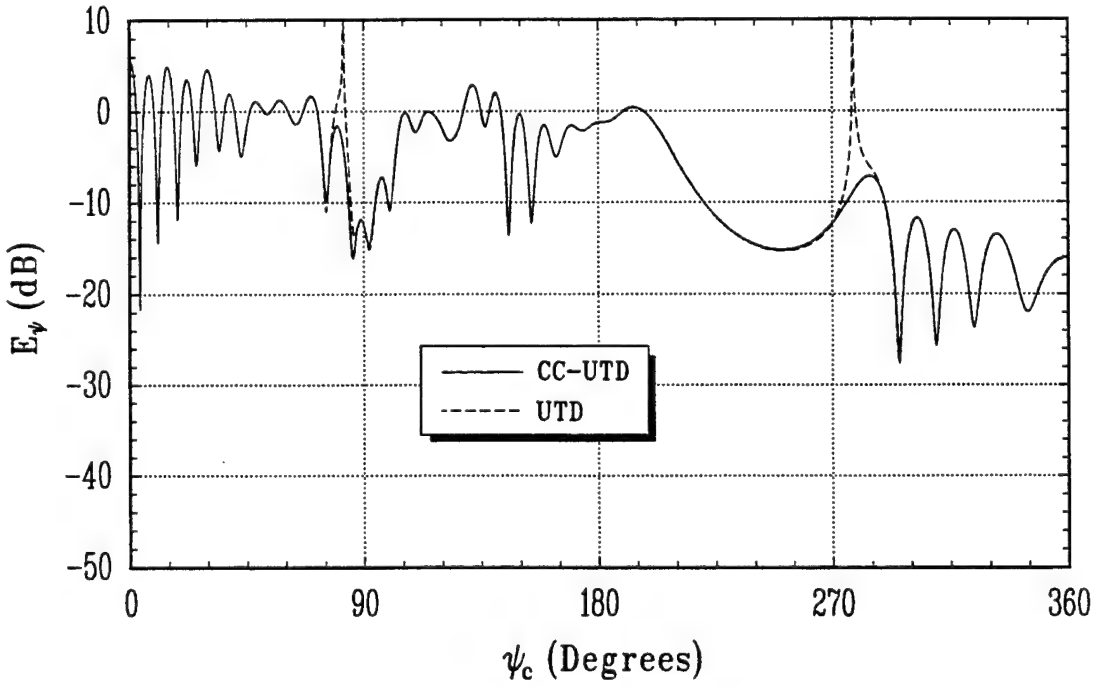

Figure 52: Total field comparison in the $\hat{\psi}_c$ direction for a plate with a focal length of $a = 4\lambda$, an observation distance of $s_c = 8\lambda$ and an incidence angle of $\psi_c' = 30°$.

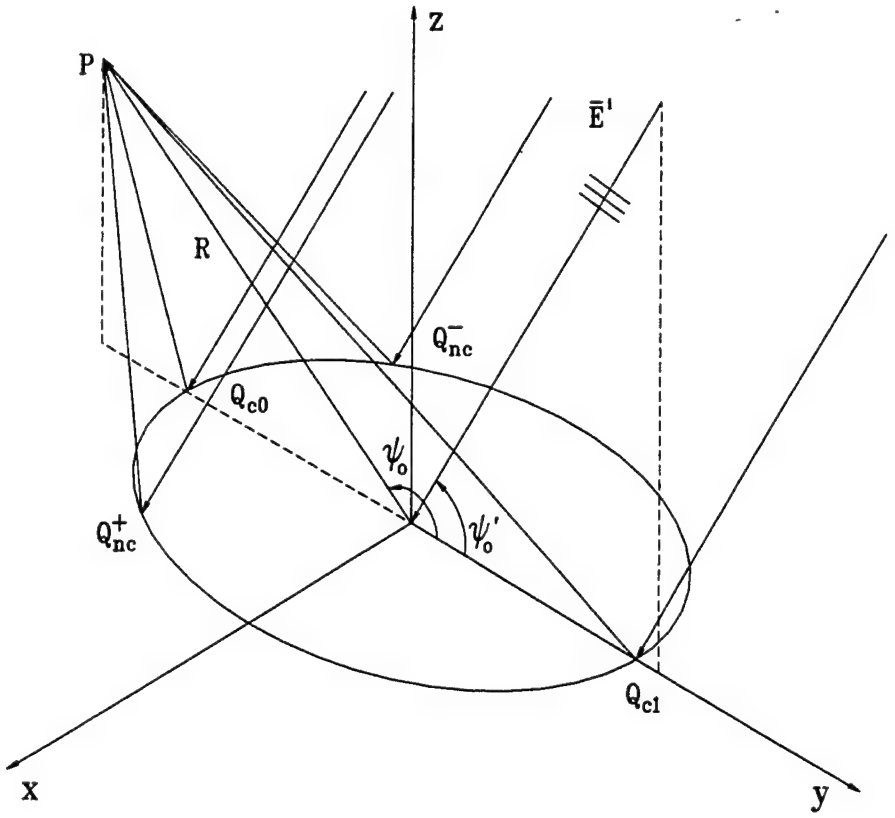

Figure 53: Geometry for the scattering by an elliptic disk.

axis of symmetry and the bistatic pattern must be taken in the plane of symmetry of the ellipse. This geometry is shown in Figure 53. This section consists of two parts. First, the parameters required for the CC-UTD and the UTD solutions are determined. Next, the scattered field is calculated using the CC-UTD and the UTD. These results are compared to a MM solution.

2.1 Elliptic Disk Scattered Field Parameters

It is important to accurately define the edge of the elliptic disk in order to determine the diffraction parameters required to use the CC-UTD and the UTD. An ellipse is defined by

$$\left(\frac{x_e}{a}\right)^2 + \left(\frac{y_e}{b}\right)^2 = 1 \tag{503}$$

where a and b are the principle axes of the ellipse in the x and y directions, respectively. The x and y coordinates of a point of the edge of the elliptic disk can now be related

by

$$x_e = a\cos v \tag{504a}$$

$$y_e = b\sin v \tag{504b}$$

where v is the only variable. The diffraction points on the edge of the disk can be determined by recalling that $\cos\beta = \cos\beta'$ at these points. In doing so, we find that $v_{c0} = \frac{3\pi}{2}$, $v_{c1} = \frac{\pi}{2}$ and

$$\sin v_{nc} = \begin{cases} \dfrac{-C_1}{2C_2} + \dfrac{\varepsilon_v}{2C_2}\left|\sqrt{C_1^2 - 4C_0C_2}\right| & ;\text{ if } C_1^2 - 4C_0C_2 > 0 \\ \dfrac{-C_1}{2C_2} - j\dfrac{\varepsilon_v}{2C_2}\left|\sqrt{C_1^2 - 4C_0C_2}\right| & ;\text{ if } C_1^2 - 4C_0C_2 < 0 \end{cases} \tag{505}$$

are the diffraction points as shown in Figure 53. Also, $\varepsilon_v = \pm 1$ is determined by enforcing the fact that $\cos\beta = \cos\beta'$ and the constants C_0, C_1 and C_2 are given by

$$C_0 = b^2\left[\left(a^2 + R^2\right)\cos^2\psi_o' - R^2\cos^2\psi_o\right] \tag{506a}$$

$$C_1 = 2bR\left(b^2\sin^2\psi_o' - a^2\right)\cos\psi_o \tag{506b}$$

$$C_2 = b^2\left(b^2 - a^2\right)\cos^2\psi_o' - \left(b^2 - a^2\right)^2 \tag{506c}$$

and are used to determine the locations of the non-central diffraction points. Now that the diffraction points have been found, it is easy to see that if $|\sin v_{nc}| < 1$ the observation point is in the caustic lit region and all other cases correspond to the caustic shadow region. Next, it is easily shown that

$$s_{c0} = \sqrt{R^2 + b^2 + 2bR\cos\psi_o} \tag{507}$$

and

$$s_{c1} = \sqrt{R^2 + b^2 - 2bR\cos\psi_o} \tag{508}$$

are the distances from the central diffraction points to the observation point and

$$s_{nc} = \varepsilon_s\left|\sqrt{(R^2 + a^2) - (2bR\cos\psi_o)\,\sin v_{nc} + (b^2 - a^2)\,\sin^2 v_{nc}}\right| \tag{509}$$

with

$$\varepsilon_s = \begin{cases} +1 & ;\text{ if } |\sin v_{nc}| < 1 \\ -j & ;\text{ otherwise} \end{cases} \tag{510}$$

is the distances from the non-central diffraction points to the observation point. The curvature at any point on the edge of the disk is found to be

$$\begin{aligned} \kappa_g(Q') &= \frac{a^4 b}{\left[a^4 + (b^2 - a^2)\, x_e^2\right]^{3/2}} \\ &= \frac{ab}{\left[(a\sin v)^2 + (b\cos v)^2\right]^{3/2}} \end{aligned} \tag{511}$$

from (470). Evaluating (511) at Q_{c0}, Q_{c1} and Q_{nc} we obtain

$$\kappa_g(Q_{c0}) = \kappa_g(Q_{c1}) = \frac{b}{a^2} \tag{512}$$

and

$$\kappa_g(Q_{nc}) = \frac{ab}{\left[b^2 + (a^2 - b^2)\sin^2 v_{nc}\right]^{3/2}}, \tag{513}$$

respectively. Also, differentiating (511) four times with respect to x_e, using (758) and (763) of Appendix D to convert the derivatives and evaluating them at Q_{c0} and Q_{c1} we get

$$\kappa_g^{\mathrm{II}}(Q_{c0}) = \kappa_g^{\mathrm{II}}(Q_{c1}) = \frac{3b\,(a^2 - b^2)}{a^6} \tag{514}$$

and

$$\kappa_g^{\mathrm{IV}}(Q_{c0}) = \kappa_g^{\mathrm{IV}}(Q_{c1}) = \frac{45b\,(a^2 - b^2)^2 + 12b^3\,(a^2 - b^2)}{a^{10}} \tag{515}$$

as the second and fourth derivatives of the curvature with respect to arc length. Using the fact that $\beta = \beta'$ at the diffraction points,

$$\beta_{c0} = \beta_{c1} = \frac{\pi}{2} \tag{516}$$

and

$$\sin\beta_{nc} = \sqrt{\frac{(b\sin\psi_o')^2 + \left(a^2 - b^2\sin^2\psi_o'\right)\sin^2 v_{nc}}{b^2 + (a^2 - b^2)\sin^2 v_{nc}}} \tag{517}$$

are the oblique incidence angles at the diffraction points. The incident angles ψ_{c0}' and ψ_{c1}' are

$$\psi_{c0}' = \psi_o' \tag{518}$$

and

$$\psi_{c1}' = \begin{cases} \pi - \psi_o' & ;\ \text{if } \psi_o' < \pi \\ 3\pi - \psi_o' & ;\ \text{if } \psi_o' > \pi \end{cases}; \tag{519}$$

respectively, at the central diffraction points and the incident angle ψ'_{nc} is determined using

$$\cos\psi'_{nc} = \frac{-a\cos\psi'_o \sin v_{nc}}{\sin\beta_{nc}\sqrt{b^2+(a^2-b^2)\sin^2 v_{nc}}} \tag{520}$$

at the non-central diffraction points. The diffraction angles ψ_{c0} and ψ_{c1} are found using

$$\cos\psi_{c0} = \frac{b+R\cos\psi_o}{s_{c0}} \tag{521}$$

and

$$\cos\psi_{c1} = \frac{b-R\cos\psi_o}{s_{c1}}\ ; \tag{522}$$

respectively, at the central diffraction points and the incident angle ψ_{nc} is found using

$$\cos\psi_{nc} = \frac{ab - aR\cos\psi_o \sin v_{nc}}{s_{nc}\sin\beta_{nc}\sqrt{b^2+(a^2-b^2)\sin^2 v_{nc}}} \tag{523}$$

at the non-central diffraction points. The caustic distances can now be determined using (10) of Chapter 2 and are given by

$$\rho^d(Q_{c0}) = \frac{-a^2 s_{c0}}{b\left(R\cos\psi_o + s_{c0}\cos\psi'_o + b\right)} \tag{524}$$

and

$$\rho^d(Q_{c1}) = \frac{a^2 s_{c1}}{b\left(R\cos\psi_o + s_{c1}\cos\psi'_o - b\right)} \tag{525}$$

at the central diffraction points and

$$\rho^d(Q_{nc}) = \frac{\left[b^2+(a^2-b^2)\sin^2 v_{nc}\right]^2 s_{nc}\sin^2\beta_{nc}}{a^2 b\left(R\sin v_{nc}\cos\psi_o + s_{nc}\sin v_{nc}\cos\psi'_o - b\right)} \tag{526}$$

at the non-central diffraction points. Finally, it is necessary to determine the Geometrical Optics (GO) field and the incident field at each of the diffraction points. The incident field at the observation point is

$$\begin{aligned}\vec{E}^i(P) &= \left\{\hat{\beta}'_o E^i_{\beta_o} + \hat{\psi}'_o E^i_{\psi_o}\right\} e^{jkR\cos(\psi_o-\psi'_o)} \\ &\quad \times\left\{\mathrm{U}\left[\tilde{\psi}_1-\psi_o\right] + \mathrm{U}\left[\psi_o-\tilde{\psi}_2\right]\right\}\end{aligned} \tag{527}$$

which is determined using classical GO techniques and

$$\tilde{\psi}_1 = \pi + \psi'_o - \sin^{-1}\left(\frac{b}{R}\sin\psi'_o\right) \tag{528}$$

$$\tilde{\psi}_2 = \pi + \psi'_o + \sin^{-1}\left(\frac{b}{R}\sin\psi'_o\right) \tag{529}$$

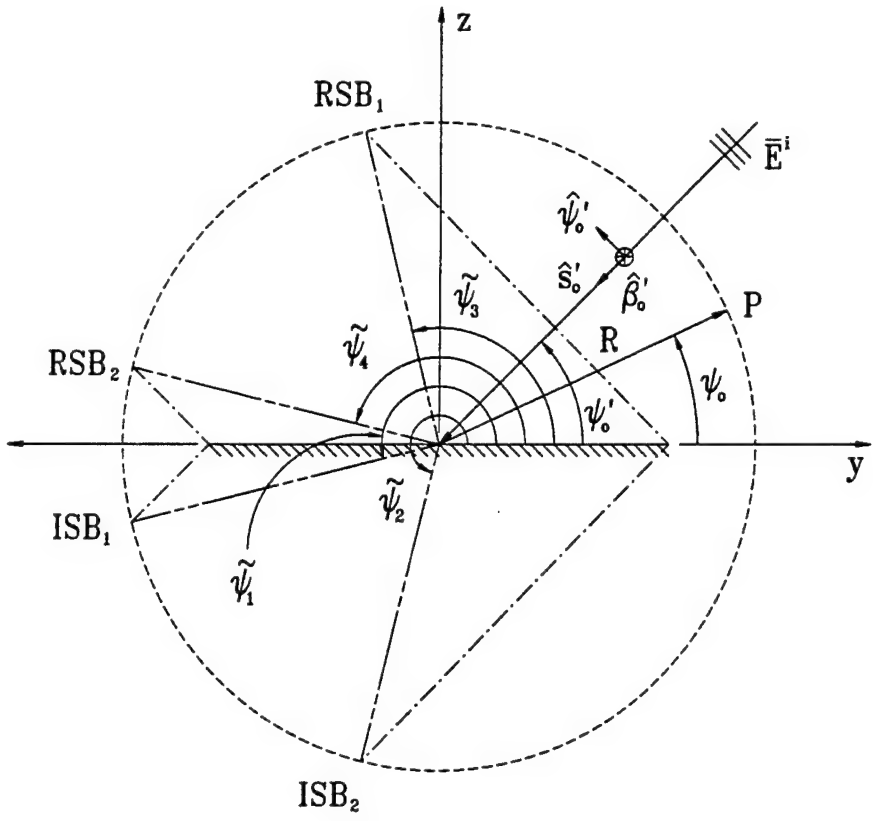

Figure 54: Incident and reflection shadow boundaries of an elliptic disk.

are the angles corresponding to the two incident shadow boundaries as shown in Figure 54. The incident wave polarization vectors $\widehat{\beta}'_o$ and $\widehat{\psi}'_o$ must be transformed into the global polarization unit vectors $\widehat{s}_o$, $\widehat{\beta}_o$ and $\widehat{\psi}_o$ as shown in Figure 55. Using the coordinate transformation

$$\widehat{\beta}'_o = -\widehat{\beta}_o \tag{530}$$

$$\widehat{\psi}'_o = \widehat{s}_o \sin(\psi_o - \psi'_o) + \widehat{\psi}_o \cos(\psi_o - \psi'_o) \tag{531}$$

it is found that

$$\begin{aligned} \vec{E}^i(P) = & \left\{ \widehat{s}_o E^i_{\psi_o} \sin(\psi_o - \psi'_o) - \widehat{\beta}_o E^i_{\beta_o} + \widehat{\psi}_o E^i_{\psi_o} \cos(\psi_o - \psi'_o) \right\} \\ & \times e^{jkR\cos(\psi_o - \psi'_o)} \left\{ \mathrm{U}\left[\tilde{\psi}_1 - \psi_o\right] + \mathrm{U}\left[\psi_o - \tilde{\psi}_2\right] \right\} \end{aligned} \tag{532}$$

is the incident field at the observation point. Next, the reflected field at the observation point is

$$\vec{E}^r(P) = \left\{ \widehat{\beta}_r E^i_{\beta_o} R_s + \widehat{\psi}_r E^i_{\psi_o} R_h \right\} e^{jkR\cos(\psi_o + \psi'_o)} \mathrm{U}\left[\psi_o - \tilde{\psi}_3\right] \mathrm{U}\left[\tilde{\psi}_4 - \psi_o\right] \tag{533}$$

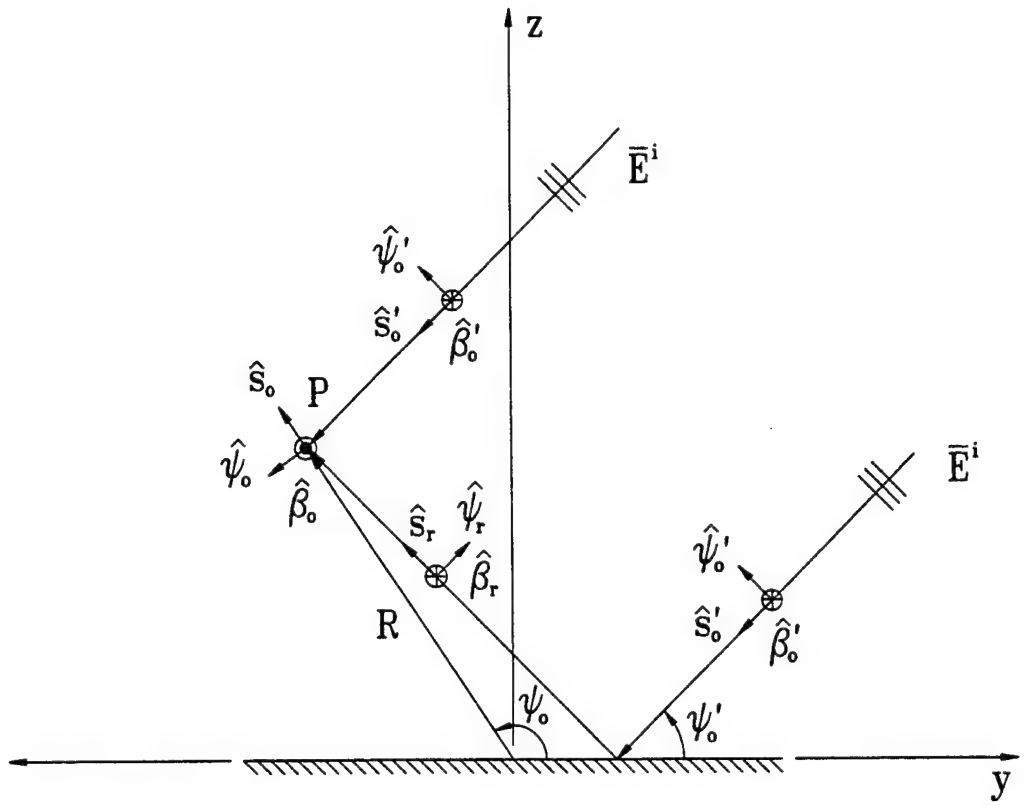

Figure 55: Polarization unit vector definition for the incident and reflected fields in the presence of an elliptic disk.

where the reflection coefficients are $R_{s,h} = \mp 1$ and

$$\tilde{\psi}_3 = \pi - \psi_o' - \sin^{-1}\left(\frac{b}{R}\sin\psi_o'\right) \tag{534}$$

$$\tilde{\psi}_4 = \pi - \psi_o' + \sin^{-1}\left(\frac{b}{R}\sin\psi_o'\right) \tag{535}$$

are the angles corresponding to the two reflection shadow boundaries as shown in Figure 54. The reflected wave polarization vectors $\hat{\beta}_r$ and $\hat{\psi}_r$ must be transformed into the global polarization unit vectors $\hat{s}_o$, $\hat{\beta}_o$ and $\hat{\psi}_o$ as shown in Figure 55. Using the coordinate transformation

$$\hat{\beta}_r = -\hat{\beta}_o \tag{536}$$

$$\hat{\psi}_r = \hat{s}_o \sin(\psi_o + \psi_o') + \hat{\psi}_o \cos(\psi_o + \psi_o') \tag{537}$$

it is found that

$$\begin{aligned}\vec{E}^r(P) = {} & \left\{\hat{s}_o\, E^i_{\psi_o} \sin(\psi_o + \psi_o') + \hat{\beta}_o\, E^i_{\beta_o} + \hat{\psi}_o\, E^i_{\psi_o} \cos(\psi_o + \psi_o')\right\} \\ & \times e^{jkR\cos(\psi_o + \psi_o')}\, \mathrm{U}\left[\psi_o - \tilde{\psi}_3\right] \mathrm{U}\left[\tilde{\psi}_4 - \psi_o\right]\end{aligned} \tag{538}$$

is the reflected field at the observation point. The GO field at the observation point is the sum of the incident field and the reflected field at the observation point. The diffracted field can now be determined using the diffraction parameters found previously.

The incident field at each diffraction point and polarization vectors are required to determine the diffracted field near the caustic. The incident field at the central diffraction points are

$$\vec{E}^i(Q_{c0}) = \left\{\hat{\beta}'_o\, E^i_{\beta_o} + \hat{\psi}'_o\, E^i_{\psi_o}\right\} e^{-jkb\cos\psi_o'} \tag{539}$$

at Q_{c0} and

$$\vec{E}^i(Q_{c1}) = \left\{\hat{\beta}'_o\, E^i_{\beta_o} + \hat{\psi}'_o\, E^i_{\psi_o}\right\} e^{jkb\cos\psi_o'} \tag{540}$$

at Q_{c1}. The incident wave polarization unit vectors at the two central diffraction points are $\hat{\beta}'_{c0} = \hat{\beta}'_o$ and $\hat{\psi}'_{c0} = \hat{\psi}'_o$ at Q_{c0}, and $\hat{\beta}'_{c1} = -\hat{\beta}'_o$ and $\hat{\psi}'_{c1} = -\hat{\psi}'_o$ at Q_{c1}. These polarization unit vectors are shown in Figure 56. Also, the diffracted field

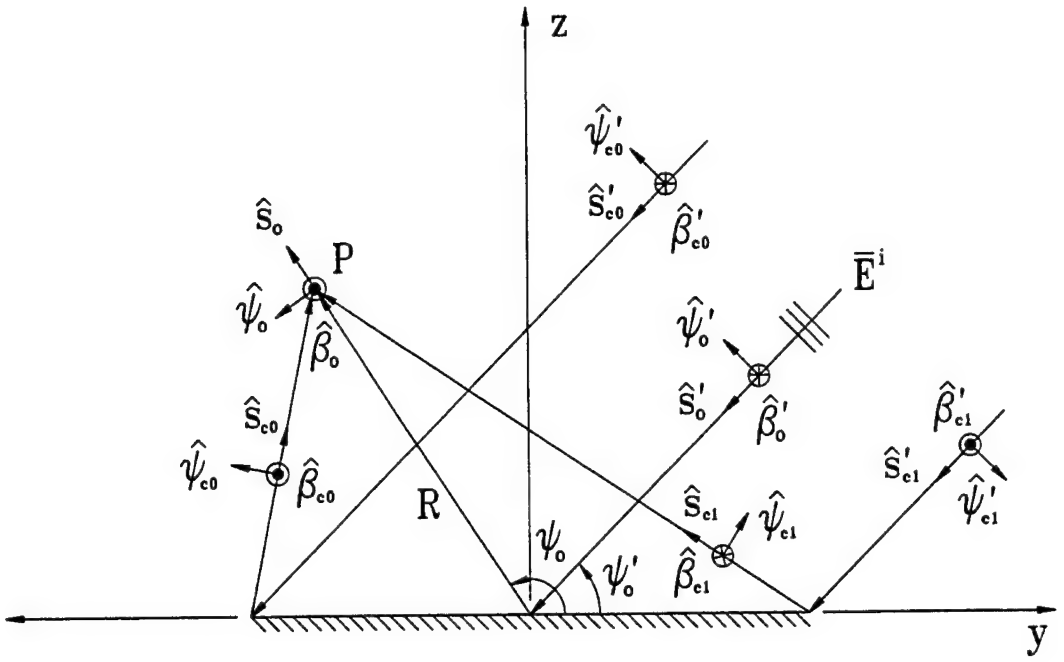

Figure 56: Polarization unit vector definition for the fields diffracted by an elliptic disk.

polarization unit vectors are transformed to the global polarization unit vectors $\hat{s}_o$, $\hat{\beta}_o$ and $\hat{\psi}_o$ using

$$\hat{s}_{c0} = \hat{s}_o \cos(\psi_{c0} - \psi_o) + \hat{\psi}_o \sin(\psi_{c0} - \psi_o) \quad (541)$$

$$\hat{\beta}_{c0} = \hat{\beta}_o \quad (542)$$

$$\hat{\psi}_{c0} = -\hat{s}_o \sin(\psi_{c0} - \psi_o) + \hat{\psi}_o \cos(\psi_{c0} - \psi_o) \quad (543)$$

for the field diffracted from Q_{c0} and

$$\hat{s}_{c1} = -\hat{s}_o \cos(\psi_{c1} + \psi_o) + \hat{\psi}_o \sin(\psi_{c1} + \psi_o) \quad (544)$$

$$\hat{\beta}_{c1} = -\hat{\beta}_o \quad (545)$$

$$\hat{\psi}_{c1} = \hat{s}_o \sin(\psi_{c1} + \psi_o) + \hat{\psi}_o \cos(\psi_{c1} + \psi_o) \quad (546)$$

for the field diffracted from Q_{c1}. These polarization unit vectors are shown in Figure 56. These vectors can be used in conjunction with the diffracted field parameters derived earlier in this subsection to obtain the expressions for the field diffracted from the central diffraction points. The only quantities remaining in these expressions are

the caustic correction transition functions. The argument of the caustic correction transition functions of the field diffracted from Q_{c0} are

$$\xi_0 = \left| \sqrt{2k \left[(\sin v_{nc} + 1)\, b \cos \psi_o' - s_{nc} + s_{c0} \right]} \right| e^{-j3\eta_0 \pi/4} \tag{547}$$

on the lit side of the caustic and

$$\xi_0 = \left| \sqrt{2k \left[(\sin v_{nc} + 1)\, b \cos \psi_o' - s_{nc} + s_{c0} \right]} \right| e^{-j\eta_0 \pi/4} \tag{548}$$

on the shadow side of the caustic where

$$\eta_0 = -\operatorname{sgn} \left\{ \frac{\rho^d(Q_{c0})}{s_{c0} \left[\rho^d(Q_{c0}) + s_{c0} \right]} \right\} . \tag{549}$$

The argument of the caustic correction transition functions of the field diffracted from Q_{c1} are

$$\xi_1 = \left| \sqrt{2k \left[(\sin v_{nc} - 1)\, b \cos \psi_o' - s_{nc} + s_{c1} \right]} \right| e^{-j3\eta_1 \pi/4} \tag{550}$$

on the lit side of the caustic and

$$\xi_1 = \left| \sqrt{2k \left[(\sin v_{nc} - 1)\, b \cos \psi_o' - s_{nc} + s_{c1} \right]} \right| e^{-j\eta_1 \pi/4} \tag{551}$$

on the shadow side of the caustic where

$$\eta_1 = -\operatorname{sgn} \left\{ \frac{\rho^d(Q_{c1})}{s_{c1} \left[\rho^d(Q_{c1}) + s_{c1} \right]} \right\} . \tag{552}$$

The expressions derived in Chapter 7 can now be used to determine the field diffracted by the two central diffraction points.

The field diffracted by the two non-central diffraction points must be determined. The incident field at the non-central diffraction points

$$\vec{E}^i(Q_{nc}) = \left\{ \hat{\beta}'_o E^i_{\beta_o} + \hat{\psi}'_o E^i_{\psi_o} \right\} e^{jkb \sin v_{nc} \cos \psi_o'} \tag{553}$$

along with the incident wave polarization unit vectors

$$\hat{\beta}' = \frac{\hat{\beta}'_o (-a \sin v_{nc}) + \hat{\psi}'_o (b \sin \psi_o' \cos v_{nc})}{\sin \beta_{nc} \sqrt{b^2 + (a^2 - b^2) \sin^2 v_{nc}}} \tag{554}$$

and

$$\hat{\psi}' = \frac{\hat{\beta}'_o (-b \sin \psi_o' \cos v_{nc}) + \hat{\psi}'_o (-a \sin v_{nc})}{\sin \beta_{nc} \sqrt{b^2 + (a^2 - b^2) \sin^2 v_{nc}}} \tag{555}$$

are necessary in determining the field diffracted by the non-central diffraction points. Finally, it is necessary to determine the uniform polarization vectors $\vec{\mathbf{B}}_u(\xi)$ and $\vec{\Psi}_u(\xi)$ as given by (415) and (416) of Chapter 7, respectively. Since the non-central diffraction points can coalesce to either Q_{c0} or Q_{c1}, we must refer these vectors to the appropriate point. First, if $-1 < \sin v_{nc} < 0$ then the non-central diffraction points are closer to Q_{c0}. Therefore, referring $\vec{\mathbf{B}}_u(\xi)$ and $\vec{\Psi}_u(\xi)$ to Q_{c0} we obtain

$$\begin{aligned}
\vec{\mathbf{B}}_u(\xi) &= \widehat{s}_{c0}\left\{\frac{-s_{c0}\,a^2\sin v_{nc}\cos v_{nc}\,T_{nc}(\xi_0,\eta_0,2)}{s_{nc}^2\sin\beta_{nc}\sqrt{b^2+(a^2-b^2)\sin^2 v_{nc}}}\right. \\
&+ \left.\frac{b\left\{a^2\cos\psi_{c0}+s_{c0}b\sin^2\psi_{c0}\right\}\cos v_{nc}\,(\sin v_{nc}+1)\,T_{nc}(\xi_0,\eta_0,4)}{s_{nc}^2\sin\beta_{nc}\sqrt{b^2+(a^2-b^2)\sin^2 v_{nc}}}\right\} \\
&+ \widehat{\beta}_{c0}\left\{\frac{-s_{c0}^2\,a\sin v_{nc}\,T_{nc}(\xi_0,\eta_0,0)}{s_{nc}^2\sin\beta_{nc}\sqrt{b^2+(a^2-b^2)\sin^2 v_{nc}}}\right. \\
&+ \left.\frac{ab\left\{s_{c0}\cos\psi_{c0}-b\right\}(\sin v_{nc}+1)^2\,T_{nc}(\xi_0,\eta_0,4)}{s_{nc}^2\sin\beta_{nc}\sqrt{b^2+(a^2-b^2)\sin^2 v_{nc}}}\right\} \\
&+ \widehat{\psi}_{c0}\left\{\frac{-s_{c0}^2\,b\sin\psi_{c0}\cos v_{nc}\,T_{nc}(\xi_0,\eta_0,2)}{s_{nc}^2\sin\beta_{nc}\sqrt{b^2+(a^2-b^2)\sin^2 v_{nc}}}\right. \\
&+ \left.\frac{b\sin\psi_{c0}\left\{s_{c0}b\cos\psi_{c0}-a^2\right\}\cos v_{nc}\,(\sin v_{nc}+1)\,T_{nc}(\xi_0,\eta_0,4)}{s_{nc}^2\sin\beta_{nc}\sqrt{b^2+(a^2-b^2)\sin^2 v_{nc}}}\right\} \qquad (556)
\end{aligned}$$

and

$$\begin{aligned}
\vec{\Psi}_u(\xi) &= \widehat{s}_{c0}\left\{\frac{ab\sin\psi_{c0}\,(\sin v_{nc}+1)\,T_{nc}(\xi_0,\eta_0,2)}{s_{nc}\sin\beta_{nc}\sqrt{b^2+(a^2-b^2)\sin^2 v_{nc}}}\right\} \\
&+ \widehat{\beta}_{c0}\left\{\frac{s_{c0}\,b\sin\psi_{c0}\cos v_{nc}\,T_{nc}(\xi_0,\eta_0,2)}{s_{nc}\sin\beta_{nc}\sqrt{b^2+(a^2-b^2)\sin^2 v_{nc}}}\right\} \\
&+ \widehat{\psi}_{c0}\left\{\frac{-s_{c0}\,a\sin v_{nc}\,T_{nc}(\xi_0,\eta_0,0)}{s_{nc}\sin\beta_{nc}\sqrt{b^2+(a^2-b^2)\sin^2 v_{nc}}}\right. \\
&\qquad \left.+\frac{ab\cos\psi_{c0}\,(\sin v_{nc}+1)\,T_{nc}(\xi_0,\eta_0,2)}{s_{nc}\sin\beta_{nc}\sqrt{b^2+(a^2-b^2)\sin^2 v_{nc}}}\right\}, \qquad (557)
\end{aligned}$$

respectively. The coordinate transformation in (541) through (543) is then used to transform this expression into the global coordinates $\widehat{s}_o$, $\widehat{\beta}_o$ and $\widehat{\psi}_o$. Next, if $0 < \sin v_{nc} < 1$ then the non-central diffraction points are closer to Q_{c1}. Therefore,

referring $\vec{\mathbf{B}}_u(\xi)$ and $\vec{\Psi}_u(\xi)$ to Q_{c1} we obtain

$$\begin{aligned}
\vec{\mathbf{B}}_u(\xi) &= \widehat{s}_{c1}\left\{\frac{-s_{c1}\,a^2\sin v_{nc}\cos v_{nc}\,T_{nc}(\xi_1,\eta_1,2)}{s_{nc}^2\sin\beta_{nc}\sqrt{b^2+(a^2-b^2)\sin^2 v_{nc}}}\right.\\
&+\left.\frac{b\left\{a^2\cos\psi_{c1}+s_{c1}b\sin^2\psi_{c1}\right\}\cos v_{nc}\,(\sin v_{nc}-1)\,T_{nc}(\xi_1,\eta_1,4)}{s_{nc}^2\sin\beta_{nc}\sqrt{b^2+(a^2-b^2)\sin^2 v_{nc}}}\right\}\\
&+\widehat{\beta}_{c1}\left\{\frac{s_{c1}^2\,a\sin v_{nc}\,T_{nc}(\xi_1,\eta_1,0)}{s_{nc}^2\sin\beta_{nc}\sqrt{b^2+(a^2-b^2)\sin^2 v_{nc}}}\right.\\
&+\left.\frac{ab\left\{s_{c1}\cos\psi_{c1}-b\right\}(\sin v_{nc}-1)^2\,T_{nc}(\xi_1,\eta_1,4)}{s_{nc}^2\sin\beta_{nc}\sqrt{b^2+(a^2-b^2)\sin^2 v_{nc}}}\right\}\\
&+\widehat{\psi}_{c1}\left\{\frac{s_{c1}^2\,b\sin\psi_{c1}\cos v_{nc}\,T_{nc}(\xi_1,\eta_1,2)}{s_{nc}^2\sin\beta_{nc}\sqrt{b^2+(a^2-b^2)\sin^2 v_{nc}}}\right.\\
&+\left.\frac{b\sin\psi_{c1}\left\{s_{c1}b\cos\psi_{c1}-a^2\right\}\cos v_{nc}\,(\sin v_{nc}-1)\,T_{nc}(\xi_1,\eta_1,4)}{s_{nc}^2\sin\beta_{nc}\sqrt{b^2+(a^2-b^2)\sin^2 v_{nc}}}\right\} \qquad (558)
\end{aligned}$$

and

$$\begin{aligned}
\vec{\Psi}_u(\xi) &= \widehat{s}_{c1}\left\{\frac{-ab\sin\psi_{c1}\,(\sin v_{nc}-1)\,T_{nc}(\xi_1,\eta_1,2)}{s_{nc}\sin\beta_{nc}\sqrt{b^2+(a^2-b^2)\sin^2 v_{nc}}}\right\}\\
&+\widehat{\beta}_{c1}\left\{\frac{-s_{c1}\,b\sin\psi_{c1}\cos v_{nc}\,T_{nc}(\xi_1,\eta_1,2)}{s_{nc}\sin\beta_{nc}\sqrt{b^2+(a^2-b^2)\sin^2 v_{nc}}}\right\}\\
&+\widehat{\psi}_{c1}\left\{\frac{s_{c1}\,a\sin v_{nc}\,T_{nc}(\xi_1,\eta_1,0)}{s_{nc}\sin\beta_{nc}\sqrt{b^2+(a^2-b^2)\sin^2 v_{nc}}}\right.\\
&\qquad+\left.\frac{-ab\cos\psi_{c1}\,(\sin v_{nc}-1)\,T_{nc}(\xi_1,\eta_1,2)}{s_{nc}\sin\beta_{nc}\sqrt{b^2+(a^2-b^2)\sin^2 v_{nc}}}\right\}, \qquad (559)
\end{aligned}$$

respectively. The coordinate transformation in (544) through (546) is then used to transform this expression into the global coordinates $\widehat{s}_o$, $\widehat{\beta}_o$ and $\widehat{\psi}_o$. These vectors along with the diffracted field parameters derive earlier in this subsection can now be used to calculate the field diffracted by the non-central diffraction points.

2.2 Numerical Calculation of the Field Scattered by an Elliptic Disk

The numerical calculation of the field expressions derived in Subsection 2.1 confirms the uniformity of the CC-UTD. This geometry is representative of a typical practical

problem. This subsection is devoted to the numerical calculation of the field scattered by an elliptic disk.

The results generated in this subsection will be presented in terms of the scattered field. The field scattered by an object is given by

$$\vec{E}^s(P) = \vec{E}^t(P) - \vec{E}^i(P) \tag{560}$$

where $\vec{E}^t(P)$ is the total electric field and $\vec{E}^i(P)$ is the incident field. It is important to note that throughout this subsection, $\vec{E}^i(P)$ is the incident field at the observation point in the absence of the object and not the incident field part of the GO field. Also, the scattered field components will be normalized using

$$\sigma_{\beta'\beta} = 4\pi R^2 \left| \frac{\hat{\beta}_o \cdot \vec{E}^s(P)}{\hat{\beta}'_o \cdot \vec{E}^i(P)} \right|^2 , \tag{561}$$

$$\sigma_{\psi's} = 4\pi R^2 \left| \frac{\hat{s}_o \cdot \vec{E}^s(P)}{\hat{\psi}'_o \cdot \vec{E}^i(P)} \right|^2 \tag{562}$$

and

$$\sigma_{\psi'\psi} = 4\pi R^2 \left| \frac{\hat{\psi}_o \cdot \vec{E}^s(P)}{\hat{\psi}'_o \cdot \vec{E}^i(P)} \right|^2 \tag{563}$$

which are consistent with the definition of the far-zone radar cross section. These results are converted into units of decibels per square meter (dBsm) using

$$\sigma\,(\text{dBsm}) = 10 \log_{10}[\sigma] \tag{564}$$

since the expressions in (561) through (563) are power ratios multiplied by length squared. This subsection is a comparison of the CC-UTD, UTD and Moment Method solutions. The MM solution used to determine the scattered field is generated using a general program developed by Nehrbass, Gupta and Newman [37].

The first geometry considered here is the plane wave scattering by an elliptic disk with $a = 3.0$ m and $b = 1.5$ m. Also, the incidence angle is taken to be $\psi'_o = 45^\circ$ and the observation distance is $R = 2.5$ m. All of the calculations for this geometry are performed at a frequency of 300 MHz.

It is easy to show that the ISB's for this geometry occur at $\bar{\psi}_1 = 199.8959^\circ$ and $\bar{\psi}_2 = 250.1041^\circ$ using (528) and (529), respectively. Also, the RSB's for this geometry

occur at $\tilde{\psi}_3 = 109.8959°$ and $\tilde{\psi}_4 = 160.1041°$ using (534) and (535), respectively. The CB's for the elliptic disk occur when $\rho^d + s$ in the amplitude spreading factors approaches zero. Using this fact, the CB's of Q_{c0} are found using

$$bs_{c0}\cos\psi_o' + bR\cos\psi_o + b^2 - a^2 = 0 \tag{565}$$

and the CB's of Q_{c1} are found using

$$bs_{c1}\cos\psi_o' + bR\cos\psi_o - b^2 + a^2 = 0 \tag{566}$$

where each of these must be solved separately for $\cos\psi_o$. For the geometry chosen here, the non-central diffraction points only coalesce at Q_{c0}. Therefore, using (565) we find that

$$25\cos^2\psi_o - 105\cos\psi_o + 64 = 0 \tag{567}$$

must be solved for $\cos\psi_o$. Solving this equation, the valid root is $\cos\psi_{CB0} = .73985$ which results in CB's occurring at $\psi_{CB0} = 42.2811°, 317.7189°$.

First, the scattered field comparison of the $\widehat{\beta}_o$ component is discussed. The CC-UTD, UTD and MM solutions are computed and shown in Figure 57. This component is discussed first because it is effected the least by slope diffraction and double diffraction effects. It is seen from Figure 57 that the CC-UTD solution is not only bounded, but also smooth and continuous across the caustics. Also, the CC-UTD solution smoothly reduces to the classical UTD solution away from the caustics as expected. There is excellent agreement between the CC-UTD solution and the MM solution throughout the pattern.

Next, the scattered field comparison of the $\widehat{s}_o$ and $\widehat{\psi}_o$ components are discussed. The CC-UTD, UTD and MM solutions are computed and shown in Figure 58 for the $\widehat{s}_o$ component. First, the $\widehat{s}_o$ component shown in Figure 58 is highly dependent on slope diffraction near the incident and reflection shadow boundaries. Also, double diffraction plays an important role near grazing to the disk. However, these effects have been neglected in these calculations. The scattered field in the caustic regions is dominated by the coalescing diffraction points. This fact can be seen in Figure 58. The field predicted by the CC-UTD near the caustics is in excellent agreement with

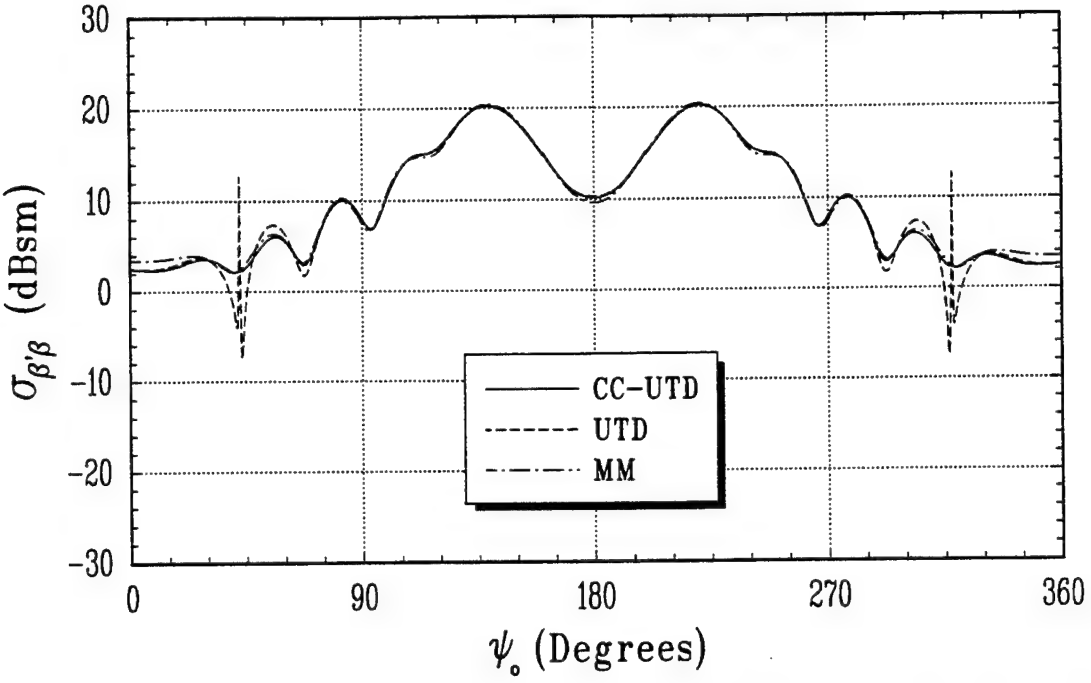

Figure 57: Scattered field comparison of the $\hat{\beta}_o$ component in the y-z plane of an elliptic disk with $a = 3.0$ m, $b = 1.5$ m, an observation distance of $R = 2.5$ m and an incidence angle of $\psi'_o = 45°$ at a frequency of 300 MHz.

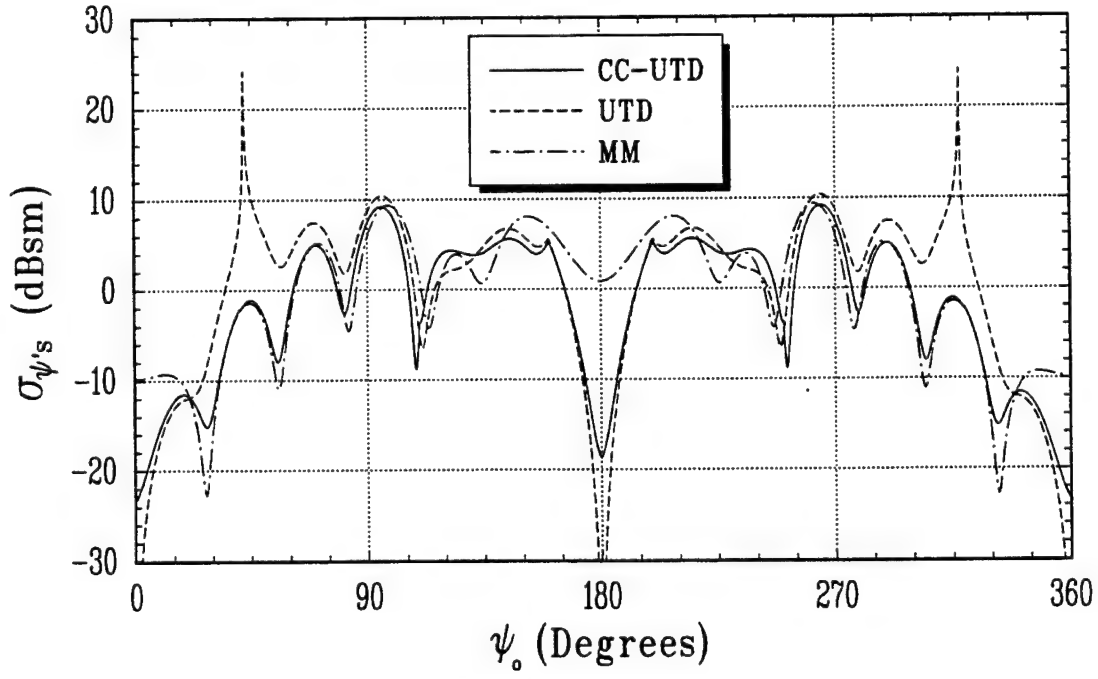

Figure 58: Scattered field comparison of the $\hat{s}_o$ component in the y-z plane of an elliptic disk with $a = 3.0$ m, $b = 1.5$ m, an observation distance of $R = 2.5$ m and an incidence angle of $\psi'_o = 45°$ at a frequency of 300 MHz.

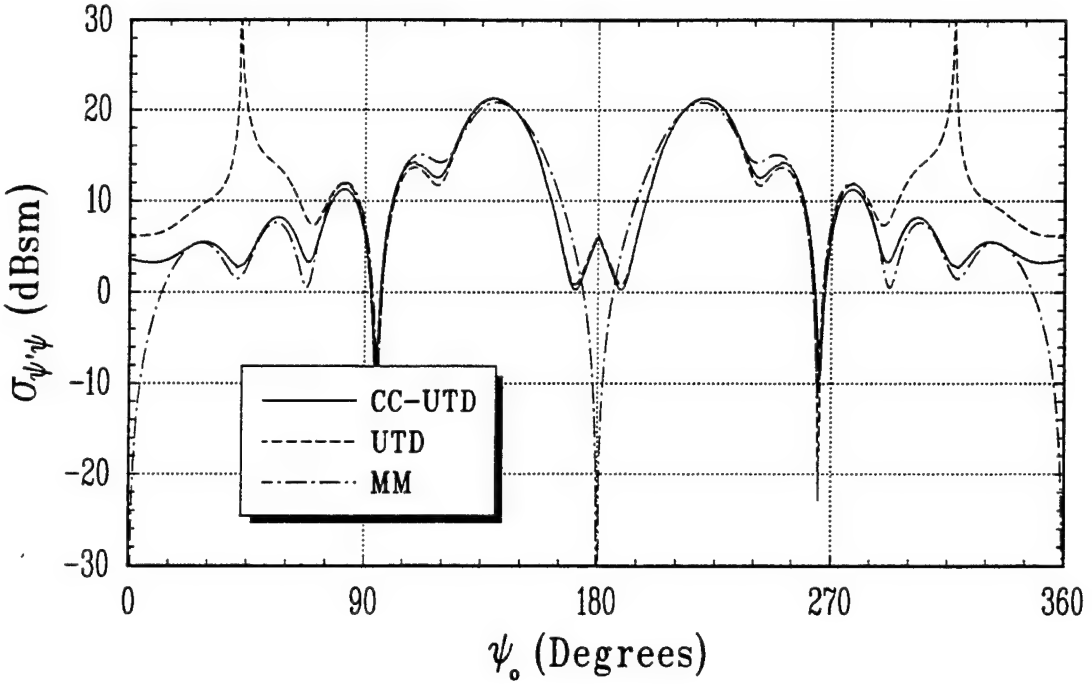

Figure 59: Scattered field comparison of the $\hat{\psi}_o$ component in the y-z plane of an elliptic disk with $a = 3.0$ m, $b = 1.5$ m, an observation distance of $R = 2.5$ m and an incidence angle of $\psi'_o = 45°$ at a frequency of 300 MHz.

the MM. Also, the CC-UTD solution smoothly reduces to the classical UTD solution away from the caustics. The inclusion of the slope diffraction terms would greatly improve the scattered field near the incident and reflection shadow boundaries. Also, the inclusion of the double diffraction terms would improve the scattered field near grazing angles. However, not including these terms is consistent with the assumptions of the classical UTD. Next, Figure 59 shows the $\hat{\psi}_o$ component of the scattered field predicted using the CC-UTD, UTD and MM. Slope diffraction has little effect for this polarization, but double diffraction has a noticeable effect near grazing angles. However, the scattered field in the caustic regions is dominated by the coalescence of diffraction points. These effects can be seen from Figure 59. First, the CC-UTD solution is smooth and continuous across the incident and reflection shadow boundaries and in good agreement with the MM. Near the caustics, the CC-UTD solution is again smooth and continuous and in excellent agreement with the MM.

One of the advantages of ray optical solutions is the computational speed of these solutions. All three of these polarization components where run at the same time using the general MM program developed by Nehrbass, Gupta and Newman [37]. For this geometry, the MM solution was run on a Silicon Graphics Indigo/R4K workstation and required 2 hours, 27 minutes and 8.31 seconds to compute. However, these three scattered field components for the CC-UTD and UTD solutions were run concurrently on the same computer and required only 3.92 seconds to compute. This is a distinct improvement in computational efficiency.

It is now of interest to study the effects of the different approximate solutions discussed in Section 5 of Chapter 7. For the sake of discussion, the first approximate solution discussed in Section 5 of Chapter 7 will be denoted by CC-UTD$_1$. The CC-UTD$_1$ solution assumes that the edge is parabolic in shape near the central diffraction point. Also, the second approximate solution discussed in Section 5 of Chapter 7 will be denoted by CC-UTD$_2$. This solution assumes that the main contribution to the diffracted field comes from two specific integrals and the rest are negligible.

The CC-UTD, CC-UTD$_1$, CC-UTD$_2$ and MM solutions are compared in the y-z plane of an elliptic disk with $a = 3.0$ m, $b = 1.5$ m, an observation distance of $R = 2.5$ m and an incidence angle of $\psi_o' = 45°$ at a frequency of 300 MHz. The comparisons of these solutions for the $\widehat{s}_o$, $\widehat{\beta}_o$ and $\widehat{\psi}_o$ components are shown in Figures 60, 61 and 62; respectively. As expected there is a negligible difference between the CC-UTD and CC-UTD$_1$ solutions. This is expected because the diffracted fields depend on the local geometry of the diffraction point. Therefore, the leading term of the Taylor series about the diffraction point accurately describes the edge and all others can be neglected. However, the difference between the CC-UTD and CC-UTD$_2$ solutions is larger. This occurs because different contributions to the diffracted field have been neglected. These solutions differ very little in the caustic regions and are still in good agreement with the MM solution.

Although Figures 60 though 62 show that these three approximate solutions agree very well with the MM solution, the differences between the CC-UTD, CC-UTD$_1$ and

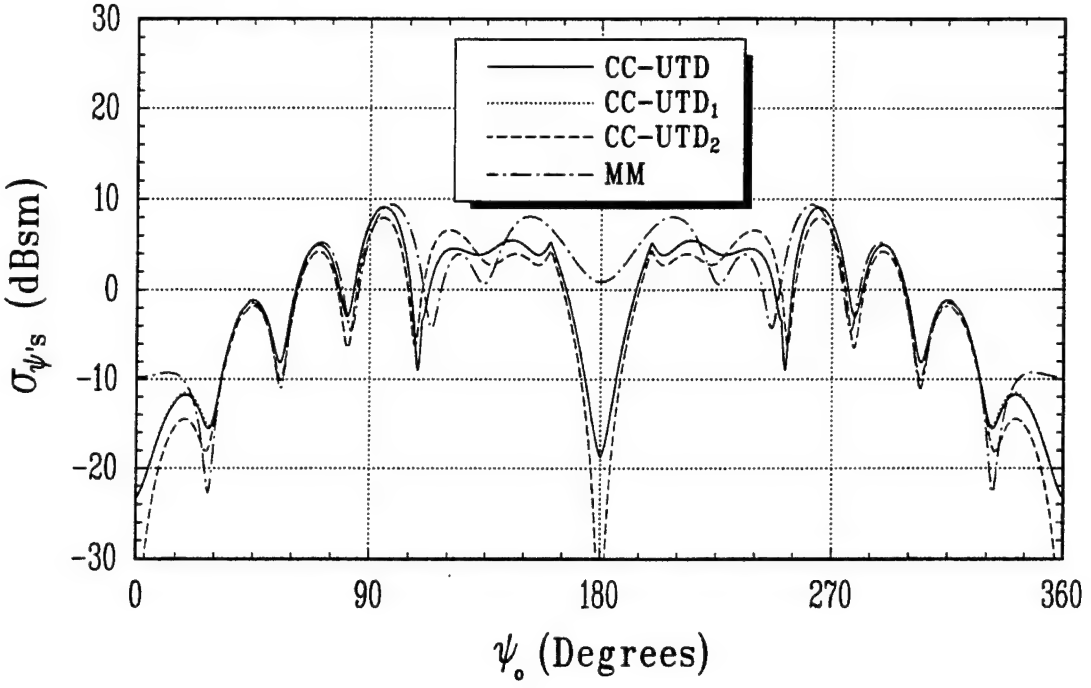

Figure 60: Scattered field approximation comparison of the $\hat{s}_o$ component in the y-z plane of an elliptic disk with $a = 3.0$ m, $b = 1.5$ m, an observation distance of $R = 2.5$ m and an incidence angle of $\psi_o' = 45°$ at a frequency of 300 MHz.

CC-UTD$_2$ are of interest. To better illustrate this, the percent difference between these three solutions will be defined as

$$\mathrm{P}_s = \frac{\left|\hat{s}_o \cdot \left\{\vec{E}^s(P) - \vec{E}_a^s(P)\right\}\right|}{\left|\hat{\psi}_o' \cdot \vec{E}^i(0)\right|} \times 100\% \tag{568}$$

for the $\hat{s}_o$ components,

$$\mathrm{P}_\beta = \frac{\left|\hat{\beta}_o \cdot \left\{\vec{E}^s(P) - \vec{E}_a^s(P)\right\}\right|}{\left|\hat{\beta}_o' \cdot \vec{E}^i(0)\right|} \times 100\% \tag{569}$$

for the $\hat{\beta}_o$ components and

$$\mathrm{P}_\psi = \frac{\left|\hat{\psi}_o \cdot \left\{\vec{E}^s(P) - \vec{E}_a^s(P)\right\}\right|}{\left|\hat{\psi}_o' \cdot \vec{E}^i(0)\right|} \times 100\% \tag{570}$$

for the $\hat{\psi}_o$ components. Also, $\vec{E}^s(P)$ is the scattered field predicted by the CC-UTD solution, $\vec{E}_a^s(P)$ is the approximate scattered field predicted by either the CC-UTD$_1$ or the CC-UTD$_2$ solution and $\vec{E}^i(0)$ is the incident field at the origin. First, the percent

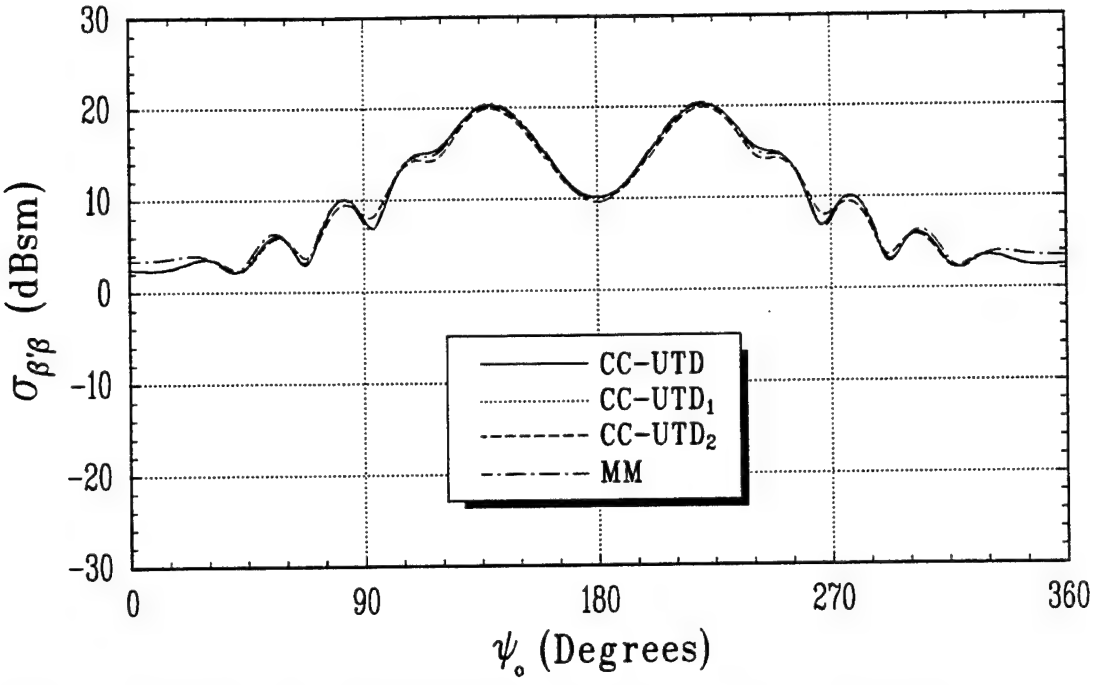

Figure 61: Scattered field approximation comparison of the $\widehat{\beta}_o$ component in the y-z plane of an elliptic disk with $a = 3.0$ m, $b = 1.5$ m, an observation distance of $R = 2.5$ m and an incidence angle of $\psi'_o = 45°$ at a frequency of 300 MHz.

difference between the CC-UTD and CC-UTD$_1$ is shown in Figure 63. This figure shows that for the $\widehat{s}_o$ and $\widehat{\psi}_o$ components of the scattered field, these solutions differ by less than 0.4%. Also, this approximation only simplifies the field in the caustic shadow region for these components. Therefore, there is no difference between these solutions in the caustic lit region for these scattered field components. This figure also shows that for the $\widehat{\beta}_o$ component of the scattered field, these solutions differ by less than 0.5% in the caustic shadow region and 4% in the caustic lit region. In most cases of interest, these differences are negligible and this approximate solution should be used. Also, the percent difference between the CC-UTD and CC-UTD$_2$ is shown in Figure 64. This figure shows that the difference between the CC-UTD solution and the CC-UTD$_2$ is less than 8%. Although this difference is greater than that of the CC-UTD$_1$ solution, it is a much simpler solution to apply. Therefore, this solution should be used first and then refined later if the need arises. However, this solution should be accurate enough for most practical problems.

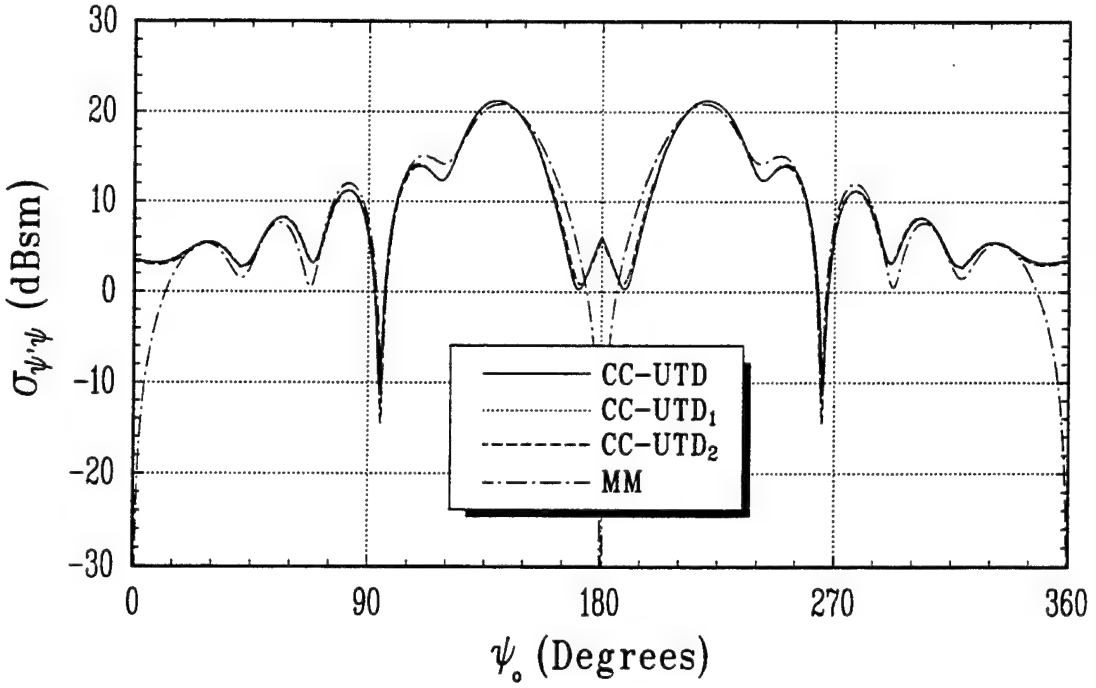

Figure 62: Scattered field approximation comparison of the $\widehat{\psi}_o$ component in the y-z plane of an elliptic disk with $a = 3.0$ m, $b = 1.5$ m, an observation distance of $R = 2.5$ m and an incidence angle of $\psi'_o = 45°$ at a frequency of 300 MHz.

The next geometry considered here is the plane wave scattering by a circular disk with $a = b = 2.5$ m. Also, the incidence angle is taken to be $\psi'_o = 70°$ and the observation distance is $R = 5.0$ m. All of the calculations for this geometry are performed at a frequency of 300 MHz. This geometry is interesting in that a circular disk is a typical geometry studied using high frequency techniques.

It is easy to show that the ISB's for this geometry occur at $\tilde{\psi}_1 = 221.9757°$ and $\tilde{\psi}_2 = 278.0243°$ using (528) and (529), respectively. Also, the RSB's for this geometry occur at $\tilde{\psi}_3 = 81.9757°$ and $\tilde{\psi}_4 = 138.0243°$ using (534) and (535), respectively. The CB's of diffraction point Q_{c0} are found by solving (565) and are $\psi_{CB0} = 109.1656°$, $250.8344°$. Similarly, the CB's of diffraction point Q_{c1} are found by solving (566) and are $\psi_{CB1} = 116.4425°$, $243.5575°$.

Again, the scattered field comparison of the $\widehat{\beta}_o$ component is discussed first because this component is effected the least by slope diffraction and double diffraction effects. The CC-UTD, UTD and MM solutions are computed and shown in Figure 65. It is

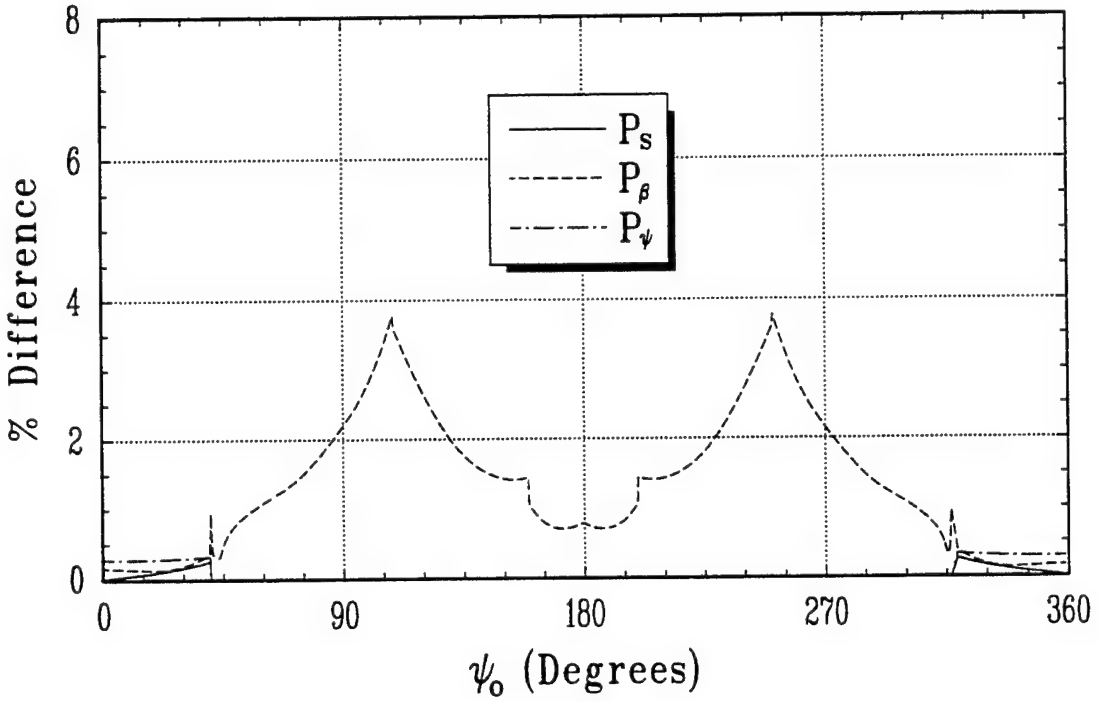

Figure 63: Percent scattered field difference between the CC-UTD and CC-UTD$_1$ solutions in the y-z plane of an elliptic disk with $a = 3.0$ m, $b = 1.5$ m, an observation distance of $R = 2.5$ m and an incidence angle of $\psi_o' = 45°$ at a frequency of 300 MHz.

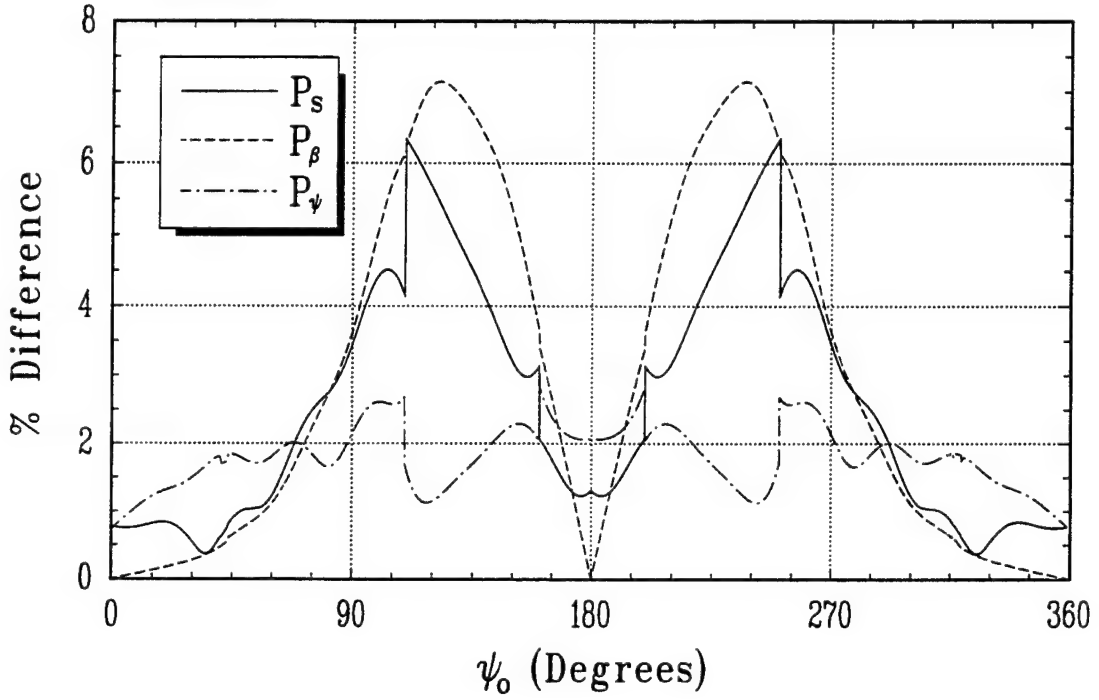

Figure 64: Percent scattered field difference between the CC-UTD and CC-UTD$_2$ solutions in the y-z plane of an elliptic disk with $a = 3.0$ m, $b = 1.5$ m, an observation distance of $R = 2.5$ m and an incidence angle of $\psi_o' = 45°$ at a frequency of 300 MHz.

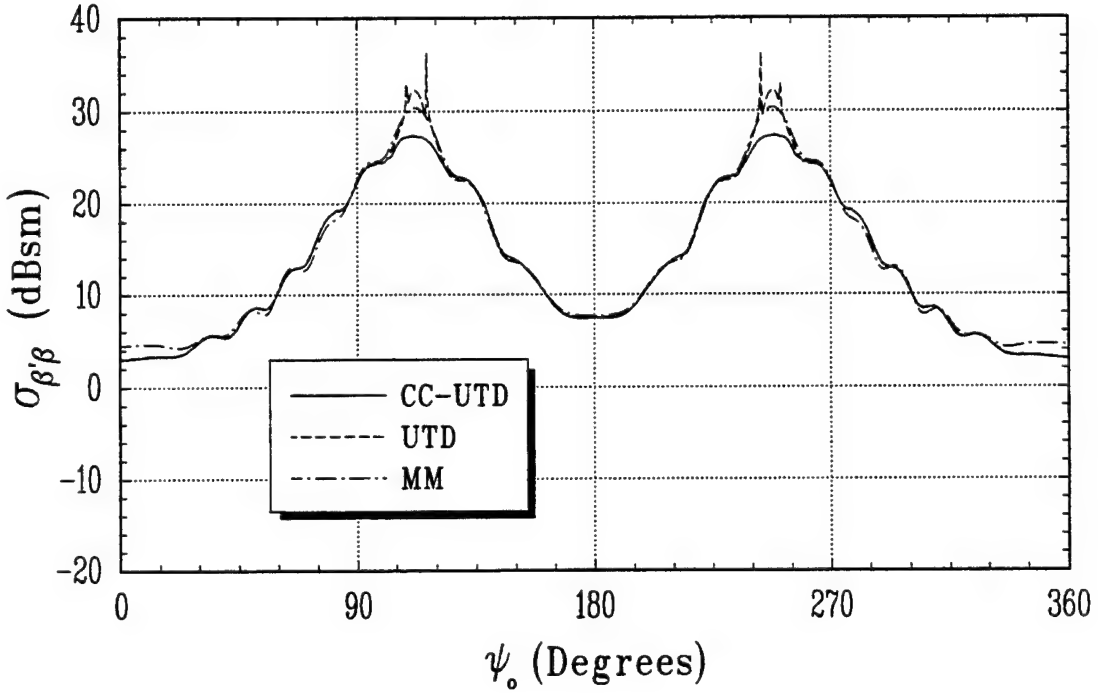

Figure 65: Scattered field comparison of the $\widehat{\beta}_o$ component in the y-z plane of a circular disk with $a = b = 2.5$ m, an observation distance of $R = 5.0$ m and an incidence angle of $\psi'_o = 70°$ at a frequency of 300 MHz.

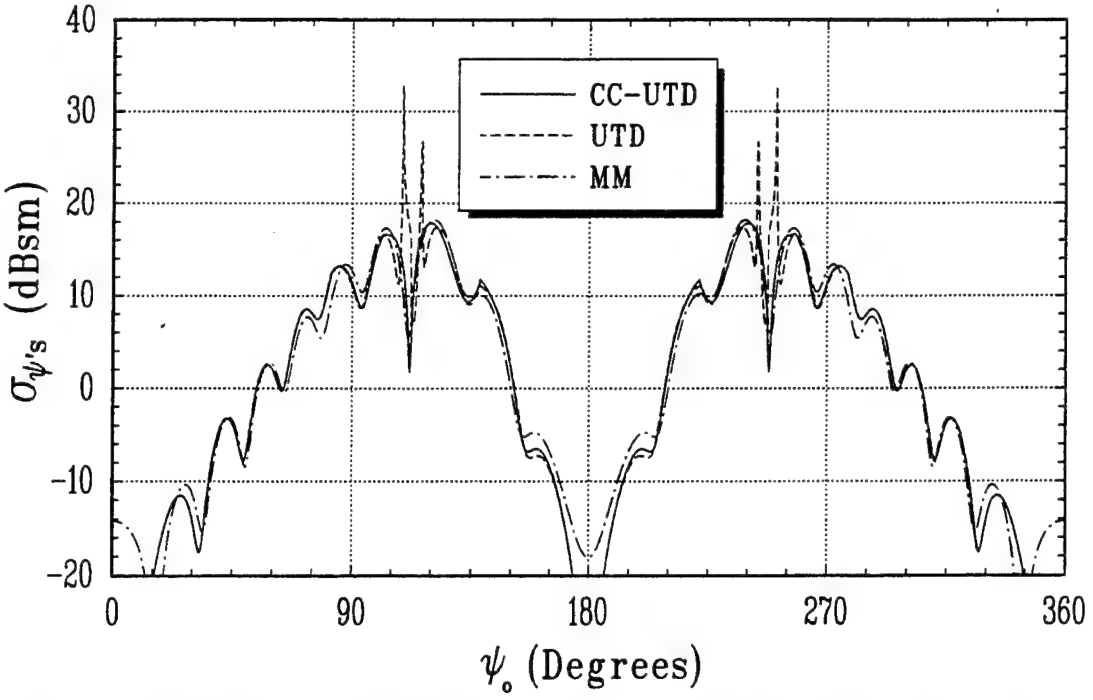

Figure 66: Scattered field comparison of the $\hat{s}_o$ component in the y-z plane of a circular disk with $a = b = 2.5$ m, an observation distance of $R = 5.0$ m and an incidence angle of $\psi'_o = 70°$ at a frequency of 300 MHz.

seen from Figure 65 that the CC-UTD solution is not only bounded, but also smooth and continuous across the caustics. Also, the CC-UTD solution smoothly reduces to the classical UTD solution away from the caustics as expected. However, the scattered field in the caustic regions is about 3 dB below the result predicted using the Method of Moments. This can be attributed to the CB's of Q_{c0} and Q_{c1} being close together. In order to obtain a more accurate result, all four diffraction points should be accounted for in the uniform asymptotic expansion. This would result in a solution that contains Swallowtail integrals [38].

Next, the scattered field comparison of the $\hat{s}_o$ and $\hat{\psi}_o$ components are discussed. The CC-UTD, UTD and MM solutions are computed and shown in Figure 66 for the $\hat{s}_o$ component. First, the $\hat{s}_o$ component shown in Figure 66 is dependent on slope diffraction near the incident and reflection shadow boundaries. Also, double diffraction plays an important role near grazing to the disk. However, these effects have been neglected in these calculations. The scattered field in the caustic regions

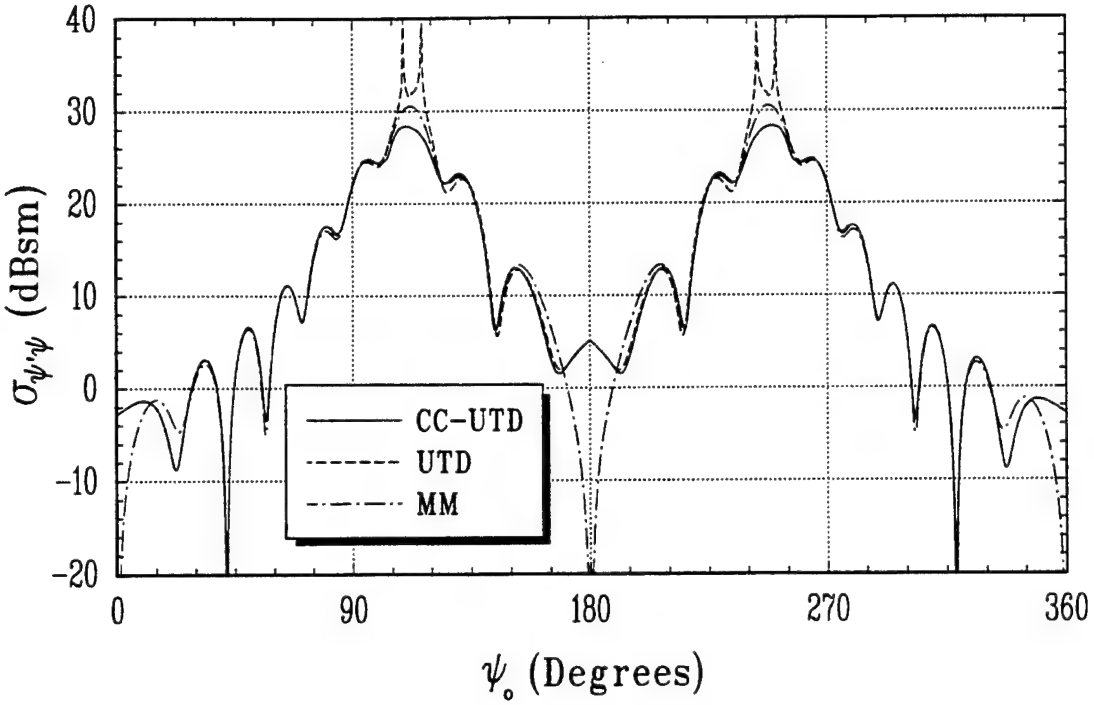

Figure 67: Scattered field comparison of the $\hat{\psi}_o$ component in the y-z plane of a circular disk with $a = b = 2.5$ m, an observation distance of $R = 5.0$ m and an incidence angle of $\psi'_o = 70°$ at a frequency of 300 MHz.

is dominated by the coalescing diffraction points. This fact can be seen in Figure 66. The field predicted by the CC-UTD near the caustics is in excellent agreement with the MM. Also, the CC-UTD solution smoothly reduces to the classical UTD solution away from the caustics. The inclusion of the slope diffraction terms would greatly improve the scattered field near the incident and reflection shadow boundaries. Also, the inclusion of the double diffraction terms would improve the scattered field near grazing angles. However, not including these terms is consistent with the assumptions of the classical UTD. Next, Figure 67 shows the $\hat{\psi}_o$ component of the scattered field predicted using the CC-UTD, UTD and MM solutions. Slope diffraction has little effect for this polarization, but double diffraction has a noticeable effect near grazing angles. However, the scattered field in the caustic regions is dominated by the coalescence of diffraction points. These effects can be seen from Figure 67. First, the CC-UTD solution is smooth and continuous across the incident and reflection shadow boundaries and in good agreement with the MM. Near the caustics, the CC-

UTD solution is again smooth and continuous, but about 3 dB below the scattered field predicted by the Method of Moments.

One of the advantages of ray optical solutions is the computational speed of these solutions. All three of these polarization components where run at the same time using the general MM program developed by Nehrbass, Gupta and Newman [37]. For this geometry, the MM solution was run on a Silicon Graphics Indigo/R4K workstation and required 2 hours, 7 minutes and 38.23 seconds to compute. However, these three scattered field components for the CC-UTD and UTD solutions were run concurrently on the same computer and required only 6.24 seconds to compute. This is a distinct improvement in computational efficiency.

SECTION 9

Conclusion

The high frequency electromagnetic field near the cusp of a caustic has been investigated. New caustic corrected UTD solutions have been developed to obtain fast and accurate results. These solutions also lead to valuable physical insight into the nature of the electromagnetic fields near the cusp. The Incremental Theory of Diffraction (ITD) has been used to obtain the ray optical solutions in this work. These solutions use the GO fields found using classical GO techniques and a caustic corrected UTD diffracted field is used to correct the GO fields. These solutions predict fields which are smooth and continuous through the diffracted field caustics and reduce to the classical UTD solution away from the caustics.

A caustic corrected UTD solution for the radiation by a source on a flat plate is derived in Chapter 5. The CC-UTD diffracted field in the caustic lit region is found to be

$$\begin{aligned}\vec{E}^d(P) \;\sim\; & \vec{E}^i(Q_c)\cdot\overline{\overline{D}}^L(Q_c)\sqrt{\rho^d(Q_c)}\,\frac{e^{-jkR_c}}{R_c} \\ & + \vec{E}^i(Q_{nc}^+)\cdot\overline{\overline{D}}^L(Q_{nc}^+)\sqrt{\rho^d(Q_{nc})}\,\frac{e^{-jkR_{nc}}}{R_{nc}} \\ & + \vec{E}^i(Q_{nc}^-)\cdot\overline{\overline{D}}^L(Q_{nc}^-)\sqrt{\rho^d(Q_{nc})}\,\frac{e^{-jkR_{nc}}}{R_{nc}} \qquad (571)\end{aligned}$$

where the dyadic diffraction coefficients for the central and non-central diffraction points are

$$\overline{\overline{D}}^L(Q_c) = -\hat{\psi}'\hat{\psi}\,D_h(Q_c)\,T_c(\xi,0) \qquad (572)$$

and

$$\overline{\overline{D}}^L(Q_{nc}) = -\hat{\psi}'\hat{\psi}\,D_h(Q_{nc})\,T_{nc}(\xi,\eta,0), \qquad (573)$$

respectively. The diffraction coefficient $D_h(Q_e)$ is identical to the UTD half-plane diffraction coefficient for the hard polarization. Also, the caustic correction transition functions $T_c(\xi,0)$ and $T_{nc}(\xi,\eta,0)$ are defined in (655) and (656) of Appendix B, respectively. The CC-UTD diffracted field in the caustic shadow region is found to be

$$\begin{aligned}\vec{E}^d(P) \;\sim\; & \vec{E}^i(Q_c)\cdot\overline{\overline{D}}^S(Q_c)\sqrt{\rho^d(Q_c)}\,\frac{e^{-jkR_c}}{R_c} \\ & + \;\vec{E}^i(Q_c)\cdot\overline{\overline{D}}^S(Q_c)\sqrt{\rho^d(Q_c)}\,\frac{e^{-jkR_c}}{R_c}\end{aligned} \tag{574}$$

where the dyadic diffraction coefficients at the central diffraction point are

$$\overline{\overline{D}}^S(Q_c) = -\hat{\psi}'\hat{\psi}\,D_h(Q_c)\,T_s(\xi,0) \tag{575}$$

and

$$\overline{\overline{\mathcal{D}}}^S(Q_c) = -\hat{\psi}'\hat{\psi}\,\mathcal{D}_h(Q_c)\,T_s(\xi,2)\,. \tag{576}$$

The caustic correction transition functions $T_s(\xi,0)$ and $T_s(\xi,2)$ are defined in (674) of Appendix B. Also, $D_h(Q_c)$ is the UTD half-plane diffraction coefficient for the hard polarization and

$$\begin{aligned}\mathcal{D}_h(Q_c) \;=\; & \frac{\rho^d(Q_c)}{2jk}\left\{\frac{d^2D_h(Q_c)}{dl^2} - D_h(Q_c)\left(\frac{1}{(s_c')^2}\left[1-\frac{s_c'}{\rho_g(Q_c)}\right]\right.\right. \\ & \left.\left. + \kappa_g^2(Q_c)\sin^2\psi_c - \frac{1}{4}\mathcal{C}(l_c)\right)\right\}\end{aligned} \tag{577}$$

is a curvature dependent diffraction coefficient. These equations can now be used to calculate the field on the both sides of the diffracted field caustic when the source is located on the face of the plate.

Chapter 7 is a derivation of a CC-UTD solution for cases when the near-zone point is not located on the face of the plate. Although a complete CC-UTD solution is derived, it is shown that a very simple approximate solution is accurate enough for most practical problems. This approximate CC-UTD diffracted field solution is written as

$$\vec{E}^d(P) \;\sim\; \vec{E}^i(Q_c)\cdot\overline{\overline{D}}^L(Q_c)\sqrt{\frac{\rho^d(Q_c)}{s_c\,[\rho^d(Q_c)+s_c]}}\,e^{-jks_c}$$

$$+ \quad \vec{E}^i(Q_{nc}^+) \cdot \overline{\overline{D}}^L(Q_{nc}^+) \sqrt{\frac{\rho^d(Q_{nc})}{s_{nc}\left[\rho^d(Q_{nc}) + s_{nc}\right]}}\, e^{-jks_{nc}}$$

$$+ \quad \vec{E}^i(Q_{nc}^-) \cdot \overline{\overline{D}}^L(Q_{nc}^-) \sqrt{\frac{\rho^d(Q_{nc})}{s_{nc}\left[\rho^d(Q_{nc}) + s_{nc}\right]}}\, e^{-jks_{nc}} \tag{578}$$

in the caustic lit region, where

$$\overline{\overline{D}}^L(Q_c) \approx -\hat{\beta}'\hat{\beta}_c\, D_s(Q_c)\, T_c(\xi, 0) - \hat{\psi}'\hat{\psi}_c\, D_h(Q_c)\, T_c(\xi, 0) \tag{579}$$

is the dyadic diffraction coefficient for the central diffracted field and

$$\begin{aligned} \overline{\overline{D}}^L(Q_{nc}) \;\approx\; & -\hat{\beta}'\hat{\beta}_c \left\{ \frac{-s_c^2 \left[\hat{e}(Q_{nc}) \cdot \hat{\beta}_c\right]}{s_{nc}^2 \sin\beta_{nc}} \right\} D_s(Q_{nc})\, T_{nc}(\xi, \eta, 0) \\ & -\hat{\psi}'\hat{\psi}_c \left\{ \frac{-s_c \left[\hat{e}(Q_{nc}) \cdot \hat{\beta}_c\right]}{s_{nc} \sin\beta_{nc}} \right\} D_h(Q_{nc})\, T_{nc}(\xi, \eta, 0) \end{aligned} \tag{580}$$

is the dyadic diffraction coefficient for the non-central diffracted fields. This approximate CC-UTD diffracted field solution is written as

$$\begin{aligned} \vec{E}^d(P) \;\sim\; & \vec{E}^i(Q_c) \cdot \overline{\overline{D}}^S(Q_c) \sqrt{\frac{\rho^d(Q_c)}{s_c\left[\rho^d(Q_c) + s_c\right]}}\, e^{-jks_c} \\ & + \vec{E}^i(Q_c) \cdot \overline{\overline{D}}^S(Q_c) \left\{ \frac{\rho^d(Q_c)}{s_c\left[\rho^d(Q_c) + s_c\right]} \right\}^{3/2} e^{-jks_c} \end{aligned} \tag{581}$$

in the caustic shadow region, where

$$\overline{\overline{D}}^S(Q_c) \approx -\hat{\beta}'\hat{\beta}_c\, D_s(Q_c)\, T_s(\xi, 0) - \hat{\psi}'\hat{\psi}_c\, D_h(Q_c)\, T_s(\xi, 0) \tag{582}$$

is the dyadic diffraction coefficient for the central diffracted field and

$$\begin{aligned} \overline{\overline{D}}^S(Q_c) \;\approx\; & -\hat{\beta}'\hat{\beta}_c \left(\frac{s_c^5}{2jk}\, \mathcal{F}_s^{\mathrm{II}}(Q_c) + \frac{s_c^2}{8jk} \right. \\ & \qquad \left. \times \left[C(l_c) - 4\kappa_g^2(Q_c) \right] D_s(Q_c) \right) T_s(\xi, 2) \\ & -\hat{\psi}'\hat{\psi}_c \left(\frac{s_c^4}{2jk}\, \mathcal{F}_h^{\mathrm{II}}(Q_c) + \frac{s_c^2}{8jk} \right. \\ & \qquad \left. \times \left[C(l_c) - 4\kappa_g^2(Q_c) \right] D_h(Q_c) \right) T_s(\xi, 2) \end{aligned} \tag{583}$$

is the dyadic diffraction coefficient for the curvature dependant central diffracted field. Again, $D_{s,h}(Q_e)$ are the UTD half-plane diffraction coefficients.

There are several restrictions on the use of the CC-UTD solutions. First, the edge of the flat plate must be symmetric about an axis and the source and observation points must lie in the plane of symmetry. This ensures that the diffraction points are symmetrically located. It is also important to note that the caustic boundaries should not be close to the incident or reflection shadow boundaries. The CC-UTD solutions begin to break down as these boundaries approach each other because only the diffracted field contribution of the ITD is integrated. In these cases, the PO integral minus its edge contribution can no longer be approximated by the GO field.

These solutions have been applied to two different problems in order to show their accuracy and practicability. The first problem is the radiation by a short monopole mounted in the center of an elliptic disk. The directive gain of this antenna has been calculated using the CC-UTD, UTD and MM solutions. These patterns were compared and shown to be in good agreement. The other problem considered was the bistatic scattering by a plane wave incident on an elliptic disk. The bistatic scattering patterns have been generated using the CC-UTD, UTD and MM solutions. These scattering patterns were compared and shown to be in good agreement.

Several generalizations of these results can be performed in future research endeavors. First, the coalescence of two diffraction points can be investigated using the ITD and the uniform asymptotic expansion of Chester, Friedman and Ursell [18]. Also, three unequally spaced and nearly coincident diffraction points can be investigated. This can be accomplished using the ITD and the uniform asymptotic expansions in [38, 39, 40, 41]. These expansions involve the Pearcey integral [42] and its derivatives. These functions can be computed using the small and large argument formulas found in [41, 43, 44, 45].

Appendix A

Auxiliary Integral Evaluation

Three different auxiliary integrals are encountered in the evaluation of the incremental diffracted field as shown in Chapter 3. These integrals are identical to those defined by Michaeli in the appendix of [21, 22]. The closed form evaluation of these auxiliary integrals is performed in this appendix using the same procedure as the one described by Michaeli in [21, 22]. It is important to note that the purpose of Chapter 3 is to obtain an expression for the field diffracted by an infinitesimal length of the edge of a wedge. Therefore, the contribution from the lower limit of the auxiliary integrals is to be determined. To illustrate this fact, only the lower limit of these integrals will be displayed throughout this appendix.

The first integral treated here as given by (46) of Chapter 3 is

$$U_1 = \int_0 u(X,\psi')\, e^{jX\zeta} dX, \tag{584}$$

where the integral representation of $u(X,\psi')$ as given by (31) of Chapter 3

$$u(X,\psi') = \frac{1}{2\pi jn} \int_\Gamma G_h(\xi)\, e^{jX\cos\xi}\, d\xi \tag{585}$$

and

$$G_h(\xi) = \frac{\sin\left(\frac{\xi}{n}\right)}{\cos\left(\frac{\xi}{n}\right) - \cos\left(\frac{\psi'}{n}\right)} \tag{586}$$

is to be used here. The contour of integration in (585) is shown in Figure 68. To begin the evaluation of (584) we wish to perform the integration in X first because of its simplicity. However, care must be taken when interchanging the order of integration in (584). The order of integration can only be changed if the integral on X converges

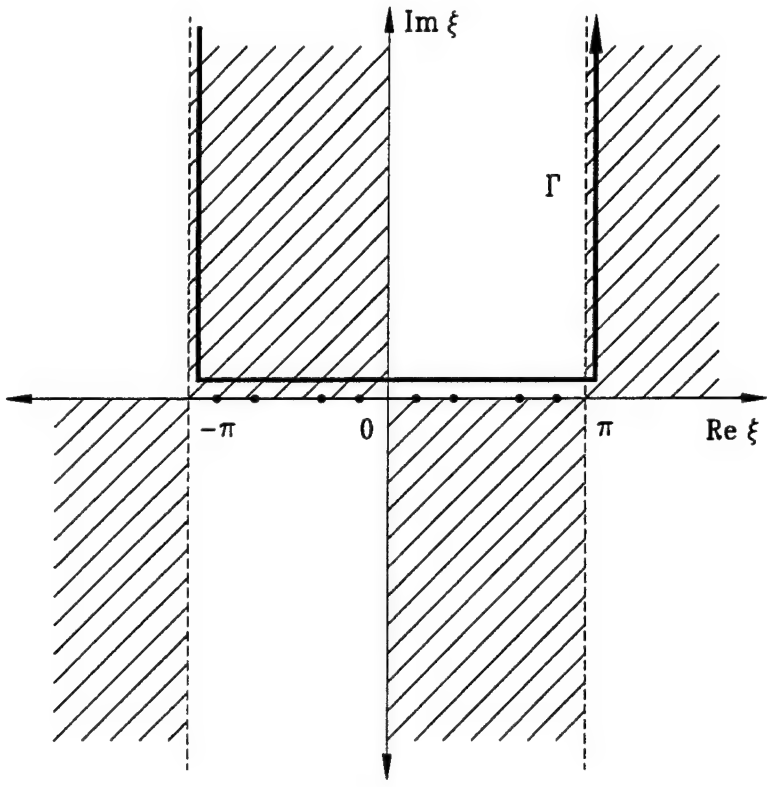

Figure 68: Contour of integration for the exact solution for the total field in the presence of a wedge.

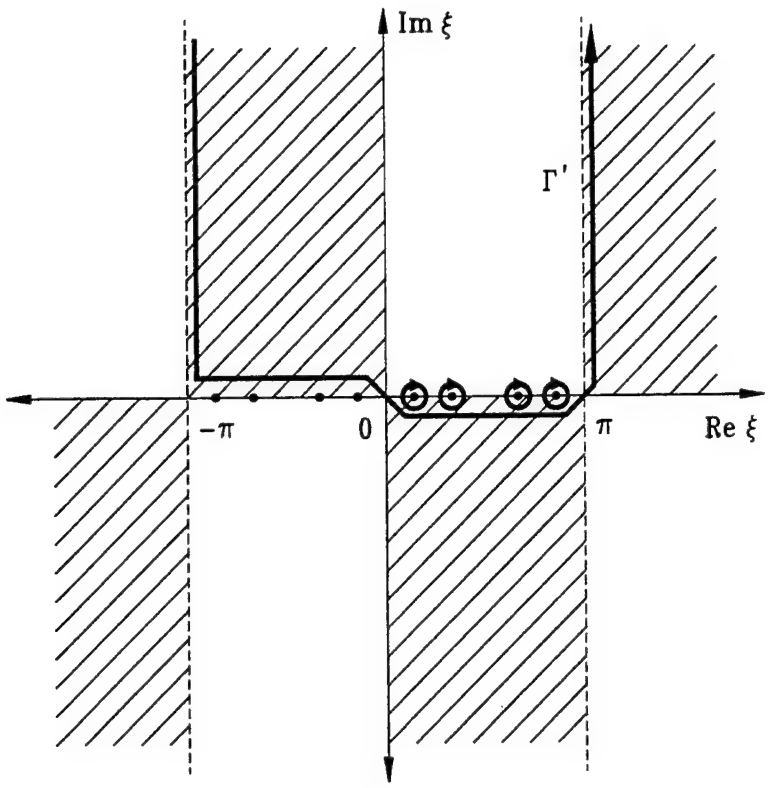

Figure 69: Deformed contour of integration for the total field in the presence of a wedge.

at $X \to +\infty$ for all ξ on the contour of integration in the ξ plane. This condition is not satisfied on the contour Γ. However, deforming the contour of integration from Γ to Γ' as shown in Figure 69 will ensure convergence. Figure 69 shows that several poles of the integrand are crossed when the contour of integration is deformed to Γ'. Therefore, including the residue contributions from these poles, (585) becomes

$$u(X,\psi') = \frac{1}{2\pi jn}\int_{\Gamma'} G_h(\xi)\, e^{jX\cos\xi}\, d\xi + \sum_m e^{jX\cos\xi_m} \tag{587}$$

where ξ_m are the roots of

$$\cos\left(\frac{\xi}{n}\right) - \cos\left(\frac{\psi'}{n}\right) = 0 \tag{588}$$

in the interval $0 < \xi_m < \pi$. Substituting (587) into (584) we obtain an expression

$$U_1 = \int_0 \frac{1}{2\pi jn}\int_{\Gamma'} G_h(\xi)\, e^{jX(\cos\xi+\zeta)}\, d\xi\, dX + \sum_m \int_0 e^{jX(\cos\xi_m+\zeta)} dX \tag{589}$$

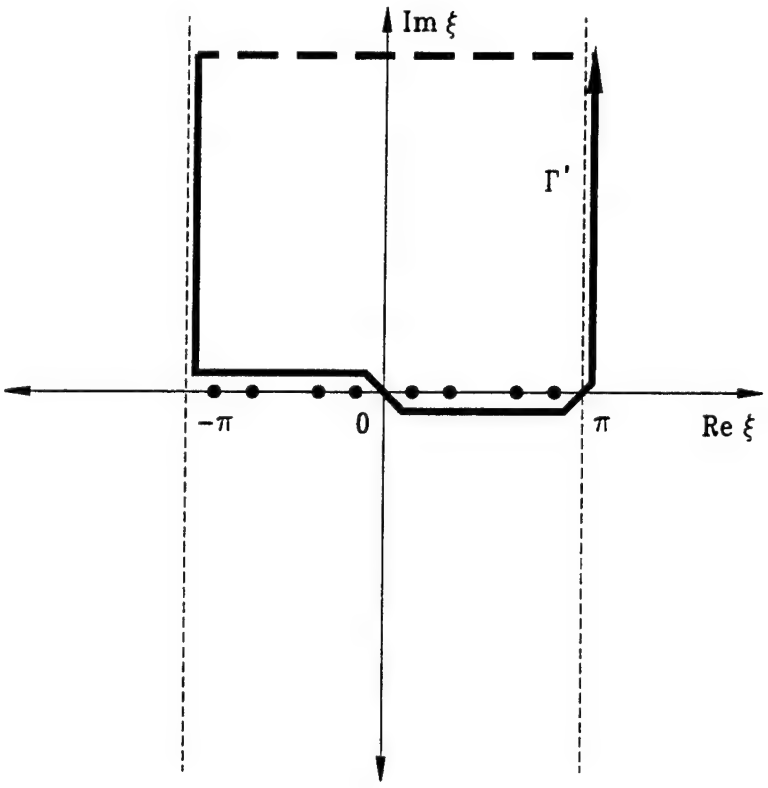

Figure 70: Deformed contour of integration enclosed at infinity.

which will allow us to interchange the order of integration

$$U_1 = \frac{1}{2\pi jn} \int_{\Gamma'} \int_0 G_h(\xi)\, e^{jX(\cos\xi+\zeta)}\, dX\, d\xi + \sum_m \int_0 e^{jX(\cos\xi_m+\zeta)} dX. \tag{590}$$

Since the convergence of the integral is now ensured, the integration with respect to X is performed

$$U_1 = \frac{-1}{2\pi n} \int_{\Gamma'} \frac{G_h(\xi)}{\cos\xi+\zeta}\, e^{jX(\cos\xi+\zeta)} \Big|_0 d\xi + \sum_m \frac{-j\, e^{jX(\cos\xi_m+\zeta)}}{\cos\xi_m+\zeta} \Big|_0 \tag{591}$$

which results in

$$U_1 = \frac{1}{2\pi n} \int_{\Gamma'} \frac{G_h(\xi)}{\cos\xi+\zeta}\, d\xi + \sum_m \frac{j}{\cos\xi_m+\zeta} \tag{592}$$

as the contribution from the edge. The remaining integral can be evaluated by enclosing the contour Γ' at infinity as shown in Figure 70. The Cauchy Residue Theorem can be applied by including the poles at ξ_m and the additional pole at

$$\xi_p = \cos^{-1}(-\zeta) = \pi - \cos^{-1}\zeta = \pi - \alpha \tag{593}$$

enclosed by the contour of integration. To completely determine the pole at $\xi = \xi_p$ we must define $\cos^{-1}\zeta$. For any real ζ,

$$\alpha = \cos^{-1}\zeta = -j\ln\left(\zeta + \sqrt{\zeta^2 - 1}\right) \tag{594}$$

where the proper branch of the square root is

$$\sqrt{\zeta^2-1} = \begin{cases} -\left|\sqrt{\zeta^2-1}\right| & ;\text{if } \zeta < -1 \\ j\left|\sqrt{\zeta^2-1}\right| & ;\text{if } -1 \le \zeta \le 1 \\ \left|\sqrt{\zeta^2-1}\right| & ;\text{if } \zeta > 1 \end{cases} \tag{595}$$

and the principal branch of $\ln(z)$ is used. That is $\ln(z) = \ln|z| + j\arg(z)$ where $0 \le \arg(z) \le \pi$. Now that the pole is completely defined, the evaluation of (592) can be completed. Using the Cauchy Residue Theorem including the indicated poles, (592) is

$$\begin{aligned} U_1 &= \sum_m \frac{-j}{\cos\xi_m + \zeta} + \frac{1}{j\sin\alpha}\, G_h^o(\alpha) + \sum_m \frac{j}{\cos\xi_m + \zeta} \\ &= \frac{1}{j\sin\alpha}\, G_h^o(\alpha) \end{aligned} \tag{596}$$

where

$$\begin{aligned} G_h^o(\alpha) &= \frac{\frac{1}{n}\sin\left(\frac{\pi-\alpha}{n}\right)}{\cos\left(\frac{\pi-\alpha}{n}\right) - \cos\left(\frac{\psi'}{n}\right)} \\ &= \frac{-1}{2n}\left[\cot\left(\frac{\pi-(\alpha-\psi')}{2n}\right) + \cot\left(\frac{\pi-(\alpha+\psi')}{2n}\right)\right] \end{aligned} \tag{597}$$

is a hard diffraction coefficient in the spectral domain. This completes the closed form evaluation of the edge contribution of U_1.

The second integral as given by (47) of Chapter 3 is

$$U_2 = \int_0^{\infty} \frac{\partial u(X,\psi')}{\partial X}\, e^{jX\zeta}\, dX \tag{598}$$

where $u(X,\psi')$ is given by (585). To make the differentiation with respect to X simpler, we recognize that this integral is easier to evaluate if we use integration-by-

parts. Using integration-by-parts, (598) becomes

$$\begin{aligned} U_2 &= u(X,\psi')\,e^{jX\zeta}\Big|_0 - \int_0 u(X,\psi')\,\frac{\partial}{\partial X}\left(e^{jX\zeta}\right)dX \\ &= -j\zeta\int_0 u(X,\psi')\,e^{jX\zeta}\,dX - u(0,\psi') \end{aligned} \tag{599}$$

where we recognize the integral as U_1 and $\zeta = \cos\alpha$ from (594). Therefore, we obtain

$$U_2 = -j\cos\alpha\, U_1 - u(0,\psi') \tag{600}$$

where

$$u(0,\psi') = \frac{1}{n} \tag{601}$$

from the eigenfunction solution in (30) of Chapter 3. Thus, substituting (596) and (601) into (600) we arrive at

$$U_2 = -\cot\alpha\, G_h^o(\alpha) - \frac{1}{n} \tag{602}$$

where again $G_h^o(\alpha)$ is a hard diffraction coefficient in the spectral domain.

Finally, the third integral as given by (48) of Chapter 3 is

$$U_3 = \int_0 \frac{1}{X}\,\frac{\partial u(X,\psi')}{\partial\psi'}\,e^{jX\zeta}\,dX \tag{603}$$

where $u(X,\psi')$ is given by (585). The evaluation of U_3 begins with the evaluation of the derivative of $u(X,\psi')$ with respect to ψ'. Again, we wish to use integration-by-parts to make the evaluation easier. Therefore if we recognize

$$\begin{aligned} \frac{1}{X}\,\frac{\partial u(X,\psi')}{\partial\psi'} &= \frac{1}{2\pi jnX}\int_\Gamma \left\{\frac{\partial}{\partial\psi'}\,G_h(\xi)\right\}\,e^{jX\cos\xi}\,d\xi \\ &= \frac{-1}{2\pi jnX}\int_\Gamma \left\{\frac{\partial}{\partial\xi}\,G_s(\xi)\right\}\,e^{jX\cos\xi}\,d\xi \end{aligned} \tag{604}$$

where

$$G_s(\xi) = \frac{\sin\left(\frac{\psi'}{n}\right)}{\cos\left(\frac{\xi}{n}\right) - \cos\left(\frac{\psi'}{n}\right)} \tag{605}$$

we obtain a form that can be integrated by parts. Using integration-by-parts, (604) becomes

$$\frac{1}{X}\,\frac{\partial u(X,\psi')}{\partial\psi'} = \frac{-1}{2\pi jnX}\,G_s(\xi)\,e^{jX\cos\xi}\Big|_{-\pi+j\infty}^{\pi+j\infty}$$

$$+ \quad \frac{1}{2\pi jnX} \int_{\Gamma} G_s(\xi) \, \frac{\partial}{\partial \xi} \left(e^{jX \cos \xi} \right) \, d\xi$$

$$= \quad \frac{-1}{2\pi n} \int_{\Gamma} \sin \xi \, G_s(\xi) \, e^{jX \cos \xi} \, d\xi \tag{606}$$

and it is important to recognize that the value of the integrand at $\pm\pi + j\infty$ is zero. Again, the contour of integration is deformed from Γ to Γ' to ensure convergence. Including the residue contributions from the poles that are crossed,

$$\frac{1}{X} \frac{\partial u(X, \psi')}{\partial \psi'} = \frac{-1}{2\pi n} \int_{\Gamma'} \sin \xi \, G_s(\xi) \, e^{jX \cos \xi} \, d\xi$$

$$+ \sum_m \frac{\sin \xi_m \sin \left(\frac{\psi'}{n} \right)}{\sin \left(\frac{\xi_m}{n} \right)} \, e^{jX \cos \xi_m} \tag{607}$$

which is now in a form that allows us to interchange the order of integration. Substituting (607) into (603) we obtain

$$U_3 = \int_0 \frac{-1}{2\pi n} \int_{\Gamma'} \sin \xi \, G_s(\xi) \, e^{jX(\cos \xi + \zeta)} \, d\xi \, dX$$

$$+ \sum_m \int_0 \frac{\sin \xi_m \sin \left(\frac{\psi'}{n} \right)}{\sin \left(\frac{\xi_m}{n} \right)} \, e^{jX(\cos \xi_m + \zeta)} \, dX \tag{608}$$

where by interchanging the order of integration

$$U_3 = \frac{-1}{2\pi n} \int_{\Gamma'} \int_0 \sin \xi \, G_s(\xi) \, e^{jX(\cos \xi + \zeta)} \, dX \, d\xi$$

$$+ \sum_m \int_0 \frac{\sin \xi_m \sin \left(\frac{\psi'}{n} \right)}{\sin \left(\frac{\xi_m}{n} \right)} \, e^{jX(\cos \xi_m + \zeta)} \, dX \, . \tag{609}$$

The integration with respect to X is performed,

$$U_3 = \frac{-1}{2\pi jn} \int_{\Gamma'} \frac{\sin \xi \, G_s(\xi)}{\cos \xi + \zeta} \, e^{jX(\cos \xi + \zeta)} \Bigg|_0 \, d\xi$$

$$+ \sum_m \frac{-j \sin \xi_m \sin \left(\frac{\psi'}{n} \right)}{\sin \left(\frac{\xi_m}{n} \right) \left\{ \cos \xi_m + \zeta \right\}} \, e^{jX(\cos \xi_m + \zeta)} \Bigg|_0 , \tag{610}$$

resulting in

$$U_3 = \frac{1}{2\pi jn} \int_{\Gamma'} \frac{\sin \xi \, G_s(\xi)}{\cos \xi + \zeta} \, d\xi + \sum_m \frac{j \sin \xi_m \sin \left(\frac{\psi'}{n} \right)}{\sin \left(\frac{\xi_m}{n} \right) \left\{ \cos \xi_m + \zeta \right\}} \tag{611}$$

as the edge contribution of U_3. Enclosing the contour at infinity as shown in Figure 70 and using the Cauchy Residue Theorem,

$$\begin{aligned} U_3 &= \sum_m \frac{-j \sin\xi_m \sin\left(\frac{\psi'}{n}\right)}{\sin\left(\frac{\xi_m}{n}\right)\left\{\cos\xi_m + \zeta\right\}} + G_s^o(\alpha) + \sum_m \frac{j \sin\xi_m \sin\left(\frac{\psi'}{n}\right)}{\sin\left(\frac{\xi_m}{n}\right)\left\{\cos\xi_m + \zeta\right\}} \\ &= G_s^o(\alpha) \end{aligned} \tag{612}$$

where

$$\begin{aligned} G_s^o(\alpha) &= \frac{-\frac{1}{n}\sin\left(\frac{\psi'}{n}\right)}{\cos\left(\frac{\pi-\alpha}{n}\right) - \cos\left(\frac{\psi'}{n}\right)} \\ &= \frac{-1}{2n}\left[\cot\left(\frac{\pi-(\alpha-\psi')}{2n}\right) - \cot\left(\frac{\pi-(\alpha+\psi')}{2n}\right)\right] \end{aligned} \tag{613}$$

is a soft diffraction coefficient in the spectral domain.

The expressions for U_1, U_2 and U_3 obtained here are identical to those reported by Michaeli [21, 22]. It is seen that for all three integrals, the results are proportional to the soft and hard diffraction coefficients corresponding to the 0-face as expected.

Appendix B

Uniform Asymptotic Expansions for Evaluating Integrals with Three Collinear and Equally Spaced Stationary Phase Points

The problem of asymptotically evaluating an integral near a cusp requires a uniform asymptotic expansion for an integral with three coalescing stationary phase points. The method used here was first presented by Chester, Friedman and Ursell [18] who derived a uniform asymptotic expansion for a contour integral with two coalescing saddle points. This method was later extended by Bleistein [39] to include many saddle points and algebraic singularities. Later, Ursell [40] confirmed Bleistein's result with more mathematical rigor. Most recently, this method was studied by Martin [46] to accurately determine the regions of validity of these uniform asymptotic expansions. An expansion similar to the one derived here can be found in [47, 48] except only the leading term is retained there. Also, the arguments of certain quantities are left undefined. The expansion derived here retains the first two non-vanishing terms and completely defines all quantities.

1 Canonical Integral Mapping

Let us consider an integral of the form

$$I_m(K) = \int_{-\infty}^{\infty} (z - z_c)^m g(z) e^{jKf(z)} dz \tag{614}$$

where $g(z)$ is a smooth, slowly varying and even function of z about $z = z_c$ such that $g(z_c) \neq 0$ and $f(z)$ has three equally spaced, collinear stationary phase points at $\bar{z}_s = (-z_{nc}, z_c, +z_{nc})$ defined such that $f^{\mathrm{I}}(\bar{z}_s) \equiv f^{\mathrm{III}}(\bar{z}_s) \equiv 0$. The subscripts c and nc are used to denote the central and non-central stationary phase points, respectively. It is also assumed that K is a large real number and m is a real and even integer greater then or equal to 0.

This integral must be mapped to an integral with the simplest possible phase function that has the same critical point structure as the initial integral. We begin by making the substitution

$$f(z) = F(t) = \mu t^4 + 2\eta a t^2 + b \tag{615}$$

where $\mu = \operatorname{sgn}\{f^{\mathrm{IV}}(z_c)\}$ and $\eta = \operatorname{sgn}\{f^{\mathrm{II}}(z_c)\}$. It is clearly seen that $F(t)$ has three equally spaced, collinear stationary phase points at $\bar{t}_s = (-t_{nc}, t_c, +t_{nc}) = (-\sqrt{-\mu\eta a}, 0, +\sqrt{-\mu\eta a})$.

The constants a and b must now be determined. To do so, we require that the stationary phase points in the t plane coalesce when the stationary phase points in the z plane coalesce. Therefore, if we map $f(\bar{z}_s) \rightarrow F(\bar{t}_s)$ we get

$$b = f(z_c) \tag{616}$$

and

$$a = \pm\sqrt{|f(z_{nc}) - f(z_c)|} \tag{617}$$

where the sign of a must be determined. Two conditions must be satisfied in order to completely determine the sign of a. If μ and η have the same sign, $f(z)$ has one real stationary phase point and two complex conjugate stationary phase points. Also, if μ and η have opposite signs, $f(z)$ has three real stationary phase points. Enforcing these conditions on $F(t)$ we find

$$a = \left|\sqrt{f(z_{nc}) - f(z_c)}\right|. \tag{618}$$

To properly map $(z - z_c)^m g(z)$ to the t plane, we make the substitution

$$G_m(t) = g(z)\frac{dz}{dt}\left(\frac{z - z_c}{t}\right)^m \tag{619}$$

which results in the integral

$$I_m(K) = \int_{-\infty}^{\infty} t^m G_m(t) e^{jKF(t)} dt \tag{620}$$

where $G_m(t)$ is an analytic function of t. $G_m(t)$ must be expanded in a series to obtain a uniform asymptotic expansion of $I_m(K)$.

2 A Uniform Asymptotic Expansion Using the Chester, Friedman and Ursell Technique

Since $G_m(t)$ is an analytic function, we can expand it in terms of the power series

$$\begin{aligned} G_m(t) &= \sum_{n=0}^{\infty} (a_n + b_n t + c_n t^2)(4\mu t^3 + 4\eta a t)^n \\ &= a_0 + b_0 t + c_0 t^2 + \sum_{n=1}^{\infty} (a_n + b_n t + c_n t^2)(4\mu t^3 + 4\eta a t)^n \end{aligned} \tag{621}$$

where a_n, b_n and c_n must be determined. Substituting this into (620) we obtain

$$\begin{aligned} I_m(K) \sim\ & a_0 \int_{-\infty}^{\infty} t^m e^{jKF(t)} dt + b_0 \int_{-\infty}^{\infty} t^{m+1} e^{jKF(t)} dt + c_0 \int_{-\infty}^{\infty} t^{m+2} e^{jKF(t)} dt \\ & + \int_{-\infty}^{\infty} \sum_{n=1}^{\infty} (a_n + b_n t + c_n t^2)(4\mu t^3 + 4\eta a t)^n t^m e^{jKF(t)} dt \end{aligned} \tag{622}$$

where the last term is the remainder of the asymptotic expansion and will be given by

$$I_m^R(K) = \int_{-\infty}^{\infty} \sum_{n=1}^{\infty} (a_n + b_n t + c_n t^2)(4\mu t^3 + 4\eta a t)^n t^m e^{jKF(t)} dt. \tag{623}$$

If we now define the canonical integral as

$$J_k(K) = \int_{-\infty}^{\infty} t^k e^{jKF(t)} dt \tag{624}$$

(622) is given by

$$I_m(K) \sim a_0 J_m(K) + b_0 J_{m+1}(K) + c_0 J_{m+2}(K) + I_m^R(K). \tag{625}$$

We now want to reduce the canonical integral $J_k(K)$ to a standard form. Making the variable substitutions

$$\xi = \frac{-j2K\eta a}{\sqrt{-j2K\mu}} = \left| \sqrt{2K[f(z_{nc}) - f(z_c)]} \right| e^{j(\mu - 2\eta)\pi/4} \tag{626}$$

and

$$p = (2K)^{1/4} t e^{-j\mu\pi/8} \tag{627}$$

in (624) and deforming the contour of integration back to the real axis we obtain the integral

$$J_k(K) = \frac{e^{jKf(z_c)} e^{\xi^2/2}}{(-j2K\mu)^{(k+1)/4}} \int_{-\infty}^{\infty} p^k e^{-\frac{1}{2}(\xi+p^2)^2} dp. \tag{628}$$

A Parabolic Cylinder function of order $-\nu$ and argument ξ is defined by [47, 48]

$$D_{-\nu}(\xi) = \frac{2e^{\xi^2/4}}{\Gamma(\nu)} \int_0^{\infty} p^{2\nu-1} e^{-\frac{1}{2}(\xi+p^2)^2} dp \quad ; \ \mathrm{Re}(\nu) > 0. \tag{629}$$

The canonical integral in (628) can be written in terms of these Parabolic Cylinder functions. Rewriting (629) and solving for the integral we get

$$\int_{-\infty}^{\infty} p^{2\nu-1} e^{-\frac{1}{2}(\xi+p^2)^2} dp = \left[1 + \frac{1}{(-1)^{2\nu-1}}\right] \frac{\Gamma(\nu) e^{-\xi^2/4}}{2} D_{-\nu}(\xi) \tag{630}$$

which is of the same form as the canonical integral in (628). Using this relation in (628) we get

$$\begin{aligned} J_k(K) &= \frac{\Gamma\left(\frac{k+1}{2}\right) e^{jKf(z_c)} e^{\xi^2/4}}{(-j2K\mu)^{(k+1)/4}} D_{-\left(\frac{k+1}{2}\right)}(\xi) \\ &= \frac{\sqrt{2\pi}\,(k+1)!!\ e^{jKf(z_c)} e^{\xi^2/4}}{(k+1)\,2^{(k+1)/2}(-j2K\mu)^{(k+1)/4}} D_{-\left(\frac{k+1}{2}\right)}(\xi) \end{aligned} \tag{631}$$

if k is even, and

$$J_k(K) = 0 \tag{632}$$

if k is odd. The double factorial function in (631) is define as

$$(k+1)!! = 1 \cdot 3 \cdot 5 \cdot \ldots \cdot (k-3) \cdot (k-1) \cdot (k+1) \tag{633}$$

for even k greater than or equal to zero.

From (621) we can solve for a_0, b_0 and c_0 by letting $t = \bar{t}_s$ and solving the system of three equations. This results in the constants

$$a_0 = G_m(t_c), \tag{634}$$

$$b_0 = \frac{G_m(t_{nc}) - G_m(-t_{nc})}{2t_{nc}} \tag{635}$$

and

$$c_0 = \frac{G_m(t_{nc}) + G_m(-t_{nc}) - 2G_m(t_c)}{2t_{nc}^2} \tag{636}$$

which are in terms of the three quantities $G_m(\bar{t}_s)$. To find $G_m(t)$ from (619) we begin by differentiating both sides of (615) with respect to t to get

$$\frac{dz}{dt} = \frac{F^{\mathrm{I}}(t)}{f^{\mathrm{I}}(z)} = \frac{4\mu t^3 + 4\eta a t}{f^{\mathrm{I}}(z)}. \tag{637}$$

This equation is not defined at the stationary phase points because we found $\bar{z}_s$ and $\bar{t}_s$ by requiring $f^{\mathrm{I}}(\bar{z}_s) \equiv 0$ and $F^{\mathrm{I}}(\bar{t}_s) \equiv 0$, respectively. Using l'Hôpital's rule on (637), it can be shown that

$$\left(\frac{dz}{dt}\right)^2 = \frac{12\mu t^2 + 4\eta a}{f^{\mathrm{II}}(z)}. \tag{638}$$

Therefore, at $t = t_c$ and $z = z_c$,

$$\left(\frac{dz}{dt}\right)_c^2 = \frac{4\eta a}{f^{\mathrm{II}}(z_c)} = \frac{4a}{|f^{\mathrm{II}}(z_c)|} > 0. \tag{639}$$

Requiring that the path of integration at $z = z_c$ remains unchanged by the mapping (i.e., $\frac{dz}{dt} > 0$),

$$\left(\frac{dz}{dt}\right)_c = \left|\sqrt{\frac{4a}{f^{\mathrm{II}}(z_c)}}\right| \tag{640}$$

which allows us to write

$$G_m(t_c) = g(z_c)\left(\frac{dz}{dt}\right)_c \left(\lim_{\substack{z\to z_c \\ t\to t_c}} \frac{z - z_c}{t}\right)^m. \tag{641}$$

Using l'Hôpital's rule to find the limit in (641),

$$G_m(t_c) = g(z_c)\left(\frac{dz}{dt}\right)_c^{m+1} = g(z_c)\left|\frac{4a}{f^{\mathrm{II}}(z_c)}\right|^{\frac{m+1}{2}}. \tag{642}$$

Similarly, at $t = t_{nc}$ and $z = z_{nc}$,

$$\left(\frac{dz}{dt}\right)_{nc}^2 = \frac{-8\eta a}{f^{\mathrm{II}}(z_{nc})} \tag{643}$$

where we must determine $\operatorname{sgn}\{f^{\mathrm{II}}(z_{nc})\}$ to ensure the proper mapping. Expanding $f(z)$ in a Taylor series around $z = z_c$ and differentiating twice with respect to z we

obtain three equations:

$$f(z) \approx f(z_c) + \frac{1}{2}f^{II}(z_c)(z-z_c)^2 + \frac{1}{24}f^{IV}(z_c)(z-z_c)^4 \quad (644)$$

$$f^{I}(z) \approx f^{II}(z_c)(z-z_c) + \frac{1}{6}f^{IV}(z_c)(z-z_c)^3 \quad (645)$$

$$f^{II}(z) \approx f^{II}(z_c) + \frac{1}{2}f^{IV}(z_c)(z-z_c)^2. \quad (646)$$

Since $f^{I}(z_{nc}) \equiv 0$ we can evaluate (645) at $z = z_{nc}$ and equate it to zero and get

$$\frac{1}{2}f^{IV}(z_c)(z_{nc}-z_c)^2 \approx -3f^{II}(z_c). \quad (647)$$

Next, evaluating (646) at $z = z_{nc}$ and substituting in (647) we arrive at

$$f^{II}(z_{nc}) \approx -2f^{II}(z_c). \quad (648)$$

Finally, we have found that

$$\operatorname{sgn}\{f^{II}(z_{nc})\} = -\operatorname{sgn}\{f^{II}(z_c)\} = -\eta, \quad (649)$$

and using this result in (643) we obtain

$$\left(\frac{dz}{dt}\right)^2_{nc} = \frac{8a}{|f^{II}(z_{nc})|} > 0. \quad (650)$$

Requiring that the path of integration at $z = z_{nc}$ remains unchanged by the mapping (i.e., $\frac{dz}{dt} > 0$),

$$\left(\frac{dz}{dt}\right)_{nc} = \left|\sqrt{\frac{8a}{f^{II}(z_{nc})}}\right| \quad (651)$$

which allows us to write

$$\begin{aligned} G_m(t_{nc}) &= g(z_{nc})\left(\frac{dz}{dt}\right)_{nc}\left(\frac{z_{nc}-z_c}{t_{nc}}\right)^m \\ &= g(z_{nc})\left|\sqrt{\frac{8a}{f^{II}(z_{nc})}}\right|\left(\frac{z_{nc}-z_c}{t_{nc}}\right)^m. \end{aligned} \quad (652)$$

This is the final item required for the uniform asymptotic expansion.

The leading term of the uniform asymptotic expansion is found by substituting (631), (634) and (642) into (625) such that

$$\begin{aligned} a_0 J_m(K) &= g(z_c)\frac{\sqrt{2\pi}}{|Kf^{II}(z_c)|^{(m+1)/2}}\frac{(m+1)!!}{m+1}e^{j\eta(m+1)\pi/4}e^{jKf(z_c)} \\ &\quad \times\left\{\xi^{(m+1)/2}e^{\xi^2/4}D_{-\left(\frac{m+1}{2}\right)}(\xi)\right\} \end{aligned} \quad (653)$$

where ξ is defined in (626). Since m is an even integer that is greater than or equal to zero, $m+1$ is an odd integer that is greater than or equal to one. From (632), $J_k(K) = 0$ for odd k; therefore, $b_0 J_{m+1}(K) = 0$. This means that the second term of the uniform asymptotic expansion is zero. This is a result of the fact that the stationary phase points are equally spaced. The third term in the uniform asymptotic expansion is determined by substituting (631), (636), (642) and (652) into (625)

$$\begin{aligned} c_0 J_{m+2}(K) &= g(z_c)\frac{\sqrt{2\pi}}{|Kf^{II}(z_c)|^{(m+1)/2}}\frac{(m+1)!!}{m+1}e^{j\eta(m+1)\pi/4}e^{jKf(z_c)} \\ &\quad \times\left\{\frac{m+1}{2}\xi^{(m-1)/2}e^{\xi^2/4}D_{-(\frac{m+3}{2})}(\xi)\right\} \\ &+ 2(z_{nc}-z_c)^m g(z_{nc})\left|\sqrt{\frac{2\pi}{Kf^{II}(z_{nc})}}\right|e^{-j\eta\pi/4}e^{jKf(z_{nc})} \\ &\quad \times\left\{(-1)^{m/2}\frac{\eta(m+1)!!}{2j(2\xi)^{(m+1)/2}}e^{-\xi^2/4}D_{-(\frac{m+3}{2})}(\xi)\right\} \end{aligned} \tag{654}$$

where ξ is again defined in (626). The terms can now be regrouped and transition functions for the central and non-central stationary phase contributions defined as

$$\begin{aligned} T_c(\xi,m) &= \xi^{(m+1)/2}e^{\xi^2/4}D_{-(\frac{m+1}{2})}(\xi) \\ &+ \frac{m+1}{2}\xi^{(m-1)/2}e^{\xi^2/4}D_{-(\frac{m+3}{2})}(\xi) \end{aligned} \tag{655}$$

and

$$T_{nc}(\xi,\eta,m) = (-1)^{m/2}\frac{\eta(m+1)!!}{2j(2\xi)^{(m+1)/2}}e^{-\xi^2/4}D_{-(\frac{m+3}{2})}(\xi), \tag{656}$$

respectively. Therefore, the uniform asymptotic expansion of $I_m(K)$ is

$$\begin{aligned} I_m(K) &\sim g(z_c)\frac{\sqrt{2\pi}}{|Kf^{II}(z_c)|^{(m+1)/2}}\frac{(m+1)!!}{m+1}e^{j\eta(m+1)\pi/4}e^{jKf(z_c)}T_c(\xi,m) \\ &+ 2(z_{nc}-z_c)^m g(z_{nc})\left|\sqrt{\frac{2\pi}{Kf^{II}(z_{nc})}}\right|e^{-j\eta\pi/4}e^{jKf(z_{nc})}T_{nc}(\xi,\eta,m) \\ &+ I_m^R(K). \end{aligned} \tag{657}$$

The transition functions are used to correct the non-uniform stationary phase contributions from the central and non-central stationary phase points. The inclusion of these transition functions properly accounts for the three nearly coincident stationary phase points.

3 A Uniform Asymptotic Expansion Using the Classical Stationary Phase Technique

One of the drawbacks of the expansion developed in Section 2 is that when the non-central stationary phase points are complex, $g(z)$ may be an extremely difficult function to evaluate at the complex point $z = z_{nc}$. Therefore, it is advantageous to derive an alternate uniform asymptotic expansion in this region. As explained earlier, if μ and η both have the same sign, $f(z)$ has one real stationary phase point and two complex conjugate stationary phase points. When this is the case, we can expand $G_m(t)$ in a Maclaurin series around $t = t_c = 0$. That is, let

$$\begin{aligned} G_m(t) &= \sum_{n=0}^{\infty} \frac{G_m^{(n)}(0)}{n!} t^n \\ &= G_m^{(0)}(0) + G_m^{(1)}(0)\, t + \frac{1}{2} G_m^{(2)}(0)\, t^2 + \sum_{n=3}^{\infty} \frac{G_m^{(n)}(0)}{n!} t^n. \end{aligned} \tag{658}$$

Substituting this into (620) we obtain

$$\begin{aligned} I_m(K) \sim\ & G_m^{(0)}(0) \int_{-\infty}^{\infty} t^m e^{jKF(t)} dt + G_m^{(1)}(0) \int_{-\infty}^{\infty} t^{m+1} e^{jKF(t)} dt \\ &+ \frac{1}{2} G_m^{(2)}(0) \int_{-\infty}^{\infty} t^{m+2} e^{jKF(t)} dt \\ &+ \sum_{n=3}^{\infty} \frac{G_m^{(n)}(0)}{n!} \int_{-\infty}^{\infty} t^{m+n} e^{jKF(t)} dt \end{aligned} \tag{659}$$

where the last term is the remainder of the asymptotic expansion and will be given by

$$I_m^R(K) = \sum_{n=3}^{\infty} \frac{G_m^{(n)}(0)}{n!} \int_{-\infty}^{\infty} t^{m+n} e^{jKF(t)} dt = \sum_{n=3}^{\infty} \frac{G_m^{(n)}(0)}{n!} J_{m+n}(K) \tag{660}$$

and $J_k(K)$ is the canonical integral defined in (624). Since $J_{m+1}(K) = 0$ as explained in Section 2 we get

$$I_m(K) \sim G_m^{(0)}(0) J_m(K) + \frac{1}{2} G_m^{(2)}(0) J_{m+2}(K) + I_m^R(K). \tag{661}$$

Also from Section 2, we recognize

$$G_m^{(0)}(0) = G_m(t_c) = g(z_c) \left(\frac{dz}{dt}\right)_c^{m+1} = g(z_c) \left| \frac{4a}{f^{\,\mathrm{II}}(z_c)} \right|^{\frac{m+1}{2}} \tag{662}$$

and note that the leading two terms of this expansion are identical to the leading two terms of the expansion presented in Section 2 since $a_0 = G_m(t_c)$. Therefore, it remains to find $G_m^{(2)}(0)$. Differentiating (619) twice with respect to t and using l'Hôpital's rule, it can be shown that

$$\begin{aligned} G_m^{(2)}(0) &= g^{\text{II}}(z_c)\left(\frac{dz}{dt}\right)_c^{m+3} + (3+m)g^{\text{I}}(z_c)\left(\frac{dz}{dt}\right)_c^{m+1}\left(\frac{d^2z}{dt^2}\right)_c \\ &+ m\left(1+\frac{m-1}{4}\right)g(z_c)\left(\frac{dz}{dt}\right)_c^{m-1}\left(\frac{d^2z}{dt^2}\right)_c^2 \\ &+ \left(1+\frac{m}{3}\right)g(z_c)\left(\frac{dz}{dt}\right)_c^{m}\left(\frac{d^3z}{dt^3}\right)_c . \end{aligned} \tag{663}$$

The differentials in (663) are determined by successively differentiating (615) with respect to t to get:

$$f(z) = \mu t^4 + 2\eta a t^2 + b \tag{664}$$

$$f^{\text{I}}(z)\left(\frac{dz}{dt}\right) = 4\mu t^3 + 4\eta a t \tag{665}$$

$$f^{\text{II}}(z)\left(\frac{dz}{dt}\right)^2 + f^{\text{I}}(z)\left(\frac{d^2z}{dt^2}\right) = 12\mu t^2 + 4\eta a \tag{666}$$

$$f^{\text{III}}(z)\left(\frac{dz}{dt}\right)^3 + 3f^{\text{II}}(z)\left(\frac{dz}{dt}\right)\left(\frac{d^2z}{dt^2}\right) + f^{\text{I}}(z)\left(\frac{d^3z}{dt^3}\right) = 24\mu t \tag{667}$$

$$\begin{aligned} &f^{\text{IV}}(z)\left(\frac{dz}{dt}\right)^4 + 6f^{\text{III}}(z)\left(\frac{dz}{dt}\right)^2\left(\frac{d^2z}{dt^2}\right) \\ &+f^{\text{II}}(z)\left[3\left(\frac{d^2z}{dt^2}\right)^2 + 4\left(\frac{dz}{dt}\right)\left(\frac{d^3z}{dt^3}\right)\right] + f^{\text{I}}(z)\left(\frac{d^4z}{dt^4}\right) = 24\mu \end{aligned} \tag{668}$$

Evaluating (666) at $z = z_c$ and $t = t_c = 0$, and recalling that $f^{\text{I}}(z_c) \equiv 0$ we find

$$\left(\frac{dz}{dt}\right)_c = \left|\sqrt{\frac{4a}{f^{\text{II}}(z_c)}}\right| \tag{669}$$

which is the same as (640) in Section 2. Next, evaluating (667) at $z = z_c$ and $t = t_c = 0$, and recalling that $f^{\text{I}}(z_c) \equiv f^{\text{III}}(z_c) \equiv 0$ we find

$$\left(\frac{d^2z}{dt^2}\right)_c = 0. \tag{670}$$

Lastly, evaluating (668) at $z = z_c$ and $t = t_c = 0$, and recalling that $f^{\text{I}}(z_c) \equiv f^{\text{III}}(z_c) \equiv 0$ and (670) we find

$$\left(\frac{dz}{dt}\right)_c \left(\frac{d^3z}{dt^3}\right)_c = \frac{6\mu}{f^{\text{II}}(z_c)} - \frac{f^{\text{IV}}(z_c)}{4f^{\text{II}}(z_c)} \left(\frac{dz}{dt}\right)_c^4. \tag{671}$$

Therefore, substituting (669) through (671) into (663) we obtain

$$\begin{aligned} G_m^{(2)}(0) &= g^{\text{II}}(z_c) \left|\frac{4a}{f^{\text{II}}(z_c)}\right|^{\frac{m+3}{2}} + g(z_c) \left|\frac{4a}{f^{\text{II}}(z_c)}\right|^{\frac{m+3}{2}} \left(\frac{3+m}{12}\right) \\ &\quad \times \left\{\frac{3|Kf^{\text{II}}(z_c)|}{|\xi|^2} - \frac{Kf^{\text{IV}}(z_c)}{Kf^{\text{II}}(z_c)}\right\} \end{aligned} \tag{672}$$

where ξ is defined in (626). Finally, substituting (631), (662) and (672) into (661) and simplifying, the uniform asymptotic expansion of $I_m(K)$ is

$$\begin{aligned} I_m(K) &\sim g(z_c) \frac{\sqrt{2\pi}}{|Kf^{\text{II}}(z_c)|^{(m+1)/2}} \frac{(m+1)!!}{m+1} e^{j\eta(m+1)\pi/4} e^{jKf(z_c)} T_s(\xi, m) \\ &+ g^{\text{II}}(z_c) \frac{\sqrt{2\pi}(m+1)!!}{2|Kf^{\text{II}}(z_c)|^{(m+3)/2}} e^{j\eta(m+3)\pi/4} e^{jKf(z_c)} T_s(\xi, m+2) \\ &+ g(z_c) \frac{\sqrt{2\pi}(m+1)!!}{2|Kf^{\text{II}}(z_c)|^{(m+3)/2}} e^{j\eta(m+3)\pi/4} e^{jKf(z_c)} \left(\frac{3+m}{12}\right) \\ &\quad \times \left\{\frac{3|Kf^{\text{II}}(z_c)|}{|\xi|^2} - \frac{Kf^{\text{IV}}(z_c)}{Kf^{\text{II}}(z_c)}\right\} T_s(\xi, m+2) + I_m^R(K) \end{aligned} \tag{673}$$

where the transition function is defined as

$$T_s(\xi, k) = \xi^{(k+1)/2} e^{\xi^2/4} D_{-\left(\frac{k+1}{2}\right)}(\xi) \tag{674}$$

with ξ being given in (626). It is important to recall that this asymptotic expansion is valid only if $f(z)$ has one real stationary phase point and two complex conjugate stationary phase points (i.e., $\mu = \eta$). Again, the transition function is used to correct the non-uniform stationary phase contributions when the three stationary phase points are nearly coincident.

4 Verification of Uniformity

In order to show the results in Sections 2 and 3 are uniform, two things must be shown. First, it must be shown that the uniform asymptotic expansion in Section 2

and the uniform asymptotic expansion in Section 3 are approximately equal near the point where the three stationary phase points coalesce. Second, it must be shown that these asymptotic expansions give a bounded result near the point where the three stationary phase points coalesce. This includes the fact that in the limit as $|f^{II}(z_c)| \to 0$, both expansions must reduce to the known result for an integral with a third-order stationary phase point.

It is a simple task to verify the first of these conditions. The first two terms of each expansion are identical since $a_0 = G_m^{(0)}(0)$ and the second term in each expansion is zero as pointed out in Section 3. Therefore, it remains to be shown that the third term of each expansion is approximately equal when $z_{nc} \approx z_c$. To show this, we recognize that in the limit as $z_{nc} \to z_c$ the constant c_0 in (636) is proportional to the limit form of the second derivative of $G_m(t)$. More specifically,

$$c_0 \approx \frac{1}{2} G_m^{(2)}(0) \tag{675}$$

for $z_{nc} \approx z_c$. It is now easy to see that this agrees with the third term in the Maclaurin expansion of $G_m(t)$ used in Section 3. Therefore, if $z_{nc} \approx z_c$ the uniform asymptotic expansion developed in Section 2 reduces to the uniform asymptotic expansion developed in Section 3.

The expansion in Section 3 must be bounded for $z_{nc} \approx z_c$ to verify the second condition. We must determine the small argument form of the argument of these transition functions since the transition functions are used to correct for the nearly coincident stationary phase points. We begin by evaluating (644) at $z = z_{nc}$ and recombining terms to obtain

$$f(z_{nc}) - f(z_c) \approx \frac{1}{24} f^{IV}(z_c)(z_{nc} - z_c)^4 + \frac{1}{2} f^{II}(z_c)(z_{nc} - z_c)^2 \tag{676}$$

for $z_{nc} \approx z_c$. Next, since $f^{I}(z_{nc}) \equiv 0$, we evaluate (645) at $z = z_{nc}$ and equate it to zero to obtain

$$(z_{nc} - z_c)^2 \approx \frac{-6 f^{II}(z_c)}{f^{IV}(z_c)} \tag{677}$$

which is substituted into (676) to get

$$|f(z_{nc}) - f(z_c)| \approx \frac{3}{2} \frac{|f^{II}(z_c)|^2}{|f^{IV}(z_c)|}. \tag{678}$$

Finally, substituting (678) into (626) we end up with

$$\xi \approx |Kf^{II}(z_c)|\sqrt{\frac{3}{|Kf^{IV}(z_c)|}}\, e^{j(\mu-2\eta)\pi/4} \tag{679}$$

which is the small argument form of the argument of the transition functions. This result is identical to the transition function argument used in [12].

The transition function in (674) can be approximated now that an approximation of ξ has been obtained for $f^{II}(z_c) \to 0$. An approximate form of the transition function is found by substituting (679) into (674)

$$\begin{aligned} T_s(\xi,k) \;\approx\; & |Kf^{II}(z_c)|^{(k+1)/2}\left[\frac{3}{|Kf^{IV}(z_c)|}\right]^{\frac{k+1}{4}} e^{j\mu(k+1)\pi/8} \\ & \times e^{-j\eta(k+1)\pi/4}\, e^{\xi^2/4}\, D_{-\left(\frac{k+1}{2}\right)}(\xi) \end{aligned} \tag{680}$$

where the approximate form of ξ given by (679) is to be used in this equation. This result can also be used to show

$$\left\{\frac{3|Kf^{II}(z_c)|}{|\xi|^2} - \frac{Kf^{IV}(z_c)}{Kf^{II}(z_c)}\right\} \approx 0, \tag{681}$$

which implies that the last term in (673) corrects for the slope near the point of coalescence. Using this fact and the approximate form of the transition function given by (680), (673) can be approximated for small ξ as

$$\begin{aligned} I_m(K) \;\sim\; & g(z_c)\sqrt{2\pi}\,\frac{(m+1)!!}{m+1}\left[\frac{3}{|Kf^{IV}(z_c)|}\right]^{\frac{m+1}{4}} e^{j\mu(m+1)\pi/8} \\ & \times e^{jKf(z_c)}\, e^{\xi^2/4}\, D_{-\left(\frac{m+1}{2}\right)}(\xi) \\ + \;\; & g^{II}(z_c)\sqrt{\frac{\pi}{2}}(m+1)!!\left[\frac{3}{|Kf^{IV}(z_c)|}\right]^{\frac{m+3}{4}} e^{j\mu(m+3)\pi/8} \\ & \times e^{jKf(z_c)}\, e^{\xi^2/4}\, D_{-\left(\frac{m+3}{2}\right)}(\xi) + I_m^R(K) \end{aligned} \tag{682}$$

which is valid for $f^{II}(z_c) \to 0$. It is easy to see that for small ξ this is a bounded result. Therefore, the final condition to be shown is that for $\xi = 0$, this reduces to the known solution for an integral with a third-order stationary phase point.

Referring to Appendix C, it is a simple task to show that

$$e^{\xi^2/4}\, D_{-\left(\frac{k+1}{2}\right)}(\xi)\,\Big|_{\xi=0} = D_{-\left(\frac{k+1}{2}\right)}(0) = \frac{\sqrt{\pi}}{2^{(k+1)/4}\Gamma\left(\frac{k+3}{4}\right)}\,. \tag{683}$$

Therefore, substituting (683) into (682) we obtain

$$I_m(K) \sim g(z_c)\frac{\sqrt{2}\pi}{\Gamma\left(\frac{m+3}{4}\right)}\frac{(m+1)!!}{(m+1)}\left[\frac{3}{2|Kf^{\text{IV}}(z_c)|}\right]^{\frac{m+1}{4}} \times e^{j\mu(m+1)\pi/8}\, e^{jKf(z_c)}$$
$$+ g^{\text{II}}(z_c)\frac{\sqrt{2}\pi}{\Gamma\left(\frac{m+5}{4}\right)}\frac{(m+1)!!}{2}\left[\frac{3}{2|Kf^{\text{IV}}(z_c)|}\right]^{\frac{m+3}{4}} \times e^{j\mu(m+3)\pi/8}\, e^{jKf(z_c)} + I_m^R(K) \qquad (684)$$

which is recognizable as the first two non-vanishing terms of the asymptotic expansion for an integral with a third-order stationary phase point.

Appendix C

Parabolic Cylinder Functions

An efficient means of calculating Parabolic Cylinder functions is required when examining the field near the cusp of a caustic caused by the coalescence of three equally spaced diffraction points. This appendix contains definitions, a series formula, large argument formulas, relationships between certain orders of Parabolic Cylinder functions and modified Bessel functions and other useful properties.

A Parabolic Cylinder function can be defined as the solution of the differential equation

$$\frac{d^2u}{dz^2} - \left(a + \frac{z^2}{4}\right) u = 0 \tag{685}$$

which has four linearly dependent solutions

$$u = D_{-(a+1/2)}(z),\ \ D_{-(a+1/2)}(-z),\ \ D_{(a-1/2)}(jz),\ \ D_{(a-1/2)}(-jz) \tag{686}$$

as defined in [49]. The standard solution used here is taken to be the first of these which has an integral form [47, 48, 49, 50]

$$D_{-(a+1/2)}(z) = \frac{e^{-z^2/4}}{\Gamma\left(a+\frac{1}{2}\right)} \int_0^\infty t^{(a-1/2)}\, e^{-\frac{1}{2}t^2 - zt}\, dt \tag{687}$$

$$= \frac{2e^{z^2/4}}{\Gamma\left(a+\frac{1}{2}\right)} \int_0^\infty t^{2a}\, e^{-\frac{1}{2}(z+t^2)^2}\, dt \tag{688}$$

for $\mathrm{Re}\left(a+\frac{1}{2}\right) > 0$. It is easily seen from the integral form of the solution that Parabolic Cylinder functions contain the proper form to be used in the study of the field near the cusp of a caustic caused by the coalescence of three equally spaced diffraction points.

From [50] the series form of the Parabolic Cylinder function is

$$D_{-(a+1/2)}(z) = \frac{\sqrt{\pi}}{2^{(2a+1)/4}\Gamma\left(\frac{2a+3}{4}\right)}\, y_1(z,a) \; - \; \frac{\sqrt{\pi}}{2^{(2a-1)/4}\Gamma\left(\frac{2a+1}{4}\right)}\, y_2(z,a) \tag{689}$$

where

$$y_1(z,a) = \sum_{n=0}^{\infty} \mathcal{A}_{2n} \frac{z^{2n}}{(2n)!} \tag{690}$$

and

$$y_2(z,a) = \sum_{n=0}^{\infty} \mathcal{B}_{2n+1} \frac{z^{2n+1}}{(2n+1)!} \tag{691}$$

are two auxiliary power series. The coefficients of $y_1(z,a)$ and $y_2(z,a)$ can be calculated recursively using

$$\mathcal{A}_0 = 1 \tag{692}$$

$$\mathcal{A}_2 = a \tag{693}$$

$$\mathcal{A}_{2n} = a\,\mathcal{A}_{2n-2} + \frac{(2n-2)(2n-3)}{4}\,\mathcal{A}_{2n-4} \tag{694}$$

and

$$\mathcal{B}_1 = 1 \tag{695}$$

$$\mathcal{B}_3 = a \tag{696}$$

$$\mathcal{B}_{2n+1} = a\,\mathcal{B}_{2n-1} + \frac{(2n-1)(2n-2)}{4}\,\mathcal{B}_{2n-3}, \tag{697}$$

respectively. A useful quantity that can be obtained from this series is

$$D_{-(a+1/2)}(0) = \frac{\sqrt{\pi}}{2^{(2a+1)/4}\Gamma\left(\frac{2a+3}{4}\right)} \tag{698}$$

for $z = 0$. Although this series is an exact solution, it becomes computationally inefficient if $|z|$ becomes large. Therefore, it is best used to calculate Parabolic Cylinder functions if $|z|$ is small.

If $|z|$ is large, asymptotic expansions of the Parabolic Cylinder function can be used. From [49] with $|z| \gg 1$ and $|z| \gg |a + \frac{1}{2}|$, the asymptotic series must be divided into three separate regions depending on the argument of z. Therefore, as given in [49] the asymptotic series of the Parabolic Cylinder functions are

$$D_{-(a+1/2)}(z) \sim e^{-z^2/4} z^{-(a+1/2)}\, S_c(z,a) \tag{699}$$

for $|\arg(z)| < \frac{3\pi}{4}$,

$$D_{-(a+1/2)}(z) \sim e^{-z^2/4} z^{-(a+1/2)} S_c(z,a) - \frac{\sqrt{2\pi}}{\Gamma\left(a+\frac{1}{2}\right)} e^{-j(2a+1)\pi/2} e^{z^2/4} z^{(a-1/2)} S_{nc}(z,a) \quad (700)$$

for $\frac{\pi}{4} < \arg(z) < \frac{5\pi}{4}$ and

$$D_{-(a+1/2)}(z) \sim e^{-z^2/4} z^{-(a+1/2)} S_c(z,a) - \frac{\sqrt{2\pi}}{\Gamma\left(a+\frac{1}{2}\right)} e^{j(2a+1)\pi/2} e^{z^2/4} z^{(a-1/2)} S_{nc}(z,a) \quad (701)$$

for $\frac{3\pi}{4} < \arg(z) < \frac{7\pi}{4}$. All three of these asymptotic formulas are written in terms of the two auxiliary asymptotic series

$$S_c(z,a) = \sum_{n=0}^{\infty} (-1)^n \frac{\left(a+\frac{1}{2}\right)_{2n}}{(2n)!!\, z^{2n}} \quad (702)$$

corresponding to the central stationary phase point contribution and

$$S_{nc}(z,a) = \sum_{n=0}^{\infty} \frac{\left(-a+\frac{1}{2}\right)_{2n}}{(2n)!!\, z^{2n}} \quad (703)$$

corresponding to the non-central stationary phase point contributions. These series contain the function

$$(x)_{2n} = x \cdot (x+1) \cdot (x+2) \cdot \ldots \cdot (x+2n-2) \cdot (x+2n-1) \quad (704)$$

with $(x)_0 = 1$ and the double factorial function defined in [33]

$$(2n)!! = 2 \cdot 4 \cdot 6 \cdot \ldots \cdot (2n-2) \cdot (2n) \quad (705)$$

with $(0)!! = 1$. These asymptotic series can now be used to calculate Parabolic Cylinder functions with large arguments.

The relationship between modified Bessel functions and certain Parabolic Cylinder functions may be useful due to the abundance of computer subroutines for accurately calculating modified Bessel functions. In particular, the Parabolic Cylinder function can be written in terms of modified Bessel functions [50] for integer values of a. Therefore, for $a = 0$ and $|\arg(z)| < \frac{\pi}{2}$,

$$D_{-1/2}(z) = \sqrt{\frac{z}{2\pi}} K_{1/4}\left(\frac{1}{4}z^2\right) \quad (706)$$

and

$$D_{-1/2}(-z) = \sqrt{\frac{\pi z}{2}}\left[\sqrt{2}I_{1/4}\left(\frac{1}{4}z^2\right) + \frac{1}{\pi}K_{1/4}\left(\frac{1}{4}z^2\right)\right] \tag{707}$$

where $I_\mu(x)$ and $K_\mu(x)$ are modified Bessel functions of the first and second kind of order μ and argument x, respectively. For computational purposes, if $|z| \approx 0$,

$$D_{-1/2}(0) = \frac{\sqrt{\pi}}{2^{1/4}\Gamma\left(\frac{3}{4}\right)} = 1.216280215 \tag{708}$$

can be used. Also, for $a = 1$ and $|\arg(z)| < \frac{\pi}{2}$,

$$D_{-3/2}(z) = z\sqrt{\frac{z}{2\pi}}\left[K_{3/4}\left(\frac{1}{4}z^2\right) - K_{1/4}\left(\frac{1}{4}z^2\right)\right] \tag{709}$$

and

$$\begin{aligned} D_{-3/2}(-z) &= z\sqrt{\pi z}\left\{\left[I_{3/4}\left(\frac{1}{4}z^2\right) + I_{1/4}\left(\frac{1}{4}z^2\right)\right]\right. \\ &+ \left.\frac{1}{\sqrt{2\pi}}\left[K_{3/4}\left(\frac{1}{4}z^2\right) + K_{1/4}\left(\frac{1}{4}z^2\right)\right]\right\} \end{aligned} \tag{710}$$

where the modified Bessel functions are defined as before. Again, for computational purposes, if $|z| \approx 0$,

$$D_{-3/2}(0) = \frac{4\sqrt{\pi}}{2^{3/4}\Gamma\left(\frac{1}{4}\right)} = 1.162736634 \tag{711}$$

can be used. The recursion relation [49]

$$D_\nu(z) = \frac{z}{\nu+1}D_{\nu+1}(z) - \frac{1}{\nu+1}D_{\nu+2}(z) \tag{712}$$

should be used to obtain all other Parabolic Cylinder functions with orders that are integer multiples of these in order to reduce the computation time. It is important to note that this recursion relation is valid for all Parabolic Cylinder functions regardless of order or argument. Another important property that can be exploited in the computation of Parabolic Cylinder functions is

$$D_\nu(z^*) = D_\nu^*(z) \tag{713}$$

which can be used to limit the scope of computations.

As examples, two Parabolic Cylinder functions of different order are presented. These correspond to those required for the uniform asymptotic expansion developed

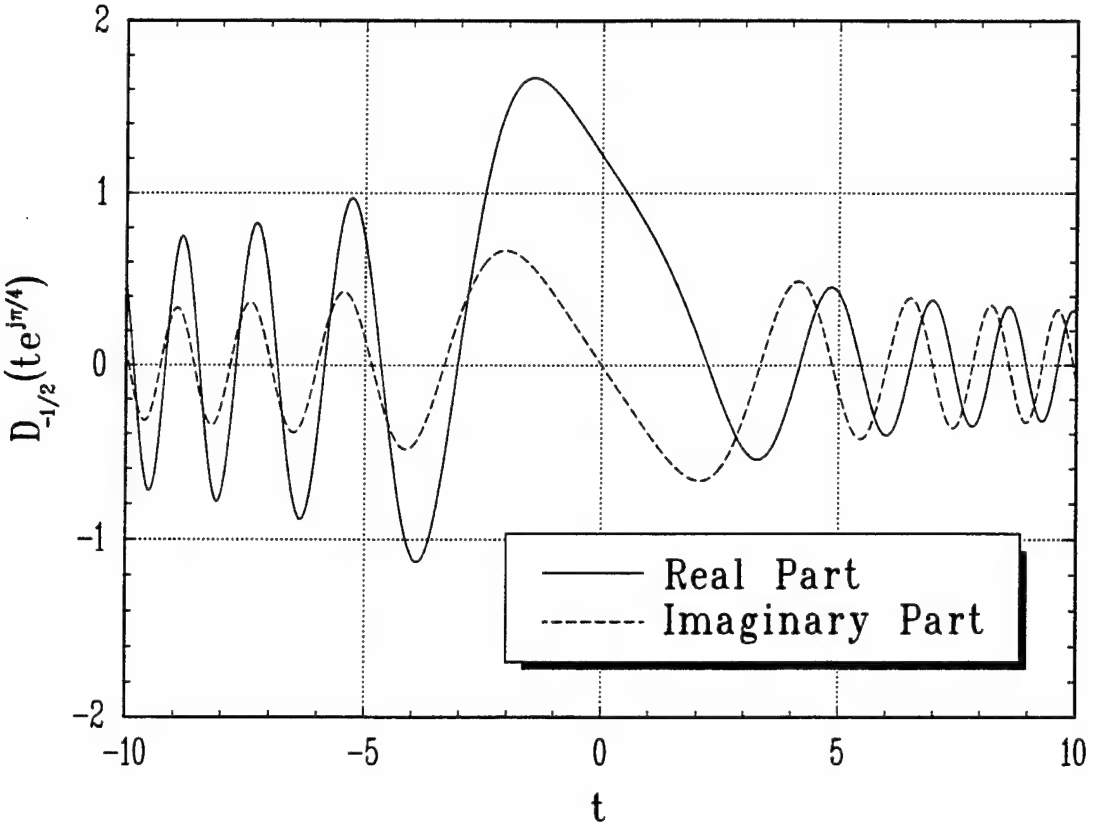

Figure 71: This is a plot of a Parabolic Cylinder function of order -0.5 (i.e., $a = 0$) and argument $z = te^{j\pi/4}$.

in Appendix B. Parabolic Cylinder functions of argument $z = te^{j\pi/4}$ and orders $-\frac{1}{2}$ and $-\frac{3}{2}$ are shown in Figures 71 and 72, respectively. It is important to note that all the Parabolic Cylinder functions required for the calculation of the transition functions in Appendix B can be obtained from these. These two results can be used in conjunction with the recursion relation in (712) to obtain the necessary order since the orders of all the Parabolic Cylinder functions are integer multiples of $-\frac{1}{2}$. Also, the conjugate relation in (713) can be used to obtain the proper argument since the argument of transition functions are restricted to $\arg(\xi) = \pm\frac{\pi}{4}, \pm\frac{3\pi}{4}$.

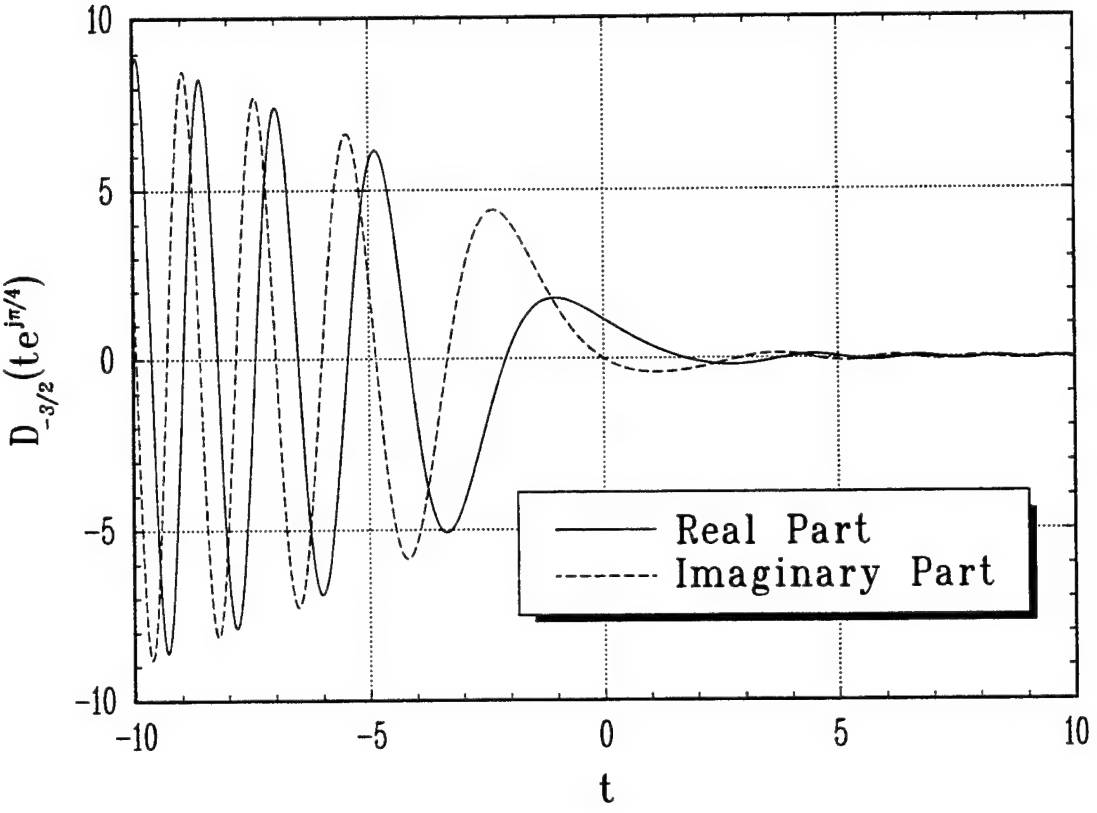

Figure 72: This is a plot of a Parabolic Cylinder function of order -1.5 (i.e., $a = 1$) and argument $z = te^{j\pi/4}$.

Appendix D

The Geometric Interpretation of the Phase Function, Diffraction Parameter and Half-Plane Diffraction Coefficient Derivatives Required for the Uniform Asymptotic Expansion of the Diffracted Field Integral Equations

Any asymptotic expansion depends on the derivatives of the phase and amplitude functions of the initial integral. These derivatives can be performed on an integral obtained for a specific problem, but they may be difficult to write in a geometry independent form. To alleviate this problem, these derivatives can be performed on general expressions using differential geometry. This appendix is devoted to the differentiation of the phase function, diffraction parameters and half-plane diffraction coefficients required for the use of the uniform asymptotic expansions derived in Appendix B.

1 Phase Function Derivatives

The first few derivatives of the phase function are required for both of the uniform asymptotic expansions of Sections 2 and 3. The second derivative of the phase function evaluated at the central and non-central stationary phase points are required for the expansion in Section 2. The second and fourth derivatives of the phase function evaluated at the central stationary phase point are required for the expansion in Section 3. This section is a derivation of the second and fourth derivatives of the phase function evaluated at the central stationary phase point and the second derivative of the phase function evaluated at the non-central stationary phase points. This is accomplished using differential geometry.

This derivation begins by writing the phase function in terms of some geometric parameters of the edge. This geometry is shown in Figure 73 and l is defined as the arc length along the edge from the origin to the diffraction point Q'. It should also be noted at this point that all derivatives in this section are performed with respect to arc length unless stated otherwise. The phase function of the diffraction integrals is

$$h(l) = -r_i(Q') - r_d(Q') \tag{714}$$

where,

$$\begin{aligned} r_i^2(Q') &= \left\{\left[\vec{R}_i + \vec{r}_e(Q')\right] \cdot \hat{b}\right\}^2 + \left\{\left[\vec{R}_i + \vec{r}_e(Q')\right] \cdot \hat{n}_e(Q')\right\}^2 \\ &+ \left\{\left[\vec{R}_i + \vec{r}_e(Q')\right] \cdot \hat{e}(Q')\right\}^2 \end{aligned} \tag{715}$$

and

$$\begin{aligned} r_d^2(Q') &= \left\{\left[\vec{R}_d - \vec{r}_e(Q')\right] \cdot \hat{b}\right\}^2 + \left\{\left[\vec{R}_d - \vec{r}_e(Q')\right] \cdot \hat{n}_e(Q')\right\}^2 \\ &+ \left\{\left[\vec{R}_d - \vec{r}_e(Q')\right] \cdot \hat{e}(Q')\right\}^2 . \end{aligned} \tag{716}$$

The parameters that are a function of arc length will be denoted by Q' to obtain a result that is consistent with the UTD. This will allow us to evaluate the results at different diffraction points and easily distinguish between them. The phase function itself will be left as a function of arc length to be consistent with the integral equation

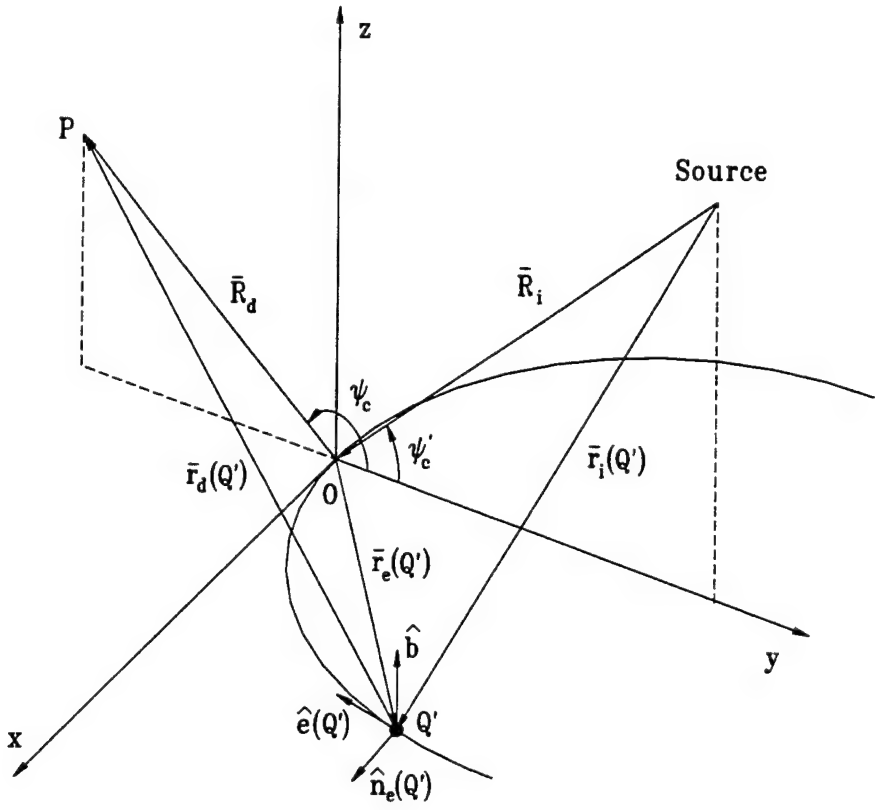

Figure 73: Geometric parameter definitions for the phase function derivatives of the diffraction integrals.

it came from. The chain rule will be used to differentiate these expressions; therefore, the derivatives of $\hat{n}_e(Q')$, $\hat{e}(Q')$ and $\vec{r}_e(Q')$ are performed first. The derivatives of the unit vectors $\hat{n}_e(Q')$ and $\hat{e}(Q')$ are known as the Serret-Frenet equations [51] and are

$$\hat{e}^{\,\mathrm{I}}(Q') = \kappa_g(Q')\,\hat{n}_e(Q') \tag{717a}$$

$$\hat{n}_e^{\,\mathrm{I}}(Q') = -\kappa_g(Q')\,\hat{e}(Q') \tag{717b}$$

where $\kappa_g(Q')$ is the curvature of the edge at a point, Q', of arc length l away from the origin. The first derivative of the position vector, $\vec{r}_e(Q')$, from the origin to the diffraction point is

$$\vec{r}_e^{\,\mathrm{I}}(Q') = -\,\hat{e}(Q') \tag{718}$$

from the definition of the tangent vector $\hat{e}(Q')$. By successively differentiating (718) and using the Serret-Frenet equations (717), we obtain the next five derivatives of the position vector as:

$$\vec{r}_e^{\,\mathrm{II}}(Q') = -\hat{e}^{\,\mathrm{I}}(Q') = -\kappa_g(Q')\,\hat{n}_e(Q') \tag{719}$$

$$\begin{aligned}\vec{r}_e^{\,\mathrm{III}}(Q') &= -\kappa_g^{\mathrm{I}}(Q')\,\hat{n}_e(Q') - \kappa_g(Q')\,\hat{n}_e^{\,\mathrm{I}}(Q') \\ &= -\kappa_g^{\mathrm{I}}(Q')\,\hat{n}_e(Q') + \kappa_g^2(Q')\,\hat{e}(Q')\end{aligned} \tag{720}$$

$$\begin{aligned}\vec{r}_e^{\,\mathrm{IV}}(Q') &= -\kappa_g^{\mathrm{II}}(Q')\,\hat{n}_e(Q') - \kappa_g^{\mathrm{I}}(Q')\,\hat{n}_e^{\,\mathrm{I}}(Q') \\ &\qquad +2\kappa_g(Q')\kappa_g^{\mathrm{I}}(Q')\,\hat{e}(Q') + \kappa_g^2(Q')\,\hat{e}^{\,\mathrm{I}}(Q') \\ &= -\left[\kappa_g^{\mathrm{II}}(Q') - \kappa_g^3(Q')\right]\hat{n}_e(Q') + 3\kappa_g(Q')\kappa_g^{\mathrm{I}}(Q')\,\hat{e}(Q')\end{aligned} \tag{721}$$

$$\begin{aligned}\vec{r}_e^{\,\mathrm{V}}(Q') &= -\kappa_g^{\mathrm{III}}(Q')\,\hat{n}_e(Q') - \kappa_g^{\mathrm{II}}(Q')\,\hat{n}_e^{\,\mathrm{I}}(Q') + 3\kappa_g^2(Q')\kappa_g^{\mathrm{I}}(Q')\,\hat{n}_e(Q') \\ &\qquad +\kappa_g^3(Q')\,\hat{n}_e^{\,\mathrm{I}}(Q') + 3\{\kappa_g^{\mathrm{I}}(Q')\}^2\,\hat{e}(Q') \\ &\qquad +3\kappa_g(Q')\kappa_g^{\mathrm{II}}(Q')\,\hat{e}(Q') + 3\kappa_g(Q')\kappa_g^{\mathrm{I}}(Q')\,\hat{e}^{\,\mathrm{I}}(Q') \\ &= \left[6\kappa_g^2(Q')\kappa_g^{\mathrm{I}}(Q') - \kappa_g^{\mathrm{III}}(Q')\right]\hat{n}_e(Q') \\ &\qquad + \left[4\kappa_g(Q')\kappa_g^{\mathrm{II}}(Q') - \kappa_g^4(Q') + 3\{\kappa_g^{\mathrm{I}}(Q')\}^2\right]\hat{e}(Q')\end{aligned} \tag{722}$$

$$\vec{r}_e^{\,\mathrm{VI}}(Q') = -\kappa_g^{\mathrm{IV}}(Q')\,\hat{n}_e(Q') - \kappa_g^{\mathrm{III}}(Q')\,\hat{n}_e^{\,\mathrm{I}}(Q') + 4\kappa_g^{\mathrm{I}}(Q')\kappa_g^{\mathrm{II}}(Q')\,\hat{e}(Q')$$

$$
\begin{aligned}
&+4\kappa_g(Q')\kappa_g^{\mathrm{III}}(Q')\,\widehat{e}\,(Q')+4\kappa_g(Q')\kappa_g^{\mathrm{II}}(Q')\,\widehat{e}^{\,\mathrm{I}}(Q')\\
&+12\kappa_g(Q')\{\kappa_g^{\mathrm{I}}(Q')\}^2\,\widehat{n}_e(Q')+6\kappa_g^2(Q')\kappa_g^{\mathrm{II}}(Q')\,\widehat{n}_e(Q')\\
&+6\kappa_g^2(Q')\kappa_g^{\mathrm{I}}(Q')\,\widehat{n}_e^{\,\mathrm{I}}(Q')-4\kappa_g^3(Q')\kappa_g^{\mathrm{I}}(Q')\,\widehat{e}\,(Q')\\
&-\kappa_g^4(Q')\,\widehat{e}^{\,\mathrm{I}}(Q')+6\kappa_g^{\mathrm{I}}(Q')\kappa_g^{\mathrm{II}}(Q')\,\widehat{e}\,(Q')+3\{\kappa_g^{\mathrm{I}}(Q')\}^2\,\widehat{e}^{\,\mathrm{I}}(Q')\\
=\;&\left[10\kappa_g^2(Q')\kappa_g^{\mathrm{II}}(Q')-\kappa_g^5(Q')-\kappa_g^{\mathrm{IV}}(Q')+15\kappa_g(Q')\{\kappa_g^{\mathrm{I}}(Q')\}^2\right]\widehat{n}_e(Q')\\
&+\left[5\kappa_g(Q')\kappa_g^{\mathrm{III}}(Q')+10\kappa_g^{\mathrm{I}}(Q')\kappa_g^{\mathrm{II}}(Q')\right.\\
&\left.-10\kappa_g^3(Q')\kappa_g^{\mathrm{I}}(Q')\right]\widehat{e}\,(Q') \qquad (723)
\end{aligned}
$$

Next, we wish to evaluate these derivatives at the central and non-central diffraction points. The central diffraction point, Q_c, is located at the origin of the coordinate system shown in Figure 73. Also, $\kappa_g^{\mathrm{I}}(Q_c)=\kappa_g^{\mathrm{III}}(Q_c)=0$ due to the symmetry of the assumed geometry. Therefore, the derivatives of the position vector evaluated at the central diffraction point are:

$$
\begin{aligned}
\vec{r}_e(Q_c) &= 0 && (724a)\\
\vec{r}_e^{\,\mathrm{I}}(Q_c) &= -\widehat{e}\,(Q_c) && (724b)\\
\vec{r}_e^{\,\mathrm{II}}(Q_c) &= -\kappa_g(Q_c)\,\widehat{n}_e(Q_c) && (724c)\\
\vec{r}_e^{\,\mathrm{III}}(Q_c) &= \kappa_g^2(Q_c)\,\widehat{e}\,(Q_c) && (724d)\\
\vec{r}_e^{\,\mathrm{IV}}(Q_c) &= -\left[\kappa_g^{\mathrm{II}}(Q_c)-\kappa_g^3(Q_c)\right]\widehat{n}_e(Q_c) && (724e)\\
\vec{r}_e^{\,\mathrm{V}}(Q_c) &= -\left[\kappa_g^4(Q_c)-4\kappa_g(Q_c)\kappa_g^{\mathrm{II}}(Q_c)\right]\widehat{e}\,(Q_c) && (724f)\\
\vec{r}_e^{\,\mathrm{VI}}(Q_c) &= -\left[\kappa_g^{\mathrm{IV}}(Q_c)-10\kappa_g^2(Q_c)\kappa_g^{\mathrm{II}}(Q_c)+\kappa_g^5(Q_c)\right]\widehat{n}_e(Q_c) && (724g)
\end{aligned}
$$

The non-central diffraction points, Q_{nc}, are assumed here to be located at an arc length of $l=l_{nc}$ from the origin of the coordinate system. Therefore, the derivatives of the position vector evaluated at the non-central diffraction points are:

$$
\begin{aligned}
\vec{r}_e^{\,\mathrm{I}}(Q_{nc}) &= -\widehat{e}\,(Q_{nc}) && (725a)\\
\vec{r}_e^{\,\mathrm{II}}(Q_{nc}) &= -\kappa_g(Q_{nc})\,\widehat{n}_e(Q_{nc}) && (725b)
\end{aligned}
$$

where only the first two derivatives are required by the uniform asymptotic expansion in Section 2.

The first derivative of $r_i(Q')$ can now be derived by differentiating both sides of (715) with respect to arc length l as

$$\begin{aligned} 2r_i(Q')r_i^{\mathrm{I}}(Q') &= 2\left\{\left[\vec{R}_i+\vec{r}_e(Q')\right]\cdot\hat{b}\right\}\left\{\vec{r}_e^{\,\mathrm{I}}(Q')\cdot\hat{b}\right\} \\ &+ 2\left\{\left[\vec{R}_i+\vec{r}_e(Q')\right]\cdot\hat{n}_e(Q')\right\}\left\{\vec{r}_e^{\,\mathrm{I}}(Q')\cdot\hat{n}_e(Q')\right. \\ &\qquad \left.+\left[\vec{R}_i+\vec{r}_e(Q')\right]\cdot\hat{n}_e^{\mathrm{I}}(Q')\right\} \\ &+ 2\left\{\left[\vec{R}_i+\vec{r}_e(Q')\right]\cdot\hat{e}(Q')\right\}\left\{\vec{r}_e^{\,\mathrm{I}}(Q')\cdot\hat{e}(Q')\right. \\ &\qquad \left.+\left[\vec{R}_i+\vec{r}_e(Q')\right]\cdot\hat{e}^{\mathrm{I}}(Q')\right\} \end{aligned} \tag{726}$$

where, by using (717) and simplifying, we obtain

$$\begin{aligned} r_i(Q')r_i^{\mathrm{I}}(Q') &= \left\{\left[\vec{R}_i+\vec{r}_e(Q')\right]\cdot\hat{b}\right\}\left\{\vec{r}_e^{\,\mathrm{I}}(Q')\cdot\hat{b}\right\} \\ &+ \left\{\left[\vec{R}_i+\vec{r}_e(Q')\right]\cdot\hat{n}_e(Q')\right\}\left\{\vec{r}_e^{\,\mathrm{I}}(Q')\cdot\hat{n}_e(Q')\right\} \\ &+ \left\{\left[\vec{R}_i+\vec{r}_e(Q')\right]\cdot\hat{e}(Q')\right\}\left\{\vec{r}_e^{\,\mathrm{I}}(Q')\cdot\hat{e}(Q')\right\}. \end{aligned} \tag{727}$$

Following a similar procedure, the first derivative of $r_d(Q')$ is

$$\begin{aligned} r_d(Q')r_d^{\mathrm{I}}(Q') &= -\left\{\left[\vec{R}_d-\vec{r}_e(Q')\right]\cdot\hat{b}\right\}\left\{\vec{r}_e^{\,\mathrm{I}}(Q')\cdot\hat{b}\right\} \\ &- \left\{\left[\vec{R}_d-\vec{r}_e(Q')\right]\cdot\hat{n}_e(Q')\right\}\left\{\vec{r}_e^{\,\mathrm{I}}(Q')\cdot\hat{n}_e(Q')\right\} \\ &- \left\{\left[\vec{R}_d-\vec{r}_e(Q')\right]\cdot\hat{e}(Q')\right\}\left\{\vec{r}_e^{\,\mathrm{I}}(Q')\cdot\hat{e}(Q')\right\}. \end{aligned} \tag{728}$$

It is now a simple task to show that the first derivatives of $r_i(Q')$ and $r_d(Q')$ are

$$r_i^{\mathrm{I}}(Q_c) = r_d^{\mathrm{I}}(Q_c) = 0 \tag{729}$$

at the central diffraction point and

$$r_i^{\mathrm{I}}(Q_{nc}) = -\cos\beta'_{nc} \tag{730}$$

and

$$r_d^{\mathrm{I}}(Q_{nc}) = \cos\beta_{nc}\,; \tag{731}$$

respectively, at the non-central diffraction points.

Next, the second derivative of $r_i(Q')$ is determined by differentiating both sides of (727) with respect to arc length,

$$\begin{aligned}
[r_i^{\mathrm{I}}(Q')]^2 \;+\; & r_i(Q')r_i^{\mathrm{II}}(Q') = \left\{\vec{r}_e^{\,\mathrm{I}}(Q')\cdot\hat{b}\right\}^2 + \left\{\left[\vec{R}_i+\vec{r}_e(Q')\right]\cdot\hat{b}\right\}\left\{\vec{r}_e^{\,\mathrm{II}}(Q')\cdot\hat{b}\right\} \\
+\; & \left\{\vec{r}_e^{\,\mathrm{I}}(Q')\cdot\hat{n}_e(Q')\right\}^2 + \left\{\left[\vec{R}_i+\vec{r}_e(Q')\right]\cdot\hat{n}_e^{\,\mathrm{I}}(Q')\right\}\left\{\vec{r}_e^{\,\mathrm{I}}(Q')\cdot\hat{n}_e(Q')\right\} \\
+\; & \left\{\left[\vec{R}_i+\vec{r}_e(Q')\right]\cdot\hat{n}_e(Q')\right\}\left\{\vec{r}_e^{\,\mathrm{II}}(Q')\cdot\hat{n}_e(Q')+\vec{r}_e^{\,\mathrm{I}}(Q')\cdot\hat{n}_e^{\,\mathrm{I}}(Q')\right\} \\
+\; & \left\{\vec{r}_e^{\,\mathrm{I}}(Q')\cdot\hat{e}(Q')\right\}^2 + \left\{\left[\vec{R}_i+\vec{r}_e(Q')\right]\cdot\hat{e}^{\,\mathrm{I}}(Q')\right\}\left\{\vec{r}_e^{\,\mathrm{I}}(Q')\cdot\hat{e}(Q')\right\} \\
+\; & \left\{\left[\vec{R}_i+\vec{r}_e(Q')\right]\cdot\hat{e}(Q')\right\}\left\{\vec{r}_e^{\,\mathrm{II}}(Q')\cdot\hat{e}(Q')+\vec{r}_e^{\,\mathrm{I}}(Q')\cdot\hat{e}^{\,\mathrm{I}}(Q')\right\} \qquad (732)
\end{aligned}$$

where, using (717) and simplifying, we obtain

$$\begin{aligned}
[r_i^{\mathrm{I}}(Q')]^2 \;+\; & r_i(Q')r_i^{\mathrm{II}}(Q') = \left\{\vec{r}_e^{\,\mathrm{I}}(Q')\cdot\hat{b}\right\}^2 + \left\{\vec{r}_e^{\,\mathrm{I}}(Q')\cdot\hat{n}_e(Q')\right\}^2 \\
+\; & \left\{\vec{r}_e^{\,\mathrm{I}}(Q')\cdot\hat{e}(Q')\right\}^2 \\
+\; & \left\{\left[\vec{R}_i+\vec{r}_e(Q')\right]\cdot\hat{b}\right\}\left\{\vec{r}_e^{\,\mathrm{II}}(Q')\cdot\hat{b}\right\} \\
+\; & \left\{\left[\vec{R}_i+\vec{r}_e(Q')\right]\cdot\hat{n}_e(Q')\right\}\left\{\vec{r}_e^{\,\mathrm{II}}(Q')\cdot\hat{n}_e(Q')\right\} \\
+\; & \left\{\left[\vec{R}_i+\vec{r}_e(Q')\right]\cdot\hat{e}(Q')\right\}\left\{\vec{r}_e^{\,\mathrm{II}}(Q')\cdot\hat{e}(Q')\right\}. \qquad (733)
\end{aligned}$$

Following a similar procedure, we obtain

$$\begin{aligned}
[r_d^{\mathrm{I}}(Q')]^2 \;+\; & r_d(Q')r_d^{\mathrm{II}}(Q') = \left\{\vec{r}_e^{\,\mathrm{I}}(Q')\cdot\hat{b}\right\}^2 + \left\{\vec{r}_e^{\,\mathrm{I}}(Q')\cdot\hat{n}_e(Q')\right\}^2 \\
+\; & \left\{\vec{r}_e^{\,\mathrm{I}}(Q')\cdot\hat{e}(Q')\right\}^2 \\
-\; & \left\{\left[\vec{R}_d-\vec{r}_e(Q')\right]\cdot\hat{b}\right\}\left\{\vec{r}_e^{\,\mathrm{II}}(Q')\cdot\hat{b}\right\} \\
-\; & \left\{\left[\vec{R}_d-\vec{r}_e(Q')\right]\cdot\hat{n}_e(Q')\right\}\left\{\vec{r}_e^{\,\mathrm{II}}(Q')\cdot\hat{n}_e(Q')\right\} \\
-\; & \left\{\left[\vec{R}_d-\vec{r}_e(Q')\right]\cdot\hat{e}(Q')\right\}\left\{\vec{r}_e^{\,\mathrm{II}}(Q')\cdot\hat{e}(Q')\right\} \qquad (734)
\end{aligned}$$

as the second derivative $r_d(Q')$ with respect to arc length. Evaluating (733) at the central diffraction point,

$$r_i^{\mathrm{II}}(Q_c) = \frac{1}{R_i} - \kappa_g(Q_c)\left[\hat{R}_i\cdot\hat{n}_e(Q_c)\right] - \frac{\left[\hat{R}_i\cdot\hat{e}(Q_c)\right]^2}{R_i} \qquad (735)$$

where, for a plane wave incidence (i.e., $R_i\to\infty$) and $\hat{R}_i\cdot\hat{n}_e(Q_c)=\cos\psi_c'$,

$$r_i^{\mathrm{II}}(Q_c) = -\kappa_g(Q_c)\left[\hat{R}_i\cdot\hat{n}_e(Q_c)\right] = -\kappa_g(Q_c)\cos\psi_c'. \qquad (736)$$

Also, evaluating (734) at the central diffraction point,

$$r_d^{\text{II}}(Q_c) = \frac{1}{s_c} + \kappa_g(Q_c)\left[\widehat{R}_d \cdot \widehat{n}_e(Q_c)\right] - \frac{\left[\widehat{R}_d \cdot \widehat{e}\,(Q_c)\right]^2}{s_c} \tag{737}$$

and since $\widehat{R}_d \cdot \widehat{n}_e(Q_c) = -\cos\psi_c$ and $\widehat{R}_d \cdot \widehat{e}\,(Q_c) = 0$,

$$r_d^{\text{II}}(Q_c) = \frac{1}{s_c} - \kappa_g(Q_c)\cos\psi_c. \tag{738}$$

Evaluating (733) at the non-central diffraction points,

$$r_i^{\text{II}}(Q_{nc}) = \frac{1}{s_i} - \kappa_g(Q_{nc})\left[\widehat{s}\,' \cdot \widehat{n}_e(Q_{nc})\right] - \frac{\left[\widehat{s}\,' \cdot \widehat{e}\,(Q_{nc})\right]^2}{s_i} \tag{739}$$

where for a plane wave incidence (i.e., $s_i \to \infty$)

$$r_i^{\text{II}}(Q_{nc}) = -\kappa_g(Q_{nc})\left[\widehat{s}\,' \cdot \widehat{n}_e(Q_{nc})\right]. \tag{740}$$

Also, evaluating (734) at the non-central diffraction points,

$$r_d^{\text{II}}(Q_{nc}) = \frac{1}{s_{nc}} + \kappa_g(Q_{nc})\left[\widehat{s} \cdot \widehat{n}_e(Q_{nc})\right] - \frac{\left[\widehat{s} \cdot \widehat{e}\,(Q_{nc})\right]^2}{s_{nc}} \tag{741}$$

and since $\widehat{s} \cdot \widehat{e}\,(Q_{nc}) = \cos\beta_{nc}$ we get,

$$r_d^{\text{II}}(Q_{nc}) = \frac{\sin^2\beta_{nc}}{s_{nc}} + \kappa_g(Q_{nc})\left[\widehat{s} \cdot \widehat{n}_e(Q_{nc})\right]. \tag{742}$$

This completes the derivation of the second derivatives.

The third derivative of (715) is found by differentiating both sides of (733) with respect to arc length

$$\begin{aligned}
3r_i^{\text{I}}(Q')r_i^{\text{II}}(Q') \;+\; & r_i(Q')r_i^{\text{III}}(Q') = 3\left\{\vec{r}_e^{\,\text{I}}(Q') \cdot \widehat{b}\right\}\left\{\vec{r}_e^{\,\text{II}}(Q') \cdot \widehat{b}\right\} \\
+\; & 2\left\{\vec{r}_e^{\,\text{I}}(Q') \cdot \widehat{n}_e(Q')\right\}\left\{\vec{r}_e^{\,\text{II}}(Q') \cdot \widehat{n}_e(Q') + \vec{r}_e^{\,\text{I}}(Q') \cdot \widehat{n}_e^{\,\text{I}}(Q')\right\} \\
+\; & 2\left\{\vec{r}_e^{\,\text{I}}(Q') \cdot \widehat{e}\,(Q')\right\}\left\{\vec{r}_e^{\,\text{II}}(Q') \cdot \widehat{e}\,(Q') + \vec{r}_e^{\,\text{I}}(Q') \cdot \widehat{e}^{\,\text{I}}(Q')\right\} \\
+\; & \left\{\left[\vec{R}_i + \vec{r}_e(Q')\right] \cdot \widehat{b}\right\}\left\{\vec{r}_e^{\,\text{III}}(Q') \cdot \widehat{b}\right\} \\
+\; & \left\{\vec{r}_e^{\,\text{I}}(Q') \cdot \widehat{n}_e(Q') + \left[\vec{R}_i + \vec{r}_e(Q')\right] \cdot \widehat{n}_e^{\,\text{I}}(Q')\right\}\left\{\vec{r}_e^{\,\text{II}}(Q') \cdot \widehat{n}_e(Q')\right\} \\
+\; & \left\{\left[\vec{R}_i + \vec{r}_e(Q')\right] \cdot \widehat{n}_e(Q')\right\}\left\{\vec{r}_e^{\,\text{III}}(Q') \cdot \widehat{n}_e(Q') + \vec{r}_e^{\,\text{II}}(Q') \cdot \widehat{n}_e^{\,\text{I}}(Q')\right\} \\
+\; & \left\{\vec{r}_e^{\,\text{I}}(Q') \cdot \widehat{e}\,(Q') + \left[\vec{R}_i + \vec{r}_e(Q')\right] \cdot \widehat{e}^{\,\text{I}}(Q')\right\}\left\{\vec{r}_e^{\,\text{II}}(Q') \cdot \widehat{e}\,(Q')\right\} \\
+\; & \left\{\left[\vec{R}_i + \vec{r}_e(Q')\right] \cdot \widehat{e}\,(Q')\right\}\left\{\vec{r}_e^{\,\text{III}}(Q') \cdot \widehat{e}\,(Q')\right. \\
& \qquad \left. + \vec{r}_e^{\,\text{II}}(Q') \cdot \widehat{e}^{\,\text{I}}(Q')\right\}
\end{aligned} \tag{743}$$

which, using (717) and simplifying, results in

$$\begin{aligned} 3r_i^{\mathrm{I}}(Q')r_i^{\mathrm{II}}(Q') \;+\; & r_i(Q')r_i^{\mathrm{III}}(Q') = 3\left\{\vec{r}_e^{\,\mathrm{I}}(Q')\cdot\hat{b}\right\}\left\{\vec{r}_e^{\,\mathrm{II}}(Q')\cdot\hat{b}\right\} \\ & + 3\left\{\vec{r}_e^{\,\mathrm{I}}(Q')\cdot\hat{n}_e(Q')\right\}\left\{\vec{r}_e^{\,\mathrm{II}}(Q')\cdot\hat{n}_e(Q')\right\} \\ & + 3\left\{\vec{r}_e^{\,\mathrm{I}}(Q')\cdot\hat{e}(Q')\right\}\left\{\vec{r}_e^{\,\mathrm{II}}(Q')\cdot\hat{e}(Q')\right\} \\ & + \left\{\left[\vec{R}_i+\vec{r}_e(Q')\right]\cdot\hat{b}\right\}\left\{\vec{r}_e^{\,\mathrm{III}}(Q')\cdot\hat{b}\right\} \\ & + \left\{\left[\vec{R}_i+\vec{r}_e(Q')\right]\cdot\hat{n}_e(Q')\right\}\left\{\vec{r}_e^{\,\mathrm{III}}(Q')\cdot\hat{n}_e(Q')\right\} \\ & + \left\{\left[\vec{R}_i+\vec{r}_e(Q')\right]\cdot\hat{e}(Q')\right\}\left\{\vec{r}_e^{\,\mathrm{III}}(Q')\cdot\hat{e}(Q')\right\}. \end{aligned} \tag{744}$$

Following a similar approach, the third derivative of $r_d(Q')$ is

$$\begin{aligned} 3r_d^{\mathrm{I}}(Q')r_d^{\mathrm{II}}(Q') \;+\; & r_d(Q')r_d^{\mathrm{III}}(Q') = 3\left\{\vec{r}_e^{\,\mathrm{I}}(Q')\cdot\hat{b}\right\}\left\{\vec{r}_e^{\,\mathrm{II}}(Q')\cdot\hat{b}\right\} \\ & + 3\left\{\vec{r}_e^{\,\mathrm{I}}(Q')\cdot\hat{n}_e(Q')\right\}\left\{\vec{r}_e^{\,\mathrm{II}}(Q')\cdot\hat{n}_e(Q')\right\} \\ & + 3\left\{\vec{r}_e^{\,\mathrm{I}}(Q')\cdot\hat{e}(Q')\right\}\left\{\vec{r}_e^{\,\mathrm{II}}(Q')\cdot\hat{e}(Q')\right\} \\ & - \left\{\left[\vec{R}_d-\vec{r}_e(Q')\right]\cdot\hat{b}\right\}\left\{\vec{r}_e^{\,\mathrm{III}}(Q')\cdot\hat{b}\right\} \\ & - \left\{\left[\vec{R}_d-\vec{r}_e(Q')\right]\cdot\hat{n}_e(Q')\right\}\left\{\vec{r}_e^{\,\mathrm{III}}(Q')\cdot\hat{n}_e(Q')\right\} \\ & - \left\{\left[\vec{R}_d-\vec{r}_e(Q')\right]\cdot\hat{e}(Q')\right\}\left\{\vec{r}_e^{\,\mathrm{III}}(Q')\cdot\hat{e}(Q')\right\} \end{aligned} \tag{745}$$

with respect to arc length. Since we only need the third derivative of the phase function at the central diffraction point,

$$r_i^{\mathrm{III}}(Q_c) = r_d^{\mathrm{III}}(Q_c) = 0 \tag{746}$$

which completes the required third derivatives. Now only the fourth derivative of the phase function must be found.

Finally, the fourth derivative of (715) is found by differentiating both sides of (744) with respect to arc length

$$\begin{aligned} 3\left[r_i^{\mathrm{II}}(Q')\right]^2 \;+\; & 4r_i^{\mathrm{I}}(Q')r_i^{\mathrm{III}}(Q') + r_i(Q')r_i^{\mathrm{IV}}(Q') = \\ & 3\left\{\vec{r}_e^{\,\mathrm{II}}(Q')\cdot\hat{b}\right\}^2 + 4\left\{\vec{r}_e^{\,\mathrm{I}}(Q')\cdot\hat{b}\right\}\left\{\vec{r}_e^{\,\mathrm{III}}(Q')\cdot\hat{b}\right\} \\ & + 3\left\{\vec{r}_e^{\,\mathrm{II}}(Q')\cdot\hat{n}_e(Q') + \vec{r}_e^{\,\mathrm{I}}(Q')\cdot\hat{n}_e^{\,\mathrm{I}}(Q')\right\}\left\{\vec{r}_e^{\,\mathrm{II}}(Q')\cdot\hat{n}_e(Q')\right\} \\ & + 3\left\{\vec{r}_e^{\,\mathrm{I}}(Q')\cdot\hat{n}_e(Q')\right\}\left\{\vec{r}_e^{\,\mathrm{III}}(Q')\cdot\hat{n}_e(Q') + \vec{r}_e^{\,\mathrm{II}}(Q')\cdot\hat{n}_e^{\,\mathrm{I}}(Q')\right\} \end{aligned}$$

$$
\begin{aligned}
&+ 3\{\vec{r}_e^{\,\mathrm{II}}(Q')\cdot\hat{e}(Q')+\vec{r}_e^{\,\mathrm{I}}(Q')\cdot\hat{e}^{\mathrm{I}}(Q')\}\{\vec{r}_e^{\,\mathrm{II}}(Q')\cdot\hat{e}(Q')\}\\
&+ 3\{\vec{r}_e^{\,\mathrm{I}}(Q')\cdot\hat{e}(Q')\}\{\vec{r}_e^{\,\mathrm{III}}(Q')\cdot\hat{e}(Q')+\vec{r}_e^{\,\mathrm{II}}(Q')\cdot\hat{e}^{\mathrm{I}}(Q')\}\\
&+ \left\{\left[\vec{R}_i+\vec{r}_e(Q')\right]\cdot\hat{b}\right\}\left\{\vec{r}_e^{\,\mathrm{IV}}(Q')\cdot\hat{b}\right\}\\
&+ \left\{\vec{r}_e^{\,\mathrm{I}}(Q')\cdot\hat{n}_e(Q')+\left[\vec{R}_i+\vec{r}_e(Q')\right]\cdot\hat{n}_e^{\mathrm{I}}(Q')\right\}\{\vec{r}_e^{\,\mathrm{III}}(Q')\cdot\hat{n}_e(Q')\}\\
&+ \left\{\left[\vec{R}_i+\vec{r}_e(Q')\right]\cdot\hat{n}_e(Q')\right\}\{\vec{r}_e^{\,\mathrm{IV}}(Q')\cdot\hat{n}_e(Q')+\vec{r}_e^{\,\mathrm{III}}(Q')\cdot\hat{n}_e^{\mathrm{I}}(Q')\}\\
&+ \left\{\vec{r}_e^{\,\mathrm{I}}(Q')\cdot\hat{e}(Q')+\left[\vec{R}_i+\vec{r}_e(Q')\right]\cdot\hat{e}^{\mathrm{I}}(Q')\right\}\{\vec{r}_e^{\,\mathrm{III}}(Q')\cdot\hat{e}(Q')\}\\
&+ \left\{\left[\vec{R}_i+\vec{r}_e(Q')\right]\cdot\hat{e}(Q')\right\}\{\vec{r}_e^{\,\mathrm{IV}}(Q')\cdot\hat{e}(Q')\\
&\qquad +\vec{r}_e^{\,\mathrm{III}}(Q')\cdot\hat{e}^{\mathrm{I}}(Q')\} \qquad (747)
\end{aligned}
$$

where, after using (717) and simplifying, we obtain

$$
\begin{aligned}
3\left[r_i^{\mathrm{II}}(Q')\right]^2 &+ 4r_i^{\mathrm{I}}(Q')r_i^{\mathrm{III}}(Q')+r_i(Q')r_i^{\mathrm{IV}}(Q')=\\
&\quad 3\left\{\vec{r}_e^{\,\mathrm{II}}(Q')\cdot\hat{b}\right\}^2+4\left\{\vec{r}_e^{\,\mathrm{I}}(Q')\cdot\hat{b}\right\}\left\{\vec{r}_e^{\,\mathrm{III}}(Q')\cdot\hat{b}\right\}\\
&+ 3\{\vec{r}_e^{\,\mathrm{II}}(Q')\cdot\hat{n}_e(Q')\}^2+4\{\vec{r}_e^{\,\mathrm{I}}(Q')\cdot\hat{n}_e(Q')\}\{\vec{r}_e^{\,\mathrm{III}}(Q')\cdot\hat{n}_e(Q')\}\\
&+ 3\{\vec{r}_e^{\,\mathrm{II}}(Q')\cdot\hat{e}(Q')\}^2+4\{\vec{r}_e^{\,\mathrm{I}}(Q')\cdot\hat{e}(Q')\}\{\vec{r}_e^{\,\mathrm{III}}(Q')\cdot\hat{e}(Q')\}\\
&+ \left\{\left[\vec{R}_i+\vec{r}_e(Q')\right]\cdot\hat{b}\right\}\left\{\vec{r}_e^{\,\mathrm{IV}}(Q')\cdot\hat{b}\right\}\\
&+ \left\{\left[\vec{R}_i+\vec{r}_e(Q')\right]\cdot\hat{n}_e(Q')\right\}\{\vec{r}_e^{\,\mathrm{IV}}(Q')\cdot\hat{n}_e(Q')\}\\
&+ \left\{\left[\vec{R}_i+\vec{r}_e(Q')\right]\cdot\hat{e}(Q')\right\}\{\vec{r}_e^{\,\mathrm{IV}}(Q')\cdot\hat{e}(Q')\}. \qquad (748)
\end{aligned}
$$

Following a similar procedure on (745) we obtain

$$
\begin{aligned}
3\left[r_d^{\mathrm{II}}(Q')\right]^2 &+ 4r_d^{\mathrm{I}}(Q')r_d^{\mathrm{III}}(Q')+r_d(Q')r_d^{\mathrm{IV}}(Q')=\\
&\quad 3\left\{\vec{r}_e^{\,\mathrm{II}}(Q')\cdot\hat{b}\right\}^2+4\left\{\vec{r}_e^{\,\mathrm{I}}(Q')\cdot\hat{b}\right\}\left\{\vec{r}_e^{\,\mathrm{III}}(Q')\cdot\hat{b}\right\}\\
&+ 3\{\vec{r}_e^{\,\mathrm{II}}(Q')\cdot\hat{n}_e(Q')\}^2+4\{\vec{r}_e^{\,\mathrm{I}}(Q')\cdot\hat{n}_e(Q')\}\{\vec{r}_e^{\,\mathrm{III}}(Q')\cdot\hat{n}_e(Q')\}\\
&+ 3\{\vec{r}_e^{\,\mathrm{II}}(Q')\cdot\hat{e}(Q')\}^2+4\{\vec{r}_e^{\,\mathrm{I}}(Q')\cdot\hat{e}(Q')\}\{\vec{r}_e^{\,\mathrm{III}}(Q')\cdot\hat{e}(Q')\}\\
&- \left\{\left[\vec{R}_d-\vec{r}_e(Q')\right]\cdot\hat{b}\right\}\left\{\vec{r}_e^{\,\mathrm{IV}}(Q')\cdot\hat{b}\right\}\\
&- \left\{\left[\vec{R}_d-\vec{r}_e(Q')\right]\cdot\hat{n}_e(Q')\right\}\{\vec{r}_e^{\,\mathrm{IV}}(Q')\cdot\hat{n}_e(Q')\}\\
&- \left\{\left[\vec{R}_d-\vec{r}_e(Q')\right]\cdot\hat{e}(Q')\right\}\{\vec{r}_e^{\,\mathrm{IV}}(Q')\cdot\hat{e}(Q')\} \qquad (749)
\end{aligned}
$$

as the fourth derivative of $r_d(Q')$. Again, we only need the fourth derivatives at the central diffraction point. Therefore, at the central diffraction point

$$\begin{aligned} r_i^{\text{IV}}(Q_c) &= -\left[\kappa_g^{\text{II}}(Q_c) - \kappa_g^3(Q_c)\right]\left[\hat{R}_i \cdot \hat{n}_e(Q_c)\right] - \frac{\kappa_g^2(Q_c)}{R_i} - \frac{3}{R_i}\left[r_i^{\text{II}}(Q_c)\right]^2 \\ &= -\left[\kappa_g^{\text{II}}(Q_c) - \kappa_g^3(Q_c)\right]\cos\psi_c' - \frac{\kappa_g^2(Q_c)}{R_i}\left[1 + 3\cos^2\psi_c'\right] \end{aligned} \tag{750}$$

where, for a plane wave incidence (i.e., $R_i \to \infty$) we get

$$r_i^{\text{IV}}(Q_c) = -\left[\kappa_g^{\text{II}}(Q_c) - \kappa_g^3(Q_c)\right]\cos\psi_c' \,. \tag{751}$$

Also at the central diffraction point,

$$\begin{aligned} r_d^{\text{IV}}(Q_c) &= \left[\kappa_g^{\text{II}}(Q_c) - \kappa_g^3(Q_c)\right]\left[\hat{R}_d \cdot \hat{n}_e(Q_c)\right] - \frac{\kappa_g^2(Q_c)}{s_c} - \frac{3}{s_c}\left[r_d^{\text{II}}(Q_c)\right]^2 \\ &= -\left[\kappa_g^{\text{II}}(Q_c) - \kappa_g^3(Q_c)\right]\cos\psi_c - \frac{\kappa_g^2(Q_c)}{s_c} \\ &\quad - \frac{3}{s_c}\left[\frac{1}{s_c} - \kappa_g(Q_c)\cos\psi_c\right]^2 . \end{aligned} \tag{752}$$

This completes the required derivatives for the determination of the necessary phase derivatives.

Finally, the derivatives of the phase function (714) can be determined using the derivatives of $r_i(Q')$ and $r_d(Q')$ evaluated at the diffraction points. First, the derivatives of the phase function at the central diffraction point located at $l = l_c$ are:

$$h(l_c) = -s_c \tag{753a}$$

$$h^{\text{I}}(l_c) = 0 \tag{753b}$$

$$\begin{aligned} h^{\text{II}}(l_c) &= -\frac{1}{s_c} + \kappa_g(Q_c)\left[\cos\psi_c + \cos\psi_c'\right] \\ &= -\left[\frac{1}{s_c} + \frac{1}{\rho^d(Q_c)}\right] \end{aligned} \tag{753c}$$

$$h^{\text{III}}(l_c) = 0 \tag{753d}$$

$$\begin{aligned} h^{\text{IV}}(l_c) &= \left[\kappa_g^{\text{II}}(Q_c) - \kappa_g^3(Q_c)\right]\left[\cos\psi_c + \cos\psi_c'\right] + \frac{\kappa_g^2(Q_c)}{s_c} \\ &\quad + \frac{3}{s_c^3}\left[1 - \frac{s_c\cos\psi_c}{\rho_g(Q_c)}\right]^2 \end{aligned} \tag{753e}$$

where the radius of curvature of the edge at the central diffraction point is

$$\rho_g(Q_c) = \frac{1}{\kappa_g(Q_c)} \tag{754}$$

and

$$\rho^d(Q_c) = \frac{-\rho_g(Q_c)}{\cos\psi_c + \cos\psi_c'} \tag{755}$$

is the second caustic distance of the central diffracted field. Also, the derivatives of the phase function at the non-central diffraction points are

$$h(l_{nc}) = -\hat{s}' \cdot \vec{r}_e(Q_{nc}) - s_{nc} \tag{756a}$$

$$h^{\mathrm{I}}(l_{nc}) = \cos\beta_{nc}' - \cos\beta_{nc} \equiv 0 \tag{756b}$$

$$\begin{aligned} h^{\mathrm{II}}(l_{nc}) &= -\frac{\sin^2\beta_{nc}}{s_{nc}} - \frac{[\hat{s} - \hat{s}'] \cdot \hat{n}_e(Q_{nc})}{\rho_g(Q_{nc})} \\ &= -\sin^2\beta_{nc}\left[\frac{1}{s_{nc}} + \frac{1}{\rho^d(Q_{nc})}\right] \end{aligned} \tag{756c}$$

where

$$\rho^d(Q_{nc}) = \frac{\rho_g(Q_{nc})\sin^2\beta_{nc}}{[\hat{s} - \hat{s}'] \cdot \hat{n}_e(Q_{nc})} \tag{757}$$

is the second caustic distance of the non-central diffracted field. This completes the derivation of the phase function derivatives.

It is advantageous at this point to derive the relationship between the derivatives with respect to l and the derivatives with respect to the x direction, x_e. To accomplish this, we note that $h(x_e) = h(l)$ and successively differentiate with respect to x_e on both sides to obtain:

$$h(x_e) = h(l) \tag{758a}$$

$$h^{\mathrm{I}}(x_e) = h^{\mathrm{I}}(l)\left(\frac{dl}{dx_e}\right) \tag{758b}$$

$$h^{\mathrm{II}}(x_e) = h^{\mathrm{II}}(l)\left(\frac{dl}{dx_e}\right)^2 + h^{\mathrm{I}}(l)\left(\frac{d^2l}{dx_e^2}\right) \tag{758c}$$

$$\begin{aligned} h^{\mathrm{III}}(x_e) &= h^{\mathrm{III}}(l)\left(\frac{dl}{dx_e}\right)^3 + 3h^{\mathrm{II}}(l)\left(\frac{dl}{dx_e}\right)\left(\frac{d^2l}{dx_e^2}\right) \\ &\quad + h^{\mathrm{I}}(l)\left(\frac{d^3l}{dx_e^3}\right) \end{aligned} \tag{758d}$$

$$\begin{aligned} h^{\mathrm{IV}}(x_e) &= h^{\mathrm{IV}}(l)\left(\frac{dl}{dx_e}\right)^4 + 6h^{\mathrm{III}}(l)\left(\frac{dl}{dx_e}\right)^2\left(\frac{d^2l}{dx_e^2}\right) \\ &\quad + 3h^{\mathrm{II}}(l)\left(\frac{d^2l}{dx_e^2}\right)^2 + 4h^{\mathrm{II}}(l)\left(\frac{dl}{dx_e}\right)\left(\frac{d^3l}{dx_e^3}\right) \end{aligned}$$

$$+h^{\mathrm{I}}(l)\left(\frac{d^4l}{dx_e^4}\right) \tag{758e}$$

$$\begin{aligned} h^{\mathrm{V}}(x_e) &= h^{\mathrm{V}}(l)\left(\frac{dl}{dx_e}\right)^5 + 10h^{\mathrm{IV}}(l)\left(\frac{dl}{dx_e}\right)^3\left(\frac{d^2l}{dx_e^2}\right) \\ &\quad +15h^{\mathrm{III}}(l)\left(\frac{dl}{dx_e}\right)\left(\frac{d^2l}{dx_e^2}\right)^2 + 10h^{\mathrm{III}}(l)\left(\frac{dl}{dx_e}\right)^2\left(\frac{d^3l}{dx_e^3}\right) \\ &\quad +10h^{\mathrm{II}}(l)\left(\frac{d^2l}{dx_e^2}\right)\left(\frac{d^3l}{dx_e^3}\right) + 5h^{\mathrm{II}}(l)\left(\frac{dl}{dx_e}\right)\left(\frac{d^4l}{dx_e^4}\right) \\ &\quad +h^{\mathrm{I}}(l)\left(\frac{d^5l}{dx_e^5}\right) \end{aligned} \tag{758f}$$

$$\begin{aligned} h^{\mathrm{VI}}(x_e) &= h^{\mathrm{VI}}(l)\left(\frac{dl}{dx_e}\right)^6 + 15h^{\mathrm{V}}(l)\left(\frac{dl}{dx_e}\right)^4\left(\frac{d^2l}{dx_e^2}\right) \\ &\quad +45h^{\mathrm{IV}}(l)\left(\frac{dl}{dx_e}\right)^2\left(\frac{d^2l}{dx_e^2}\right)^2 + 20h^{\mathrm{IV}}(l)\left(\frac{dl}{dx_e}\right)^3\left(\frac{d^3l}{dx_e^3}\right) \\ &\quad +60h^{\mathrm{III}}(l)\left(\frac{dl}{dx_e}\right)\left(\frac{d^2l}{dx_e^2}\right)\left(\frac{d^3l}{dx_e^3}\right) + 15h^{\mathrm{III}}(l)\left(\frac{d^2l}{dx_e^2}\right)^3 \\ &\quad +15h^{\mathrm{III}}(l)\left(\frac{dl}{dx_e}\right)^2\left(\frac{d^4l}{dx_e^4}\right) + 10h^{\mathrm{II}}(l)\left(\frac{d^3l}{dx_e^3}\right)^2 \\ &\quad +15h^{\mathrm{II}}(l)\left(\frac{d^2l}{dx_e^2}\right)\left(\frac{d^4l}{dx_e^4}\right) + 6h^{\mathrm{II}}(l)\left(\frac{dl}{dx_e}\right)\left(\frac{d^5l}{dx_e^5}\right) \\ &\quad +h^{\mathrm{I}}(l)\left(\frac{d^6l}{dx_e^6}\right) \end{aligned} \tag{758g}$$

where the differentials must now be determined. To do so, we begin by determining the edge vector as

$$\hat{e}(Q') = \frac{-\hat{x} - \hat{y}\,y'}{\sqrt{1+(y')^2}} \tag{759}$$

which allows us to take the dot product with $\hat{x}$ to obtain

$$-\hat{x}\cdot\hat{e}(Q') = \frac{1}{\sqrt{1+(y')^2}}. \tag{760}$$

Using this result and the definition of the first differential, we find

$$\frac{dl}{dx_e} = \sqrt{1+(y')^2} = \frac{-1}{\hat{x}\cdot\hat{e}(Q')}. \tag{761}$$

This can now be successively differentiated to find the remaining differentials as

$$\frac{d^2l}{dx_e^2} = -\kappa_g(Q')\frac{\hat{x}\cdot\hat{n}_e(Q')}{[\hat{x}\cdot\hat{e}(Q')]^3} \tag{762a}$$

$$\frac{d^3l}{dx_e^3} = -\kappa_g^2(Q')\frac{1}{[\hat{x}\cdot\hat{e}(Q')]^3} - 3\kappa_g^2(Q')\frac{[\hat{x}\cdot\hat{n}_e(Q')]^2}{[\hat{x}\cdot\hat{e}(Q')]^5}$$
$$+\kappa_g^1(Q')\frac{\hat{x}\cdot\hat{n}_e(Q')}{[\hat{x}\cdot\hat{e}(Q')]^4} \tag{762b}$$

where the Serret-Frenet equations of (717) have been used to simplify the results. Although only the first three differentials are required to transform the phase function derivatives, the first six are required in Chapter 7. Therefore, differentiating (762b) three times with respect to x_e we obtain

$$\left.\frac{dl}{dx_e}\right|_{Q_c} = 1 \tag{763a}$$
$$\left.\frac{d^2l}{dx_e^2}\right|_{Q_c} = 0 \tag{763b}$$
$$\left.\frac{d^3l}{dx_e^3}\right|_{Q_c} = \kappa_g^2(Q_c) \tag{763c}$$
$$\left.\frac{d^4l}{dx_e^4}\right|_{Q_c} = 0 \tag{763d}$$
$$\left.\frac{d^5l}{dx_e^5}\right|_{Q_c} = 4\kappa_g(Q_c)\kappa_g^{II}(Q_c) + 9\kappa_g^4(Q_c) \tag{763e}$$
$$\left.\frac{d^6l}{dx_e^6}\right|_{Q_c} = 0 \tag{763f}$$

at the central diffraction point. We can now substitute (753), (761) and (762) into (758) and evaluate at the central

$$h(x_c) = h(l_c) \tag{764a}$$
$$h^I(x_c) = 0 \tag{764b}$$
$$h^{II}(x_c) = h^{II}(l_c) \tag{764c}$$
$$h^{III}(x_c) = 0 \tag{764d}$$
$$h^{IV}(x_c) = h^{IV}(l_c) + 4\kappa_g^2(Q_c)h^{II}(l_c) \tag{764e}$$

and non-central

$$h(x_{nc}) = h(l_{nc}) \tag{765a}$$
$$h^I(x_{nc}) = 0 \tag{765b}$$
$$h^{II}(x_{nc}) = h^{II}(l_{nc})\left(\frac{-1}{\hat{x}\cdot\hat{e}(Q_{nc})}\right)^2 \tag{765c}$$

diffraction points. One last result that will become useful for the uniform asymptotic expansion in Section 3 is the ratio of $h^{\text{IV}}(x_c)$ to $h^{\text{II}}(x_c)$ is

$$\frac{h^{\text{IV}}(x_c)}{h^{\text{II}}(x_c)} = \frac{h^{\text{IV}}(l_c)}{h^{\text{II}}(l_c)} + 4\kappa_g^2(Q_c) \tag{766}$$

which can be used to convert the final result back to the derivatives with respect to arc length.

2 Diffraction Parameter Derivatives

The second derivative of the amplitude function of the integral is required in order to use the uniform asymptotic expansion developed in Section 3. This amplitude function is dependant on the specific integral, but several quantities show up repeatedly. This section is a derivation of the first two derivatives of these common functions.

An important fact that will be used extensively is that the first two derivatives of any function with respect to arc length are the same as the first two derivatives of that function with respect to x_e at the central diffraction point. This was shown in Section 1 for the phase function, but it is true for any function. The equality of the derivatives with respect to arc length and x_e will be stated without further explanation since all the derivatives obtained in this section are evaluated at the central diffraction point.

First, if we recognize that $r = r_d(Q')$, we obtain

$$r\big|_{Q_c} = s_c \tag{767a}$$

$$\left.\frac{dr}{dl}\right|_{Q_c} = \left.\frac{dr}{dx_e}\right|_{Q_c} = 0 \tag{767b}$$

$$\left.\frac{d^2r}{dl^2}\right|_{Q_c} = \left.\frac{d^2r}{dx_e^2}\right|_{Q_c} = \frac{1}{s_c} - \kappa_g(Q_c)\cos\psi_c \tag{767c}$$

from (729) and (738), respectively. Next, we wish to determine the derivatives of $\sin\beta$ and $\sin^2\beta$. To accomplish this we begin with

$$\cos\beta = \hat{r}_d(Q') \cdot \hat{e}(Q') \tag{768}$$

which is a definition of $\cos\beta$. This can be rewritten as

$$r_d(Q')\cos\beta = \vec{r}_d(Q') \cdot \hat{e}(Q') = \left[\vec{R}_d - \vec{r}_e(Q')\right] \cdot \hat{e}(Q') \tag{769}$$

which allows us to differentiate using the chain rule to get

$$\begin{aligned} r_d^{\mathrm{I}}(Q')\cos\beta + r_d(Q')\left(\frac{d\cos\beta}{dl}\right) &= \left[\vec{R}_d - \vec{r}_e(Q')\right]\cdot\hat{e}^{\mathrm{I}}(Q') - \vec{r}_e^{\mathrm{I}}(Q')\cdot\hat{e}(Q') \\ &= \kappa_g(Q')\left\{\left[\vec{R}_d - \vec{r}_e(Q')\right]\cdot\hat{n}_e(Q')\right\} \\ &\quad -\vec{r}_e^{\mathrm{I}}(Q')\cdot\hat{e}(Q') \end{aligned} \tag{770}$$

where the Serret-Frenet equations of (717) have been used to simplify the result. Again, using the chain rule and the Serret-Frenet equations of (717), (770) is differentiated to obtain

$$\begin{aligned} r_d^{\mathrm{II}}(Q')\cos\beta &+ 2r_d^{\mathrm{I}}(Q')\left(\frac{d\cos\beta}{dl}\right) + r_d(Q')\left(\frac{d^2\cos\beta}{dl^2}\right) = \\ &= \kappa_g^{\mathrm{I}}(Q')\left\{\left[\vec{R}_d - \vec{r}_e(Q')\right]\cdot\hat{n}_e(Q')\right\} \\ &+ \kappa_g(Q')\left\{\left[\vec{R}_d - \vec{r}_e(Q')\right]\cdot\hat{n}_e^{\mathrm{I}}(Q')\right\} \\ &- \kappa_g(Q')\left\{\vec{r}_e^{\mathrm{I}}(Q')\cdot\hat{n}_e(Q')\right\} \\ &- \vec{r}_e^{\mathrm{II}}(Q')\cdot\hat{e}(Q') - \vec{r}_e^{\mathrm{I}}(Q')\cdot\hat{e}^{\mathrm{I}}(Q') \\ &= \kappa_g^{\mathrm{I}}(Q')\left\{\left[\vec{R}_d - \vec{r}_e(Q')\right]\cdot\hat{n}_e(Q')\right\} \\ &- \kappa_g^2(Q')\left\{\left[\vec{R}_d - \vec{r}_e(Q')\right]\cdot\hat{e}(Q')\right\} \\ &- \kappa_g(Q')\left\{\vec{r}_e^{\mathrm{I}}(Q')\cdot\hat{n}_e(Q')\right\} \\ &- \vec{r}_e^{\mathrm{II}}(Q')\cdot\hat{e}(Q') - \kappa_g(Q')\left\{\vec{r}_e^{\mathrm{I}}(Q')\cdot\hat{n}_e(Q')\right\} \end{aligned} \tag{771}$$

which will be used to determine the second derivative of $\cos\beta$. Evaluating (769) through (771) at the central diffraction point, we get:

$$\cos\beta\big|_{Q_c} = 0 \tag{772a}$$

$$\left.\frac{d\cos\beta}{dl}\right|_{Q_c} = \left.\frac{d\cos\beta}{dx_e}\right|_{Q_c} = \frac{1}{s_c} - \kappa_g(Q_c)\cos\psi_c \tag{772b}$$

$$\left.\frac{d^2\cos\beta}{dl^2}\right|_{Q_c} = \left.\frac{d^2\cos\beta}{dx_e^2}\right|_{Q_c} = 0. \tag{772c}$$

Using the trigonometric identity, $\sin^2\beta = 1 - \cos^2\beta$, we can differentiate twice

$$\frac{d\sin^2\beta}{dl} = -2\cos\beta\left(\frac{d\cos\beta}{dl}\right) \tag{773a}$$

$$\frac{d^2\sin^2\beta}{dl^2} = -2\left(\frac{d\cos\beta}{dl}\right)^2 - 2\cos\beta\left(\frac{d^2\cos\beta}{dl^2}\right) \tag{773b}$$

and evaluate them at the central diffraction point to obtain

$$\sin^2\beta\Big|_{Q_c} = 1 \tag{774a}$$

$$\left.\frac{d\sin^2\beta}{dl}\right|_{Q_c} = \left.\frac{d\sin^2\beta}{dx_e}\right|_{Q_c} = 0 \tag{774b}$$

$$\left.\frac{d^2\sin^2\beta}{dl^2}\right|_{Q_c} = \left.\frac{d^2\sin^2\beta}{dx_e^2}\right|_{Q_c} = -2\left[\frac{1}{s_c} - \kappa_g(Q_c)\cos\psi_c\right]^2 \tag{774c}$$

as the derivatives of $\sin^2\beta$. Also, differentiating $\sin^2\beta$ using the chain rule

$$\frac{d\sin^2\beta}{dl} = 2\sin\beta\left(\frac{d\sin\beta}{dl}\right) \tag{775a}$$

$$\frac{d^2\sin^2\beta}{dl^2} = 2\left(\frac{d\sin\beta}{dl}\right)^2 + 2\sin\beta\left(\frac{d^2\sin\beta}{dl^2}\right) \tag{775b}$$

and evaluate them at the central diffraction point to obtain

$$\sin\beta|_{Q_c} = 1 \tag{776a}$$

$$\left.\frac{d\sin\beta}{dl}\right|_{Q_c} = \left.\frac{d\sin\beta}{dx_e}\right|_{Q_c} = 0 \tag{776b}$$

$$\left.\frac{d^2\sin\beta}{dl^2}\right|_{Q_c} = \left.\frac{d^2\sin\beta}{dx_e^2}\right|_{Q_c} = -\left[\frac{1}{s_c} - \kappa_g(Q_c)\cos\psi_c\right]^2 \tag{776c}$$

as the required derivatives of $\sin\beta$. Following a similar procedure and recognizing $\cos\beta' = \hat{r}_i(Q')\cdot\hat{e}(Q')$ and $R_i \to \infty$ we obtain

$$\cos\beta'|_{Q_c} = 0 \tag{777a}$$

$$\left.\frac{d\cos\beta'}{dl}\right|_{Q_c} = \left.\frac{d\cos\beta'}{dx_e}\right|_{Q_c} = -\kappa_g(Q_c)\cos\psi_c' \tag{777b}$$

$$\left.\frac{d^2\cos\beta'}{dl^2}\right|_{Q_c} = \left.\frac{d^2\cos\beta'}{dx_e^2}\right|_{Q_c} = 0 \tag{777c}$$

and

$$\sin^2\beta'\Big|_{Q_c} = 1 \tag{778a}$$

$$\left.\frac{d\sin^2\beta'}{dl}\right|_{Q_c} = \left.\frac{d\sin^2\beta'}{dx_e}\right|_{Q_c} = 0 \tag{778b}$$

$$\left.\frac{d^2\sin^2\beta'}{dl^2}\right|_{Q_c} = \left.\frac{d^2\sin^2\beta'}{dx_e^2}\right|_{Q_c} = -2\left[\kappa_g(Q_c)\cos\psi_c'\right]^2 \tag{778c}$$

which can be used to obtain

$$\sin\beta'|_{Q_c} = 1 \tag{779a}$$

$$\left.\frac{d\sin\beta'}{dl}\right|_{Q_c} = \left.\frac{d\sin\beta'}{dx_e}\right|_{Q_c} = 0 \tag{779b}$$

$$\left.\frac{d^2\sin\beta'}{dl^2}\right|_{Q_c} = \left.\frac{d^2\sin\beta'}{dx_e^2}\right|_{Q_c} = -\left[\kappa_g(Q_c)\cos\psi_c'\right]^2 \tag{779c}$$

as the required derivatives of $\cos\beta'$, $\sin^2\beta'$ and $\sin\beta'$ evaluated at the central diffraction point. The only other common quantity of the amplitude functions are the half-plane diffraction coefficients. However, these will be determined in the next section due to the extensive nature of the differentiation of the diffraction coefficients.

3 Half-Plane Diffraction Coefficient Derivatives

Other common quantities that appears in the amplitude functions of the diffraction integrals are the half-plane diffraction coefficients. The edges are assumed to be on flat plates for the purposes of the work. Therefore, the second derivatives of the half-plane diffraction coefficients are required in order to use the uniform asymptotic expansion developed in Section 3 of Appendix B. This section is devoted to the differentiation of the half-plane diffraction coefficients.

As discussed in Section 2, the first two derivatives with respect to arc length of any function is identical to the first two derivatives with respect to x_e evaluated at the central diffraction point. This fact will be used here as well. The equality of the derivatives with respect to arc length and x_e will be stated without further explanation since all of the derivatives determined in this section are evaluated at the central diffraction point.

The diffraction integrals formulated in this work are obtained using the ITD as discussed in Chapter 4. For this reason, it will be necessary to differentiate the ITD half-plane diffraction coefficients rather than the UTD half-plane diffraction coefficients. First, recall that the ITD half-plane diffraction coefficients are

$$\widetilde{D}_{s,h}(Q') = \frac{1}{2}\left\{\frac{F\left[kLa(\Psi^-)\right]}{\cos\left(\frac{\Psi^-}{2}\right)} \mp \frac{F\left[kLa(\Psi^+)\right]}{\cos\left(\frac{\Psi^+}{2}\right)}\right\}$$

$$= \frac{1}{2}\left\{\sec\left(\frac{\Psi^-}{2}\right) F\left[kLa(\Psi^-)\right] \mp \sec\left(\frac{\Psi^+}{2}\right) F\left[kLa(\Psi^+)\right]\right\} \qquad (780)$$

where

$$L = r\sin^2\beta \qquad (781)$$

is the distance parameter and

$$a(\Psi^\mp) = 2\cos^2\left(\frac{\Psi^\mp}{2}\right) \qquad (782)$$

is the angle parameter. This must now be differentiated twice in order to use the uniform asymptotic expansion derived in Section 3 of Appendix B.

Extensive use of the chain rule is employed to accomplish this differentiation. The differentiation of $\Psi^\mp = \psi \mp \psi'$ will be performed first. We can write $\cos\psi$ as

$$\cos\psi = -\frac{\hat{r}_d(Q')\cdot\hat{n}_e(Q')}{\sin\beta} \qquad (783)$$

and it can be rewritten as

$$r_d(Q')\sin\beta\cos\psi = -\vec{r}_d(Q')\cdot\hat{n}_e(Q') = -\left[\vec{R}_d - \vec{r}_e(Q')\right]\cdot\hat{n}_e(Q') \qquad (784)$$

which allows us to easily differentiate. Now, differentiating both side of (784) with respect to arc length we obtain

$$\begin{aligned} r_d^{\rm I}(Q')\sin\beta\cos\psi \;+\; & r_d(Q')\left(\frac{d\sin\beta}{dl}\right)\cos\psi + r_d(Q')\sin\beta\left(\frac{d\cos\psi}{dl}\right) = \\ &= \{\vec{r}_e^{\,\rm I}(Q')\cdot\hat{n}_e(Q')\} - \left[\vec{R}_d - \vec{r}_e(Q')\right]\cdot\hat{n}_e^{\rm I}(Q') \\ &= \{\vec{r}_e^{\,\rm I}(Q')\cdot\hat{n}_e(Q')\} \\ &+ \kappa_g(Q')\left\{\left[\vec{R}_d - \vec{r}_e(Q')\right]\cdot\hat{e}\,(Q')\right\} \end{aligned} \qquad (785)$$

where the Serret-Frenet equations of (717) were used to simplify this result which will be used to determine the first derivative of $\cos\psi$. Next, differentiating both sides of (785) with respect to arc length we get

$$\begin{aligned} & r_d^{\rm II}(Q')\sin\beta\cos\psi \;+\; 2r_d^{\rm I}(Q')\left(\frac{d\sin\beta}{dl}\right)\cos\psi + 2r_d^{\rm I}(Q')\sin\beta\left(\frac{d\cos\psi}{dl}\right) + \\ & 2r_d(Q')\left(\frac{d\sin\beta}{dl}\right)\left(\frac{d\cos\psi}{dl}\right) + r_d(Q')\left(\frac{d^2\sin\beta}{dl^2}\right)\cos\psi + r_d(Q')\sin\beta\left(\frac{d^2\cos\psi}{dl^2}\right) = \end{aligned}$$

$$
\begin{aligned}
&= \{\vec{r}_e^{\,\mathrm{II}}(Q')\cdot\hat{n}_e(Q')\} + \{\vec{r}_e^{\,\mathrm{I}}(Q')\cdot\hat{n}_e^{\mathrm{I}}(Q')\} \\
&+ \kappa_g^{\mathrm{I}}(Q')\left\{\left[\vec{R}_d - \vec{r}_e(Q')\right]\cdot\hat{e}(Q')\right\} - \kappa_g(Q')\{\vec{r}_e^{\,\mathrm{I}}(Q')\cdot\hat{e}(Q')\} \\
&+ \kappa_g(Q')\left\{\left[\vec{R}_d - \vec{r}_e(Q')\right]\cdot\hat{e}^{\mathrm{I}}(Q')\right\} \\
&= \{\vec{r}_e^{\,\mathrm{II}}(Q')\cdot\hat{n}_e(Q')\} + \kappa_g^{\mathrm{I}}(Q')\left\{\left[\vec{R}_d - \vec{r}_e(Q')\right]\cdot\hat{e}(Q')\right\} \\
&- 2\kappa_g(Q')\{\vec{r}_e^{\,\mathrm{I}}(Q')\cdot\hat{e}(Q')\} \\
&+ \kappa_g^2(Q')\left\{\left[\vec{R}_d - \vec{r}_e(Q')\right]\cdot\hat{n}_e(Q')\right\} \qquad (786)
\end{aligned}
$$

where the Serret-Frenet equations of (717) have been used to simplify this result which will be used to obtain the second derivative of $\cos\psi$. Evaluating (784) through (786) at the central diffraction point we obtain

$$\cos\psi\big|_{Q_c} = \cos\psi_c \qquad (787a)$$

$$\left.\frac{d\cos\psi}{dl}\right|_{Q_c} = \left.\frac{d\cos\psi}{dx_e}\right|_{Q_c} = 0 \qquad (787b)$$

$$\left.\frac{d^2\cos\psi}{dl^2}\right|_{Q_c} = \left.\frac{d^2\cos\psi}{dx_e^2}\right|_{Q_c} = -\frac{\sin^2\psi_c\cos\psi_c}{\rho_g^2(Q_c)} + \frac{\sin^2\psi_c}{s_c\,\rho_g(Q_c)} \qquad (787c)$$

which will now be used to determine the derivatives of ψ. Using the chain rule, $\cos\psi$ can be differentiated as

$$\frac{d\cos\psi}{dl} = -\sin\psi\left(\frac{d\psi}{dl}\right) \qquad (788a)$$

$$\frac{d^2\cos\psi}{dl^2} = -\cos\psi\left(\frac{d\psi}{dl}\right)^2 - \sin\psi\left(\frac{d^2\psi}{dl^2}\right) \qquad (788b)$$

which can be evaluated at the central diffraction point and (787) used to obtain

$$\psi\big|_{Q_c} = \psi_c \qquad (789a)$$

$$\left.\frac{d\psi}{dl}\right|_{Q_c} = \left.\frac{d\psi}{dx_e}\right|_{Q_c} = 0 \qquad (789b)$$

$$\left.\frac{d^2\psi}{dl^2}\right|_{Q_c} = \left.\frac{d^2\psi}{dx_e^2}\right|_{Q_c} = \frac{\sin\psi_c\cos\psi_c}{\rho_g^2(Q_c)} - \frac{\sin\psi_c}{s_c\,\rho_g(Q_c)} \qquad (789c)$$

as the derivatives of ψ. Following a similar differentiation process as before and evaluating the derivatives at the central diffraction points

$$\psi'\big|_{Q_c} = \psi_c' \qquad (790a)$$

$$\left.\frac{d\psi'}{dl}\right|_{Q_c} = \left.\frac{d\psi'}{dx_e}\right|_{Q_c} = 0 \tag{790b}$$

$$\left.\frac{d^2\psi'}{dl^2}\right|_{Q_c} = \left.\frac{d^2\psi'}{dx_e^2}\right|_{Q_c} = \frac{\sin\psi_c'\cos\psi_c'}{\rho_g^2(Q_c)} - \frac{\sin\psi_c'}{R_i\,\rho_g(Q_c)} \tag{790c}$$

where for plane wave incidence (i.e., $R_i \to \infty$) we obtain:

$$\psi'|_{Q_c} = \psi_c' \tag{791a}$$

$$\left.\frac{d\psi'}{dl}\right|_{Q_c} = \left.\frac{d\psi'}{dx_e}\right|_{Q_c} = 0 \tag{791b}$$

$$\left.\frac{d^2\psi'}{dl^2}\right|_{Q_c} = \left.\frac{d^2\psi'}{dx_e^2}\right|_{Q_c} = \frac{\sin\psi_c'\cos\psi_c'}{\rho_g^2(Q_c)} \tag{791c}$$

Finally, using (789) and (791) in $\Psi^{\mp} = \psi \mp \psi'$ and evaluating them at the central diffraction point we get

$$\Psi_c^{\mp} = \Psi^{\mp}\Big|_{Q_c} = \psi_c \mp \psi_c' \tag{792a}$$

$$\frac{d\Psi_c^{\mp}}{dl} = \left.\frac{d\Psi^{\mp}}{dl}\right|_{Q_c} = \left.\frac{d\Psi^{\mp}}{dx_e}\right|_{Q_c} = 0 \tag{792b}$$

$$\begin{aligned}\frac{d^2\Psi_c^{\mp}}{dl^2} &= \left.\frac{d^2\Psi^{\mp}}{dl^2}\right|_{Q_c} = \left.\frac{d^2\Psi^{\mp}}{dx_e^2}\right|_{Q_c} \\ &= \left\{\frac{\sin\psi_c\cos\psi_c}{\rho_g^2(Q_c)} - \frac{\sin\psi_c}{s_c\,\rho_g(Q_c)}\right\} \mp \left\{\frac{\sin\psi_c'\cos\psi_c'}{\rho_g^2(Q_c)}\right\}\end{aligned} \tag{792c}$$

as the required derivatives. Also, the distance parameter $L = r\sin^2\beta$ can be differentiated using the results of Section 2 to obtain

$$\frac{dL}{dl} = \left(\frac{dr}{dl}\right)\sin^2\beta + r\left(\frac{d\sin^2\beta}{dl}\right) \tag{793a}$$

$$\frac{d^2L}{dl^2} = \left(\frac{d^2r}{dl^2}\right)\sin^2\beta + 2\left(\frac{dr}{dl}\right)\left(\frac{d\sin^2\beta}{dl}\right) + r\left(\frac{d^2\sin^2\beta}{dl^2}\right) \tag{793b}$$

which is now evaluated at the central diffraction point and simplified to get

$$L|_{Q_c} = s_c \tag{794a}$$

$$\left.\frac{dL}{dl}\right|_{Q_c} = \left.\frac{dL}{dx_e}\right|_{Q_c} = 0 \tag{794b}$$

$$\begin{aligned}\left.\frac{d^2L}{dl^2}\right|_{Q_c} &= \left.\frac{d^2L}{dx_e^2}\right|_{Q_c} \\ &= s_c\left\{\frac{1}{s_c^2}\left[1 - \frac{s_c\cos\psi_c}{\rho_g(Q_c)}\right] - \frac{2}{s_c^2}\left[1 - \frac{s_c\cos\psi_c}{\rho_g(Q_c)}\right]^2\right\}\end{aligned} \tag{794c}$$

as the required derivatives. The angle parameter $a(\Psi^{\mp}) = 2\cos^2\left(\frac{\Psi^{\mp}}{2}\right)$ can now be differentiated using the chain rule

$$\frac{da(\Psi^{\mp})}{dl} = -2\left(\frac{d\Psi^{\mp}}{dl}\right)\sin\left(\frac{\Psi^{\mp}}{2}\right)\cos\left(\frac{\Psi^{\mp}}{2}\right) \tag{795a}$$

$$\frac{d^2a(\Psi^{\mp})}{dl^2} = -2\left(\frac{d^2\Psi^{\mp}}{dl^2}\right)\sin\left(\frac{\Psi^{\mp}}{2}\right)\cos\left(\frac{\Psi^{\mp}}{2}\right) - \left(\frac{d\Psi^{\mp}}{dl}\right)^2\cos\left(\Psi^{\mp}\right) \tag{795b}$$

which, at the central diffraction point gives

$$a(\Psi_c^{\mp}) = 2\cos^2\left(\frac{\Psi_c^{\mp}}{2}\right) \tag{796a}$$

$$\left.\frac{da(\Psi^{\mp})}{dl}\right|_{Q_c} = \left.\frac{da(\Psi^{\mp})}{dx_e}\right|_{Q_c} = 0 \tag{796b}$$

$$\left.\frac{d^2a(\Psi^{\mp})}{dl^2}\right|_{Q_c} = \left.\frac{d^2a(\Psi^{\mp})}{dx_e^2}\right|_{Q_c} = a(\Psi_c^{\mp})\left\{-\left(\frac{d^2\Psi_c^{\mp}}{dl^2}\right)\tan\left(\frac{\Psi_c^{\mp}}{2}\right)\right\} \tag{796c}$$

as the first two derivatives. We are now in a position to differentiate the argument of the Fresnel transition function $X^{\mp} = kLa(\Psi^{\mp})$. Using the chain rule

$$\frac{dX^{\mp}}{dl} = k\left(\frac{dL}{dl}\right)a(\Psi^{\mp}) + kL\left(\frac{da(\Psi^{\mp})}{dl}\right) \tag{797a}$$

$$\frac{d^2X^{\mp}}{dl^2} = k\left(\frac{d^2L}{dl^2}\right)a(\Psi^{\mp}) + 2k\left(\frac{dL}{dl}\right)\left(\frac{da(\Psi^{\mp})}{dl}\right) + kL\left(\frac{d^2a(\Psi^{\mp})}{dl^2}\right) \tag{797b}$$

and evaluating these at the central diffraction point and simplifying

$$X_c^{\mp} = \left.X^{\mp}\right|_{Q_c} = 2ks_c\cos^2\left(\frac{\Psi_c^{\mp}}{2}\right) \tag{798a}$$

$$\frac{dX_c^{\mp}}{dl} = \left.\frac{dX^{\mp}}{dl}\right|_{Q_c} = \left.\frac{dX^{\mp}}{dx_e}\right|_{Q_c} = 0 \tag{798b}$$

$$\frac{d^2X_c^{\mp}}{dl^2} = \left.\frac{d^2X^{\mp}}{dl^2}\right|_{Q_c} = \left.\frac{d^2X^{\mp}}{dx_e^2}\right|_{Q_c} = 2X_c^{\mp}\left\{\frac{1}{2s_c^2}\left[1-\frac{s_c\cos\psi_c}{\rho_g(Q_c)}\right] - \frac{1}{s_c^2}\left[1-\frac{s_c\cos\psi_c}{\rho_g(Q_c)}\right]^2 - \frac{1}{2}\left(\frac{d^2\Psi_c^{\mp}}{dl^2}\right)\tan\left(\frac{\Psi_c^{\mp}}{2}\right)\right\} \tag{798c}$$

which are the derivatives of interest. Next, the differentiation of the Fresnel transition function $F[X^{\mp}]$ is to be determined. Using the chain rule

$$\frac{dF[X^{\mp}]}{dl} = \frac{dX^{\mp}}{dl}\,\frac{dF[X^{\mp}]}{dX^{\mp}} \tag{799}$$

which is then differentiated again

$$\frac{d^2F[X^{\mp}]}{dl^2} = \frac{d^2X^{\mp}}{dl^2}\,\frac{dF[X^{\mp}]}{dX^{\mp}} + \left(\frac{dX^{\mp}}{dl}\right)^2 \frac{d^2F[X^{\mp}]}{dX^{\mp 2}} \tag{800}$$

where it is now necessary to determine the derivatives of the Fresnel transition function with respect to its argument. To do so, we recall (6) from Chapter 2

$$F[x] = 2j\sqrt{x}e^{jx}\int_{\sqrt{x}}^{\infty} e^{-j\tau^2}\,d\tau \tag{801}$$

which is the Fresnel transition function. We must know how to differentiate the Fresnel integral in order to correctly differentiate the Fresnel transition function. Using the fact that [50]

$$\frac{d}{dp}\int_{p}^{\infty} f(t)\,dt = -f(p) \tag{802}$$

and using the chain rule, the derivative of the Fresnel transition function is

$$\begin{aligned}\frac{dF[x]}{dx} &= 2j\left[\frac{e^{jx}}{2\sqrt{x}} + j\sqrt{x}e^{jx}\right]\int_{\sqrt{x}}^{\infty} e^{-j\tau^2}\,d\tau - j \\ &= \frac{F[x] - F_s[x]}{2x}\end{aligned} \tag{803}$$

with respect to its argument. The slope diffraction transition function is given by

$$F_s[x] = 2jx\left\{1 - F[x]\right\}. \tag{804}$$

Finally, substituting (798) and (803) into (799) and (800) and evaluating them at the central diffraction point we obtain

$$F[X_c^{\mp}] = F[ks_c a(\Psi_c^{\mp})] \tag{805a}$$

$$\frac{dF[X_c^{\mp}]}{dl} = \left.\frac{dF[X^{\mp}]}{dl}\right|_{Q_c} = \left.\frac{dF[X^{\mp}]}{dx_e}\right|_{Q_c} = 0 \tag{805b}$$

$$\frac{d^2F[X_c^{\mp}]}{dl^2} = \left.\frac{d^2F[X^{\mp}]}{dl^2}\right|_{Q_c} = \left.\frac{d^2F[X^{\mp}]}{dx_e^2}\right|_{Q_c}$$

$$= \left\{ \frac{1}{2s_c^2}\left[1 - \frac{s_c \cos\psi_c}{\rho_g(Q_c)}\right] - \frac{1}{s_c^2}\left[1 - \frac{s_c \cos\psi_c}{\rho_g(Q_c)}\right]^2 - \frac{1}{2}\left(\frac{d^2\Psi_c^{\mp}}{dl^2}\right)\tan\left(\frac{\Psi_c^{\mp}}{2}\right)\right\}\left\{F[X_c^{\mp}] - F_s[X_c^{\mp}]\right\} \quad (805c)$$

as the derivatives of the Fresnel transition function with respect to arc length. Now, differentiating the secant terms in the half-plane diffraction coefficients using the chain rule,

$$\frac{d\sec\left(\frac{\Psi^{\mp}}{2}\right)}{dl} = \frac{1}{2}\left(\frac{d\Psi^{\mp}}{dl}\right)\sec\left(\frac{\Psi^{\mp}}{2}\right)\tan\left(\frac{\Psi^{\mp}}{2}\right) \quad (806a)$$

$$\frac{d^2\sec\left(\frac{\Psi^{\mp}}{2}\right)}{dl^2} = \frac{1}{2}\left(\frac{d^2\Psi^{\mp}}{dl^2}\right)\sec\left(\frac{\Psi^{\mp}}{2}\right)\tan\left(\frac{\Psi^{\mp}}{2}\right) + \frac{1}{4}\left(\frac{d\Psi^{\mp}}{dl}\right)^2\left\{\sec\left(\frac{\Psi^{\mp}}{2}\right)\tan^2\left(\frac{\Psi^{\mp}}{2}\right) + \sec^3\left(\frac{\Psi^{\mp}}{2}\right)\right\} \quad (806b)$$

where evaluating these derivatives at the central diffraction point we get

$$\sec\left(\frac{\Psi^{\mp}}{2}\right)\Big|_{Q_c} = \sec\left(\frac{\Psi_c^{\mp}}{2}\right) \quad (807a)$$

$$\frac{d\sec\left(\frac{\Psi^{\mp}}{2}\right)}{dl}\Big|_{Q_c} = \frac{d\sec\left(\frac{\Psi^{\mp}}{2}\right)}{dx_e}\Big|_{Q_c} = 0 \quad (807b)$$

$$\frac{d^2\sec\left(\frac{\Psi^{\mp}}{2}\right)}{dl^2}\Big|_{Q_c} = \frac{d^2\sec\left(\frac{\Psi^{\mp}}{2}\right)}{dx_e^2}\Big|_{Q_c} = \sec\left(\frac{\Psi_c^{\mp}}{2}\right)\left\{\frac{1}{2}\left(\frac{d^2\Psi_c^{\mp}}{dl^2}\right)\tan\left(\frac{\Psi_c^{\mp}}{2}\right)\right\} \quad (807c)$$

which finally allows us to differentiate the half-plane diffraction coefficients using the chain rule.

We are in a position to differentiate the ITD half-plane diffraction coefficients in (780) since we have differentiated the secant terms and the Fresnel transition functions with respect to arc length. Using the chain rule,

$$\frac{d\widetilde{D}_{s,h}(Q')}{dl} = \frac{1}{2}\left\{\left[\frac{d\sec\left(\frac{\Psi^-}{2}\right)}{dl}F[X^-] + \sec\left(\frac{\Psi^-}{2}\right)\frac{dF[X^-]}{dl}\right] \mp \left[\frac{d\sec\left(\frac{\Psi^+}{2}\right)}{dl}F[X^+] + \sec\left(\frac{\Psi^+}{2}\right)\frac{dF[X^+]}{dl}\right]\right\} \quad (808)$$

is the first derivative and

$$\frac{d^2\widetilde{D}_{s,h}(Q')}{dl^2} = \frac{1}{2}\left\{\left[\frac{d^2\sec\left(\frac{\Psi^-}{2}\right)}{dl^2}F[X^-] + 2\,\frac{d\sec\left(\frac{\Psi^-}{2}\right)}{dl}\,\frac{dF[X^-]}{dl} + \sec\left(\frac{\Psi^-}{2}\right)\frac{d^2F[X^-]}{dl^2}\right] \mp \left[\frac{d^2\sec\left(\frac{\Psi^+}{2}\right)}{dl^2}F[X^+] + 2\,\frac{d\sec\left(\frac{\Psi^+}{2}\right)}{dl}\,\frac{dF[X^+]}{dl} + \sec\left(\frac{\Psi^+}{2}\right)\frac{d^2F[X^+]}{dl^2}\right]\right\} \tag{809}$$

is the second derivative of the ITD half-plane diffraction coefficients with respect to arc length. In order to place the final result in terms of auxiliary half-plane diffraction coefficients that have the same form as the UTD half-plane diffraction coefficients, let:

$$D_{s,h}(Q_c) = \frac{-e^{-j\pi/4}}{\sqrt{2\pi k}}\,\widetilde{D}_{s,h}(Q')\Big|_{Q_c} \tag{810a}$$

$$\frac{dD_{s,h}(Q_c)}{dl} = \frac{-e^{-j\pi/4}}{\sqrt{2\pi k}}\,\frac{d\widetilde{D}_{s,h}(Q')}{dl}\Big|_{Q_c} \tag{810b}$$

$$\frac{d^2D_{s,h}(Q_c)}{dl^2} = \frac{-e^{-j\pi/4}}{\sqrt{2\pi k}}\,\frac{d^2\widetilde{D}_{s,h}(Q')}{dl^2}\Big|_{Q_c} \tag{810c}$$

Therefore, substituting (805) and (807) into (810) and simplifying, we obtain

$$\frac{dD_{s,h}(Q_c)}{dl} = \frac{dD_{s,h}(Q_c)}{dx_e} = 0 \tag{811}$$

and

$$\frac{d^2D_{s,h}(Q_c)}{dl^2} = \frac{d^2D_{s,h}(Q_c)}{dx_e^2} = D_{s,h}^{(I)}(Q_c) + \left\{\frac{1}{2s_c^2}\left[1 - \frac{s_c\cos\psi_c}{\rho_g(Q_c)}\right] - \frac{1}{s_c^2}\left[1 - \frac{s_c\cos\psi_c}{\rho_g(Q_c)}\right]^2\right\}\left[D_{s,h}(Q_c) - D_{s,h}^{(II)}(Q_c)\right] \tag{812}$$

as the first two derivatives of the half-plane diffraction coefficients with respect to arc length evaluated at the central diffraction point. We note that

$$D_{s,h}(Q_c) = \frac{-e^{-j\pi/4}}{2\sqrt{2\pi k}}\left\{\frac{F[ks_ca(\Psi_c^-)]}{\cos\left(\frac{\Psi_c^-}{2}\right)} \mp \frac{F[ks_ca(\Psi_c^+)]}{\cos\left(\frac{\Psi_c^+}{2}\right)}\right\} \tag{813}$$

are the typical UTD half-plane diffraction coefficients for normal incidence. There are also two auxiliary half-plane diffraction coefficients

$$D_{s,h}^{(I)}(Q_c) = \frac{-e^{-j\pi/4}}{2\sqrt{2\pi k}} \left\{ \left[\frac{1}{2} \left(\frac{d^2\Psi_c^-}{dl^2} \right) \tan\left(\frac{\Psi_c^-}{2} \right) \right] \frac{F_s[ks_c a(\Psi_c^-)]}{\cos\left(\frac{\Psi_c^-}{2}\right)} \right.$$
$$\left. \mp \left[\frac{1}{2} \left(\frac{d^2\Psi_c^+}{dl^2} \right) \tan\left(\frac{\Psi_c^+}{2} \right) \right] \frac{F_s[ks_c a(\Psi_c^+)]}{\cos\left(\frac{\Psi_c^+}{2}\right)} \right\} \tag{814}$$

and

$$D_{s,h}^{(II)}(Q_c) = \frac{-e^{-j\pi/4}}{2\sqrt{2\pi k}} \left\{ \frac{F_s[ks_c a(\Psi_c^-)]}{\cos\left(\frac{\Psi_c^-}{2}\right)} \mp \frac{F_s[ks_c a(\Psi_c^+)]}{\cos\left(\frac{\Psi_c^+}{2}\right)} \right\} \tag{815}$$

which appear in (812), where $\Psi_c^{\mp} = \psi_c \mp \psi_c'$ and

$$a(\Psi_c^{\mp}) = 2\cos^2\left(\frac{\Psi_c^{\mp}}{2}\right). \tag{816}$$

Also, the slope diffraction transition function is defined as

$$F_s[x] = 2jx\{1 - F[x]\} \tag{817}$$

and the second derivative of $\Psi^{\mp}$ with respect to arc length is

$$\frac{d^2\Psi_c^{\mp}}{dl^2} = \left\{ \frac{\sin\psi_c \cos\psi_c}{\rho_g^2(Q_c)} - \frac{\sin\psi_c}{s_c\,\rho_g(Q_c)} \right\} \mp \left\{ \frac{\sin\psi_c' \cos\psi_c'}{\rho_g^2(Q_c)} \right\} \tag{818}$$

evaluated at the central diffraction point as given by (792).

REFERENCES

[1] R. Kouyoumjian and P. Pathak, "A uniform geometrical theory of diffraction for an edge in a perfectly-conducting surface," *Proc. IEEE*, vol. 62, pp. 1448–1461, 1974.

[2] R. Millar, "An approximate theory of diffraction of an electromagnetic wave by an aperture in a plane screen," *Proc. IEE*, vol. Monograph No. 152 R, pp. 177–185, Oct. 1955.

[3] R. Millar, "The diffraction of an electromagnetic wave by a large aperture," *Proc. IEE*, vol. Monograph No. 213 R, pp. 240–250, Dec. 1956.

[4] C. Ryan, Jr. and L. Peters, Jr., "Evaluation of edge diffracted fields including equivalent currents for the caustic regions," *IEEE Trans. Antennas Propagat.*, vol. AP-17, pp. 292–299, May 1969.

[5] C. Ryan, Jr. and L. Peters, Jr., "Correction to: Evaluation of edge diffracted fields including equivalent currents for the caustic regions," *IEEE Trans. Antennas Propagat.*, vol. AP-18, p. 275, Mar. 1970.

[6] W. Burnside and L. Peters, Jr., "Edge diffracted caustic fields," *IEEE Trans. Antennas Propagat.*, vol. AP-22, pp. 620–623, July 1974.

[7] W. Burnside and L. Peters, Jr., "Axial-radar cross section of finite cones by the equivalent-current concept with higher-order diffraction," *Radio Sci.*, vol. 7, pp. 943–948, Oct. 1972.

[8] J. Choi, N. Wang, L. Peters, Jr., and P. Levy, "Near axial backscattering from finite cones," *IEEE Trans. Antennas Propagat.*, vol. AP-38, pp. 1264–1272, Aug. 1990.

[9] E. Knott and T. Senior, "Comparison of three high-frequency diffraction techniques," *Proc. IEEE*, vol. 62, no. 11, pp. 1468–1474, Nov. 1974.

[10] F. Sikta and L. Peters, Jr., "UTD analysis of electromagnetic scattering by flat plate structures," Technical Report 711930-2, The Ohio State University ElectroScience Laboratory, Department of Electrical Engineering, Dec. 1981.

[11] E. Greer and W. Burnside, "High frequency near field scattering by an elliptic disk," Technical Report 4583-1, The Ohio State University ElectroScience Laboratory, Department of Electrical Engineering, Dec. 1976.

[12] N. Albertsen, P. Balling, and N. Jensen, "Caustics and caustic corrections to the field diffracted by a curved edge," *IEEE Trans. Antennas Propagat.*, vol. AP-25, pp. 297–303, May 1977.

[13] A. Michaeli, "Elimination of infinities in equivalent edge currents, Part I: Fringe current components," *IEEE Trans. Antennas Propagat.*, vol. AP-34, pp. 912–918, July 1986.

[14] D. Butorin, N. Martynov, and P. Ufimtsev, "Asymptotic expressions for the elementary edge waves," *Sov. J. Commun. Technol. Electron.*, vol. 33, no. 1, pp. 17–26, Jan. 1988.

[15] R. Tiberio and S. Maci, "A spectral incremental diffraction coefficient," *1992 URSI Digest*, Chicago, Illinois, July 18-25, p.498.

[16] R. Tiberio and S. Maci, "An incremental theory of diffraction: Scalar formulation," *IEEE Trans. Antennas Propagat.*, In press.

[17] R. Tiberio, S. Maci, and A. Toccafondi, "An incremental theory of diffraction: Electromagnetic formulation," *IEEE Trans. Antennas Propagat.*, Submitted for publication.

[18] C. Chester, B. Friedman, and F. Ursell, "An extension of the method of steepest descents," *Proc. Camb. Phil. Soc.*, vol. 53, pp. 599–611, 1957.

[19] J. Keller, "Diffraction by an aperture," *J. Appl. Phys.*, vol. 28, pp. 426–444, 1957.

[20] K. Mitzner, "Incremental length diffraction coefficients," Technical Report No. AFAL-TR-73-296, Northrop Corporation, Aircraft Division, Apr. 1974.

[21] A. Michaeli, "Equivalent edge currents for arbitrary aspects of observation," *IEEE Trans. Antennas Propagat.*, vol. AP-32, pp. 252–258, Mar. 1984.

[22] A. Michaeli, "Correction to: Equivalent edge currents for arbitrary aspects of observation," *IEEE Trans. Antennas Propagat.*, vol. AP-33, p. 227, Feb. 1985.

[23] E. Knott, "The relationship between Mitzner's ILDC and Michaeli's equivalent currents," *IEEE Trans. Antennas Propagat.*, vol. AP-33, pp. 112–114, Jan. 1985.

[24] D. Butorin and P. Ufimtsev, "Explicit expressions for an acoustic edge wave scattered by an infinitesimal edge element," *Sov. Phys. Acoust.*, vol. 32, no. 4, pp. 283–287, July-August 1986.

[25] M. Ando, T. Murasaki, and T. Kinoshita, "Elimination of false singularities in GTD equivalent edge currents," *Proc. IEE, Part H*, vol. 138, pp. 289–296, Aug. 1991.

[26] R. Shore and A. Yaghjian, "Incremental diffraction coefficients for planar surfaces," *IEEE Trans. Antennas Propagat.*, vol. AP-36, pp. 55–70, Jan. 1988.

[27] J. Arnold, "Spectral methods in edge diffraction theories," *J. Opt. Soc. Am.*, vol. A9, no. 12, pp. 2192–2205, Dec. 1992.

[28] R. Harrington, *Time-Harmonic Electromagnetic Fields.* McGraw-Hill Inc., New York, 1961.

[29] C. Balanis, *Advanced Engineering Electromagnetics.* John Wiley and Sons Inc., New York, 1989.

[30] G. James, *Geometrical Theory of Diffraction for Electromagnetic Waves.* Herts. SG1 1HQ. England: Peter Peregrinus Ltd., 1976.

[31] R. Kouyoumjian and P. Pathak, "The dyadic diffraction coefficient for a perfectly conducting wedge," Technical Report 2183-4, The Ohio State University ElectroScience Laboratory, Department of Electrical Engineering, June 1970.

[32] N. Bleistein and R. Handelsman, *Asymptotic Expansions of Integrals.* Dover Publications, Inc., New York, 1975.

[33] M. Boas, *Mathematical Methods in the Physical Sciences.* John Wiley and Sons Inc., New York, 1966.

[34] A. Michaeli, "Contribution of a single face to the wedge diffracted field," *IEEE Trans. Antennas Propagat.*, vol. AP-33, pp. 221–223, Feb. 1985.

[35] J. Kraus, *Antennas.* McGraw-Hill Book Company, Inc., New York, 1950.

[36] C. Balanis, *Antenna Theory: Analysis and Design.* Harper & Row, Inc., New York, 1982.

[37] J. Nehrbass, I. Gupta, and E. Newman, "VESP user's manual: Vectorized method of moments solution for EM scattering," Technical Report 721929, The Ohio State University ElectroScience Laboratory, Department of Electrical Engineering, Dec. 1993.

[38] J. Connor, "Practical methods for the uniform asymptotic evaluation of oscillating integrals with several coalescing saddle points," *Lecture Notes in Pure and Applied Mathematics: Asymptotic and Computational Analysis*, vol. 124, pp. 137–173, 1990.

[39] N. Bleistein, "Uniform asymptotic expansions of integrals with many nearby stationary points and algebraic singularities," *J. Math. and Mech.*, vol. 17, no. 6, pp. 533–559, 1967.

[40] F. Ursell, "Integrals with a large parameter. Several nearly coincident saddle-points," *Proc. Camb. Phil. Soc.*, vol. 72, pp. 49–65, 1972.

[41] J. Stamnes, *Waves in Focal Regions.* Hilger, Bristol, 1986.

[42] T. Pearcey, "The structure of an electromagnetic field in the neighbourhood of a cusp of a caustic," *Phil. Mag.*, vol. 37, pp. 311–317, 1946.

[43] D. Kaminski, "Asymptotic expansion of the Pearcey integral near the caustic," *SIAM J. Math. Anal.*, vol. 20, no. 4, pp. 987–1005, 1989.

[44] J. Connor and P. Curtis, "A method for the numerical evaluation of the oscillatory integrals associated with the cuspoid catastrophes: Application to Pearcey's integral and its derivatives," *J. Phys. A: Math. Gen.*, vol. 15, no. 4, pp. 1179–1190, 1982.

[45] R. Paris, "The asymptotics of Pearcey's integral for complex variables," *Lecture Notes in Pure and Applied Mathematics: Asymptotic and Computational Analysis*, vol. 124, pp. 653–667, 1990.

[46] J. Martin, "Integrals with a large parameter and several nearly coincident saddle-points; the continuation of uniformly asymptotic expansions," *Proc. Camb. Phil. Soc.*, vol. 76, pp. 211–231, 1974.

[47] L. Felsen, "Focusing by an anisotropic plasma interface," *IEEE Trans. Antennas Propagat.*, vol. AP-12, pp. 624–635, Sept. 1964.

[48] L. Felsen and N. Marcuvitz, *Radiation and Scattering of Waves.* Prentice-Hall, Inc., New Jersey, 1973.

[49] I. Gradshteyn and I. Ryzhik, *Table of Integrals, Series and Products.* Academic Press Inc., New York, 1980.

[50] M. Abramowitz and I. Stegun, *Handbook of Mathematical Functions.* (NBS Applied Math Series No. 55) Washington, D.C., NBS, 1964.

[51] M. Lipschutz, *Differential Geometry.* Schaum's Outline Series in Mathematics, McGraw-Hill Inc., New York, 1969.